ARO 19431.23-EG-RW

(2)

AD-A198 964

Final Report of the Center of Excellence in Rotary Wing Technology at Rensselaer Polytechnic Institute

Contract Number DAAG 29-82-K-0093
U.S. Army Research Office

April 15, 1988

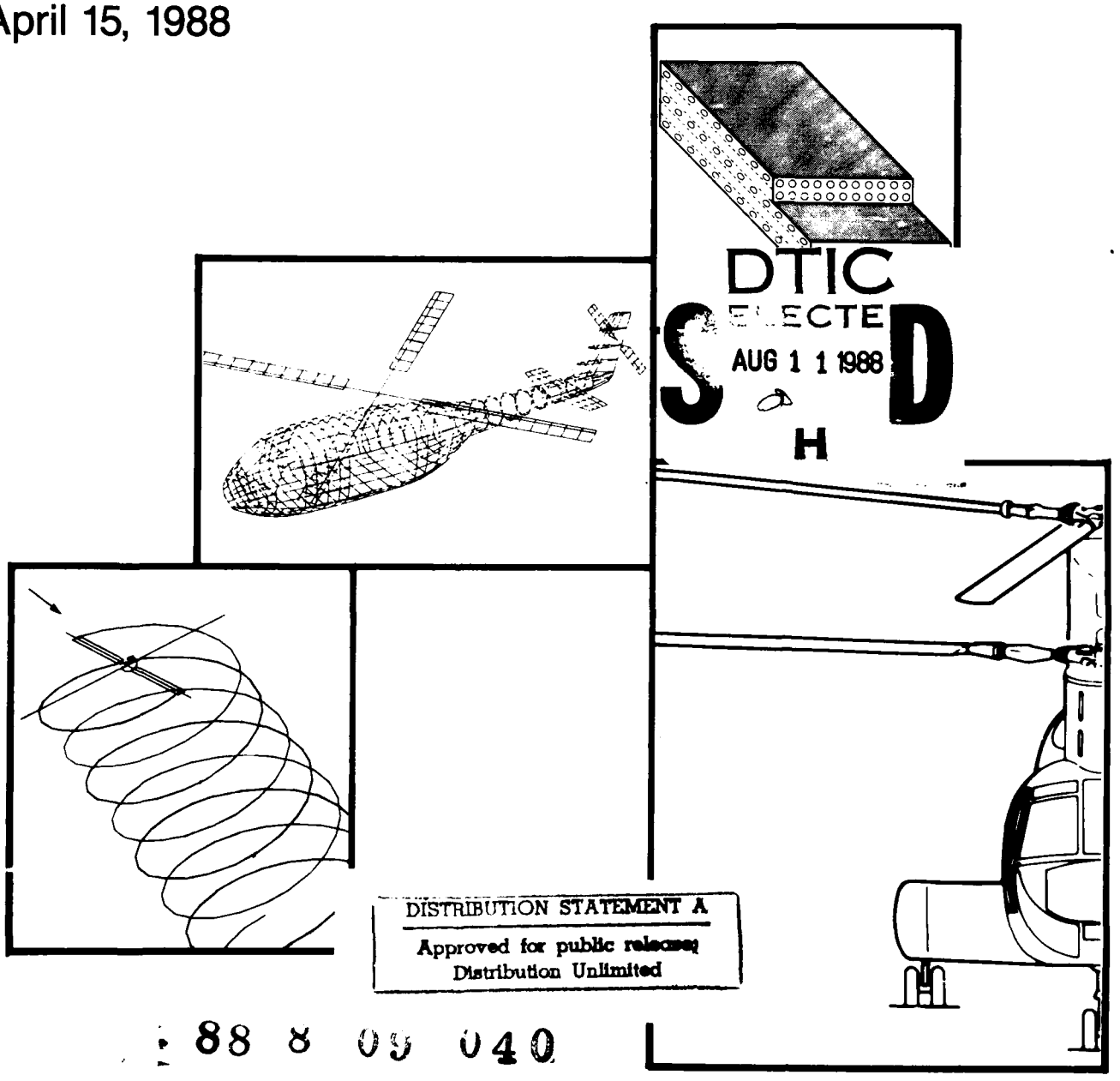

ADA198964

SECURITY CLASSIFICATION OF THIS PAGE

REPORT DOCUMENTATION PAGE

1a. REPORT SECURITY CLASSIFICATION: Unclassified	1b. RESTRICTIVE MARKINGS: -
2a. SECURITY CLASSIFICATION AUTHORITY: -	3. DISTRIBUTION/AVAILABILITY OF REPORT: Approved for public release; distribution unlimited.
2b. DECLASSIFICATION/DOWNGRADING SCHEDULE: -	
4. PERFORMING ORGANIZATION REPORT NUMBER(S): -	5. MONITORING ORGANIZATION REPORT NUMBER(S): ARO 19431.23-EG-RW
6a. NAME OF PERFORMING ORGANIZATION: Rensselaer Polytechnic Institute; 6b. OFFICE SYMBOL (If applicable): -	7a. NAME OF MONITORING ORGANIZATION: U.S. Army Research Office
6c. ADDRESS (City, State and ZIP Code): Troy, N.Y. 12180	7b. ADDRESS (City, State and ZIP Code): P.O. Box 12211 Research Triangle Park, N.C. 22709-2211
8a. NAME OF FUNDING/SPONSORING ORGANIZATION: U.S. Army Research Office; 8b. OFFICE SYMBOL (If applicable): -	9. PROCUREMENT INSTRUMENT IDENTIFICATION NUMBER: DAAG29-82-K-0093
8c. ADDRESS (City, State and ZIP Code): P.O. Box 12211 Research Triangle Parl. N.C. 27709-2211	10. SOURCE OF FUNDING NOS.

PROGRAM ELEMENT NO.	PROJECT NO.	TASK NO.	WORK UNIT NO.
-	-	-	-

11. TITLE (Include Security Classification): Center of Excellence in Rotary Wing Technology

12. PERSONAL AUTHOR(S): R.G. Loewy; Editor; O. Bauchau, R. Bielawa, M. Darlow, R.J. Diefendorf, R. Duffy, R. Mayle, H. Nagamatsu, M. Shephard, S. Winckler

13a. TYPE OF REPORT	13b. TIME COVERED	14. DATE OF REPORT (Yr., Mo., Day)	15. PAGE COUNT
Final	FROM 7/1/82 TO 4/15/88	88-4-15	330

16. SUPPLEMENTARY NOTATION: The views, opinions or findings contained in this report are those of the author(s) and should not be construed as official position(s), policies, or decision(s) of the Department of the Army unless so designated by other documentation.

17. COSATI CODES		
FIELD	GROUP	SUB. GR.

18. SUBJECT TERMS (Continue on reverse if necessary and identify by block number): Helicopters, Rotorcraft, Aeronautical Engineering Education

19. ABSTRACT (Continue on reverse if necessary and identify by block number)

The activities associated with establishing a Center of Excellence in Rotary Wing Technology at Rensselaer Polytechnic Institute under a five year contract with the U.S. Army Research Office are reported here. These include measures taken to provide comprehensive and in-depth curricula at advanced levels in rotorcraft technology; attract and retain outstanding young people in these programs; perform basic research at the leading edge of technology in structures, structural dynamics, unsteady aerodynamics and aeroelasticity disciplines as applied to rotorcraft; developing useful new national research resources in these areas; and accomplishing technology transfer to the rotorcraft community beyond the Rensselaer campus. Descriptions, references and statistics are provided to allow assessment of the extent to which these goals have been realized.

20. DISTRIBUTION/AVAILABILITY OF ABSTRACT	21. ABSTRACT SECURITY CLASSIFICATION
UNCLASSIFIED/UNLIMITED ☐ SAME AS RPT. ☒ OTIC USERS ☐	Unclassified

22a. NAME OF RESPONSIBLE INDIVIDUAL	22b. TELEPHONE NUMBER (Include Area Code)	22c. OFFICE SYMBOL
Dr.Robert Singleton	919-549-0641	

DD FORM 1473, 83 APR EDITION OF 1 JAN 73 IS OBSOLETE.

Unclassified

SECURITY CLASSIFICATION OF THIS PAGE

Final Report of the

Center of Excellence in Rotary Wing Technology

at

Rensselaer Polytechnic Institute

U.S. Army Research Office

Contract No. DAAG 29-82-K-0093

Authors

O. Bauchau
R. Bielawa
M. Darlow
R. J. Diefendorf
R. Duffy
E. Krempl
R. Mayle
H. Nagamatsu
M. Shephard
S. Winckler

Editor

R. G. Loewy

April 15, 1988

Final Report Table of Contents

Preface

This report attempts to be a rather complete summary of all that transpired under a contract covering six years of effort. The text includes summaries of pertinent information; the appendices contain fairly detailed records of activities.

Because of the length of the totality of research summaries, figures and tables are placed immediately following the text for each of the four broad disciplinary categories; ie Structures, Structural Dynamics, Unsteady Aerodynamics & Aeroelasticity. This has the effect of putting figures and tables in four groups, so that they are more easily referred to. The figures are grouped first, the tables second. All references are contained in one place, however, Section 8.

Where research results have been substantially reported in the open literature, the research summaries have been limited by referring to those publications. Thus, the degree of detail provided in research summaries is purposefully uneven, with greater numbers of figures and tables provided for those projects which were not, as of this writing, fully reported in the literature.

List of Figures

List of Tables

1. Introduction

On June 26, 1980, the U. S. Army's vertical lift technology ad hoc sub group chaired by Norman R. Augustine, submitted a report entitled "Vertical Lift Review" [Ref. 1] to the then Assistant Secretary of the Army for Research, Development and Acquisition, the Honorable Percy A. Pierre. Among six "technology" category recommendations, five "mission" category recommendations and seven "management" category recommendations, was one clearly pointed toward academia. This recommendation, number 13, said

> "Support, through a highly visible Army program, the establishment of a small number of Centers of Excellence in Rotary Wing Aircraft technology among respected U. S. universities. Nuture this through a significantly expanded program of long term research grants and invitational symposia."

The Army reacted postively to this recommendation, identifying the Army Research Office in Durham, N.C. (ARO) as the proper organization to accomplish its implementation. An announcement was made in the Commerce Business Daily, and by September '81 a supplement to the ARO Program Guide "Centers of Excellence: Rotary Wing Technology" was issued. Universities were asked to respond by December 31, 1981. A quotation from that document [Ref. 2] put the matter in a context which can hardly be improved upon as a statement of need for such centers, even seven years later:

> "Rotorcraft are only now in their third generation, are some forty years behind fixed wing aircraft in terms of total flight experience, and have enjoyed but a small fraction of the development funds allocated to fixed wing aircraft. Rotary wing aircraft design and development are therefore by no means a mature technology; in fact, today rotary wing design is nearly as much an art as it is a science. Though perhaps not widely recognized, the aerostructural complexities of a rotary wing vehicle are enormous. Rotary wing vehicles regularly operate in difficult portions of the flight envelope which fixed wing aircraft tend to encounter only on a transient basis or not at all. For example, rotary wing aircraft regularly operate in unsteady flow fields, in ground effect, with near-sonic flow conditions on lifting surfaces and in a condition of static instability. There are complex and significant interactions between the lifting rotor and other components, particularly at low speeds, which are just now beginning to be understood. Small and seemingly unimportant design changes can provide large changes in the vibration and stress levels encountered in flight as a result of the interaction. These effects all combine to make the development of rotary wing aircraft an extremely complex undertaking."

The RPI proposal [Ref. 3] responding to the ARO program announcement, expressed agreement with this point of view, stating "It is in just such an arena -- namely, where much fundamental understanding of the phenomena underlying rotary wing behavior is both needed for progress and remains to be acquired; where the inherent complexities of the systems being dealt with obscure the clues crucial to such understanding; where relatively little of the resources needed to unravel these complexities have been expended; and where the high technology which has characterized U. S. scientific and engineering programs in the last half-century can provide the needed resources -- that proper use of the graduate level educational and research capabilities of U. S. universities can be a strong force in achieving significant advances."

In accordance with this view, Rensselaer submitted a proposal with three basic program components: Educational, Research and efforts to develop new National Resources. The educational component expressed the intent of establishing distinguished graduate fellowships to attract some of the most outstanding U.S. students to the study of rotorcraft technology, would institute new and revised courses and degree options in rotorcraft technology and integrate graduate and undergraduate coursework for students who chose this option into a basic and comprehensive education in the important underlying disciplines. The research component would concentrate on four closely-related, interactive sub-disciplines; namely, materials & structures -- particularly composites -- structural dynamics, unsteady aerodynamics and aeroelasticity; all of these, of course, specialized to rotorcraft applications. The establishment of new national resources of potential use to researchers at other universities, in industry or government laboratories was pictured as naturally arising from the research component of the program. At the proposal stage, this was anticipated as involving computer graphics applications and/or new facility/equipment developments aimed at blade vortex interaction studies.

Notice that RPI had been chosen as one of the U. S. Army Centers of Excellence in Rotary Wing Aircraft Technology was received on 18 February 1982 and the contract was effective on the following July 1st.

2. Funding and Contractual History

A four year contract [Ref. 4] was received at Rensselaer for the purpose of establishing a Center of Excellence in Rotorcraft Technology with total funding of $3.101 million. Support increments were made available on July 1st of each of four successive years, in amounts shown on the financial forecast and expenditure chart of Fig. 1. Plans for future research tasks and other performance matters were established for each up-coming year on the basis of site visits to the RPI campus by the Army Research Office project monitors and evaluative panels and subsequent discussions. Initiation and termination of research projects, described in Section 5 of this report, were carried out, fundamentally, in accordance with ARO guidance formulated in this way. A list of the ARO evaluative panel members is shown in Table 1, and their years of activity on the panel indicated in Fig. 2. The dates of periodic site visits is shown in Table 2, attendees and their agenda in Appendix A.

As part of the original program planning and in response to a request from ARO, Rensselaer submitted on March 28, 1986 a proposal in which the Center would continue its development for the optional 5th year under ARO sponsorship. ARO awarded an additional $.781 million for this 5th year. In final fiscal actions under the original five year program, a one-half year contract extension proposal was submitted on April 29, 1987 with the intent of carrying the rotorcraft technology center contract forward to the end of December 1987, with additional funding of $.403 million. A favorable response on the part of ARO effective July 1, 1987 made the total 5 and one-half year funding for Rensselaer's Rotorcraft Technology Center $4.284 million. Requests for no-cost extensions resulted in the contract end date of April 15, 1988; for a total performance period of five years and nine and one-half months. The time history of actual expenditures is also shown in Fig. 1. A comparison of budget and expenditures by major categories is shown in Table 3.

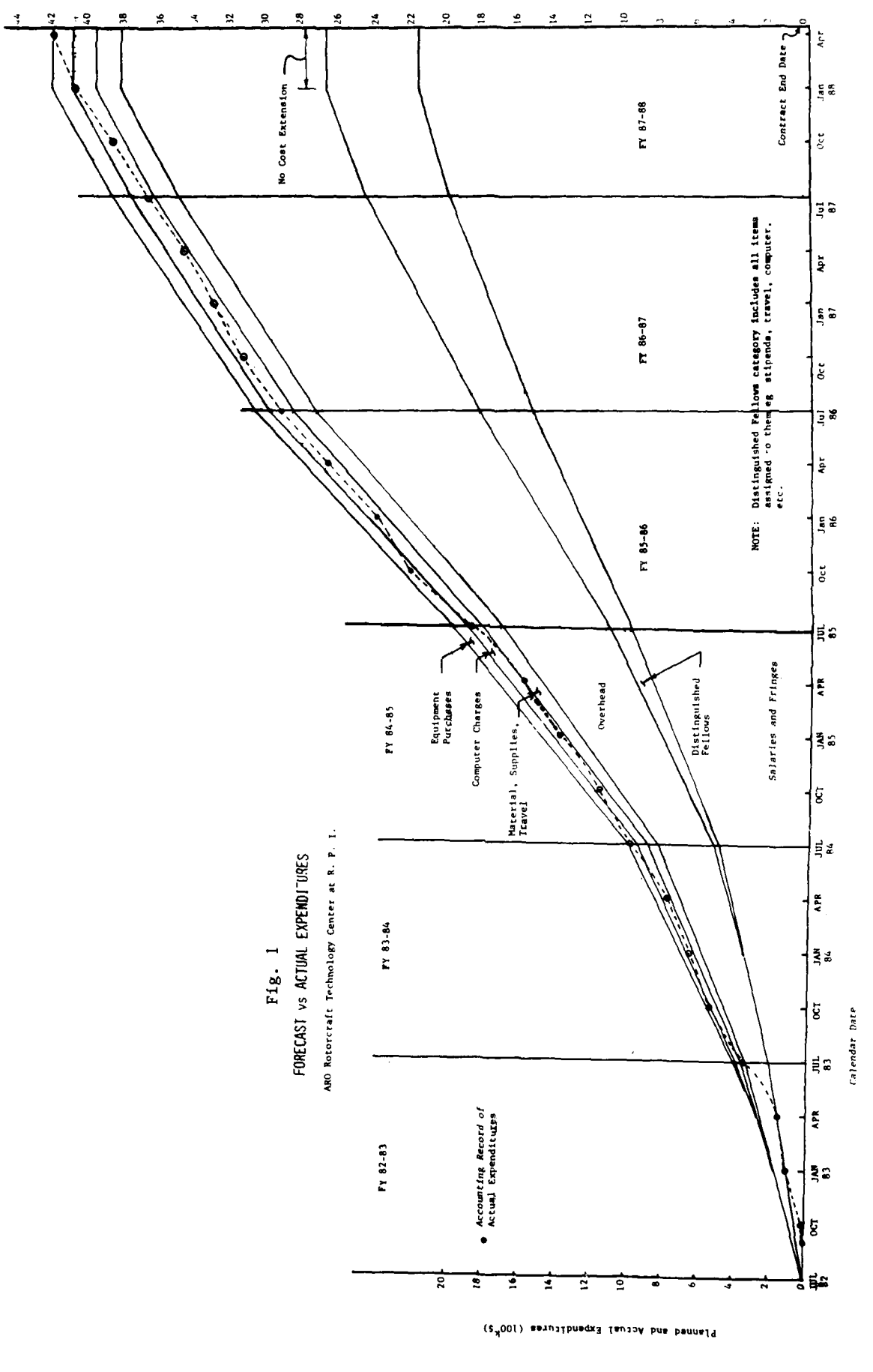

Fig. 1
FORECAST vs ACTUAL EXPENDITURES
ARO Rotorcraft Technology Center at R. P. I.

Fig. 2

Evaluative Panel Membership

Rensselaer RTC

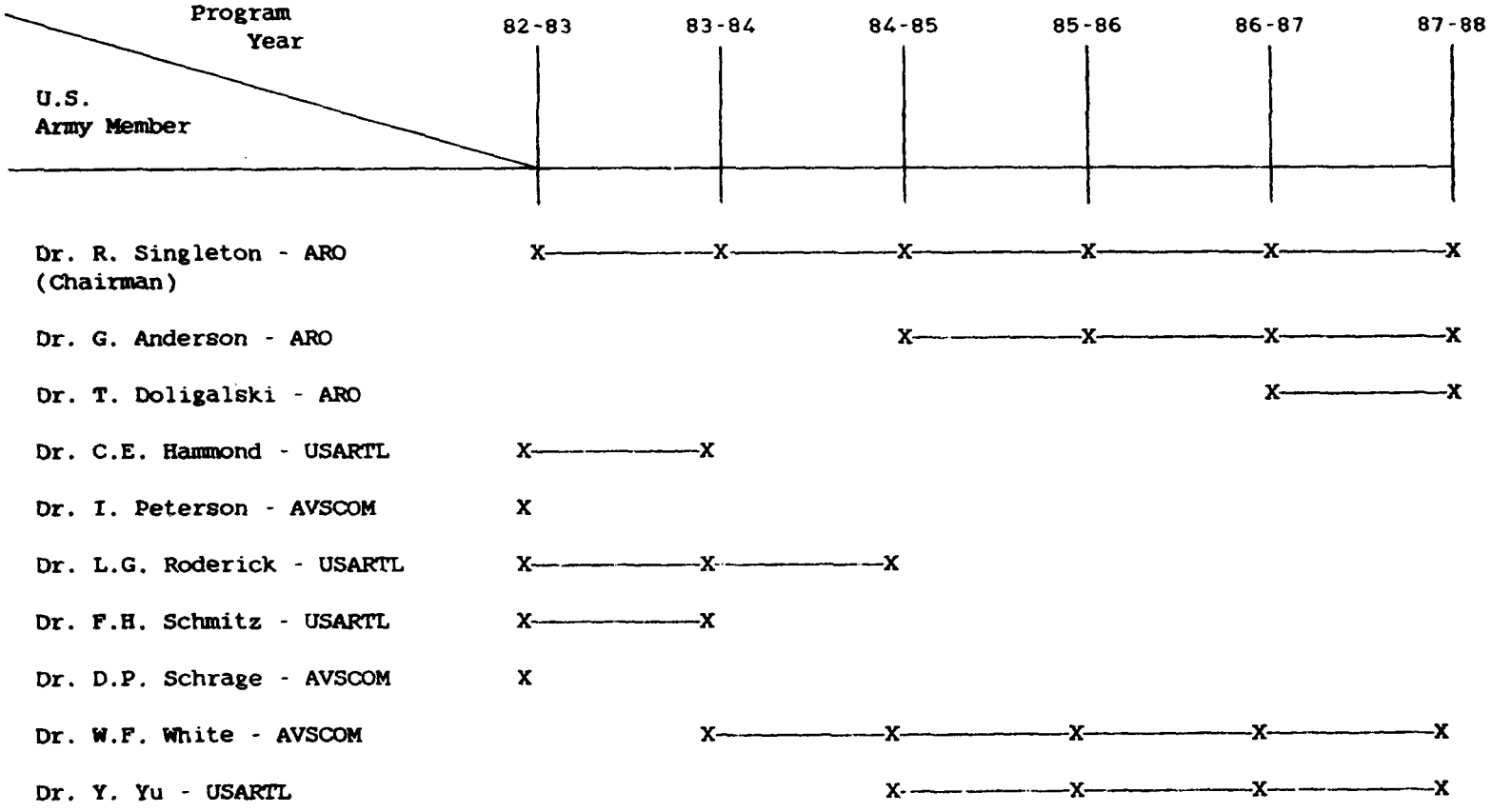

TABLE 1

Evaluative Panel Membership

Rensselaer RTC

Member	Member
Dr. Robert Singleton (Chairman) Director, Engineering Sciences Division U.S. Army Research Office	Dr. Larry G. Roderick Chief, Army Aeronautical Research Group USARTL - AVRADCOM
Dr. Gary Anderson Chief, Structures and Dynamics Branch U.S. Army Research Office	Dr. Fred H. Schmitz Chief, Fluid Mechanics Division USARTL - AVSCOM
Dr. Thomas Doligalski Chief, Aerodynamics Branch U.S. Army Research Office	Dr. Daniel P. Schrage Director of Advanced Systems USA Aviation Systems Command
Dr. C. Eugene Hammond Chief, Aeromechanics Technical Area USARTL - AVSCOM	Dr. William F. White Aerospace Engineer USA Aviation Systems Command
Dr. Idelle Peterson Aerospace Engineer USA Aviation Systems Command	Dr. Yung Yu Group Leader, Acoustics USARTL - AVRaDCOM

TABLE 2

Dates of Yearly Site Visits

ARO Evaluative Committees to Rensselaer RTC

June 28, 1983

June 19, 1984

June 12, 1985

February 3, 1987

TABLE 3

Comparison of Accumulative Budget and Expenditures by Category

Rensselaer RTC

Category	Budget	Expenditures
Salary & Benefits	56.2 %	49.6 %
Travel	1.8 %	1.9 %
Supplies & Services	3.5 %	8.9 %
Equipment	2.6 %	2.9 %
Computer	3.7 %	2.2 %
Overhead	32.2 %	34.5 %
	100.0 %	100.0 %

3. Center Organization and Management

The Rensselaer Rotorcraft Technology Center (RRTC) is organized as shown in Fig. 3. Professors Robert G. Loewy and R. Judd Diefendorf, were named as Co-Principal Investigators under the contract and function as Director & Assistant Director of the Center, respectively. Members of the Industrial Technical Advisory Panel, Table 4, were chosen deliberately as the first-line supervisors who had responsibility for across the board technology within each of the major helicopter development and production companies in the United States.

The faculty committee shown in Fig. 3 as the Budget Advisory Committee, periodically reviews progress and accomplishments in all program performance areas: namely course development and revision; distinguished fellowship candidate attraction, selection & retention; continuing education; and research projects. The specific "next year" planned program of research presented for consideration at ARO site visits (see Appendix A), was selected by the Director from faculty proposals on the basis of advice from the committee, and allocations from each year's contract funding were made by the Director on the basis of their advice for the next years' research project budgets to accomplish what had been outlined in ARO guidance. Members of the Budget Advisory Committee are listed in Table 5.

Day to day supervision of the tasks extablished as described above, was carried out by each of the faculty members listed under research project headings in Sections 4 & 5 as "Senior Investigators". A complete list of the faculty contributing to the goals of the center are listed in Table 6. They are identified there as to chronology of involvement, research specialty, center role and whether directly funded by the ARO contract or not. For convenience, their years of funding under the contract are shown in Fig. 4. It is noteworthy, that of these faculty, four were appointed to tenure-track positions subsequent to, and largely a result of the establishment of the RRTC.

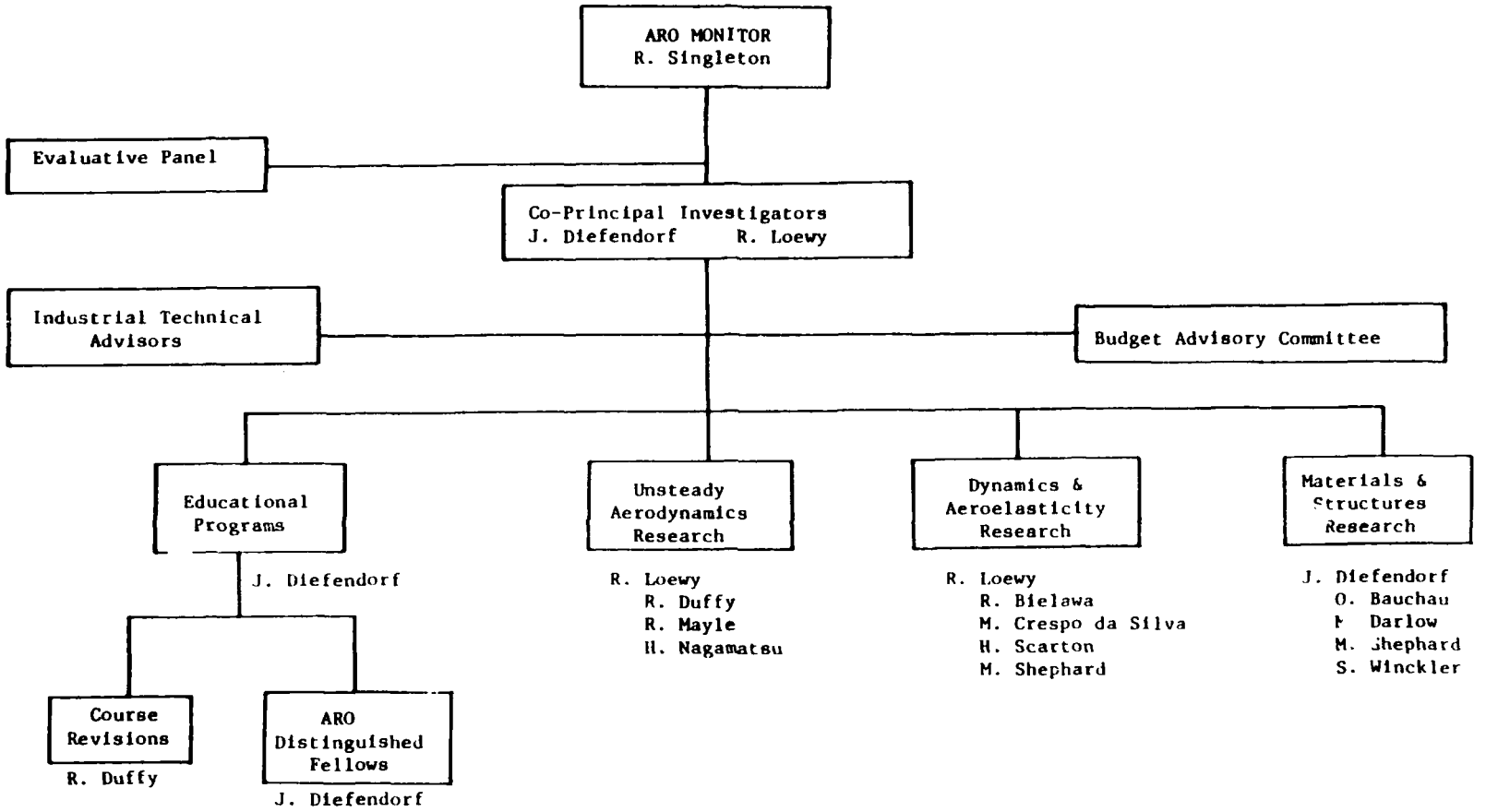

Fig. 3 - Organizational Diagram Rensselaer RTC

Fig. 4 - Faculty with Support under the Rensselaer RTC Contract

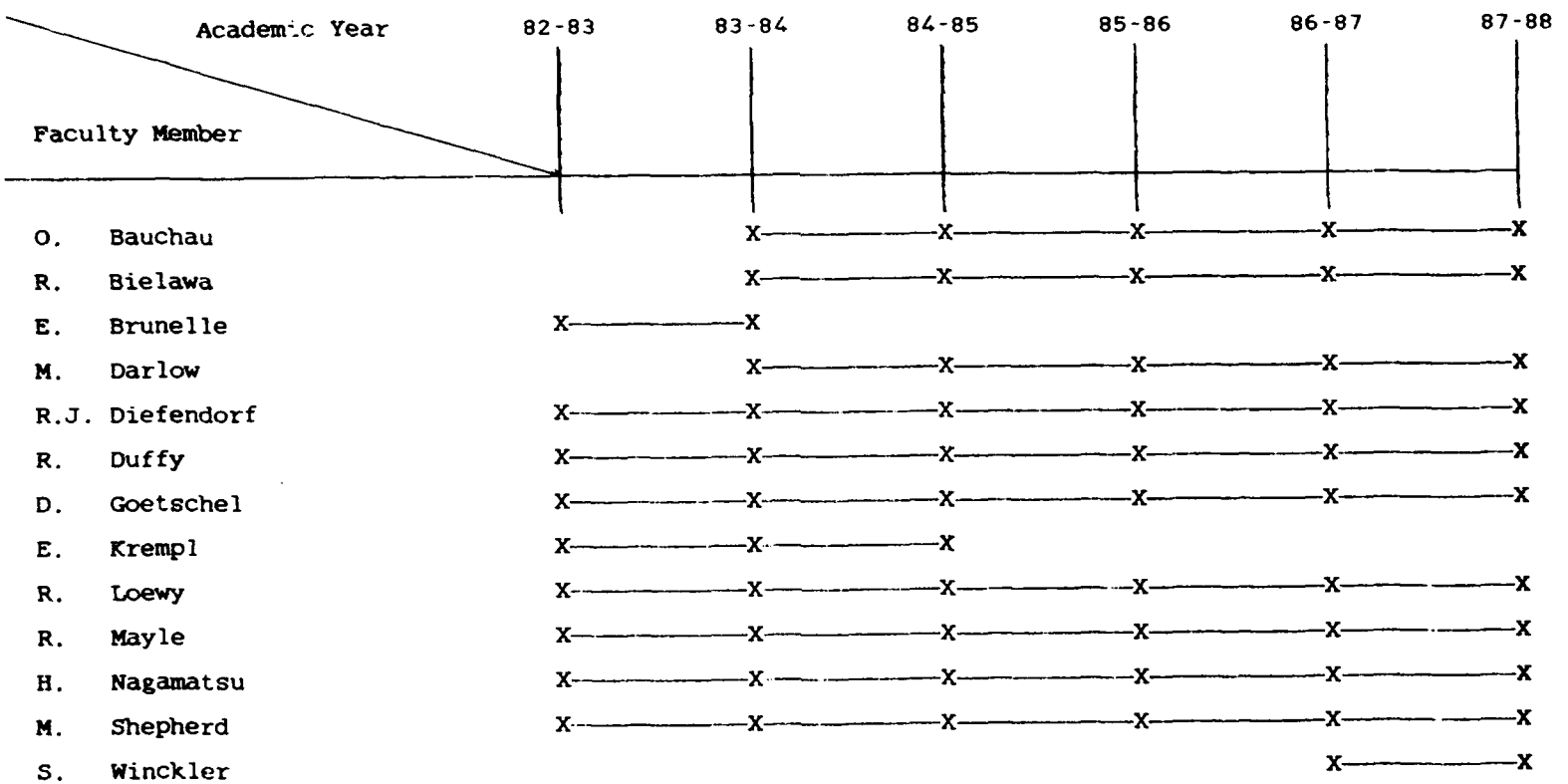

TABLE 4

Industrial Technical Advisory Panel Membership

Rensselaer RTC

Member	(Years Active)	Member	(Years Active)
Mr. Troy Gaffey Manager, JVX Technology Bell Helicopter Textron	(82 thru 87)	Dr. Herbert G. Somerson Chief Scientist Boeing Vertol Company	(85 thru 87)
Mr. David Jenney Chief of Technical Engineering Sikorsky Aircraft Division, UTC	(82 thru 87)	Mr. Al Schoen Chief Technical Engineer Boeing Vertol Company	(85)
Dr. Andrew Lemnios Director, Research & Technology Kaman Aerospace Corporation	(85 thru 87)	Mr. Robert Taylor Manager, V-22 Technology Boeing Vertol Company	(84)
Mr. Andrew H. Logan Director, Research and Technology McDonnell-Douglas Helicopter Company	(85 thru 87)	Mr. Williams Walls Director of Technology Product Assurance and R & O Boeing Vertol	(82 and 83)
Mr. Raymond Prouty Chief, Stability & Control Hughes Helicopter, Inc.	(84)	Dr. E. Roberts Wood Manager of Aeromechanics Hughes Helicopters, Inc.	(83 and 85)

TABLE 5

Faculty Budget Advisory Committee

Rensselaer RTC

Dr. Robert G. Loewy

Institute Professor
Department of Mechanical Engineering,
Aeronautical Engineering and Mechanics

Dr. R. Judd Diefendorf

Professor
Department of Materials Engineering

Dr. Robert Duffy

Associate Professor
Department of Mechanical Engineering,
Aeronautical Engineering and Mechanics

Dr. Erhard Krempl

Chairman
Department of Mechanical Engineering,
Aeronautical Engineering and Mechanics

Dr. Robert Mayle

Associate Professor
Department of Mechanical Engineering,
Aeronautical Engineering and Mechanics

TABLE 6

Faculty Members Contributing to Rensselaer RTC Program

Name	Title	Academic Department	Research Specialty	Program Role	Years of Involvement
Bauchau, O.	Assistant Professor	ME, AE & M	Aeroelasticity	Senior Investigator	07/01/84-04/15/88 (1)
Bielawa, R.	Associate Professor	ME, AE & M	Aeroelasticity	Senior Investigator	07/01/85-04/15/88 (1)
Brower, W.	Associate Professor	ME, AE & M	Computational Fluid Mechanics	Supporting Investigator	07/01/85-04/15/86
Brunelle, E.	Associate Professor	ME, AE & M	Mechanics of Composites	Senior Investigator Supporting Investigator	07/01/82-09/01/84 (1) 07/01/86-04/15/86
Crespo de Silva, M.	Professor	ME, AE & M	Structural Dynamics	Supporting Investigator	07/01/86-04/15/88
Darlow, M.	Associate Professor	ME, AE & M	Structural Dynamics	Senior Investigator	07/01/83-04/15/88 (1)
Diefendorf, R.J.	Professor	Materials Engineering	Composite Materials	Senior Investigator	07/01/82-04/15/88 (1)(2)(3)
Duffy, R.	Associate Professor	ME, AE & M	Unsteady Aerodynamics	Senior Investigator	07/01/82-04/15/88 (1)(2)
Goetshel, D.	Assistant Professor	ME, AE & M	Structures	Senior Investigator	07/01/82-07/01/85 (1)
Krempl, E.	Professor	ME, AE & M	Fatigue of Composites	Senior Investigator Supporting Investigator	07/01/82-07/01/85 (1) 07/01/85-04/15/88 (2)
Loewy, R.	Institute Professor	ME, AE & M	Aeroelasticity	Senior Investigator	07/01/82-04/15/88 (1)(2)(3)
Mayle, R.	Professor	ME, AE & M	Unsteady Aerodynamics	Senior Investigator	07/01/82-04/15/88 (1)(2)
Nagamatsu, H.	Professor	ME, AE & M	Transonic Aerodynamics	Senior Investigator	07/01/82-04/15/88 (1)
Scarton, H.	Associate Professor	ME, AE & M	Structural Dynamics	Supporting Investigator	07/01/82-04/15/88
Shepherd, M.	Professor	Civil Engineering	Finite Element Methods	Senior Investigator	07/01/82-04/15/88 (1)
Winckler, S.	Assistant Professor	ME, AE & M	Mechanics of Composites	Supporting Investigator	07/01/86-04/15/88

(1) With funding from the ARO contract (2) Member of Budget Advisory Committee (3) Co-Principal Investigator

4. Educational Components

4.a. Distinguished Fellowship Program

(Responsible Faculty: R. J. Diefendorf)

As part of the Center's efforts to attract promising young people to the study of rotorcraft technology at the graduate level, posters with self-addressed, postage-paid, tear-off return cards were designed, printed and mailed to 179 colleges and universities in the United States and Canada. New posters were sent in each of the years 83, 84, 85, and 86. In the first two years, the return reply card asked if the respondent would be interested in attending a rotorcraft seminar at RPI. Of the 68 replies in 1983/4, 41 expressed interest in an introductory seminar. Accordingly, on August 23 and 24, 1982, such a seminar was held on the campus with speakers representing 4 companies and 4 government agencies. The meeting agenda is given in Appendix B. Attendees at this seminar numbered 46, including 9 young people from beyond the RPI campus. Subsequent year's reply cards showed that it was impossible to schedule introductory seminars satisfactorily because of varying school calendars, and so no follow-up meetings of this kind were held, even though interest was higher, as a result of the program's growing visibility.

The benefits of being chosen an ARO Distinguished Fellow include a stipend of $12,000 for eleven months keyed to the Consumer Price Index (C.P.I.) as published in the Economic Report to the President. Stipends actually disbursed under this program are shown in Table 7. In addition, all academic year tuition is paid by the fellowship. An unspecified travel allowance is also provided, usually as necessary to provide one trip to a national meeting per year. This is customarily the American Helicopter Society Annual Forum, but may be another meeting, as mutually agreeable to the particular ARO Fellow and Program Director. A computer allowance of $1500/year, in addition to those which Rensselaer makes available to all students for specific courses is also provided. And finally, office space contiguous or shared with other ARO Distinguished Fellows is offered, at the student's option.

Selection among candidates for ARO distinguished fellowships is based on the following criteria: (1) U.S. citizenship (a stated ARO requirement); (2) outstanding academic record, including the emminence of the institution at which it was attained; (3) a credible statement, in writing, of strong interest in rotorcraft technology; (4) some industrial experience (eg summer employment) was seen as highly desirable if not mandatory; (5) a commitment to participate as fully as possible in the program of the RRTC. Dossiers of candidates are considered by the Budget Advisory Committee (See Section 3 of this report). Those candidates this committee recommends for ARO Distinguished Fellowships are then reviewed by the Institute-wide "Topper" Committee. The "Topper" Committee consists of faculty chosen from among the Institute's five schools (i.e. colleges) and is charged by the Dean of the Graduate School with deciding which graduate students are so outstanding as to merit additional (i.e. "Topper") monetary support from the Institute. Their function in the case of the ARO Distinguished Fellowships is to insure that these highly desirable fellowships are being awarded to students whose credentials are consistent with the highest standards being

met in Rensselaer's graduate program.

That these difficult criteria were and are being met is best evidenced by the credentials and status of those students awarded RRTC ARO Distinguished Fellowships from program inception to the contract end date. This is summarized in Table 8.

4.b. New Course Offerings and Revisions
(Responsible Faculty: R. Duffy)

A number of existing courses were revised and new course offerings formulated and entered into the curricula of the Institute as a direct or indirect result of the establishment of the RRTC. There were seven such existing courses at the program's inception and seven new courses offered during the period covered by this report. These courses are listed in Table 9. As a result of these offerings and the ARO Distinguished Fellowship program graduate enrollments with rotorcraft technology grew as shown in Fig. 5.

4.c. Graduate Level Thesis Research

Although Rensselaer has a Master's Degree option which does not require a dissertation, a large majority of all masters recipients, and - of course - all doctoral level candidates, submit a thesis reporting the results of original research, as a part of their degree requirements. A list of graduate students involved in RRTC program research, their faculty advisor, research topic(s), and whether they received ARO contract funding support is given in Table 10. Results produced by such thesis research are, of course, incorporated in dissertations, titles for which are given in Appendix C, listed by degree year.

4.d. Intramural Exchange

Any multifaceted program which hopes to enhance synergism among its varied projects will set up as many avenues of interchange among its faculty, staff and students as possible. Such will, of course, enhance research performance as is reported in Section 5, of this report. In many ways, however, the process is an important element of the students' education, all too often under-emphasized. One such activity of the RRTC, instituted at the program's inception, has been highly successful from both research interchange aspects and as an educational tool. It is reported briefly here for the latter reason. The mechanism is known as the "BBL", short for "Brown Bag Lunch".

Once a week during the academic year, all faculty and graduate students are invited to join in (bringing and) having lunch in a conference room at which informal presentations and discussions are held over the lunch hour. Subjects for these meetings are fourfold, of which two or three kinds are generally present in a single meeting: (1) brief "administrative" announcements (i.e. untechnical subjects of

general RRTC interest); (2) reports of plans, problems, approaches to solutions, and progress on individual research projects; (3) general discussion of a single, relatively broad RRTC technical issue, the subject of which has been previously announced; and (4) a summary of matters of interest which arose in the course of a national or international level professional conference, off campus, which the presenter was able to attend.

A summary of BBL agenda's over the period covered by this report are given in Appendix D. It is important to note that the technical progress reports are listed by faculty name only to indicate who is responsible. The vast majority of these reports are given by the student(s) involved in that research. Students also join in the general discussions, of course, and make some of the "administrative reports" and professional meeting reviews.

The instructional aspects of these BBL's have been found to be substantial and significant. They include experience in making presentations; becoming accustomed to revealing difficulties and plans as well as results; "thinking on your feet" and responding "off the cuff" to questions and suggestions which can be challenging; receiving critiques and suggestions on style and preparation from your mentor (in private and often reflecting the reactions of other faculty and, occasionally, other students), engaging in technical discussions "from the floor"; and generally learning the benefits and pitfalls of interchange meetings and discussions. The reaction of visitors (who attend when appropriate), of faculty participants and of the students themselves, all indicate that this is an activity well worth the time and effort.

Fig. 5
Graduate Students Active In Rotorcraft Technology Research
Rensselaer Rotorcraft Technology Center

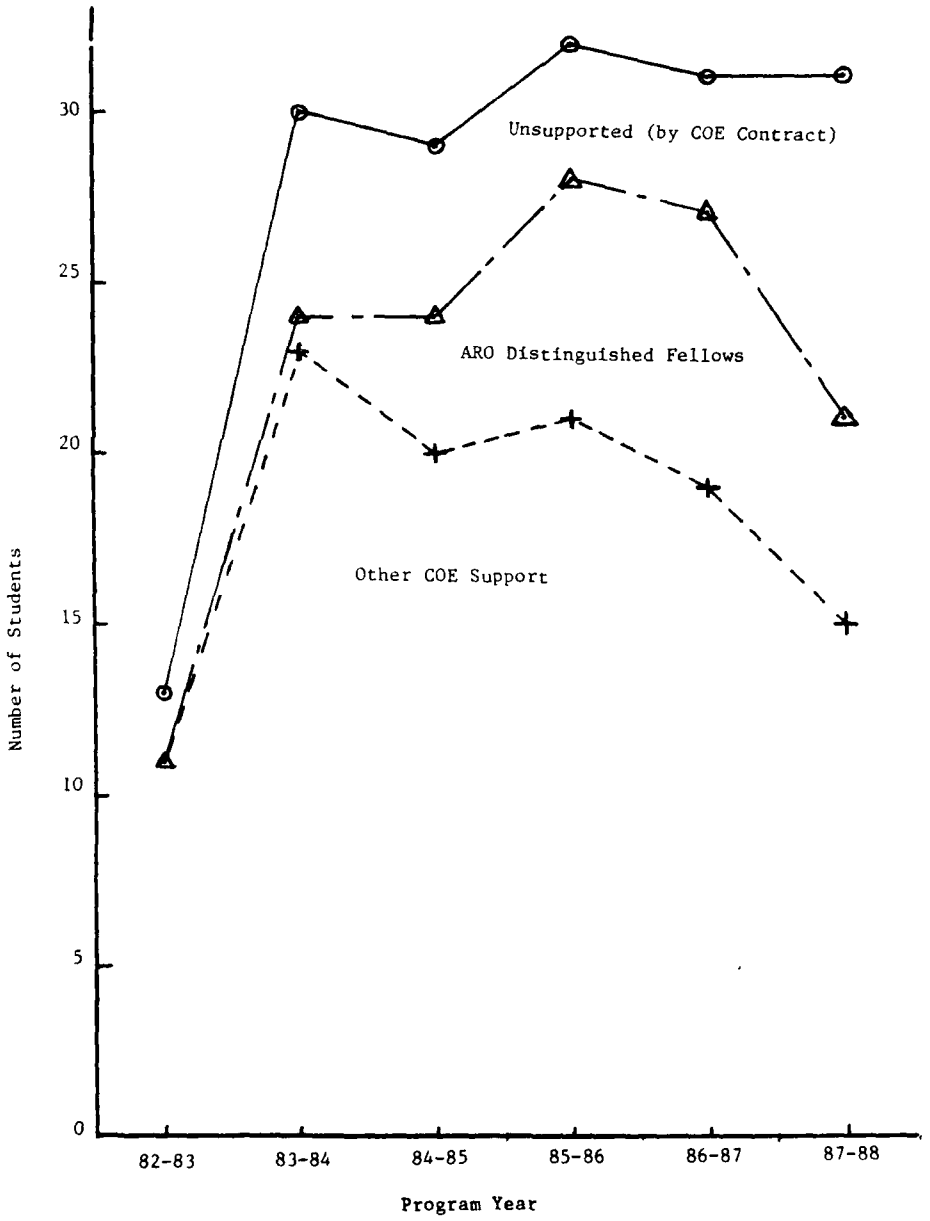

TABLE 7

Rensselaer RTC ARO Distinguished Fellowship Stipends by Year

Year	82-83	83-84	84-85	85-86	86-87	87-88
Change in CPI* (%)	base year	3.2	4.3	3.6	1.9	3.7
Stipend (Eleven Months)	12,000	12,300	12,800	13,310	13,560	14,060

*Between 2 previous years (from Economic Report of the President)

TABLE 8

Summary of Rensselaer's RTC ARO Distinguished Research Fellows' Credentials and Status

Name	Undergraduate or Graduate University	Entering Grade Point Average (out of 4.0)	Employment Experience	Date Entered Program	Status
Winckler, S.	Rensselaer Rensselaer	(B.S. Magna Cum Laude) 3.7 (Graduate)	Exxon Enterprises	January 1984	Ph.D. Received September 1986
Garing, S.	Princeton	4.0 (Undergraduate)	Sikorsky	September 1984	M.S. Received May 1985
Arcaro, D.	New Mexico	3.87 (Undergraduate)	Bell Labs Hewlett Packard	September 1984	M.S. Received May 1985
Martin, R.	Clarkson	3.7 (Graduate)	Teaching Ass't at Clarkson Tutor - St. Lawrence (Special Services)	July 1985	M.S. Received August 1987
Halvorsen, R.	University of Wisconsin	3.465 (Undergraduate)	Martin Marietta Aircraft Engineering & Modification Services	September 1985	M.S. Received December 1986
Jaran, C.	Rensselaer Rensselaer	3.5 (Graduate)	Mitre Corporation Fairchild	September 1985	Ph.D. Completed Degree Held Pending Thesis Submittal

TABLE 8 (Cont'd.)

Name	Undergraduate or Graduate University	Entering Grade Point Average (out of 4.0)	Employment Experience	Date Entered Program	Status
Kraus, R.	Gannon (Undergraduate) Rensselaer (Graduate)	3.78 (Graduate)	General Electric (Schenectady)	September 1985	Ph.D. Expected June 1988
Straus, J.	I.I.T	3.71 (Undergraduate)	U.S.A.F. - W.P.A.F.B. (Engineering Assistant)	September 1985	M.S. Received December 1986 Ph.D. in Progress
Milliken, R.	Univeristy of Maine George Washington University (J.I.A.P.S.)	3.87 (Undergraduate) (B.S. with Highest Distinction) 4.0 (Graduate)	Mt. Washington Cog Railway: Locomotive Engineer	September 1986	Ph.D. Expected August 1988
Nyberg, G.	Rensselaer	3.75 (Undergraduate)	RPI - Research Ass't	January* 1987	M.S. Received August 1987
Trilling, T.	Rensselaer	3.7 (Undergraduate)	RPI - Research Ass't	July* 1987	M.S. Received May 1988
Zotto, M.	Rensselaer	3.6 (Undergraduate)	Big V Corporation (Florida) - Manager	July 1987	M.S. in Progress

* Appointments delayed due to funding uncertainties

TABLE 9

Courses Specialized To Rotorcraft Technology

New Course No.*	Title & Catalogue Description	Semester First Offered**
37.486	Introduction to Helicopter Design Aerodynamics and dynamics of lifting rotors. Design concepts by which rotor weight and stress are minimized and vehicle control is provided. Weight and engine power trends for configuration definition. Center of gravity and aerodynamic lift and moment for equilibrium and desired aircraft attitude. Methods for determining size, weight and cost for a given payload, useful volume, and specified performance. Spring term annually. 3 credit hours.	S 78
37.606	Rotorcraft Performance & Stability Topics in flight dynamics generic to rotorcraft. Lift and propulsion systems, hovering, forward flight. Longitudinal and lateral trim. Dynamic stability. Prerequisite: 37421. Spring term annually. 3 credit hours.	S 84
37.607	Aerodynamics of Rotors Momentum, Blade Element, Vortex and Cascade Theories. Nonuniform inflow, rigid and non-rigid wakes; rotating and fixed system interactions; steady and nonsteady flow. Axial flow (rotor ascent and descent, propeller forward flight), cross flow (rotor forward flight, propeller yaw) flight conditions. Prerequisites: 37240, 37481 or equivalent. Fall term annually. 3 credit hours.	F 83

* Refers to Rensselaer Graduate Catalogue 87-88.
** S refers to Spring, F to Fall

New Course No.*	Title & Catalogue Description	First Offered
37.608	Rotorcraft Vibration and Acoustics Basic vibration and acoustical theory tailored to helicopters. Spring-mass-dashpot systems; blade models; Lagrange's equations; normal modes; system response; resonance; rotating imbalance; absorbers; isolaters, active feedback. Wave equation solutions; transmission through boundaries; monopole, dipole, quadropole sources; rotor, engine, gearbox noise; source, path receiver noise control; aerodynamic generation of sound. Prerequisite; permission of instructor. Offered on sufficient demand. 3 credit hours.	S 84
37.613	Dynamics of Rotating Machinery Analytical basis of design for rotating machinery mounted on various types of bearing supports, as exemplified by turboshaft engines, centrifugal or axial flow compressors, vehicle drive trains, etc. Description of analytical and numerical tools for evaluation of dynamic stability, critical speeds, and unbalance response of rotor-bearing systems. Special problems encountered in modern applications operating through and above the critical speeds, and means of their solution, including rigid and flexible rotor balancing and support damper design. Several informal laboratory sessions are included to enhance visualization of rotordynamic phenomena. Seniors and graduate students only. Prerequisite: 37417. Annually. 3 credit hours.	S 85
37.616	Advanced Design with Composites Advanced topics in structural design with continuous fiber advanced composites. Development of plate equations including interlaminar stresses. Introduction to and use of constrained numerical optimization program. Statistical effects on failure. Saint Venant's principle for anisotropic materials. Failure criteria, including stress concentration effects. Plate and shell buckling. A detailed student design project is assigned. Prerequisites: 37413, 37610 or permission of instructor. Spring term annually. 3 credit hours.	S 83

New Course No.*	Title & Catalogue Description	First Offered
37.686	Rotary Wing Structural Dynamics I: Vibrations Dynamics of flexible rotating beams, gyroscopic motion, drive system dynamics. Analysis of fuselage vibrations, with emphasis on rotor-fuselage coupling and design for minimum vibration; vibration test procedures. Prerequisite: 37461. Fall term annually. 3 credit hours.	S 85***
37.687	Rotary Wing Structural Dynamics II: Aeroelastic Stability Continuation of 37686 with emphasis on aero-mechanical and aeroelastic stability of rotors and rotor-pylon systems; stability of linear multi-degree-of-freedom systems, Floquet theory, ground and air resonance, unsteady aerodynamics, stall flutter, test procedures. Prerequisites: 37686, 37481, and 37430. Spring term annually.	S 85***
37.696	Radio Controlled Helicopter Project This course attempts to give a small group of students hands-on experience with an unmanned radio-controlled helicopter of considerable realism and scale. (Rotor Diameter = 11 ft; Engine Power = 12 HP) Theory and laboratory instruction are put to use so as to consolidate skills already acquired and to motivate the student to learn new skills. Experience is provided in setting engineering goals, milestones and schedules. Insight is imparted into the workings of a typical industry-type organization, by setting-up the project and conducting it much as it would be in professional practice. Grades assigned based on contributions to planning and conducting group operations, work accomplished with hardware and analysis, memos and reports. Prerequisites: Permission of the instructor. Offered on sufficient demand. 3 credit hours.	S 80

*** Originally offered as a one-semester course; changed to a two-semester sequence in F 85.

TABLE 10

Student Involvement in Rensselaer RTC Research

Student	Faculty Advisor	For Program Year Beginning In						Research Area
		82	83	84	85	86	87	
S. Amos	M. Darlow			X				Optimizing Composite Drive Shafts
D. An	E. Krempl				X			Fatigue and Failure of Composite Materials
S. Anderson	D. Goetschel		X*					Optimizing Mechanical Connections in Composite Drive Shafts
F. Arabia	R. Mayle	X*	X*					Blade Tip Vortex Interaction
D. Arcaro	F. Ling			X**	X**			Curing Techniques for Thick Cylinders made of Polyimide Resin Composites
D. Avidar	M. Darlow				X*	X*		Optimizing Composite Drive Shafts
D. Barnard	H. Nagamatsu		X*	X*				Passive Reduction of Rotor Airfoil Wave Drag
W. Bayles	M. Shephard		X***	X***				Structural Dynamic Analysis of Helicopter Airframes
R. Benson	D. Goetschel		X*	Y*				Mechanical Connections in Composite Shafts
R. Bergman	R. Mayle		X*	X*	X*			Blade Tip Vortex Interaction
M. Berube	H. Nagamatsu		X*					Passive Reduction of Rotor Airfoil Wave Drag
T. Bidlack	H. Nagamatsu	X*	X*	X*	X*	X		Passive Reduction of Rotor Airfoil Wave Drag
C. Bonner	R. Loewy						X*	Use of Generalized Coordinates in Composite Blade Analysis
J. Bossard	H. Nagamatsu				X*			Passive Reduction of Rotor Airfoil Wave Drag

* With support under the subject contract

**ARO Distinguished Fellow

*** Officer on Active Duty, U.S. Army

Student	Faculty Advisor	For Program Year Beginning In						Research Area
		82	83	84	85	86	87	
P. Bryan	O. Bauchau					X*		Damage Tolerance of Composite Drive Shafts
Y. Chang	M. Shephard			X*	X*	X*		Structural Dynamic Analysis of Helicopter Airframes
	M. Shephard					X*	X*	Combined FEM-Transfer Matrix Analysis of Helicopter Fuselage
Y. Cho	M. Crespo da Silva						X	Nonlinear Rotor Blade Dynamics
J. Colasante	R. Duffy				X*	X*		Aerodynamic and Structural Considerations of Snap-Through Airfoils
W. Conley	M. Darlow					X*	X*	Optimizing Composite Drive Shafts
E. Czajkowski	R. Duffy	X*	X*					F.E. Approx. to Theodorsen's Solution of Oscillating Airfoils
E. Degen	M. Shephard	X*	X*	X*	X			Structural Dynamic Analysis of Helicopter Airframes
D. Deyo	R. Bielawa					X*	X	Design and Fabrication of an Air Resonance Model
H. Dondes	R. Duffy					X		Aero Response to Snap-Through Airfoils: Theory and Experiments
J. Dubben	R. Duffy					X	X*	Torsion Response of Blades Equipped with Snap-Through Airfoil Panels
D. Elzey	E. Krempl		X					Fatigue and Failure in Composite Materials
N. Fortier	H. Nagamatsu				X***			Passive Reduction of Rotor Airfoil Wave Drag
K. Furnes	D. Goetschel	X*	X*					Optimizing Mechanical Connections in Composite Drive Shafts
S. Garing	R. Bielawa			X**				Rotor Impedance Test Rig Design
J. Gordis	R. Bielawa				X*	X*	X*	Shake Test Facility Development for Full-Scale Fuselage Components
B. Gregory	M. Shephard			X*	X*			Structural Dynamic Analysis of Helicopter Airframes

* With support under the subject contract

**ARO Distinguished Fellow

*** Officer on Active Duty, U.S. Army

Student	Faculty Advisor	For Program Year Beginning In						Research Area
		82	83	84	85	86	87	
R. Halvorson	O. Bauchau				X**	X**		FEM Analysis of Rotor Blade Aeroelasticity
J. Hayes	O. Bauchau				X*			Ballistic Damage Tolerance
R. Hefner	R. Bielawa						X	Shake Test Facility Development for Full-Scale Fuselage Components
S. Hill	S. Winckler						X	Hygrothermal Effects on Composite Coupling Characteristics
B. Hong	E. Krempl			X*	X*	X*		Fatigue and Failure in Composite Materials
C. Hong	O. Bauchau			X*	X*	X*	X*	FEM Analysis of Rotor Blade Aeroelasticity
K. Hsueh	R. Bielawa			X*	X*	X*	X*	Rotor Impedance Test Rig Design
G. Hu	D. Goetschel	X	X					Shear Lag in Lightly Loaded Structures
	D. Goetschel		X*	X*				Mechanical Connections in Composite Shafts
T. Hughes	R. Bielawa						X	Vibration Isolation for Radio Controlled Helicopter Model
C. Jaran	R. Duffy		X	X*	X**	X**		F.E. Approximation for 2 & 3-D Rotor Unstady Aerodynamics
	R. Duffy				X**			Aerodynamic and Structural Considerations of Snap Through Airfoils
M. Jenks	R. Duffy	X*						Position of Trailing Vortices in Closed Rectangular Tunnels
B. Jetmundsen	R. Bielawa				X*	X*		Generalized Airframe Analysis/Testing Methodology
B. Johnston	M. Shephard	X*	X*	X*				Helicopter Airframe Design Program
	M. Shephard			X*				Helicopter Airframe Structure Preprocessor
P. Jones	M. Darlow						X*	Optimizing Composite Drive Shafts
D. Kim	W. Brower						X	CFM Transonic Drag Studies
H. Kim	M. Crespo da Silva						X	Nonlinear Rotor Blade Dynamics

* With support under the subject contract

**ARO Distinguished Fellow

*** Officer on Active Duty, U.S. Army

Student	Faculty Advisor	For Program Year Beginning In						Research Area
		82	83	84	85	86	87	
M. Kolotylo	R. Duffy		X	X*				F.E. Approx. to Theodorsen's Solution of Oscillating Airfoils Aerodynamics and Structural Considerations of Snap-Through Airfoil
T. Krafchak	O. Bauchau			X*				Ballistic Damage Tolerance
R. Kraus	M. Darlow			X**	X**	X**	X**	Optimizing Composite Drive Shafts
J. Lim	M. Darlow		X*	X*				Optimizing Composite Drive Shafts
S. Liu	O. Bauchau						X	FEM Analysis of Rotor Blade Aeroelasticity
R. Martin	R. Bielawa				X**	X**	X**	Rotor Impedance Test Rig Design
M. Mathew	R. Loewy		X*	X*	X*	X*	X*	Nonlinear Rotor Dynamics, Natural Frequencies and Forced Response
T. Mavromatis	R. Loewy	X*	X*					Rotor Dynamics for Small Motions of a Flexible Blade; Natural Frequencies and Forced Response
R. Milliken	R. Duffy					X**	X**	Aero Response to Snap-Through Airfoils: Theory and Experiments
T. Mitty	H. Nagamatsu				X*	X*	X*	Passive Reduction of Rotor Airfoil Wave Drag
M. Murdock	H. Nagamatsu		X*					Passive Reduction of Rotor Airfoil Wave Drag
T. Naki	S. Winckler						X	Using Thermal Deformations in Composite Structures
J. Nickerson	R. Duffy				X*	X*		Aerodynamic and Structural Considerations of Snap-Through Airfoils
M. Niederer	D. Goetschel	X	X X					Elastic Swashplate "Scissor" Optimizing Mechanical Connections in Composite Drive Shafts
G. Nyberg	H. Nagamatsu				X*	X**	X**	Passive Reduction of Rotor Airfoil Wave Drag
M. O'Connor	R. Duffy					X*	X*	Aero Response to Snap-Through Airfoils: Theory and Experiments
A. Peck	O. Bauchau						X*	Damage Tolerance of Composite Drive Shafts

* With support under the subject contract

**ARO Distinguished Fellow

*** Officer on Active Duty, U.S. Army

Student	Faculty Advisor	For Program Year Beginning In						Research Area
		82	83	84	85	86	87	
J. Planchak	R. Duffy		X***	X***				Development of Rotor Wake Modelling
D. Radford	J.D. Diefendorf		X*	X*	X*	X*		Application of Advanced Composites to Rotorcraft Structures
P. Renzoni	R. Mayle			X*	X*	X*	X*	Blade Tip Vortex Interaction: Experiments and Correlative Theory
C. Rumsey	R. Duffy	X*	X*					Influence of the Near Wake on Steady Non-Steady Aeronautical Rotors
P. Singh	R. Bielawa			X				Rotor Impedance Test Rig Design
R. Smith	R. Loewy	X*	X*					Use of Nonrotating Modes to Predict Rotation; Natural Frequencies and Forced Response
J. Straus	R. Mayle				X**	X**	X**	Blade Tip Vortex Interaction Experiments and Correlative Theory
M. Sütcü	E. Krempl			X	X			*Fatigue and Failure in Composite Materials*
J. Terng	R. Bielawa					X*	X	Rotor Impedance Test Rig Design
N. Theron	O. Bauchau						X	FEM Analysis of Rotor Blade Aeroelasticity
R. Thieren	H. Nagamatsu		X*					Passive Reduction of Rotor Airfoil Wave Drag
M. Tomlin	R. Duffy		X*	X*				F.E. Approx. to Theodorsen's Solution of Oscillating Airfoils Aerodynamics and Structural Considerations of Snap-Through Airfoil
T. Trilling	H. Nagamatsu				X*	X	X**	Passive Reduction of Rotor Airfoil Wave Drag
N. VanDresar	R. Mayle	X*						Blade Tip Vortex Interaction
P. Vaney	D. Goetschel		X*					Optimizing Mechanical Connections in Composite Drive Shafts
E. White	H. Nagamatsu		X*					Passive Reduction of Rotor Airfoil Wave Drag
S. Winckler	R.J. Diefendorf		X**	X**	X**	X**		Application of Advanced Composites to Rotorcraft Structures
M. Zotto	R. Loewy				X*	X*	X*	Ground and Air Resonance with Shaft Flexibility and Control Feedback

* With support under the subject contract

**ARO Distinguished Fellow

*** Officer on Active Duty, U.S. Army

5. Research Components

5.a. Materials & Structures: Hygrothermal Stability

5.a.(1). Asymmetric Composites: Hygrothermal Stability

(Sr. Investigators: R. J. Diefendorf & S. J. Winckler)

Asymmetric laminates are a sub-class of composite laminates that provide designers with a unique set of properties. Whether they be cross-ply or angle-ply, asymmetric laminated plates yield an out-of-plane deflection to an in-plane stress as illustrated in Fig. 6. In most of these asymmetric laminates, both mechanical and hygrothermal in-plane stresses lead to out-of-plane deflections. Hence, laminates which are designed to twist or bend due to an in-plane load will, in general, react to changes in temperature or humidity. This combined response to mechanical and hygrothermal stresses has been a practical barrier to the use of these laminates in situations calling for aeroelastic tailoring.

One goal of the portion of this project dealing with flat plates was to determine the long-term stability of out-of-plane deflections in classical asymmetric laminates when they are hygrothermally cycled. The results were intended to provide a greater appreciation for the types of problems that are encountered in designs utilizing hygrothermally activated shape changes due to laminate asymmetry. Secondly, a group of asymmetric laminates denoted as HygroThermally Curvature stable Coupling (HTCC) laminates were identified. These asymmetric laminates were found to retain mechanical coupling, but to be free of out-of-plane reactions to steady state environmental variations.

The second portion of this project deals with composite laminates of more complex geometries. While HTCC flat plates are of basic interest, the concept of HTCC tubes seemed to hold even more promise in terms of structural design. Thus, HTCC tubes were investigated, using both theoretical and experimental techniques. Finally, it was noted that open, unconstrained shells, in general, warp during fabrication even when symmetric stacking sequences are used. This warpage makes control of part tolerance extremely difficult, and tooling design often becomes an iterative process. Asymmetric laminates were seen as a potential solution to this problem and as a result, research was undertaken into means by which part warpage could be eliminated.

The coupling between in-plane stresses and out-of-plane deflections encountered with asymmetric laminates, and shown as matrix elements B in Fig. 6 can be predicted using laminated plate theory [Ref. 5]. Laminated plate theory allows the calculation of the overall properties of the bulk laminate from properties of the constituent materials or of the individual laminae. Asymmetric laminates have unsymmetric stacking sequences with respect to the mid-plane and most react to both mechanical and hygrothermal stresses. Such asymmetries may be planned or unplanned, with the unplanned cases including inaccurate layup and non-uniform cure.

A variety of researchers have studied asymmetric laminates. Usually the research deals with either attempting to accurately predict the deformed shapes of these laminates [Refs. 6 & 7] or with using the deformed shape as an indication of the internal residual stress state of the composite.

Asymmetric cross-ply laminates, which produce a tension-bending couple, are often used as a basis for obtaining certain desired deformed shapes. Laminate theory predicts that, as a result of a temperature change or an applied load, the deformed shape of such a laminate will be anticlastic (saddle shaped). In practice, the resulting shape is often observed to be almost cylindrical, rather than having the predicted anticlastic curvature. The key to this unpredicted behavior is that the transverse deflections are not small compared to the laminate thickness, as is assumed in laminated plate theory. As might be expected, the difference between the observed deformed shapes and those resulting from these predictions is not negligible and must be considered in the design of a component. For many engineering applications, including helicopter rotor blades, a tension-twisting coupled laminate often is desirable. An asymmetric angle-ply form which only shows the tension-torsion couple would be an applicable laminate, but again, classical laminate theory is inadequate for predicting the out-of-plane deflections.

To actually apply asymmetric laminates, two basic problems must be overcome: first, inconsistencies in the amount of mechanical coupling obtained -- and second, elimination or exploitation of the corresponding couple produced by temperature and moisture variations. Of these, the second has greater importance. To be operationally useful, an asymmetric laminate must realize the same shape change, for a given mechanical or non-mechanical input, on each cycle throughout the design life of the component. Few authors [Ref. 7] have addressed this combined problem of cyclic temperature change and moisture uptake in asymmetric composite laminates. Our laminated plate research was, therefore, undertaken primarily to investigate hygrothermal stability.

5.a.(1).(a). Flat Plates

Material conditioning, combining elements of both temperature and moisture, was initially investigated to assess its overall effect on the shape reproducibility of asymmetric laminates. By using total water immersion and temperature cycling, the process of moisture uptake and the resulting hygrothermal fatigue was accelerated. Such extremes of temperature and humidity are not unrealistic and tend to establish a worst case. Drying rates are of concern, however, since it is well documented that fast drying induces damage.

Sample strips of thin asymmetric carbon fiber/epoxy cross-ply laminates [[0/90] and $[0_2/90_2]$] were fabricated from Fiberite HY-E 3048A1 prepreg tape. These asymmetric laminates took on a cylindrical curvature at room temperature due to the asymmetric stacking sequence, the elevated temperature (121°C) necessary for cure, and the sample geometry. Once weighed and measured, the laminates were immersed in water and then thermally cycled from room temperature to boiling. During this

temperature cycle the curvature of the strips changed from its room temperature value and sign, to a zero curvature state, and then to a reverse curvature state. The temperature at which the laminate has zero curvature is denoted the Zero Curvature Temperature (ZCT). Fatigue is simultaneously induced by thermal cycling, moisture absorption and desorption, and mechanical shape change.

As expected, the ZCT decreases during the period of transient moisture content (from ~90 to ~55-60°C), leveling off as the samples become saturated (~2.5wt% H_2O). This moisture uptake corresponds to a typical diffusion controlled process with a saturation time of approximately 50 cycles, or 150 hours for these thin laminates. The uptake leads to lower values of curvature at room temperature due to the moisture induced swelling of the epoxy matrix material. Upon removal from the water bath, the room temperature curvature recovers during drying. Unexpectedly, this recovery does not stop at, or before, the as-cured curvature, but continues, to yield almost double the initial pre-immersion value. Similar results were repeated by simply immersing samples in elevated temperature water baths until they were saturated, and then drying at room temperature. This result is unexpected, since published work [Ref. 7] reports decreased curvature associated with any form of degradation of such asymmetric laminates. In fact, trying to predict this increased curvature using ony laminate theory would lead to the conclusion that either the transverse modulus increases dramatically or that there has been a decrease in the fiber controlled, longitudinal modulus. These conclusions stem from the relationship between increased values of the modulus ratio (E_1/E_2) and the decreased values of curvature (k), as shown in Fig. 7.

Cycled and redried samples were retested to investigate the effect of dry-wet cycling. The value of the ZCT on the first repeat cycle was approximately 5°C higher than the initial run, but quickly decayed (~5 cycles or 15 hours) to a temperature comparable to the initial run data. Upon redrying, these retested samples returned to the same curvature as at the start of the retest. However, the saturation moisture content was approximately 50% greater than that of the corresponding as-cured case. Hence, some process is permanently affecting the laminate and yielding a new, more stable curvature.

The effect of temperature was evaluated by a long-term immersion test in room temperature water(~25C). After several months, these samples had not reached saturation due to the low thermal driving force. Upon redrying, these samples showed the same curvature as they had at pre-immersion. We conclude that elevated temperature in combination with moisture causes the increased curvature.

Creep in the matrix of the transverse plies could be a source of permanent shape change, but creep in this orientation would lead to a flattening of the samples. Creep could occur within the longitudinal plies, however, allowing the fibers to, effectively, slide with respect to one another. To test this idea, flat, uni-directional samples were prepared and immersed while bent under stress, in four-point static bending jigs. If such a uni-directional sample remained bent after saturation and subsequent redrying, then creep must be occurring.

Samples were immersed in three separate water baths, at different temperatures. Room temperature was used first, since no increased curvature had been noted in the previous room temperature tests. Next 60°C was used to match the ZCT for the saturated samples. The final temperature used was 80°C which is near the glass transition temperature (T_g) for the matrix. The samples showed a dry T_g of ~110°C, which is above the test temperatures, but moisture acts as a plasticizer for these epoxy systems, lowering the effective T_g. The samples were immersed for about 5 months to allow time for the creep process to take place and to allow the room temperature samples to approach saturation. After slow cooling - to minimize micro-mechanical damage - and redrying, only the sample immersed at 80°C showed substantial irreversible deformation. This uni-directional sample showed that inter-fiber creep in the longitudinal direction is occurring, and that the T_g is being substantially lowered during saturation.

This evidence as to the existence of inter-fiber creep, which allows fibers to shear past one another, leads to the following proposed mechanism for substantial curvature increases associated with conditioning and redrying of asymmetric cross-ply laminates:

When dry, the T_g and ZCT are ~110°C, which is higher than the 100°C test temperature, thus precluding creep. In the presence of moisture, the T_g drops below the test temperature, having two effects on the asymmetric sample. Since the thermal response is faster than the moisture pickup, which occurs faster than the subsequent creep, the sample changes shape as these various phenomena take place. When at 100C and dry, the sample shows a lesser curvature, having the same sign as that at room temperature. As the absorption of moisture plasticizes the matrix, the T_g drops, resulting in a test temperature above the effective T_g. Also, moisture absorption swells the matrix which leads to a new curvature of opposite sign to the room temperature value. Continued moisture uptake and subsequent swelling of the matrix only increases this negative curvature. Since the test temperature is above the T_g, creep also occurs. Creep always has the effect of reducing the internal stresses, and in this case the result is a flattening of the sample leading, in the limit, to a sample with zero curvature. Due to creep, the negative curvature of a saturated sample disappears and the stress-free temperature will shift from the plasticized T_g (~80°C) to the test temperature (100°C). This shift leads to a larger temperature difference between the stress free temperature and room temperature, which in turn leads to a greater room temperature dry curvature and higher ZCT.

This is presented in another way in Fig. 8, in which the effect of temperature dwell on laminate stability is being shown schematically. The area under the curve represents the time/temperature domain in which the sample is shape stable. If we move outside the right boundary of the domain, we exceed the T_g and creep begins to occur. The time dependence of creep is also shown by the short periods of time the laminate may be considered stable at temperatures in excess of the glass transition. Creep is shown to occur at temperatures below the glass transition by the dip in the top of the curve. the reason for the rise again pecisely at T_g is that this temperature corresponds to the ZCT, or the temperature at which the laminate is flat. Since creep must work to decrease the internal stresses, and the laminate is already

flat at this temperature, the sample should thus be stable. Combining this effect with the effect of temperature as a driving force for creep, we can now see why the minimum in the dip below T_g is displaced to the left. This displacement of the dip is due to a balance between high temperatures and large deviations from the ZCT, favoring creep. Another interesting point regarding the instability denoted by this dip in the curve is that samples operated in this region would be predicted to show a resulting decrease in room temperature curvature, not the increase seen in all the experimental results.

Fig. 9 extends the time/temperature representation into the moisture domain. Once the above discussion of the time/temperature domain is understood, the addition of moisture readily follows. In this case the front face of the stable volume shows the same results as the dry case in the previous figure. However, as the moisture content increases, the effective glass transition drops, decreasing the size of the stable domain and "bending" the high temperature face of the stable volume.

These representations of the stable domain allow the designer to choose a material system to meet the requirements of a particular design. Since, data gathered using asymmetric laminates relate directly to the stability of symmetric laminates under conditions of external loading, the concept of a stable volume in time/temperature/moisture space is of much more general applicability than simply to the shape stability of unsymmetric laminates. Thus, the results available regarding flat asymmetric laminates are important in the prediction of shape changes in composite components and ultimately on designing useful, shape stable structures.

Most of the composites literature dealing with such subjects, states that an asymmetric laminate with mechanical coupling will also produce hygrothermal coupling. One of the goals of the current research program, however, was to show that, for steady state conditions, a subset of the classical coupled asymmetric laminates exists whose members do not show environmental coupling, but do retain mechanical coupling. These laminates have been termed Hygro Thermally Curvature stable Coupling (HTCC) laminates. When used as flat plates or symmetric, closed geometry tubes, these laminates yield hygrothermal shape stability that was previously only thought possible through the use of symmetrically stacked laminates. This behavior has been verified by laminated plate theory and gives the designer an option free of many of the problems discussed in the previous paragraphs.

Surprisingly, the solution for curvature stability is obtainable over a wide range of coupling coefficients and is independent of the thermal expansion and moisture swelling coeffiients of the individual lamina. It is useful to review the logic that led to the definition of HTCC laminates and to present a detailed description of this group of laminates.

Fig. 10 is a schematic in which the circled items are possible properties of a laminate, and the arrows are used to show that one property implies the other. (In the direction drawn only!) First, arrows (1) and (2) are drawn because a laminate having extension-torsion coupling, or temperature induced warpings must be unsymmetric. These two statements are essentially identical. Arrow (3) is shown broken

with a question mark. If arrow (3) is solid (always true) then bending-extension or torsion-extension coupling would always imply temperature induced warping, and it would be impossible to make a component with tension-torsion coupling that is also thermally curvature stable. Because the unsymmetric laminates studied in the literature are prone to warping, the inductive conclusion that all unsymmetric laminates warp, must have seemed reasonable. According to the literature on unsymmetric laminates, laminate asymmetry implies thermally induced warping and arrow (3) should always be solid, but in no case was formal proof attempted.

The general linear laminated plate equation, relating stress resultants (N_i) and moments (M_i) to in-plane strains (ϵ_j) and curvatures (K_j), given by Tsai and Hahn[5], is

$$\left| \begin{array}{c} N_i \\ \hline M_i \end{array} \right| = \left[\begin{array}{c|c} A_{ij} & B_{ij} \\ \hline B_{ij} & D_{ij} \end{array} \right] \left| \begin{array}{c} \epsilon_j \\ \hline K_j \end{array} \right| \qquad \text{a-1-(1)}$$

where A_{ij}, B_{ij} and D_{ij} are respectively the extensional, extension-bending, and flexural stiffness matrices from Fig. 6. The stress resultants and moments (N_i & M_i) are the forces and moments per unit length of the plate, acting along edges which are parallel as shown in Fig. 6. The B_{16} and B_{26} terms are what produce the tension-torsion couplig in the 1 and 2 directions respectively. For example, an in-plane tensile force in the 1 direction (N_1) will cause the plate to twist about the 1 axis (K_6) if the B_{16} term is non-zero. For a symmetric laminated plate the entire B_{ij} matrix is zero. Thus, to have a thermally curvature stable laminate with tension-torsion coupling, the coupling term (B_{16}) must be non-zero and the thermal plate curvatures (K_i^T) must be zero.

A partial solution is possible if a laminate satisfies the following three conditions: 1) laminate symmetry; 2) zero thermal shear strain; and 3) a non-zero tension-shear coupling (A_{16}). This laminate would have the property of undergoing a shear deformation due to an in-plane tension force but would not shear due to a change in temperature.

Once the above conditions are met, the total solution is obtained by combining two of these laminates back to back to produce the tension-torsion "B_{16}" coupling of the combination. This is illustrated in Fig. 11, where the upper and lower plates have positive and negative tension-shear strain coupling, respectively. After they are bonded, the tension-shear strain coupling of the total laminate is zero and the tension-torsion coupling becomes active.

This combination is thermally curvature stable because; 1) the upper and lower halves are each symmetric and in themselves thermally curvature stable, 2) the thermal shear strain is zero, so there is no thermal shear strain interaction between the two halves to cause a thermal twist and 3) the thermal expansion properties of the halves are the same, so that no thermal bending can occur.

With these three postulated conditions in mind, two facts about lamiated composite plates are now added. For in-plane thermal expansion isotropy, a minimum of two fiber directions are needed, balanced with equal angle spacing $[(0/90)_S]$. This implies that the thermal shear strain is zero even if the laminate is rotated by an arbitrary angle. Secondly, for in-plane mechanical isotropy a minimum of three directions are needed; balanced with equal angle spacing $[(0/60/120)_S]$.

The solution to the problem, therefore, is simply a $(0/90)_S$ laminate rotated by an angle θ (i.e. $(\theta/\theta+90)_S$). This laminate satisfies the three conditions because: 1) it is a symmetric laminate; 2) it is thermally isotropic, which gives zero thermal shear strain for all θ, and 3) it is not mechanically isotropic because only two fiber directions are used, which produces a non-zero tension-shear strain coupling (A_{16}) when the angle θ is not 0^o or 90^o.

The total solution for an HTCC Laminate is then obtained by combining two of these laminates back to back, which results in a hygrothermally curvature stable laminate. One group of HTCC laminates is

$$[\theta_n/(\theta+90)_{2n}/\theta_n/-\theta_n/(-\theta+90)_{2n}/-\theta_n]_{mT} \qquad \text{a-1-(2)}$$

$$n = 1,2,3... \qquad m = 1,2,3...$$

It should be noted that this solution is valid for all "θ", and is independent of the longitudinal and transverse thermal expansion coefficients of the individual layers.

In this research it has also been shown that the level of the tension-torsion coupling of the HTCC laminate is strong. The maximum value was shown to be only about 15% less than that of the corresponding classical asymmetric laminate $[(\theta_2/\theta_1)_T]$ which warps hygrothermally. These results have been reported in the literature [Ref. 8], and are now rather widely used [Ref. 9, for example]. It is noted, however, that non-uniform application of a hostile environment, as may occur when only one side of the laminate is exposed, will cause warping of HTCC composites. Even isotropic materials will yield an out-of-plane deflection in response to environmental gradients or to transient environmental effects. The hygrothermally curvature stable laminates will, in addition, show an out-of-plane deflection for the case of an environmental gradient which is symmetric about the laminate mid-plane. To add to the difficulty of dealing with non-steady state environmental effects, is noted that various components of the environment reach steady state conditions at different rates. Thus, while solutions to the shape instability problem may work well in steady state environments, additional complexities arise when dealing with transient environmental effects.

One final point needs to be clarified regardind HTCC laminates. Once the designer achieves an HygroThermally Curvature stable Coupling laminate that meets his "elastic tailoring" objectives, he is likely to attempt to modify that laminate to meet certain other structural requirements. Doing this by simply adding an equal group of plies (i.e. uni-directional) to each surface of the HTCC laminate will usually defeat the HTCC effect. To assure that a design remains HTCC, the laminate must be checked using classical laminate theory.

5.a.(1).(b). Cylinders and Tubes

Since many structural elements of interest are single cell and tubular in geometry, attention turned from the earlier investigations of hygrothermally curvature stable laminates (plates) with tension-torsion coupling to shape stability problems for cylinders & tubes. An objective was set for an "HTCC Tube"; namely to provide tension-torsion coupling (tension induced twist) with zero hygrothermally induced twist, as well as the kind of structural geometry needed to satisfy torsional and flexural stiffness requirements.

Review of the literature showed only one investigation of environmentally induced twist in balanced [i.e., $[90/0\pm45]_S$] thin walled tubes [Ref. 10]. The order of magnitude of the induced twist measured was, as expected for a tube with zero tension-torsion coupling, very small, roughly a 1/10 degree change in total twist for a typical helicopter rotor blade, even with 100°C change in temperature. This research produced a large discrepancy between measured and predicted values for induced twist, probably because the authors assumed that $M_x = M_y = 0$ rather than the more reasonable $K_x = K_y = 0$.

As a first approximation to our HTCC problem, we assumed that, for thin walled composite tubes, the overall elastic and environmental deformations are dominated by the in-plane properties of the wall. The effect of changes in wall curvature are therefore neglected in this development.

The twist rate of these tubes is controlled by the in-plane shear strain of the tube wall, whether mechanically or environmentally induced. The HTCC tube problem is thus reduced to finding laminates with zero hygrothermally induced shear strain and large tension-shear strain coupling. In other words, the solution must satisfy the same conditions as the reduced solution of the flat plate previously discussed. It follows that one HTCC thin walled tube solution is simply to provide a $(\theta,\theta+90^\circ)_T$ two layer wall structure. This will produce tubes with tension-torsion coupling when $\theta \neq 0^\circ$ or 90°, and still eliminate thermally induced twist. Other solutions with more than two layers can be obtained from:

$$(\theta_n/(\theta+90)_n)_{mT}$$

$$n = 1,2,3,\ldots \; ; \; m = 1,2,3,\ldots$$

For an even more general solution, in which each ply group may have a different orientation angle $(\theta_1,\theta_2,\theta_3,\ldots,\theta_n)$ we have

$$(\theta_1/(\theta_1+90)/\theta_2/(\theta_2+90)/\theta_3(\theta_3+90)/\ldots/\theta_n/(\theta_n+90))_T \qquad \text{a-1-(3)}$$

$$n = 1,2,3,\ldots$$

where $\theta_1, \theta_2, \theta_3, \ldots, \theta_n$ are the ply group (θ_i/θ_i+90^o) orientation angles of the i^{th} layer.

To maximize tension-torsion coupling and find the maximum values which establish for the designer bounds on such coupling for optimization purposes, only the HTCC Tube results were used. The procedure, however, can be used on any general layup.

If a designer decides to use the tension-torsion coupling available with an HTCC tube in a new rotor blade, a number of additional considerations enter its implementation. The design must meet constraints such as flap and lag bending, torsional and extensional stiffnesses; strength; and mass and mass distribution requirements. Thus, while a simple maximization of tension-torsion coupling results in a solution of $\theta = 22.5^o$ for the HTCC laminate and tube, this angle lay-up will not provide maximum coupling when stiffness constraints are imposed. Finding the conditions for constrained maxima was, therefore, the purpose of the investigations conducted next.

For a thin walled, single cell beam, an approximate relationship between twist rate (ψ') and axial load (P) is:

$$\psi' = \frac{-a_{16}}{2A} P \qquad \text{a-1-(4)}$$

where A is the enclosed cross sectional area of the beam and a_{16} is the in-plane coupling compliance, "A_{ij}^{-1}" (tension-shear strain coupling) of the beam wall. There are two independent ways to force ψ' toward a maximum; minimizing "A" and maximizing a_{16}. Cross sectional area, A, will be influenced greatly by strength and stiffness requirements. To insure hygrothermal stability, an attempt to maximize a_{16} will be made using an HTCC wall layup of $(\theta,\theta+90)_s$.

Starting with the in-plane compliance matrix of a $(0,90)_s$ laminate [i.e. $[a^o_{ij}]$] and transforming it through a rotation of "θ", yields coupling compliance $a_{16}(\theta)$ as follows:

$$a_{16}(\theta) = (2m^3n - 2mn^3)(a^o_{11} - a^o_{12} - 1/2a^o_{66}) \qquad \text{a-1-(5)}$$

where $m = \cos(\theta)$
$n = \sin(\theta)$

This shows the angle parameters m and n to be uncoupled from the material properties (a_{ij}) in this case. Setting the first derivation of $a_{16}(\theta)$ with respect to θ equal to zero results in the equation

$$\sin 2\theta = \pm\frac{1}{2}$$

as a condition for an $a_{16}(\theta)$ extremum, given the material property $(a^o_{11} - a^o_{12} - 1/2a^o_{66})$. There are two "$\theta$" values which satisfy this relation between

0° and 90°, they are 22.5° and 65.5°. They yield equal magnitudes for $a_{16}(\theta)$ but opposite sign. The maximum a_{16} occurs at 22.5° for all materials, then, if no other constraints are imposed.

Aeroelastic stability, classical "flutter" in particular, imposes a torsional stiffness requirement. Current designs for composite rotor blades use fiber orientations of $\pm 45^{\circ}$ in the outer skin to provide most of the required torsional stiffness. If tension-torsional coupling is to be obtained, this can best be done by changing the $\pm 45^{\circ}$ orientation to give both high shear and coupling stiffness in layups of single $\pm$ orientation, rather than adding layers to provide that coupling in addition to the $\pm 45^{\circ}$ layers. Maximixing, now, the ratio of tension-torsion coupling compliance to torsion compliance, yields:

$$\frac{a_{16}}{a_{66}} = \frac{(2m^3n-2mn^3)}{8m^2n^2+(m^2+n^2)2a^{\circ}_{66}/(a^{\circ}_{11}-a^{\circ}_{12}-a^{\circ}_{66}/2)} \qquad \text{a-1-(6)}$$

where the material parameter $a^{\circ}_{66}/(a^{\circ}_{11}-a^{\circ}_{12}-1/2a^{\circ}_{66})$ is negative for all composite materials considered, and has the effect of maximizing the ratio a_{16}/a_{66} as its magnitude increases.

The need to avoid bending resonance with integer harmonics of rotor speed imposes a bending stiffness requirement. To maximize tension-torsion coupling, while satisfying a bending stiffness constraint, involves maximizing the ratio of tension-torsion coupling compliance; to bending compliance in this case, for example, flatwise bending. For a thin wall, rectangular box beam (with constant properties around the cross section), this relation becomes:

$$\frac{a_{16}}{a_{11}} = \frac{(mn^3-m^3n)}{m^2n^2+(m^2+n^2)^2a^{\circ}_{11}/(a^{\circ}_{66}+2a^{\circ}_{12}-2a^{\circ}_{11})} \qquad \text{a-1-(7)}$$

where the $a^{\circ}_{11}/(a^{\circ}_{66}+2a^{\circ}_{12}-2a^{\circ}_{11})$ term, which was positive for all materials investigated, affects the ratio in an inverse form.

Tests were conducted on various HTCC tube configurations to confirm the tension-torsion coupling and the degree of thermal shape stability achieved. As a means of checking the HTCC design concept, both $(20/-70)_T$ and $(30/-60)T$ which are HTCC tubes and $(0/30)_T$ $(0/20)_T$ and $(0,10)_T$, which are non HTCC tubes were included. The material used was HYE1048AE graphite/epoxy. One $(+45/-45)_T$ tube was also used to calibrate the appa-atus; the coupling for this tube should have been essentially zero.

The testing apparatus for tension-torsion coupling measurement allowed a 1" diameter tube to be subjected to axial tension with one end free to rotate. Twist rate measurements were made between points two inches from each end plug, to minimize end effects. A laser beam, two 90° prisms, and one beam splitter were used to detect changes in twist. Thermal twist rates were measured for all tubes at

temperatures between 25 and 66° C. The tension-torsion test equipment was used with a glass enclosure over the entire apparatus creating the thermal environment. Heat was added using a heat gun insert through a port in the end of the enclosure; temperature was measured by a thermocouple mounted 1/4" above the center of the tubes.

The $(+45/-45)_T$ tube which should have shown nearly zero coupling, did not. This is believed to have been caused by bearing misalignment in the testing apparatus. Consequently, all coupling coefficients were corrected, using the indicated coupling of the $(+45/-45)_T$ tube as the test fixture alinement calibration. Theoretical values were calcualted from Classical Lamination Theory (CLT). The results for these tubes showed much better correlation between experimental and theorietical coupling coefficients than did the flat plate prediction. Further, thermal twist results did, indeed, confirm the fact that HTCC tubes are far superior to non HTCC tubes as regards thermal twist stability.

5.a.(1).(c). Shape Stability of Curved Laminates

A problem which is related to those of asymmetric laminates for flat or closed-curved shapes, is that of symmetric laminates with curved, open shapes. Warpage during manufacture of such composite components is a serious matter. Large scale warpage can occur in the production of open geometries such as right angle stiffeners using anisotropic laminated composites - as typically occur in sub-structure in helicopter fixed airframe components, or in leading edge blade spar components - even when the laminates have symmetric stacking sequences. Since inconsistencies in manufacturing can result in warpage of flat symmetric plates, warpage in these more complex geometries has often been considered an unfortunate result of the particular manufacturing process; e.g., uneven bleeding of resin or laminate sticking to the tooling.

Research in this instance, therefore, specifically addressed problems of instability relating to components of more complex geometry. In particular, an analytical solution was developed to predict the warpage and instability of an anisotropic cylindrical shell. This was then used to arrive at a method for optimizing the laminate for shape stability. The following discussion and derivations are based on the idea that a typical composite component is a laminated structure having vastly different material properties in the thickness direction from those in the plane of the reinforcements. The properties of primary consideration in composite manufacture are:

i) coefficient of thermal expansion (CTE)

ii) cure shrinkage

iii) moisture swelling coefficient.

thermally curvature stable. Because the unsymmetric laminates studied in the literature are prone to warping, the inductive conclusion that all unsymmetric laminates warp,

must have seemed reasonable. According to the literature on unsymmetric laminates, laminate asymmetry implies thermally induced warping and arrow (3) should always be solid, but in no case was formal proof attempted.

The belief that symmetric laminates are shape-stable is largely based on flat plate experience; but unfortunately, extensions to cases with more complex geometries cannot be done without additional considerations. In the field of composites, "quasi-isotropic" laminates are often the designers' choice, in an effort to make the material react more like the metal that is often being replaced. The term "quasi-isotropic", however, only applies to the in-plane composite properties, and it must be realized that the out-of-plane properties are often vastly different. This difference between in-plane and out-of-plane properties is a major factor in the warpage and shape instability of geometrically unsymmetric components with symmetric stacking sequence.

In this context it should be noted that by warpage we imply an irreversible shape change which often occurs during the manufacturing, but can also occur in service. Effects such as cure shrinkage or consolidation would yield manufacturing warpage, while creep could introduce in-service warpage. Conversely, the second area, instability, deals with reversible changes of shape that occur as factors such as environment vary. This instability would be important for designs which must retain acceptable dimensional tolerances over a broad range of environmental conditions.

Relations were sought that could be used equally well for either area, since both of these shape changes stem from forms of anisotropy. An analytical solution was derived for the case of an anisotropic semi-cylindrical shell as a first step to gaining understanding of the problem. The in-plane expansion coefficients were taken to be isotropic (note that only two orthogonal fiber directions are necessary) and so small as to be considered zero compared to the through-thickness values, as a first approximation. To keep the sources of anisotropy as general as possible, the most basic expression was derived only in terms of the initial and final thicknesses, as defined in Fig. 12.

If $\ell = r\theta$, $\ell = \ell'$ and plane surfaces remain plane, then,

$$d\theta = \theta[(t/t')-1] \qquad \text{a-1-(8)}$$

By leaving equation (1) only in terms of the thickness, it should be clear that any effect resulting in a much greater change in thickness (from t to t') than the corresponding in-plane changes (here assumed zero) will have a similar effect on the included angle θ.

In-plane expansion and contraction can be accounted for by including an inequality between ℓ and ℓ'

$$d\theta = \theta[(\alpha_I-\alpha_T)dT/1+(\alpha_T)dT] \qquad \text{a-1-(9)}$$
$$d\theta = f(\alpha_I,\alpha_T,dT)$$

where,

dT = temperature change

α_I = in-plane coefficient of thermal expansion

α_T = through thickness coefficient of thermal expansion

Note that, this equation has been written for the specific case of a temperature change; the coefficient of thermal expansion and the change in temperature, however, can readily be replaced by one or more different expansion effects. Thus, it is straightforward to extend Equation a-1-(2) so as to include terms accounting for more complex environmental and manufacturing conditions, as follows:

$$d\theta = \theta\left\{[(\alpha_I-\alpha_T)dT/1+\alpha_T dT]+[(\beta_I-\beta T)/1+\beta T]+[(\Phi_I-\Phi_T)/1+\Phi_T]\right\} \qquad \text{a-1-(9a)}$$

where,

β_I = in-plane moisture swelling

β_T = through-thickness moisture swelling

Φ_I = in-plane fabrication expansion (shrinkage negative)

Φ_T = through-thickness fabrication expansion

Here fabrication expansion terms are meant to include all "one time only" variations that lead to warpage. Note that Equation a-1-(2) is in terms of only the in-plane and out-of-plane expansion coefficients and the environmental variable; further, that if $\alpha_I = 0$, Equation a-1-(1) becomes identical to Equation a-1-(2); and that if $\alpha_I = \alpha_T$, no shape change is predicted ($d\theta = 0$), since this is the isotropic material case.

These equations strongly suggested that shape change phenomena in geometrically unsymmetric components can be explained by material anisotropy and not simply as a result of problems during manufacture. When rough values of cure shrinkage, thermal expansion, and moisture swelling were used in Equation a-1-(2), the effects of shrinkage and moistue swelling were found to be of the same order of magnitude, while the effect of thermal expansion is several times smaller. Thus, warpage during cure, due to cure shrinkage, is predicted to give relatively large shape change at room temperature as compared to that produced by hygrothermal shape instability over a normal atmospheric operating environment.

Based on these results, the method used to attempt to minimize warpage builds in the mid-plane curvature which occurs in response to hygrothermal variations in asymmetric laminated plates, as a result of in-plane/out-of-plane coupling. by balancing the change in curvature predicted by Equations a-1-(1) and a-1-(2) of the previous paragraphs with an equal and opposite curvature, (k), predicted for a flat asymmetric laminate by classical laminate theory (CLT), a solution became available for variations in both moisture and temperature simultaneously. As noted in reporting the work on HTCC laminates, classical laminate theory can be used to predict stability with some confidence, since for this case, the desired deflections are zero.) Since

CLT assumes a flat plate as a starting point, any changes in curvature predicted for the unsymmetric geometry must also be based on an initially flat plate. This indicated the need to derive "equivalent flat plate curvatures" for components with unsymmetric geometry by transforming the change in curvature change in a flat plate. For the case of thermal expansion, the equivalent flat plate curvature became;

$$K_{ef} = \theta[(\alpha_I - \alpha_T)dT/1+\alpha_T dT]/\theta r(1+\alpha_I dT)$$
$$= (\alpha_I - \alpha_T - dT/r(1+\alpha_I dT)(1+\alpha_T dT) \qquad a\text{-}1\text{-}(10)$$

$$k_{ef} = f(\alpha_I, \alpha_T, dT, r)$$

If $k-k_{ef}=0$ then the component is predicted to be shape stable. Perhaps more important from a manufacturing viewpoint, while the predicted shape change ($d\theta$) is only a function of the in-plane and out-of-plane expansions, the term necessary to predict shape stability (k_{ef}) is also dependent on the initial component radius (r).

Thus, the process developed to arrive at an environmentally shape stable component of unsymmetric geometry which will not warp during cure is:

1) Calculate the shape change ($d\theta$) of the component using the planned (symmetric) stacking sequence.

2) Calculate the "equivalent flat plate curvature".

3) Using CLT, iterate the stacking sequence until $k \neq k_{ef}$.

The resulting shape stable component will then have an area of localized asymmetry in the corner of the angle which just balances the geometry-induced shape change. If the "arms", however, are initially flat, they will remain flat only if the laminate is symmetric in those areas. Fig. 13 shows, schematically, the stacking sequence of an optimized curved composite component.

Since neither the sample thickness nor the corner radius were prediced to affect the change in shape of symmetric laminates with temperature, they could be used as variables to investigate the accuracy of the theory derived for predicting shape stability. Further, to test the capabilities of this analysis as a means of optimizing laminates, it seemed necessary to include variations in localized stacking sequence as another variable.

In planning these tests it was noted that both the thoery and initial evaluation samples indicated that angular variations would be a maximum of less than two degrees for a right angle geometry, carbon fiber/epoxy component, over a temperature range of 50 to 350°F. Hence, a very accurate method of measuring the shape change would be necessary. A LASER light source was, therefore, reflected off the sample and the resulting deflection changes with temperature measured on a screen located a substantial distance from the sample. This allowed the measurement of angular changes as small as $<0.01^{\circ}$ due to sample shape change as a result of variations in temperature.

Using this LASER measurement technique tests were performed on a variety of carbon fiber/epoxy samples in the as-cured state. Three different thicknesses (4, 8, and 12 plies) and both symmetric and locally asymmetric stacking sequences were included for each test sample. Sections of each sample were mounted, polished, and anayzed using optical microscopy to assure the quality of the samples being tested. Once reproducible angle change versus temperature data had been obtained for these as-cured samples, the samples were themally ycled for approximatelyt one month (225 cycles) over a temperature range from 80 to 300°F. Upon completion of this thermal cycling the samples were retested to investigate their susceptibility to "in-service" damage and the long term reproducibility of the shape variations with temperature.

The results obtained during the experimental program generally showed good correlation with the predictions of the closed-form analytical solution. Changes in angle with temperature were, as predicted, independent of thickness. The different volume fractions testes did, in fact, show differing degrees of instability. The greatest degree of uncertainty in applying the theory arises in estimating out-of-plane material properties. Experimental results obtained using unstable symmetric samples, however, allowed through-thickness data to be determined, subsequently to be used for the superposition equations needed to accurately arrive at shape-stable laminates. Micromechanics is a second method for obtaining through-thickness material properties from constituent properties.

The samples that were thermally cycled showed good reproducibility. This was expected, since the environmental conditions chosen feel within the stable domain defined in the earlier work on hygrothermal fatigue. This reproducibility also showed, however, that the region of laminate asymmetry within the component does not degrade under these conditions. If a debond in this area were to occur, for example, the reproducibility of the measured instabilities, and of the stability within optimized samples, would have been compromised.

These experimental results, together with the rational used in arriving at the design methodology established in this research, lends confidence that the criteria advanced are sufficient to satisfy the shape stability criteria. There may, however, result in a laminate that does not meet other structural criteria imposed by the designer. As the number of plies increase, to meet such other design requirements, the number of stacking sequences that must meet the shape stability criteria will also grow.

5.a.(1).(d). Summary

- A safe environmental domain exists, in which a specific composite material reacts in a reproducible fashion.

- A subset of classical asymmetric laminates has been discovered which do not show in-plane/out-of-plane hygrothermal coupling, yet do retain strong mechanical coupling. These HygroThermally Curvature Stable Coupling (HTCC) Laminates allow design of coupled panels which are stable under steady state hygrothermal conditioning.

- HTCC tubes have been developed which give the designer the option of using tubular structural members which are tension-torsion coupled and hydro-thermally shape-stable.

- Symmetric laminates of unsymmetric geometry are shape unstable with respect to changing temperature or himidity.

- Closed-form analytical methods for predicting of the degree of shape change for an anisotropic material of two dimensional (2D) unsymmetric geometry have been derived. The results of such predictions have been substantiated both experimentally and through the use of a finite element technique.

- Closed-form optimization for shape stability of the same 2D geometry has been derived. The results of this derivation have been substantiated by experiment and by finite element analysis.

- Shape stable/shape correct components must be developed by addressing shape stability and shape correctness individually.

- More complex unsymmetric component geometries may show a combination of shape change and internal residual stress in response to environmental variations.

5.a.(2). Fatigue in Composites

(Sr. Investigator: E. Krempl)

The superior performance of composites in fatigue compared to metals was well established by the time the RPI-RTC was initiated. Fatigue is an especially important structural design criterion for rotorcraft, since load cycles of significance build up at rates as high as 6 to 10 times per rotor revolution. It is not surprising then, that use of composite materials in the structure of rotorcraft was (and is) increasing rapidly. Most experience prior to 1982, however, was in tension-tension fatigue of composites, i.e. where no load reversals to compression occur during the fatigue cycles. In RPI's program, fatigue characteristics where compressive stress is a part of the cycle and in biaxial stress were to be examined experimentally. Furthermore, development of a theory of material behavior from a visco-plastic viewpoint was to proceed hand-in-hand with these experiments, to better understand and characterize composite material behavior in fatigue. In short, the purpose of this research was to obtain fatigue properties of advanced composite material for negative R-ratios and model the time-dependent deformation behavior found in epoxy-fiber composites - all for material combinations of interest to the rotorcraft industry.

5.a.(2).(a). Fatigue Tests

Building on the results of earlier research in biaxial fatigue of Graphite/Epoxy tubes [Refs. 10 & 11] fatigue experiments proceeded using a unique tubular specimen developed by the Senior Investigator (Fig. 14). With its use, the concentrations of interlaminar shear stress encountered in test specimens with edges (e.g., the typical "dogbone" specimens) would not be enountered and the results obtained, therefore, would be more truly a material characteristic and less influenced by geometry. Tubular specimen geometry and the applied loads, of course, had to be such that the "pop-off" normal stress encountered by curved outer fibers in compression and curved inner fibers in tension would always be below failure levels. In a separate program, therefore, internal pressure was introduced to reduce interlaminar normal stresses as experienced by the inner surface fibers of the tubular specimens. It was shown [Ref. 12] that the fatigue life with and without internal pressure is essentially the same. Based on these results it was concluded that the interlaminar normal stresses were not a factor in the fatigue life results obtained in these experiments.

Prompted by design needs in the helicopter industry the fatigue behavior of nearly unidirectional Kevlar/Epoxy material was studied. Early attempts to manufacture a tubular specimen of $[\pm 5^{o}]_{s}$ Kevlar/Epoxy resulted in longitudinal cracks appearing after the cure process. Further, in fatigue testing of those specimens which were successfully fabricated (fiber orientations $\pm 5^{o}$, with respect to the tube centerline) failure locations suggested stress concentrations near the grips of the same test fixtures which worked well for high-stiffness Graphite/Epoxy laminates. These fixtures are shown in Fig. 15 and the grip-related failures sketched in Fig. 16. Special fixtures subsequently designed to study biaxial fatigue behavior of such low-stiffness composites as Kevlar, produced the same kind of end-concentrated failure locations.

By changing to a shorter gage-length in the specimen, to new prepregs and by increasing the pressure applied during the cure process, both cracking and grip-end failures were eliminated. The revised specimen designs and cure cycles are shown in Figs. 17 and 18, respectively. Successful fatigue tests were subsequently run for R = 0.1 and R = -0.2 (R = minimum stress/maximum stress), as shown in Fig. 19. Progressive fatigue failure stages are sketched in Fig. 20.

After the successful completion of uniaxial fatigue tests for the $[\pm 5^{o}]_{s}$ Kevlar/Epoxy material, steps were taken to begin multiaxial fatigue tests for this same material using a $[0/\pm 45]_{s}$ lay-up. Accordingly thirty thin-walled tubular specimens were layed-up, cured and machined. These specimens were to be used for fatigue tests in which the load on one axis is in some cases in-phase and in others out-of-phase with the load on the second axis, and also under negative R-ratios, but static tests also were initiated to establish base-point values. At moderate stresses their static behavior in tension was nearly linear elastic. Nonlinear hysteresis developed in static compression, however, at stress level magnitudes which exhibited linear behavior in tension.

Following the ARO review of the Spring of 1986, guidance was received to the effect that these fatigue studies were well-enough in hand to shift support to higher priority topics. Accordingly the fatigue studies were terminated as part of the ARO program.

5.a.(2).(b). Formulation of Constitutive Equations

As an important means to further understanding of deformation behavior and fatigue in composite materials as applied in rotorcraft design, a project was initiated in late 1982 with the goal of formulating constitutive equations capable of properly representing such effects. Consideration was given to linear elastic behavior, non-linearity and time dependent behavior as characteristics to be included. In earlier testing of thin-walled tubes, $\pm 45^{o}$ Gr/E laminates (as may be used in fuselage skins, drive shafts, etc) were found to have nonlinear and time dependent behavior when loaded axially to greater than 25% of ultimate tensile strength. On the other hand, such composites behaved linearly up to 90% of their ultimate torsion strength. Further, this behavior pertained to cyclic loading as well.

Based on such experience, an isotropic nonlinear viscoelastic constitutive equation based on overstress was chosen as a candidate for representig the observed nonlinear and time-dependent behavior, it takes the form as follows:

$$\dot{\epsilon} = \dot{\epsilon}^{el} + \dot{\epsilon}^{in} = \frac{\dot{\sigma}}{E} + \frac{\sigma - g}{Fk} \qquad \text{a-2-(1)}$$

$$\dot{g} = \psi\dot{\epsilon} - \left|\dot{\epsilon}^{in}\right| (g - E_t\epsilon)^{\frac{1}{b}}$$

where

σ = stress
ϵ = infinitesimal strain
g = equilibrium stress
E = Young's modulus
E_t = final tangent modulus

and ψ, k, b are positive continuous functions of overstress, $(\sigma-g)$.

This representation was to be modified to account for transverse isotropy or orthotropy. Specific forms for the nonlinear viscoelastic properties were subsequently found for transverse isotropy by means of tensor function representation theorems and were incorporated into the theory so as to account for properties such as depicted schematically in Fig. 21. To facilitate mechanism identification, special cases were considered in which the plastic anisotropy tensor was made proportional to the elastic anisotropy tensor.

The transversely isotropic nonlinear constitutive equation so developed represents linear elastic regions followed by inelastic, rate-dependent regions. Creep and relaxation are included in the formulations which pertain to the small strain regime. Neither yield surface, loading nor unloading conditions are used in this formulation, for which rate dependence is fundamental. These constitutive equations lead to a governing nonlinear differential equation, which was written in incremental form to facilitate numerical solution. It represents linear elasticity in the preferred direction and inelastic deformation in the plane of anisotropy. The results of this research are summarized in Ref. 13.

Following the 1984 review by ARO's evaluative panel, this work was judged to be sufficiently supported either by the rotorcraft industry or components of the fixed-wing or space community to justify terminating its continuation under the Center of Excellence contract. At that point, therefore, the fatigue and time dependent behavior of composites research was considered complete.

5.a.(3). Static Structural Design of Composite Drive Shafts

Various aspects of the design of composite helicopter drive/shafts have been investigated under this program. Results obtained in research on overall drive system design and optimization are reported under item 5.b.(1). in this report, in the Structural Dynamics research category, because of the importance of critical whirl speeds to system configuration. The static strength of bolted joints as encountered at the connecting ends of the drive shaft segments, torsional buckling and damage tolerance of drive shafts have also been considered both for their individual importance and because overall system optimization requires information on these aspects. Studies of these static structural characteristics are reported in this section of the report.

5.a.(3).(a). Strength of Mechanical Connections

(Sr. Investigator: D. Goetschel)

During the first two years of this program, the behavior of bolted joints in the connectors used at the ends of Graphite/Epoxy drive shafts was investigated both analytically and experimentally. In the experimental program, a number of shaft connector models were fabricated and tested to failure in torsion with various composite reinforcement configurations at the tube ends. The shaft lay-ups consisted of six plies, $[0,-45,45]_2$, made of Fiberite 1045 A1E, low modulus Graphite/Epoxy material. The ends of the tubes were reinforced with 4 additional plies at various angles, then bolt holes were drilled with a carbide tip drill. To minimize scatter among specimens due to fabrication processes, the Rensselaer curing pressure vessel was programmed and interfaced with a Texas Instruments Multiwriter controller/printer, to insure virtually identical cases.

The geometry of the end connection reinforcement is characterized by four parameters:

1) the fiber orientation angles of the reinforcing plies,

2) the edge distance (i.e. the distance from the bolt hole to the shaft's edge normalized by the bolt diameter),

3) the taper distance (i.e. the distance from the bolt hole to the end of the reinforced zone, normalized by the bolt diameter), and

4) the circular pitch (i.e. the circumferential length between two consecutive hole centers, normalized by the bolt diameter).

A total of 18 specimens were tested including (0^o, ±30, ±45, ±60, ±75, and 90^o) reinforcement ply angles. Table 11 lists the characteristic parameters for the various configurations, together with the experimentally measured failure torques.

These various bolted end connection configurations were also analyzed numerically using the three-dimensional finite element program, ABACUS. A laminated, triangular shell element with bending and membrane characteristics was used. The analysis assumed linear elastic material behavior, that hygrothermal effects could be neglected and that the bolt was undeformable. A single bolt hole was modeled with proper deformations on the boundary, symmetry conditions, and a cosine normal load distribution between bolt and bolt-hole. To facilitate these analyses a computer translator was written linking an in-house finite element pre-processor to ABACUS.

The stress distribution obtained from this finite element model was then used to predict failures of the bolted connections, based on a modified version of the average stress criterion developed by Whitney and Nuismer [Ref. 14]. The original average stress criterion predicts the occurence of failure when the average through-the-thickness stress (in the load direction) over a characteristic length (normal to the load direction) equals the unnotched laminate strength. In Rensselaer's study two modifications were introduced to this criterion. First, the average stress in the peak stress region was calculated on a ply-by-ply basis, as opposed to a through-the-thickness average. Second, the maximum fiber stress was utilized in all averaging calculations, as opposed to the stress in the loading direction. A post-processor for these programs was written which utilized a curve-fitting routine to provide continuous indications of stress in the areas of interest. Table 11 also lists the theoretical predictions for the failure load of the bolted connections, and the percentage deviation of these predictions from corresponding experimental measurements.

The comparisons possible within Table 11 show good agreement between tests and analytical predictions. The discrepancies range from -11% to +15% for all specimens. When cases are considered where two specimens were tested, the discrepancies decreased to ±7%. Such agreement should be considered excellent, since the theoretical predictions are, therefore, well within the observed experimental scatter.

Some idea of the impact of the various design parameters on the strength of bolted connections can also be assessed by analyzing the data in Table 11. First, the optimum fiber orientation angle for the reinforcement appears to be $\pm 45^{o}$. A sharp decrease in load carrying capability is observed for other configurations, especially when the angle is smaller than 45^{o}. Second, the strength decreases slightly with decreasing edge distance; decreasing edge distance from 6 to 3 results in a 10% strength decrease. Third, the best circular pitch distance was shown by the tests to be 3.4, among the three values of this parameter tested, corresponding to 8 quarter-inch bolts. Finally, taper distance seems to have little effect on the strength of these bolted connections, so long as this distance is greater than two; sharp decreases in strength, however, are observed below that value.

Following the second program review, ARO recommended this work be considered complete and that no further studies of this nature be carried out under the subject contract.

5.a.(3).(b). Torsional Buckling Analysis of Graphite/Epoxy Shafts
(Sr. Investigator: O. Bauchau)

The ultimate load carrying capability of helicopter drive shafts is usually limited by torsion buckling. Accordingly, an investigation into the torsional buckling behavior of Graphite/Epoxy shafts was initiated in 1985. From the outset, this project was to be both experimental and analytical, since the objective was to establish buckling criteria both for their general utility and also for application in the overall drive system optimization studies (Item 5.b.(1). below). In the experimental study, circular cylindrical specimens were fabricated from 6, 8, or 10 layers of Graphite/Epoxy prepreg wrapped around an aluminum mandrel, then cured according to the manufacturers' recommended cycle. Table 12 summarizes specimen construction and geometries and the number of specimens tested in each group. It is noted that the test shafts were bolted onto an aluminum fitting with six equally spaced bolts. This boundary condition is neither clamped nor simply supported. The theoretical predictions discussed below, therefore, considered both simply supported and clamped edges.

Static torsional tests of the specimens described in Table 12 were conducted in an MTS servo hydraulic testing machine at a constant twist rate of one degree per minute. Buckling was detected by a sharp decrease in the torque-twist curve. The buckling pattern was found to consist of helical waves winding around the cylinder; no significant post-buckling strength was observed.

A mathematical model of the torsional buckling behavior of circular cylinders was developed, based on a general shell theory. In the derivation of these equations, special care was taken to properly model the specific characteristics of laminated shaft elastic coupling effects, as well as transverse shearing deformations. The usual simplyfying assumptions (such as Donnell's or Flügge's assumptions) were not made.

Table 13 lists the experimentally measured buckling torques, T_{cr}; the corresponding critical shearing stress, T_{cr}; the number of circumferential waves n in the buckling deflection shape; and the theoretical predictions for each of two boundary conditions around the perifery (edges) of the ends of each tube; namely, clamped and simply supported. The principal findings resulting from these studies are:

1) Good agreement exists between the experimentally measured buckling loa ds and the theoretical results obtained by analysis.

2) As shaft length increases, the buckling mode circumferential wave number, n, decreases.

3) Even for very thin laminated Graphite/Epoxy shafts, the effect of transverse shearing deformations can be significant, when the number of circumferential waves is larger than three.

4) Torque direction and stacking sequence can drastically affect critical buckling loads (variations up to 80% were observed experimentally).

An attempt was made, before terminating this phase of the research, to derive a closed-form formula to predict the torsional buckling load of very long shafts. It was very inaccurate compared with the full solution; even when n = 2 the buckling load continues to depend strongly on the shaft length. In contrast to metal shafts, where the "infinite length" assumption necessary to obtain a closed form solution yields good results, it is thus shown to be invalid for composite shafts.

5.a.(3).(c). Ballistic Damage Tolerance in Composite Shafts
(Sr. Investigator: O. Bauchau)

Damage tolerant design of helicopter drive shafts can make an important contribution to increased survivability and operational reliability. Ballistic damage from a direct hit with a small caliber weapon or foreign object damage during maintenance or normal operations are major threats to drive system integrity. A complete assessment of foreign object damage on a composite structure is a formidable task that requires a considerable amount of testing because a very large number of parameters must be considered [Ref. 15]. In addition, the structural response during impact is complex, and such test data as exist show that the preload stress level for impact fracture (i.e., where a preloaded structure is destroyed by impact) on tubes can be significantly below the residual strength for similarly impacted panels. Where the structure is not destroyed, the details of impact damage will determine the residual ultimate strength and residual fatigue life.

Rensselaer considered approaching full assessment of damage tolerance of composite drive shafts to the point of including ballistic impact tests on loaded, high speed rotating shafts such as could be encountered in battlefield operations. However, considering the attendant difficulties and the number of parameters involved (including projectile type, geometry, mass, velocity and obliquity), it seemed appropriate to conduct a preliminary study, concentrating on one restricted, but important aspect of the problem; namely the residual ultimate torsional strength of composite shafts with well characterized damage. In this case "ultimate strength" was taken to mean the maximum torque the shaft is capable of carrying whether determined by buckling or material failure. Two limiting types of damage were considered: circular holes of various diameter (as would result from a high velocity impact, but in this case drilled into the composite tubes) and imbedded delaminations (as would result from non-penetrating impact, but here simulated with bonded-in teflon inserts).

In the limited work reported on impact loading of flat composite panels in the literature [Ref. 15-21], various researchers state that holes in a composite material inflicted by a bullet produce approximately the same reduction in static strength as a hole of the same diameter produced by standard drilling [Ref. 18] or by electric discharge machining [Ref. 19]. Thus it seemed reasonable to initiate this research by investigating the residual strength of composite shafts with holes and cracks deliberately made, as roughly modeling foreign object impact damage. The design of the specimens was essentially that used in the tests described in sections 5.a.(3).(b)., above, but in addition to the drilling required for test fixture

attachment bolts, it was also used to simulate damage. Circular holes of one-quarter, one-half, three- quarters, and one inch diameter were drilled in these tubes and three replicates were tested for each configuration. Two kinds of failure mechanism were observed. For the $^1/_4$, $^1/_2$, and $^3/_4$ in. diameter holes, the failure mechanism remained torsional buckling, as for the virgin specimens. The helical buckling wave pattern seems unaffected by the damage. For the large holes (i.e. 1 in. diameter) the failure mode is very different, involving extensive material failure around the hole. Fig. 22 shows the residual torsional strength of the shaft versus hole diameter and with simulated delamination for two lay-up configurations. Major findings of this study are:

i) The dominant failure mechanism for torsionally loaded shafts with circular holes is torsional buckling. Material failure did not occur until the damage size reached approximately one third of the shaft diameter.

ii) Delamination damage simulated between the outermost plies decreases the buckling load of the shaft, but not significantly.

iii) Stiffness characteristics, rather than strength characteristics appear to dominate the behavior of thin-walled shafts under torsional load.

The last conclusion seems particularly important, as it tends to give stiffness parameters a dominant role in the design of damage tolerant composite drive shafts. This constrasts with the fact that toughness and strength parameters generally play a dominant role in the design of damage tolerant composite structures.

It is interesting to note that there were differences in torsional buckling loads for lay-ups L#1 and L#2 (see Tables 12 and 13). L#2 is 35% stronger in the virgin configuration, but as the hole size increases both lay-ups tend to the same failure load. For 1 in. diameter holes, both lay-ups have the same failure mechanism, namely material failure. Since material failure shows little dependence on stacking sequence, both have nearly identical failure loads. Additional testing was performed on specimens having holes drilled through both sides of the tube. the second hole seems to have little effect on the buckling load. This result was to be expected since the buckling wave pattern seems unaffected by the presence of holes smaller than 1 in. diameter.

As a second, more realistic step in assessing damage tolerance of composite shafts, actual ballistic impact tests were conducted on shafts which were torsionally preloaded.

Given the difficulty of using firearms on a campus, the U.S. Army's Watervliet Arsenal (in Watervliet, N.Y.) was contacted, and permission obtained to use their firing range. The M-1 gun, a 30 caliber weapon, was selected for the ballistic impact testing after a review of likely threats to U.S. helicopters and the availability of weapons at the Arsenal. A testing fixture was fabricated to both hold and impose the static torsional preload on the shaft. Armor piercing rounds were used in the

M-1 rifle. Nominal damage size for a single 30 caliber shot is 0.30 inches. Significant delamination damage was observed, however, on the bullet exit side of the laminate. To obtain larger nominal damage sizes, two, three or four overlapping shots were fired at the same shaft. Firing tests were repeated for various preload levels. If the shaft survived the impact it was subsequently tested for residual torsional strength.

Fig. 23 compares the (normalized) buckling strength of specimens with drilled holes with the preload values (normalized) imposed for various nominal damage sizes inflicted ballistically. For a single 30 caliber shot, no impact fracture was observed for preload up to 90% of the torsional buckling load. For damage of 0.45 inch diameter, impact fracture occurs at about 75% of the buckling load. Fig. 24 shows the normalized residual strength for the shafts which did not exhibit impact fracture. This figure also shows the residual strength of shafts with drilled damage for comparison. The major findings of this part of the ballistic damage study are:

i) Graphite/Epoxy shafts possess significant ballistic impact damage tolerance. A direct hit by a 30 caliber weapon decreases the allowable torque by about 10%. For 0.60 inch ballistic damage, this decrease is about 30%.

ii) The damage inflicted by gunfire on composite shafts seems substantially unaffected by the static torsion preload which the shaft is carrying when it is hit, to within values quite close to its residual strength.

iii) Although the residual strength of ballistically impacted shafts appears to be slightly lower than that of shafts with drilled damage, the difference is not drastic. This means that meaningful insight can be gained into the damage tolerance of composite shafts by measuring the residual strength of shafts with drilled holes, a rather straightforward test procedure.

The results discussed here and in the preceding section [5.a.(3).(b).] are presented in more detail in Ref. 22.

5.a.(4). Composite Upper Controls Development
(Sr. Investigator: D. Goetschel)

In a conventional helicopter rotor upper control system, the rotating race of the swashplate is driven by a hinged linkage, termed the "scissor" mechanism. Without the "scissor", friction in the swashplate would tend to make the pitch links change from their proper angular position, because they must be ball-jointed at both ends. This is illustrated in Fig. 25. As can be seen from this figure, the "scissor" includes hinged or pinned joints at the main rotor shaft (A) and knee (B) and a spherical, or ball joint, at the swashplate (C). The pinned joints allow the swashplate to translate vertically and to swivel about an axis parallel to the axis of the pins. The spherical ball joint allows the swashplate to swivel about an axis perpendicular to the pins.

This mechanism oscillates once per revolution of the rotor whenever the control positions are such as to require cyclic pitch, which is virtually at all times in flight. Thus, the hinges and ball joints are subject to wear. Increased maintenance is a direct result.

As a means of improving maintenance and reliability, and with the encouragement of Sikorsky Aircraft, Rensselaer began in June '83 to examine the possibility of using an elastic hingeless scissor under the subject contract. The major requirements of this structure are that it be stiff in torsion and sufficiently soft in bending to have an infinite fatigue life for the cyclic flexing demanded by upper flight control motions.

The structural element postulated for such a member is sketched in Fig. 26, and as it would be installed in Fig. 27. A simple "strength of materials" analytical approach was used for the initial designs. This was followed by both tests and finite element analyses. The configurations investigated set the parameters shown in Fig. 26 at $\Phi = 45^{\circ}$, $\lambda = 2"$ and $w = 10"$. Materials evaluated were first, graphite cloth, Fiberite W 134, in an epoxy matrix, initially Epon V40/828; and later, a unidirectional graphite prepreg, Fiberitye 1048, with plies oriented at $\pm 45^{\circ}$.

Since torsional stiffness is determined, in this construction, by fiber properties, while bending flexibility is determined by the matrix, the graphite cloth was later combined with a number of resins. Ciba-Geigy Araldite 508 and Araldite 6010 seemed quite promising. Various combinations of 508 and 6010 in conjunction with one of two hardeners, N-amino ethylpiperazine (AEP) or metaphenyline diamine (MPDA) produced matrices with a wide variety of properties. Variations in ultimate tensile strengths from 50 psi, with 90% elongation at failure, to ultimate tensile strengths of 7050 psi, with elongation at failure of 12% were, possible.

All of the finite element analyses were run using the ABAQUS finite element system and its two-dimensional, 'S8R' shell element. This element has 4 corner nodes and 4 mid-side nodes and may consist of either one material or several layers with different properties and thicknesses. Two models were generated; one for stiffness/ displacement predictions; the other, more elaborate model for analyzing the shear stress in the bond during torsion, the predominant failure mechanism.

Whereas tests and analyses correlated reasonably well, more detailed mathematically modelling of the bond line was seen as necessary. Further, the tendency of the center plate (see Fig. 26) to buckle under shear load (swashplate torque transmission by the scissors) led to the revised structural concept involving "nesting" shown in Fig. 28.

It was concluded in this study that a large number of variables, involving both materials and configurations would have to be optimized to implement the composite scissors concept. In addition to providing the best combination of torsional rigidity and bending stiffness, the stiffest material displayed the best shear stress distribution along bond lines. As material stiffness increased, the stress distributions improved, resulting in lower peak shear stresses at free edges and larger areas over which the shear stress is distributed. Further, while a high ratio of shear stiffness to tensile stiffness is beneficial, it is - by itself - not enough. Due to the high sensitivity of bending cross-section moment of inertia to changes in web thickness, the best material is one which has a high shear modulus. This allows thin webs and results in lower bending moments. Initial attempts were made to optimize, through a formal program, the shape of the overall scissors configuration and choice of material properties. While promising, the project was brought to a conclusion during the last quarter of 1984, with completion of the masters thesis written by M. Niederer and listed in year '83 in Appendix C. The results of this research are reported in Ref. 23.

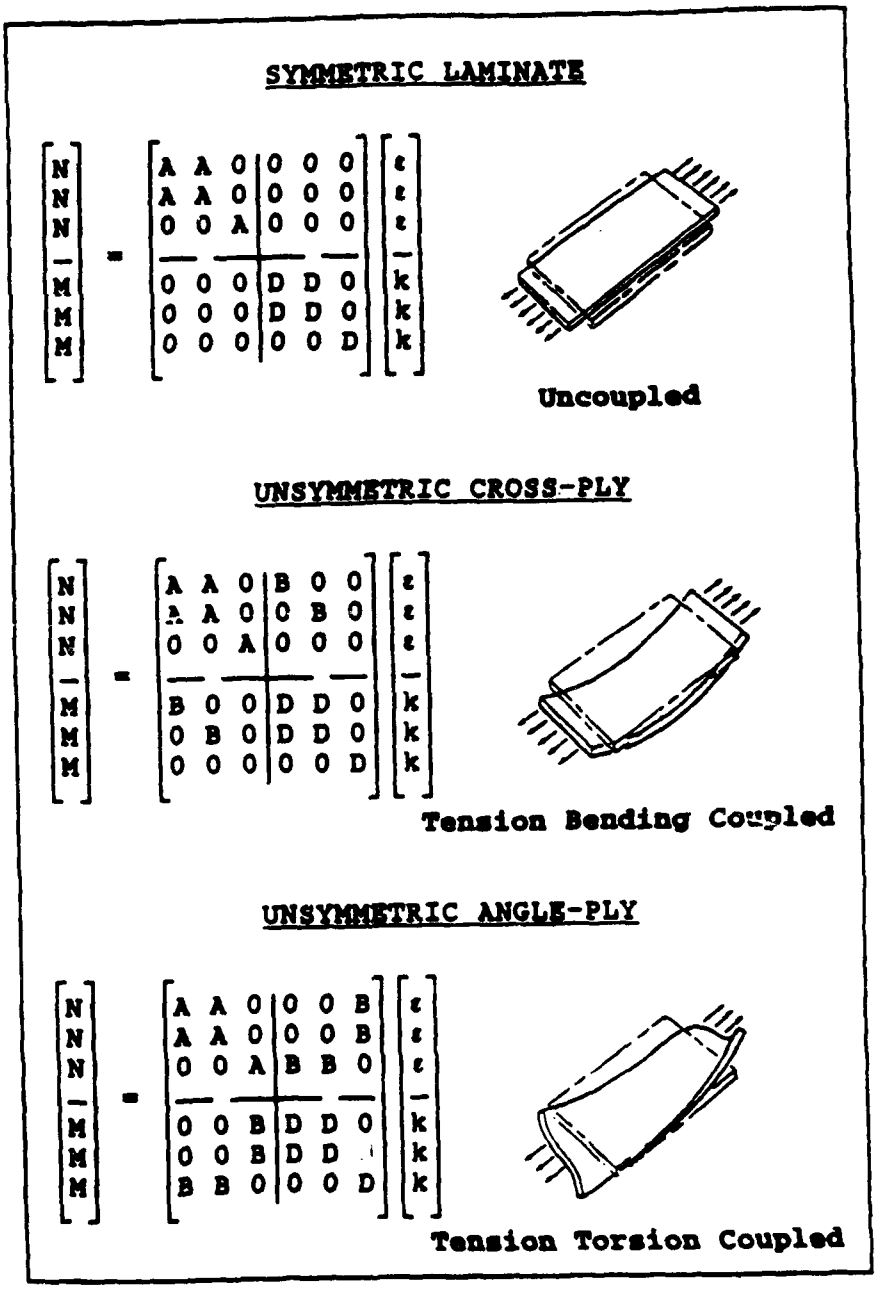

Fig. 6 - Comparison of Couplings Available with Composite Laminated Plates

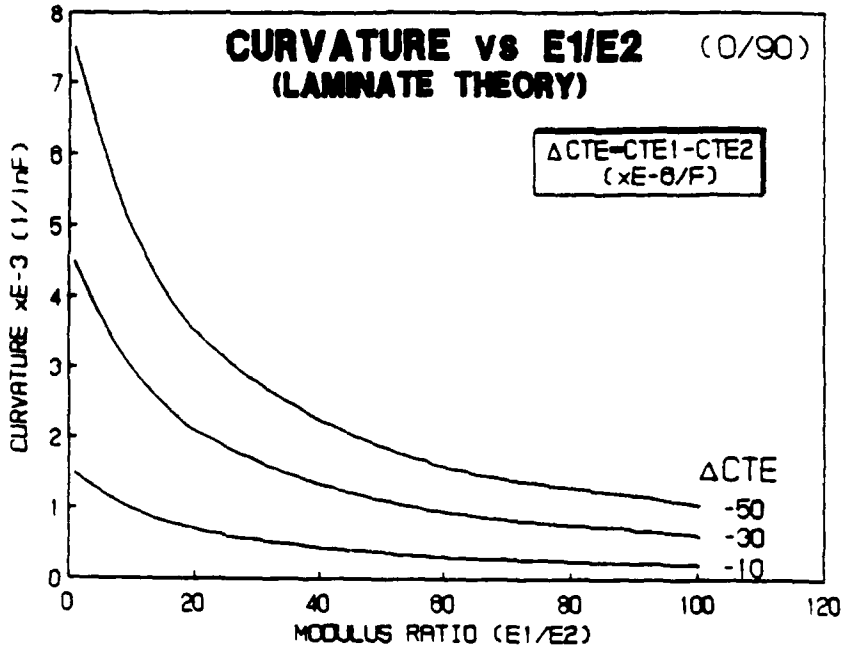

Fig. 7 - Effect of Modulus Ratio on Curvature

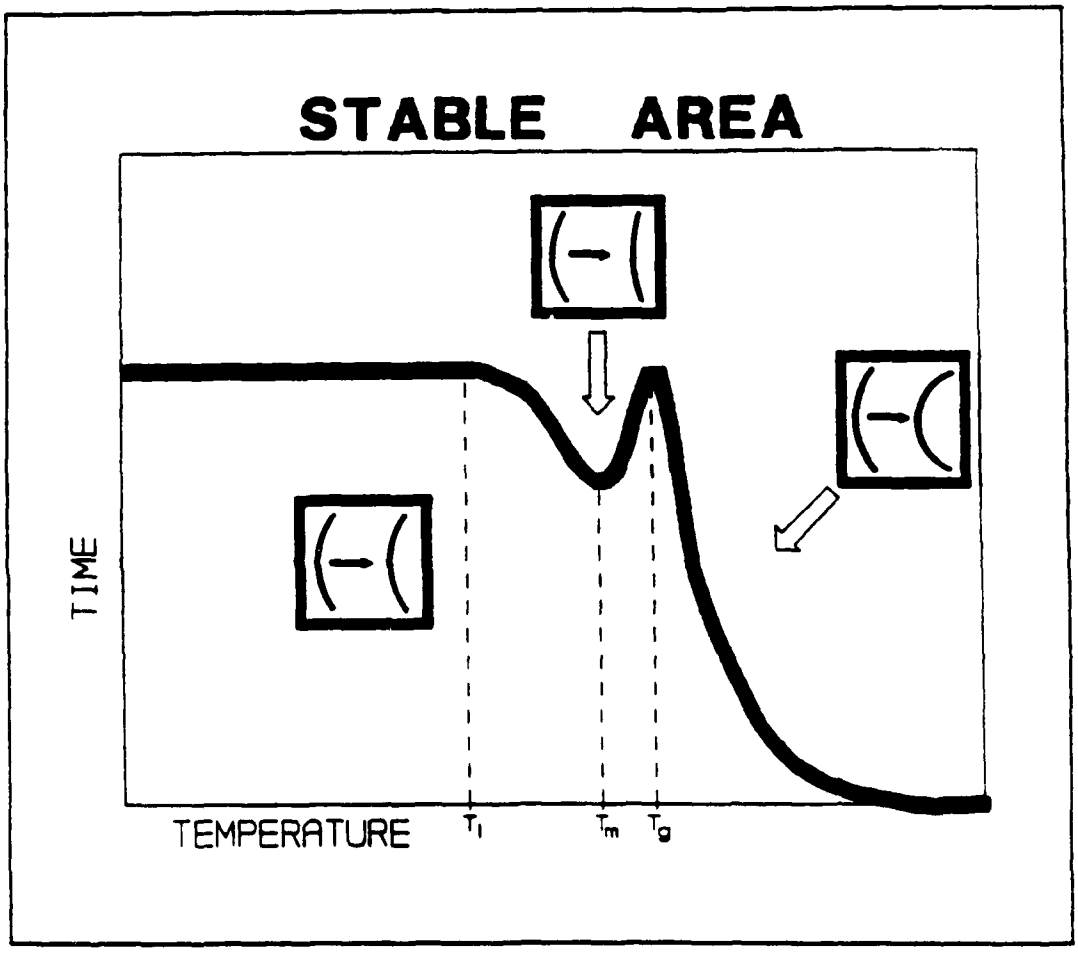

Fig. 8 - Asymmetric Laminate Stable Regions in the Time/Temperature/Moist Domain

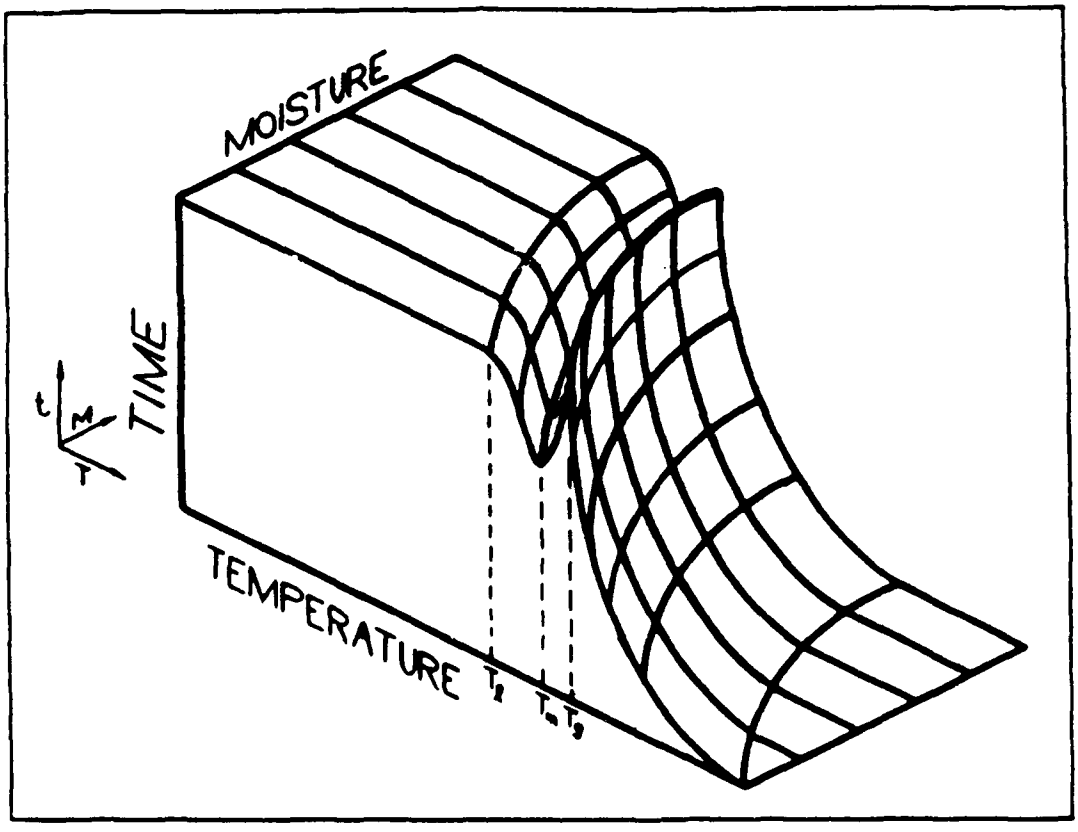

Fig. 9 - Stable Volume in the Time/Temperature/Moisture Domain

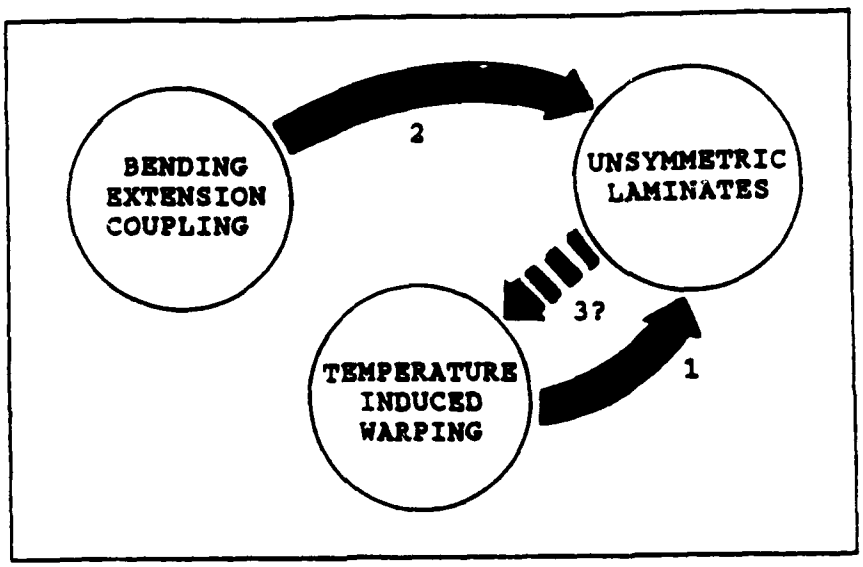

Fig. 10 - Logic Diagram for HTCC Laminates

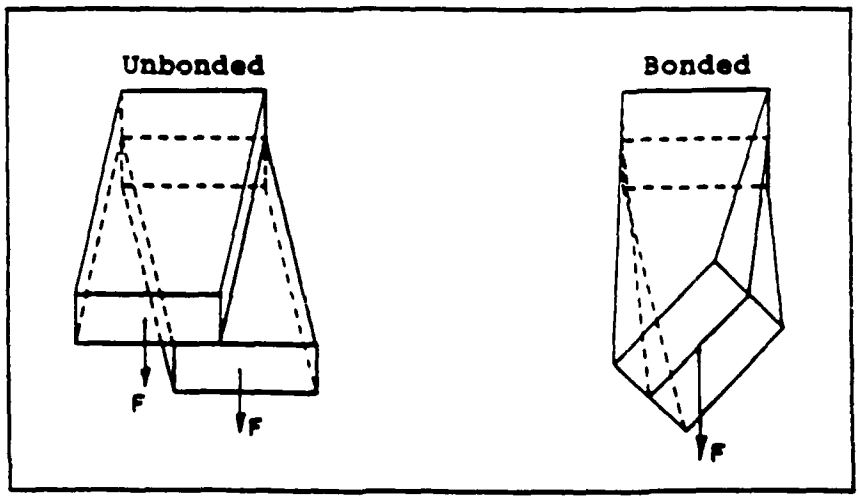

Fig. 11 - Tension-Shear Strain Coupling

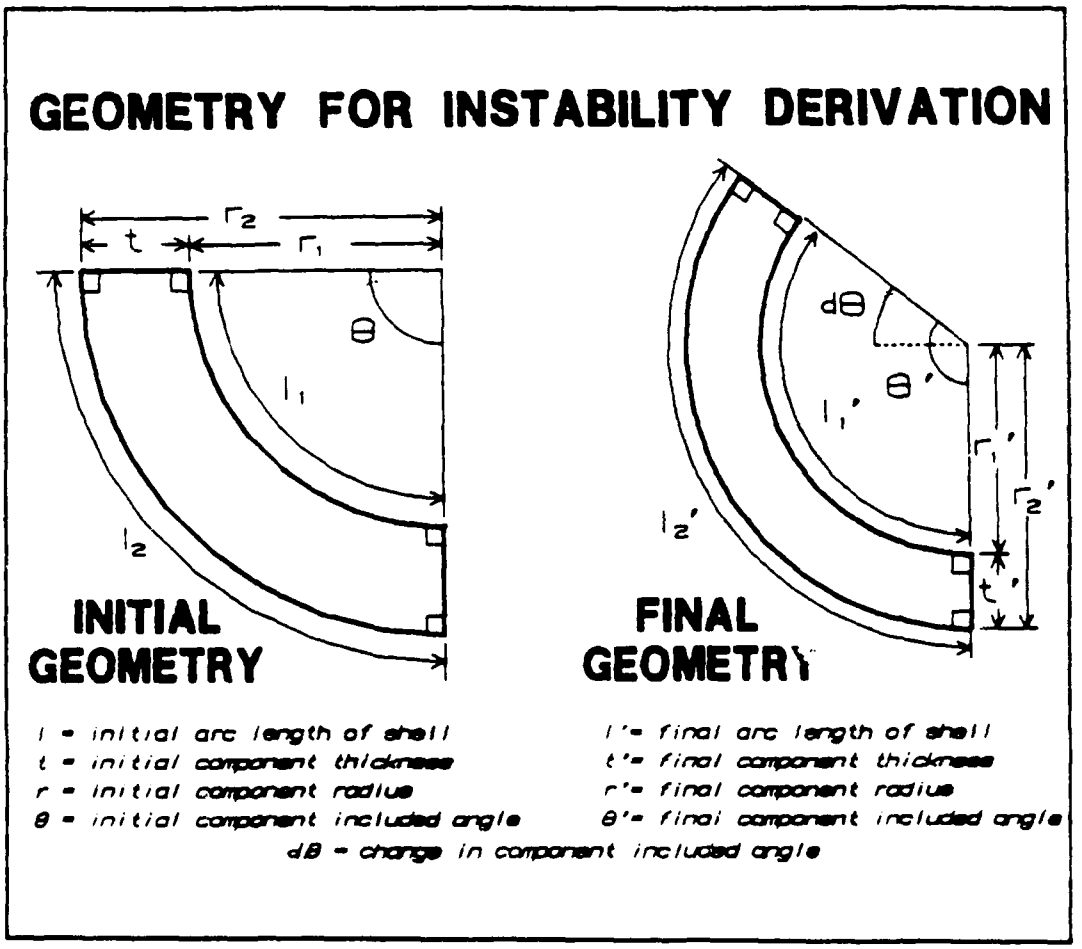

Fig. 12 - Geometry for the Derivation of Shape Instability

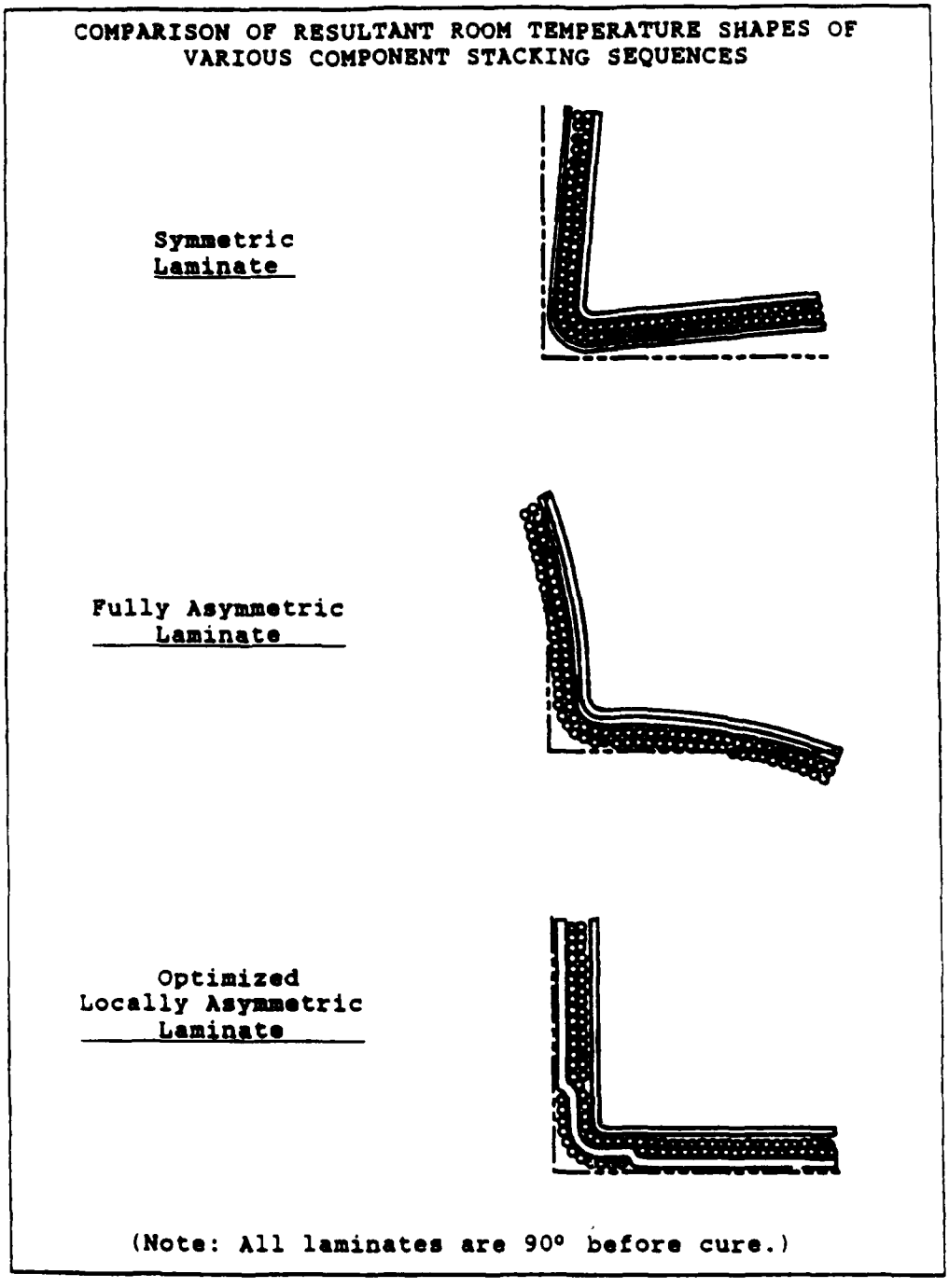

Fig. 13 - Schematics of Sample Room Temperature Composite Angle Shapes

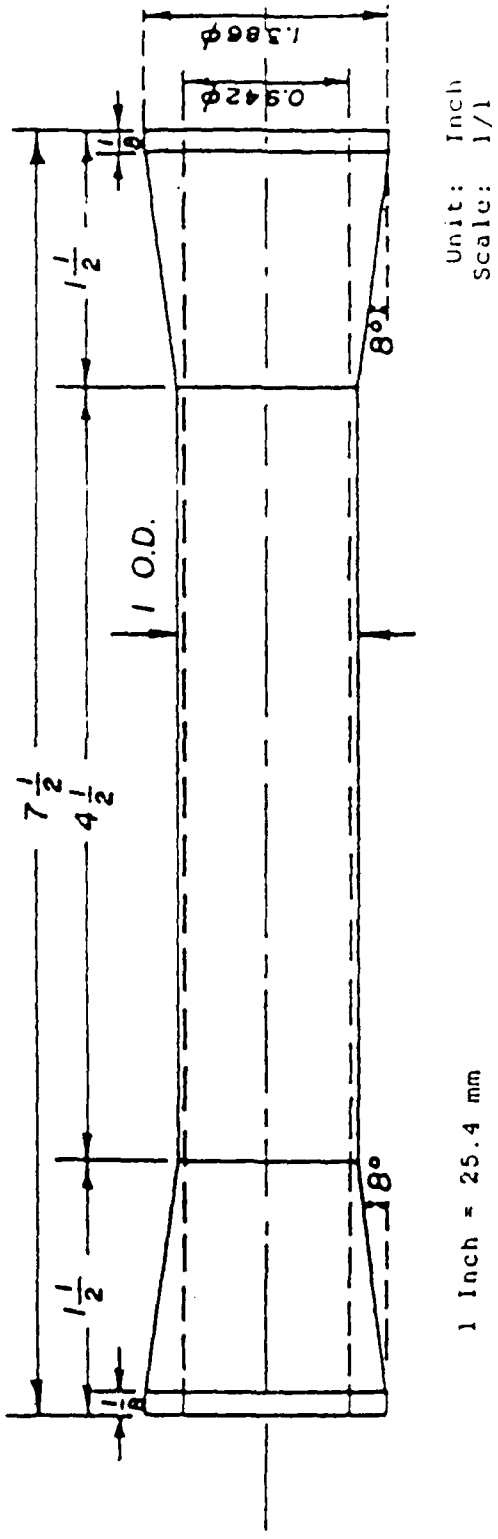

Fig. 14 · Thin-Walled Tubular Fatigue Specimen

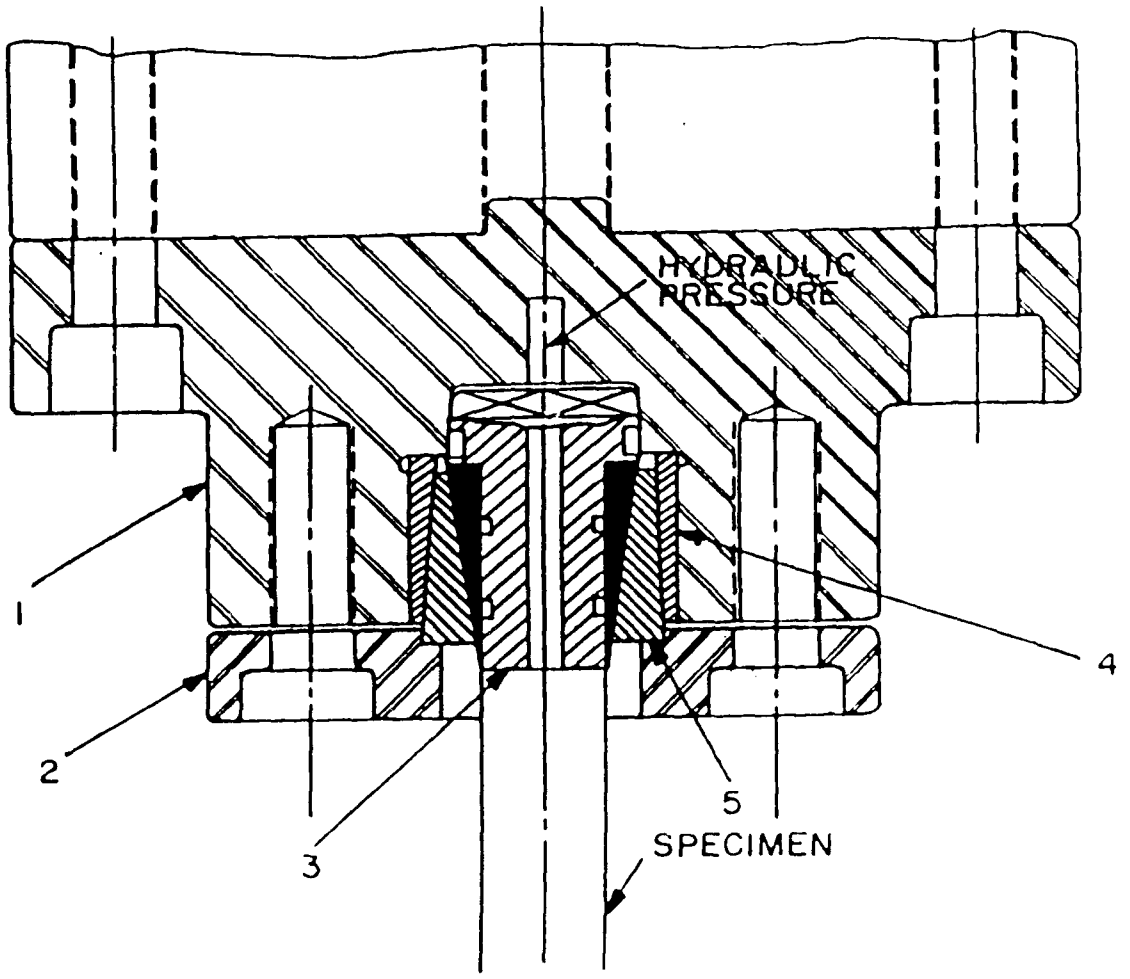

Fig. 15 - Assembly Drawing of Fixture: (1) Main Cylinder, (2) Cover Plate, (3) Insert with Square Ends, (4) Wedge, (5) Split Wedge

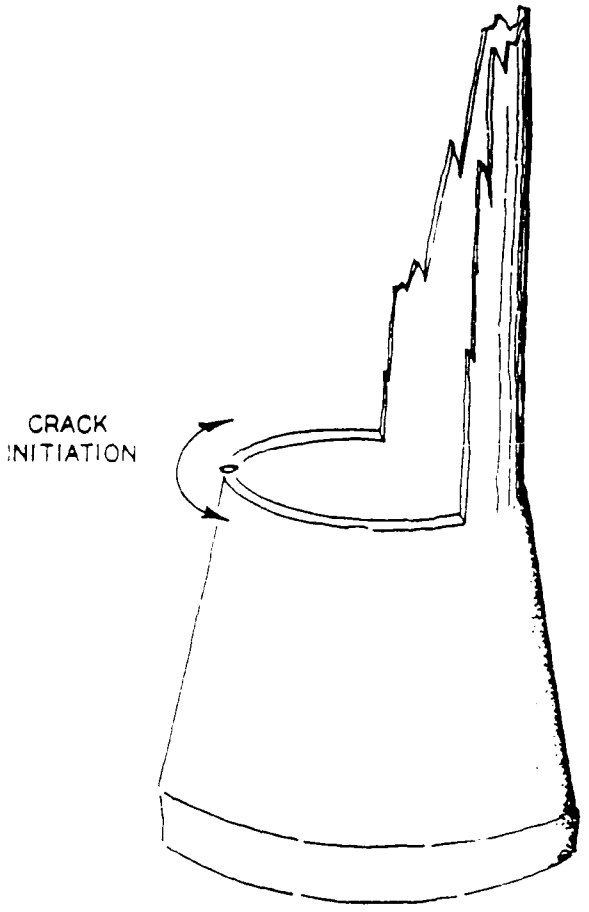

Fig. 16 - Premature End Failure of SP-328 Tapered Specimens

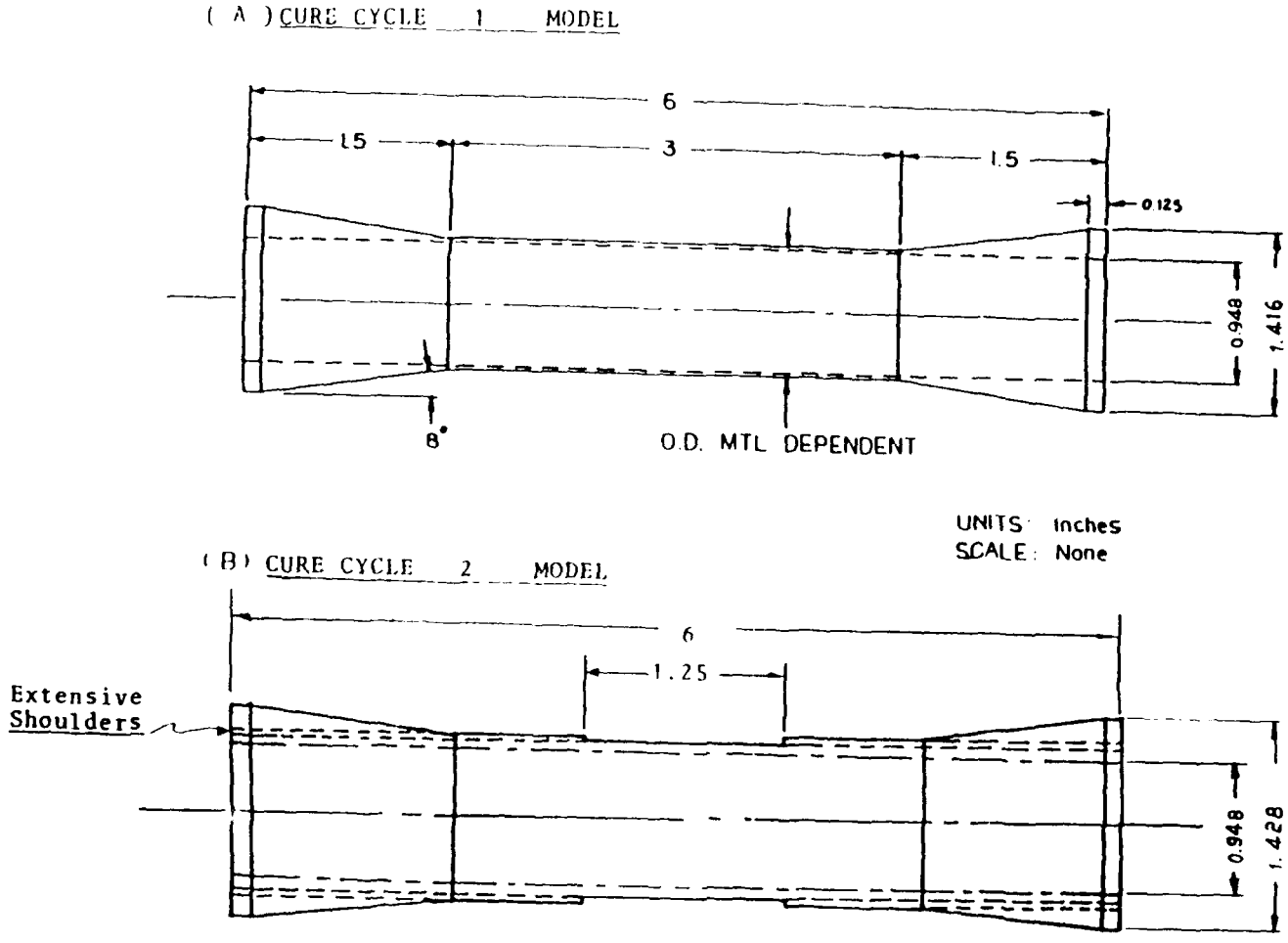

Fig. 17 - 6" Tapered Thin-Walled Tubular Specimen

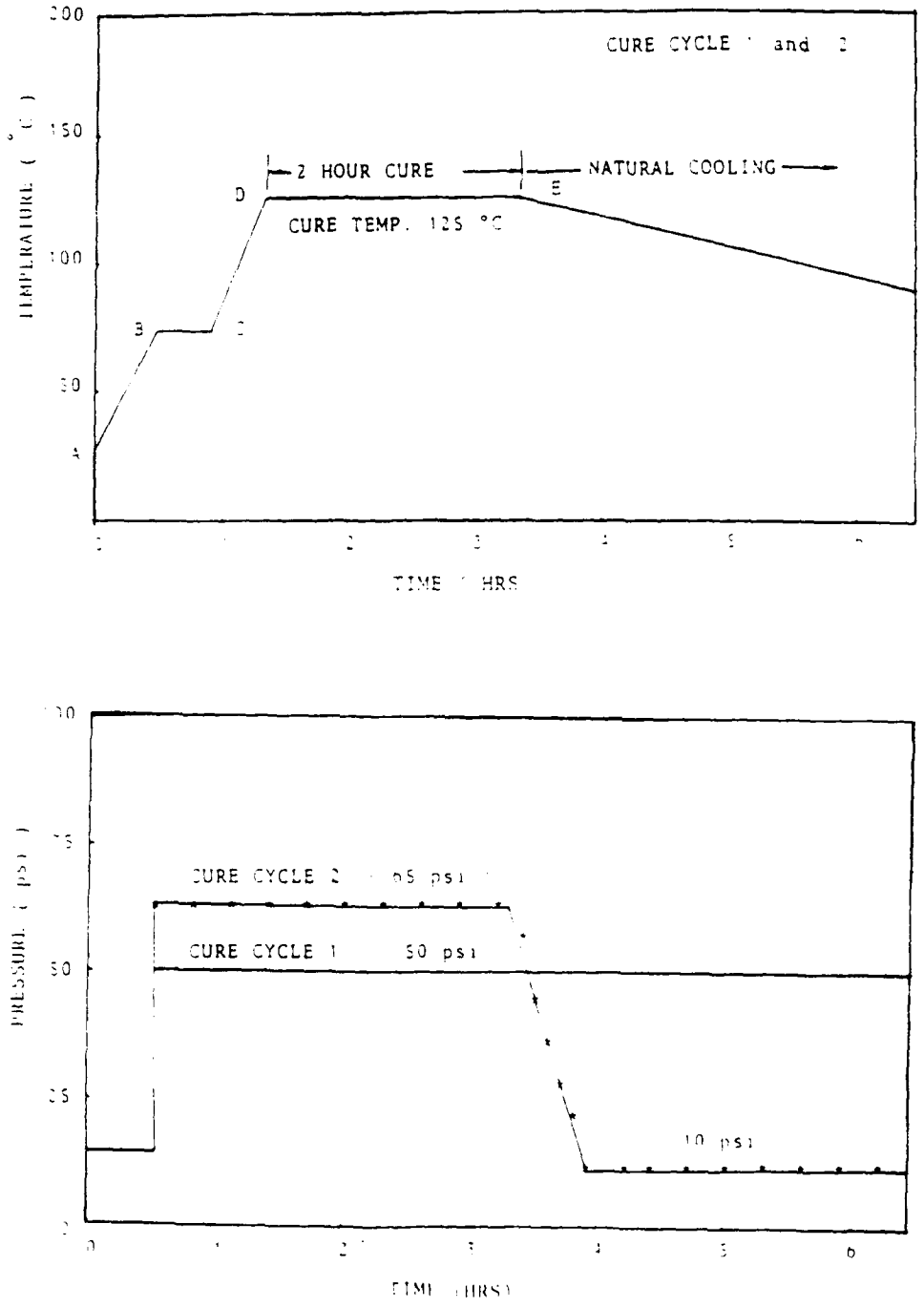

Fig. 18 - Cure Procedures (Kevlar 49 / SP-328)

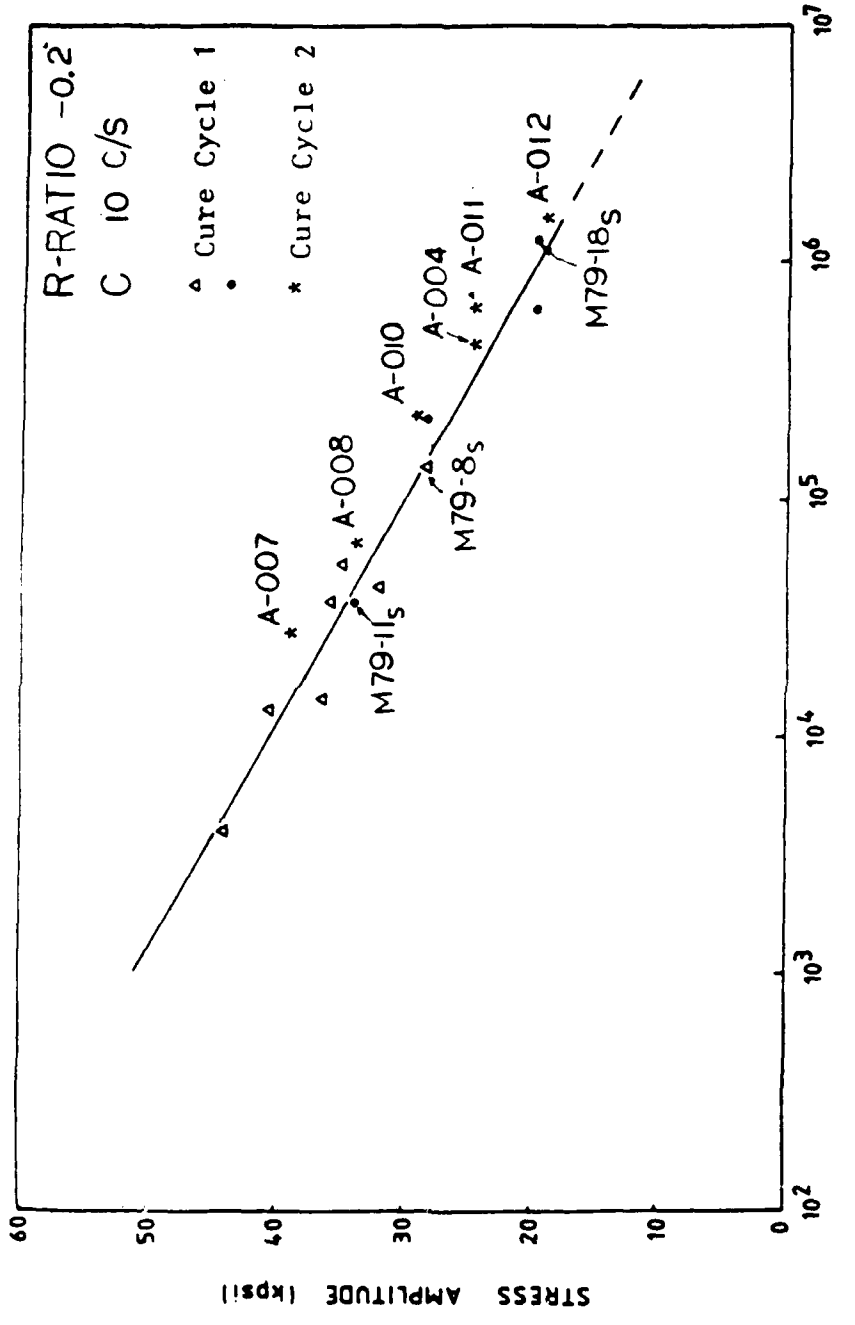

Fig. 19 · S-N Plot Kevlar 49 / SP-328 Tension-Compression Tests

Note: Specimens of Cure Cycle 1 fail near Grip Section
Specimens of Cure Cycle 2 fail near Gage Section

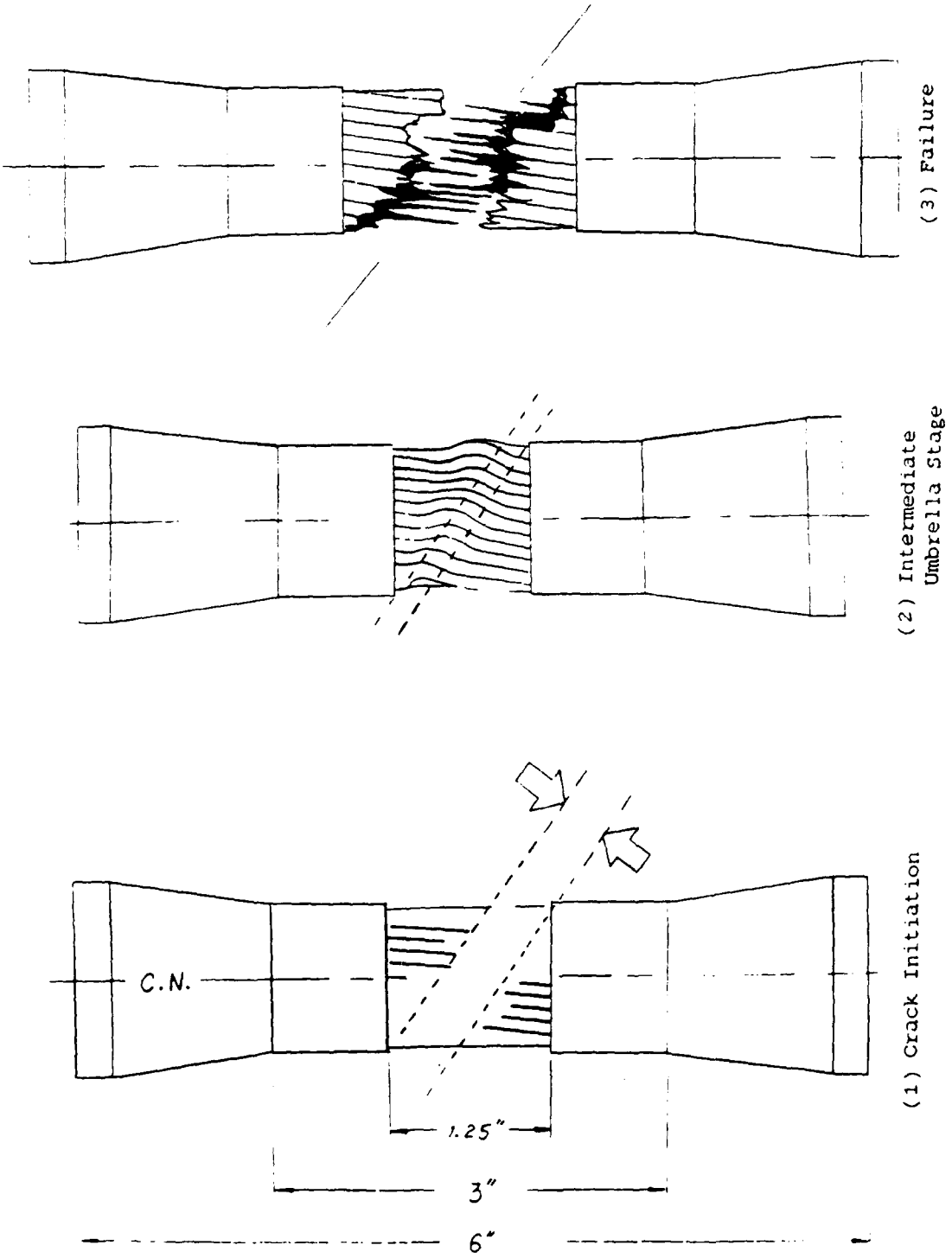

Fig. 20 - Kevlar 49 / SP-328 Tube Fatigue Failure (Cure Cycle 2 Model)

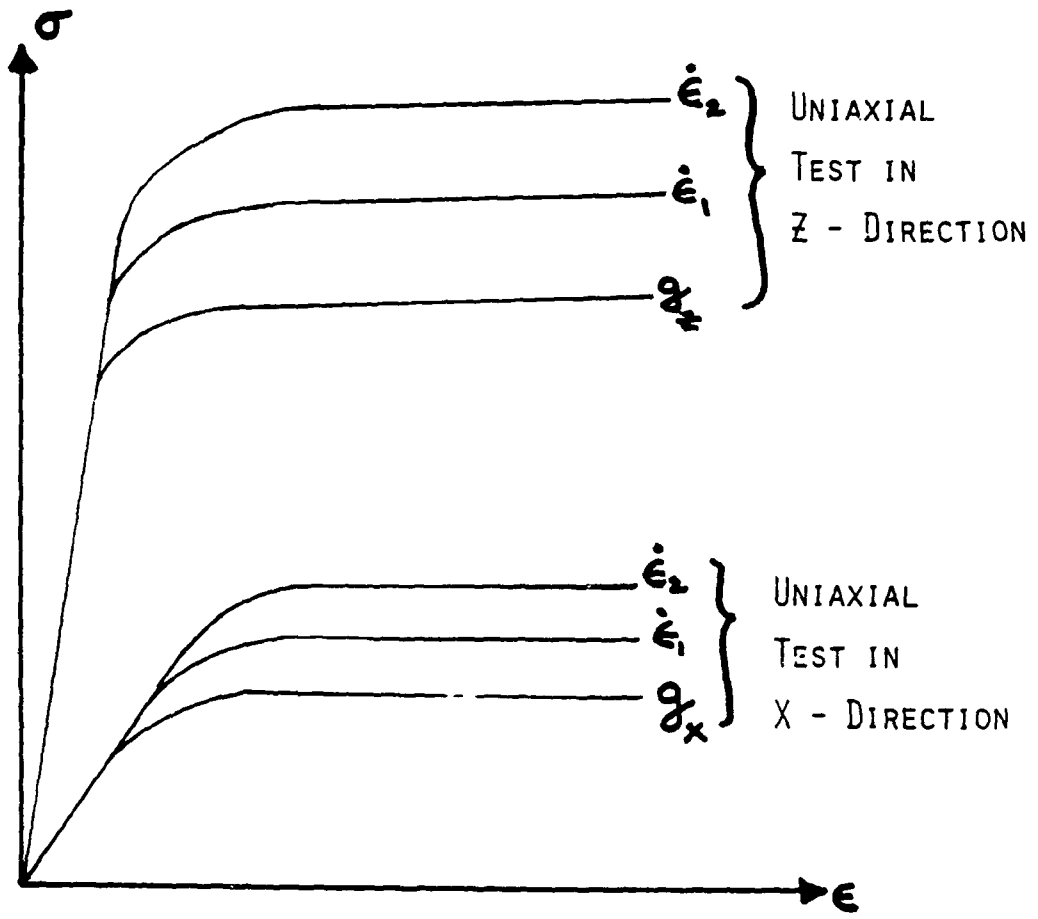

Fig. 21 - Material Behavior with Anistropic Viscoplasticity: Properties Depend on Loading Direction

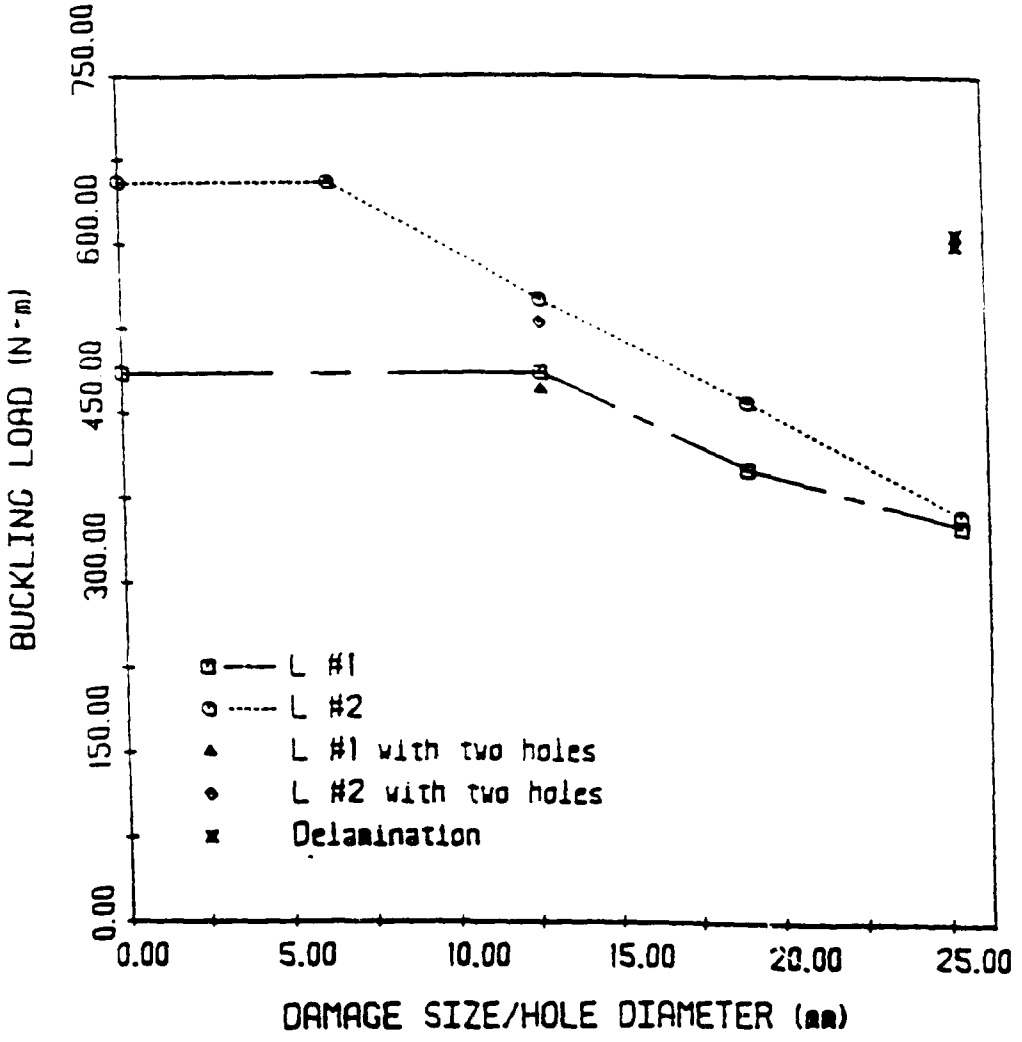

Fig. 22 - Residual Strength of Shafts with Holes and Delaminations
(Shaft layups and geometries are identified in Table 11)

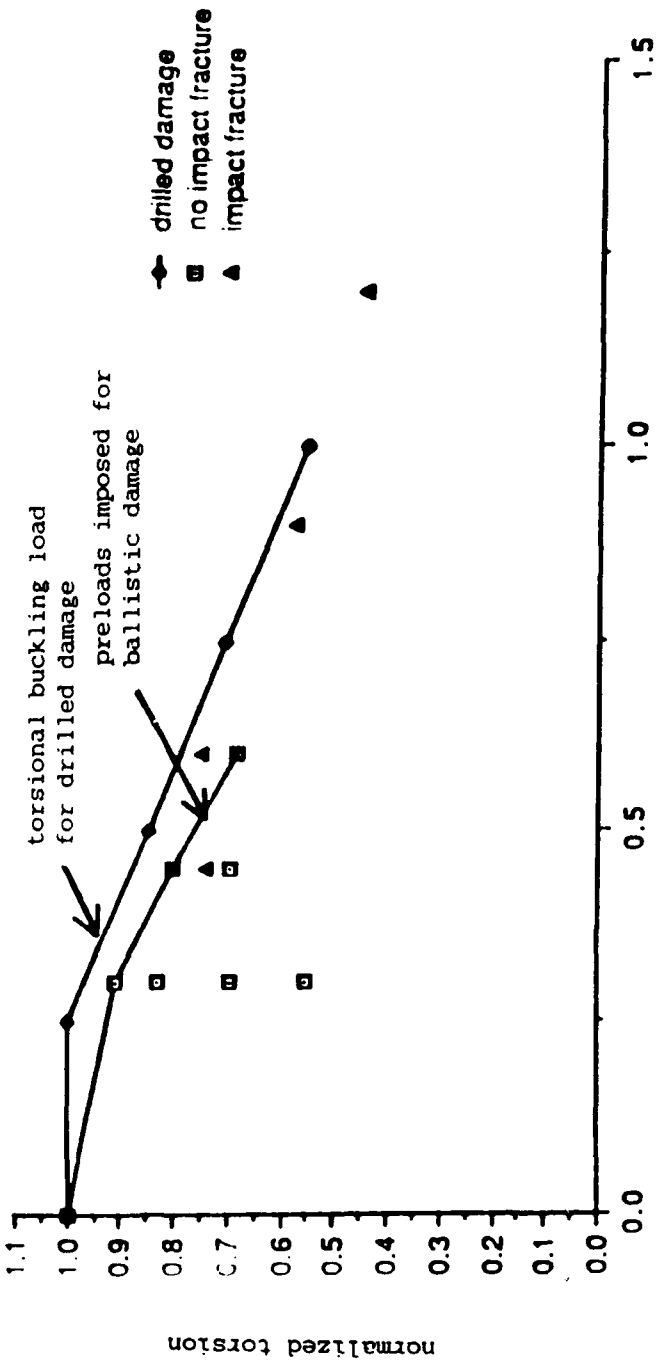

Fig. 23 - Normalized Critical Buckling Loads and Preloads vs Nominal Damage Size (in)

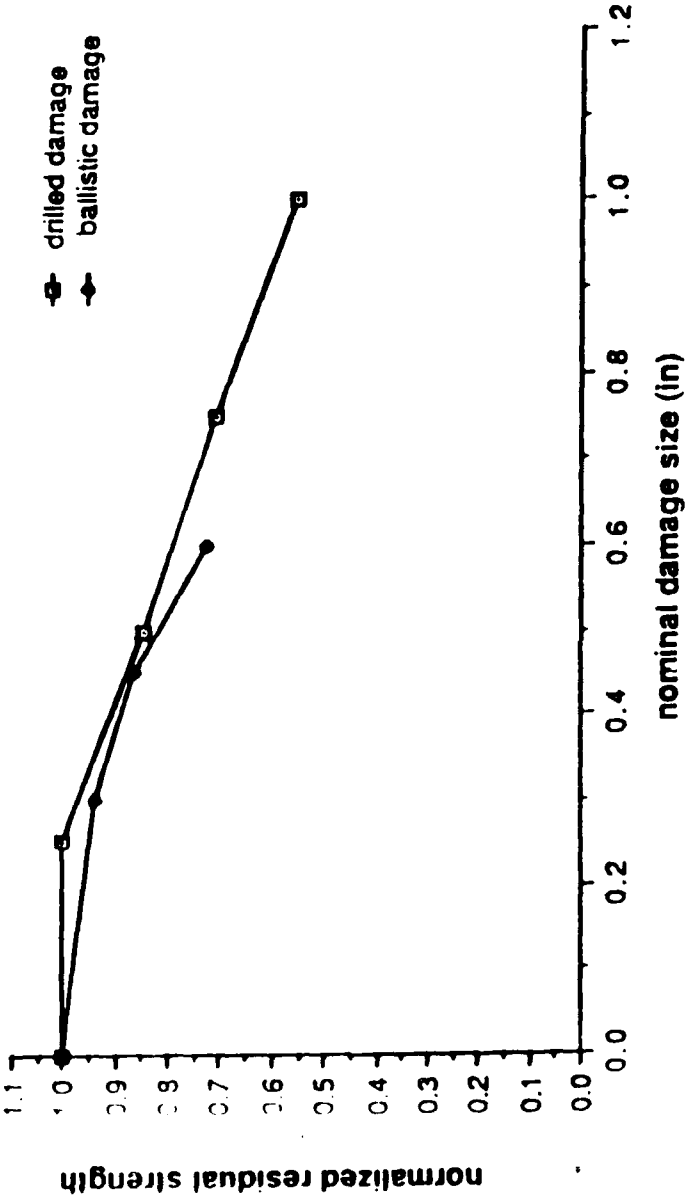

Fig. 24 - Normalized Residual Strength vs Nominal Damage Size (in)

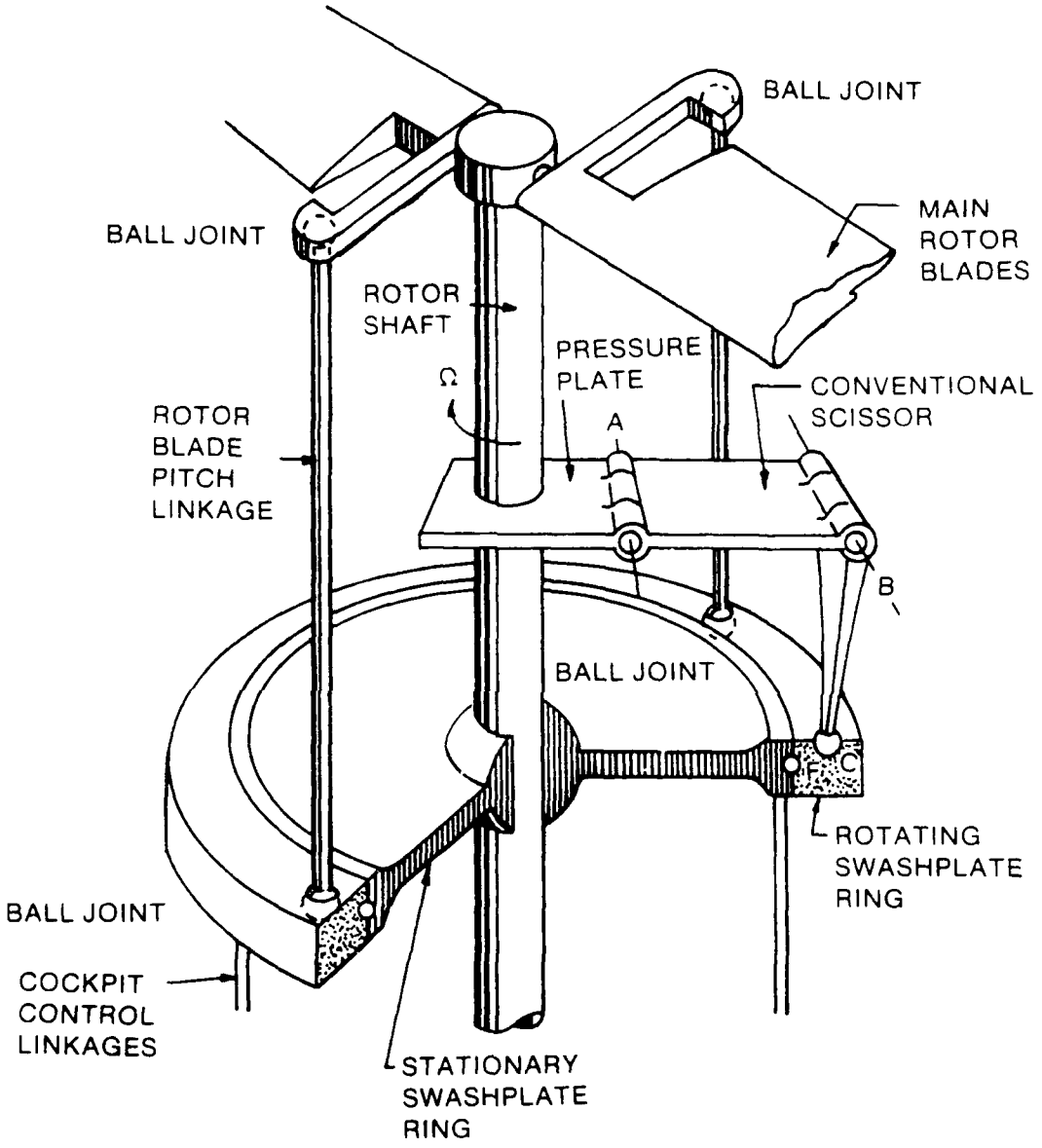

Fig. 25 - Conventional Scissor Configuration

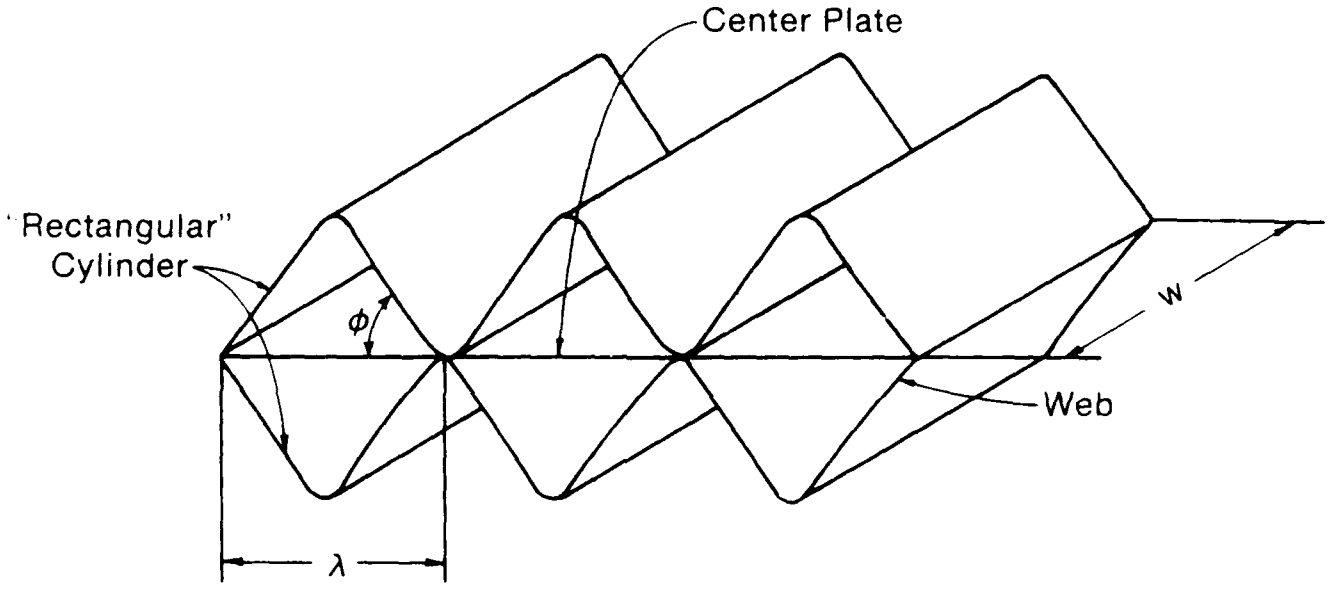

Fig. 26 - Section of Elastic Scissors Member

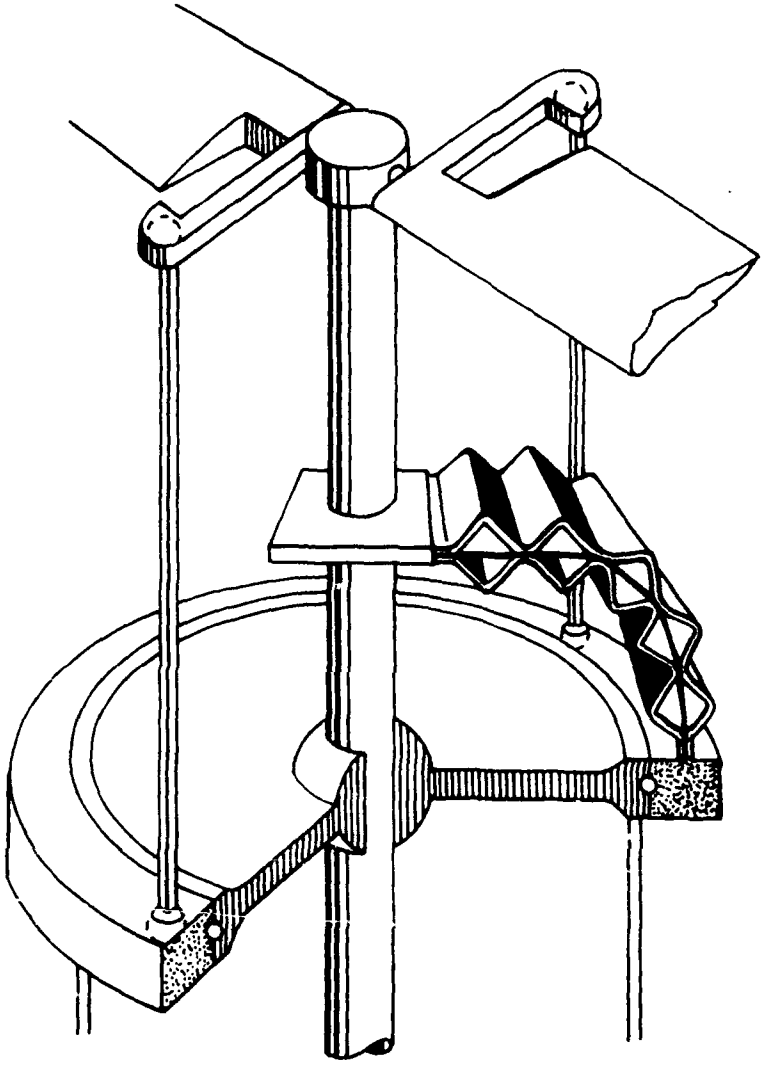

Fig. 27 - Composite Elastic Scissor Configuration Schematic

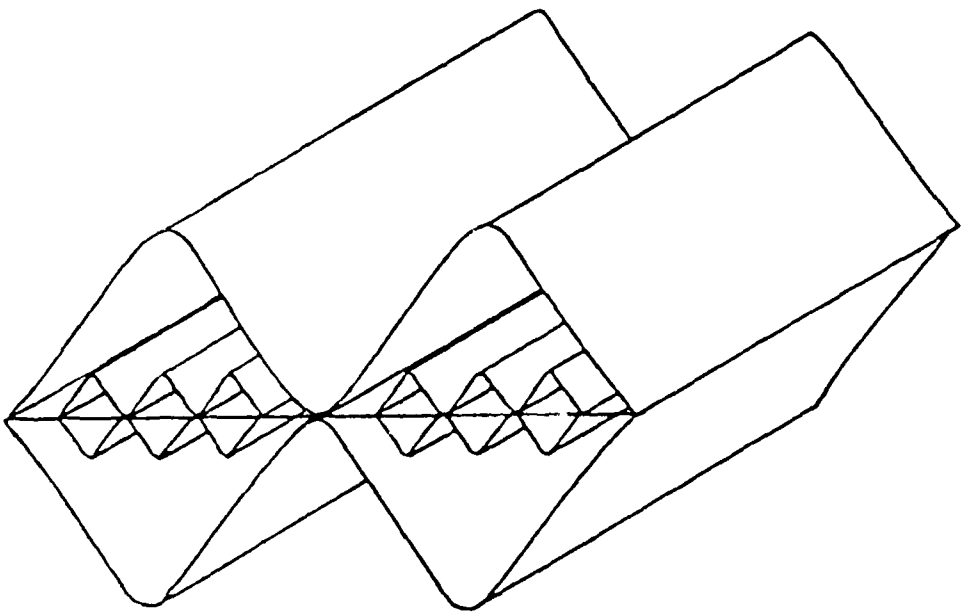

Fig. 28 - Section of Elastic Scissors Member with "Nesting"

TABLE 11

Analysis/Test Composite Shaft Connection Configurations and Results

(Material: Gr/E, Fiberite 1045 AIE)

Reinforcement Configuration	Bolt Pattern	Edge Diameter	Taper Diameter	Circular Pitch Diameter	Failure Torque lb. in	Analytical Prediction
Unreinforced	4 × 1/4" dia.	6.0	N/A	6.8	3095	2763 (-10.0%)
Ply Angle Cases:						
4 plies 0°	4 × 1/4" dia.	6.0	5.4	6.8	4355	4466 (+ 2.5%)
4 plies (total) ± 30°	4 × 1/4" dia.	6.0	5.4	6.8	4910	4765 (- 2.3%)
4 plies (total) ± 45°	4 × 1/4" dia.	6.0	5.4	6.8	5560	5843 (+ 5.1%)
4 plies (total) ± 60°	4 × 1/4" dia.	6.0	5.4	6.8	4730	5455 (+15.0%)
4 plies (total) ± 75°	4 × 1/4" dia.	6.0	5.4	6.8	4550	5252 (+15.0%)
4 plies 90°	4 × 1/4" dia.	6.0	5.4	6.8	4335	4683 (+ 8.0%)
Additional Edge Distance Cases:						
4 plies (total) ± 45°	4 × 1/4" dia.	3.0	8.4	6.8	5560	5328 (- 4.2%)
4 plies (total) ± 45°	4 × 1/4" dia.	1.5	9.9	6.8	4440	4987 (+12.0%)
Additional Circular Pitch Distance Cases:						
4 plies (total) ± 45°	8 × 1/4" dia.	6.0	5.4	8.4	9315	8931 (- 4.1%)
4 plies (total) ± 45°	4 × 3/8" dia.	5.3	6.6	4.6	7320	6492 (-11.0%)
Additional Taper Distance Cases:						
4 plies (total) ± 45°	4 × 1/4" dia.	6.0	1.8	6.8	5755	5564 (- 3.3%)
4 plies (total) ± 45°	4 × 1/4" dia.	6.0	1.1	6.8	5105	5189 (+ 1.6%)

TABLE 12

Graphite/Epoxy Torsional Buckling Specimen Construction
(Lay-ups, starting from innermost ply, and geometries)

Specimen	Ply Fiber Orientation (degs: 0 is along shaft axis)	Specimen Length L [m]	Specimen Radius R [mn]	Number of Specimens
L#1	15,-15,-45,-15,15,45	0.260	41.27	4
L#2	45,15,-15,-45,-15,15	0.260	41.27	4
L#3	-45,-15,15,45,15,-15	0.260	41.27	4
L#4	15,-15,15,-15,15,-15	0.330	37.33	6
L#5	30,-30,30,-30,30,-30	0.320	37.19	6
L#6	45,-45,45,-45,45,-45	0.320	37.42	6
L#7	0_2,45,-45,45,-45,0_2	0.320	37.42	4
L#8	0_2,45,0,-45,0,45,-45	0.320	46.86	5
L#9	0_2,45,0_2,-45,0_2,45,-45	0.320	46.90	4

TABLE 13

Comparison of Measured Values of Buckling Torque T_{cr} and Stress T_{cr} with Those of Theoretical Predictions for Clamped and Simply Supported Edges

Specimen I.D.	Experimental Data			Prediction (Clamped Edges)		Prediction (Simply Supported)	
	T_{cr} [N.m]	τ_{cr} [Mpa]	n	T_{cr} [N.m]	% Error	T_{cr} [N.m]	% Error
L#1	486	56	5	541	(11%)	523	(7.6%)
L#2	655	75	5	733	(12%)	712	(8.7%)
L#3	350	40	5	379	(8%)	366	(4.5%)
L#4	330	46	5	355	(7.6%	349	(5.8%)
L#5	390	55	4	540	(38%)	535	(37%)
L#6	490	68	4	495	(1%)	490	(0%)
L#7	543	56	4	557	(2.5%)	540	(-0.5%)
L#8	1575	105	4	1562	(-0.8%)	1544	(-2%)
L#9	2400	127	4	2543	(6%)	2491	(3.8%)

5.b. Structural Dynamics

5.b.(1). Optimizing Rotorcraft Drive Systems by Application of Advanced Composites (Sr. Investigator: M. S. Darlow)

Advancing the state-of-the art of drive shaft technology for rotorcraft through the use of advanced composites promises a number of advantages. By optimizing stiffness/weight and strength/weight relationships and facilitating supercritical operations, reduction or elimination of intermediate supports can produce reductions in empty weight and both first and life cycle costs. Furthermore, improved system reliability should result, due to a reduction in the number of components that comprise the drive train.

Both replacing an aluminum alloy shaft with one made of composite materials and minimizing the number of bearing supports result in weight savings. For a fixed distance between gearboxes, reducing the number of bearings increases the unsupported shaft lengths between the remaining bearings. This increase in unsupported shaft length decreases flexural rigidity. As this process is continued in the interest of reducing weight, the shaft flexural stiffness decreases to the point where the shaft must operate supercritically (i.e., above its fundamental flexural critical speed). This implies that a practical shaft balancing technique is necessary to control vibration amplitudes, and that external vibration dampers may be necessary to limit vibration levels. An assessment of the literatue on composite shafting indicated little effort to so optimize shaft designs and virtually no attempt at supercritical operation with composites. According, Rensselaer undertook, in July of 1983, research on advanced drive systems which has several phases. The first task was to contribute to the design of lightweight and cost-efficient composite tail rotor, synchronization, or interconnect power transmission systems for single main rotor, tandem rotor, and tilt-rotor rotorcraft, respectively, without compromising safe operation, reliability or aircraft availability, through optimization studies. Secondly, the construction of a rotating shaft test rig was undertaken which would be capable of confirming by suitable experiments the results of the theoretical and numerical studies. Lastly, shaft designs arrived at as optimal are to be so tested.

This research is seen as increasing abilities to design lighter power transmission systems with fewer components and higher reliability. But in addition the construction of an unique high speed shaft test facility available for both university and industry research is also anticipated as a substantial benefit. Through its use, it is hoped to demonstrate safe supercritical operation of composite shafts.

To ensure realism in this research, two tail rotor driveshaft designs, those used in the AH-64 and UH-60 single lifting rotor helicopters, and the synchronizing shaft design used in the CH-47 tandem helicopter were considered. The specific research goal was to maximize the weight reduction relative to the current designs. An analytical study sought to identify, for each design case and for a given number of mid-span supports, the composite fiber orientations which would provide the minimum

shaft wall thickness consistent with safe operation. Algorithms were developed, at increasing levels of sophistication, to arrive at least weight optimizations within specified constraints [Ref. 24, 25]. The features contained are: (1) lateral critical speed prediction analysis using a transfer matrix routine; (2) a Holzer routine to predict torsional natural frequencies; (3) elastic property characterization analyses for general anisotropic laminates; and (4) torsional buckling analyses for composite shafts [Ref. 22]. Constraints in an appropriate form based on the limits of acceptable shaft torsional fatigue strength and ballistic damage tolerance are still being sought for the optimization.

Optimal results were obtained for the AH-64 case showing that composite design methodology can be used to design subcritical shafts which are lighter than the conventional aluminum alloy designs, and that still greater weight savings can be obtained with supercritical composite designs. [Ref. 26]

Because the optimized designs developed during the current program are a significant departure from current production driveshaft systems, the experimental program is an inherant part of research investigating the viability of supercritical, composite driveshafts. To be specific, the purpose of the experimental study is to demonstrate that supercritical composite shafting, designed using the optimization procedures described above, can be operated safely. Thus, a test rig capable of running subscale shaft models at speeds in excess of their second flexural critical speed was designed and built. Since the experiments are to be performed at model scale, implementation of scale factors found in dimensional similtude studies ensures that the models adequately represent their fullscale counterparts.

Fabrication of the test facility is near completion at this writing. The facility consists of an enclosed test rig and a control station. Due to safety considerations, the test rig resides in its own ballistically shielded room. The test rig is powered by a 25 hp. variable speed drive capable of a speed range from near zero to 11,000 rpm. The drive and the adjacent bearing pedestal are mounted on a single plate which rests on a twelve foot long base plate. This drive and bearing assembly can be positioned anywhere along the base plate, thus providing the ability to test shafts with lengths between two and eight feet. A test shaft is supported at each end by rolling element bearing spindles which are hard-mounted to support pedestals.

The control station contains a number of instruments for monitoring shaft performance. The test shaft's speed is determined by a speed control unit with both manual (direct operator control) and automatic (closed loop) control modes. A digital tachometer measures and displays operating speed. A desktop computer has special interface boards installed which allow vibration data to be acquired in real time. Specially developed software resident on this computer calculates the magnitude and location of balance correction masses as needed to minimize the shaft's response at a given speed or set of speeds. The test shaft's vibration amplitude and phase information is measured by eddy current proximeters that output voltages to the data acquisition equipment which are proportional to the amplitude of the shaft's vibration. These signals are displayed on oscilloscopes so as to present shaft whirl orbits at several locations along the shaft in real time. A digital vector filter with an attached

plotter is also available to generate hard copy Bode and polar plots of shaft response.

The completion of this test facility is expected to provide an unique, high rotational speed, test facility featuring modern measurement and data acquisition equipment useful as a state-of-the-art test bed both for Rensselaer Rotorcraft Technology Center researchers and engineers in the broader helicopter community.

An aluminum shaft has been procured as the first article scheduled for test. This was chosen because it is desirable to deal initially with a material which has well understood characteristics. Further, since aluminum alloy shafting is in common use in production helicopters for power transmission, this shaft will establish a basis for comparison with the results of the subsequent composite test program. Four carbon/epoxy shafts are scheduled for these tests. The first composite shaft test will model an Ah-64 tail rotor driveshaft. The goals of the initial series of tests are a verification of the design criteria, a determination of the sensitivity of results to unbalance, an estimate of the influence of internal damping on supercritical operation, and a demonstration of the ability to arrive at balance configurations satisfactory for passage through multiple critical speeds.

Results obtained to date in this research and a description of the test facilities are contained in Ref. 27.

5.b.(2). Fuselage Natural Frequencies and Mode Shapes

To develop a useful structural dynamic analysis for helicopter fuselages is considerably more difficult than what has customarily been done for fixed-wing aircraft fuselages. There are several reasons for this. First, a fixed wing aircraft fuselage is fundamentally a closed structure, with relatively few openings; eg windows, doors, and - for transport - types a loading ramp. Second, the first vertical and lateral bending and first torsion modes have the greatest effect on the critical wing and tail flutter (aeroelastic instability) speeds, so that only those modes need be predicted accurately for fixed wing aircraft. These lowest modes also happen to be the easiest to predict accurately.

Helicopter fuselages are another matter. Their fuselages seem, sometimes, to be all windows, doors and ramps - especially on smaller aircraft. Furthermore, their modes and frequencies are more important in determining forced vibratory response than aeroelastic instabilities. Finally, the forced response usually is determined by frequency components at bQ -- where b is the number of blades and Ω the rotor rotational speed -- or higher, and that bQ principal excitation frequency is well above the lowest modes. Primarily for these reasons, accurate prediction of helicopter vibratory modes and frequencies continues to elude rotorcraft engineers, particularly in the design stage; this despite finite element analysis of great complexity and sophisticated test and correlation programs. This state of affairs prompted Rensselaer to initiate four structural dynamics programs aimed at improving fuselage vibration prediction capabilities; (1) improved methods for generating helicopter airframe analysis models, (2) development of new analysis techniques for efficient and accurate prediction of airframe structural dynamic characteristics, particularly in the design stage, (3) developing an experimental facility for shake-testing full scale helicopter airframe components, which can be used for basic research into the sources of difficulty in accurately quantifying the dynamic characteristics of helicopter airframe components and (4) a general methodology for efficiently analyzing the effects on the frequency responses and/or mobilities of the unmodified airframe as a result of making multidimensional changes.

5.b.(2).(a). Helicopter Airframe Analysis Model Generation
(Sr. Investigator: M. Shephard)

It is generally true that a routine, finite element vibration analysis model of a typical helicopter fuselage takes a calendar year to assemble and is not usually undertaken at all until the fuselage structure has been rather fully designed, for strength purposes. Rensselaer embarked, therefore, on the development of a geometry-based modeling technique that would allow the efficient creation of airframe analysis models within the geometric modeling environment used to define an airframe; i.e. knowing only external contours, internal spaces, the position & size of windows & doors, gear box and engine attachment points, etc. The generation of any analysis model for helicopter airframes is complicated by the fact that the geometric entities are defined so that, taken together, they constitute finite element components of a lesser geometric dimension than the structural element contained in the design system

that they represent. That is, the basic elements of the finite element model will usually only be part of a complete frame, longeron, bulkhead, etc. This dimensional reduction is carried out as part of the idealization process (Ref. 28) necessary to reduce the overall geometric representation of the airframe to one amenable to facile structural analysis. The information controlling the idealizations performed - the "break-down" for the purpose of analysis - is typically known only to the analyst. This idealization then is related to the process of generating the analysis model through a "manual" process; one in which experience, judgement and choice are involved. As a consequence, the process of generating a finite element model for an airframe is dominated by "manual" operations and is a basic reason why it typically takes something approaching one calendar year (and one person-year) of effort.

Our initial efforts (circa 82-83) at reducing the time required for this task considered the development of special purpose airframe design procedures that would facilitate the construction of analysis models from the design model. Contacts made with industry to insure relevance in this research are given in Table 14. The development of an interactive graphics program for airframe structural design progressed to the point where the basic helicopter shells could be defined and the user allowed to interactively establish frame stations by choosing either planar or non-planar "cuts" with which to intersect the cylindrical or conical airframe shell. The calculated intersection curves were then passed to a member-detailing module. Choice of frame and longeron cross-sections was also implemented, including both a library of commonly used shapes and the capability to define member cross-sections by build-up of quadrilateral primitives (Ref. 29). The next step in the development of this graphics program was to be the implementation of section property calculations, addition of a skin discretization module, and interfacing the program with analysis.

Although a technically viable approach, we soon come to the realization that this system development did not address the reality of the airframe industry, where major investments had been and continue to be made in computer-aided geometric design systems. These systems obtained at high first costs, implemented with a subsequent investment of engineering manhours and maintained with continuing input of both, clearly would not be supplanted by a university prototype, irrespective of its stand-alone virtues.

Based on this realization and industry's need to maintain and update their operative geometric design software, we began to consider an approach that would allow the specialized analysis model formulation procedures outlined above to be performed using information contained in the kinds of geometric representations which exist in the computer aided design systems currently used in industry. In this approach the first task to be carried out is taking raw geometric information from the design system data bank and grouping it by function, based on the structural entities this information defines (Refs. 30 & 31). The result of this process is a functional classification tree which carries basic input into the second part of the process. The second part then "decides" or indicates how that collected geometric information is to be idealized in the analysis model. Since the information used to perform the idealization process must be based on the knowledge of experts, knowledge-based techniques are used to computerize that information. This requires that analysis

modeling rules be loaded into the inference engine of an expert system which then examines the information in the functional classification tree and specifies how it is to be represented in the analysis model. As the third and final step, generic modeling routines then create the analysis model from these two sets of information.

In short, this research turned to the attempt to develop an "expert system"-based approach to flexible, automatic conversion of a geometric model produced in a CAD system to a generic structural model and then to a structural finite element model. The approach thus emphasizes use of existing knowledge to allow the computer to carry out as much of the time-consuming, model-building task as possible.

The definition and design of the components for such a flexible, automated conversion system, then, include:

i) Geometry Extractor - extracts geometry from the geometric modeler;

ii) Classifier - examines and orders features that are relevant to the airframe structure;

iii) Arbiter - determines, based on rules placed within it and user interaction when needed, how the geometric structural pieces will be converted to a finite element model;

iv) Rule Maintenance System - used to build and update rules in Arbiter;

v) Application Routines - based on decisions made within the Arbiter, converts the geometric pieces into a generic finite element model;

vi) FEM Translator - converts generic finite element model data into a form compatible with the specific FEM package being utilized.

The classifier was brought to the point where it currently accepts geometry from the CATIA™ modeling system. CATIA™ is being integrated into Sikorsky Aircraft's design procedures, for example. Sikorsky, which is a supporter of Rensselaer's Center for Integrated Computer Graphics industrial associates program, is actively tracking this project, and supplying technical input as well as CATIA™ models of portions of actual airframes to test with the procedures developed. Functional designs of the arbiter and rule maintenance system have also been completed using, in this portion of the procedure, an expert system developed at IBM (PRISM™).

As suggested by the four Rensselaer-generated references cited in the above paragraphs, substantial progress has been made in this research. Recent efforts have been considering how the analysis process might be moved farther forward in the design process, by allowing sensible models to be generated and useful analyses to be performed when minimal early design information is available. In particular, to be able to perform trend analyses (eg "the third coupled side-bending/torsion mode frequency will vary +3% and - 5% by increasing or decreasing the cockpit bulkhead skin gage by +.01" or -.01", respectively) before all the geometric information is

defined. In such cases the functional classification must be defined first. Next, overall geometric constraints and basic positioning decisions must be introduced and reflected in the geometric representation. Our approach contends that this is enough information to allow the numerical analysis model to be constructed, with trial properties assigned to the structural entities which remain in question. The analysis results would then be used to establish the properties needed for the structural entities. Those results would then be used to help finalize details in the geometric entities in the geometric model. This last effort is in its early stages of development. Support for this work under the ARO contract was considered to have been sufficient to make it self-supporting at the end of the subject contract, in January 1988. Continuing support is now being provided by members of the airframe industry.

5.b.(2).(b). New Helicopter Fuselage Structural Dynamics Analysis Methodology
(Sr. Investigator: M. Shephard)

The dynamic analysis of complex structures such as helicopter fuselages is usually accomplished by the application of finite element methods in which the number of variables in the solution process associated with mass motion is greatly reduced from that of the number of finite element "nodes" needed for the static analysis required to establish the load-deflection relations within the structure. The common methods of performing the reduction of system size, Guyan reduction and component mode synthesis, for example, all reduce the accuracy of the dynamic computations in ways which are difficult to predict. Furthermore, as a design methodology, the FEM - Guyar Reduction process leaves much to be desired. It is not clear how one would generalize reanalysis capabilities which preserve substantial parts of a "base-line" calculation for use in predicting the effects of structural and/or mass changes when their location is not known at the outset.

The goal of this research was, therefore, to develop an alternative analysis approach that would (a) maintain the flexibility and structural analysis accuracy of the finite element method, (b) allow the number of unknowns in the dynamic solution process to be reduced without introducing unqualified inaccuracies into the process and (c) provide for a generalized, efficient reanalysis capability. Our approach was to combine finite element methods (FEM) with transfer matrix methods (TM). The latter method suggested itself since it is known to provide accurate dynamic solutions to primarily one-dimensional structures with relatively few degrees of freedom (fuselages tend to be considerably longer in one direction). In addition, because of the associative law for matrix multiplication, the transfer matrix calculations can proceed simultaneously at a large number of independent points on the structure, thus facilitating reanalysis.

Previous attempts to combine finite elements and transfer matrix (FETM) techniques considered standard stiffness finite element representations. This lead to formulations with the restriction that the number of nodes on the two ends of the massless, structurally complex analysis element (across which one state vector must be "transferred" to another adjacent "state vector") must be the same. This restriction

if allowed to stand, would remove one of the main advantages of the finite element method. Our approach (Refs. 32 and 33), therefore, developed and employed a full, "mixed" formulation, based on the Reissner energy functional. As with the standard transfer matrix analysis method, this form has both force and displacement quantities (the "state vector") as inherent unknowns in the formulation. This additional freedom in the selection of variables removed the restriction requiring the same number of nodes on both ends of a substructure. After an Eigen value and Eigen vector extraction technique was developed, examples with both increases and decreases in the number of unknowns on either end of a set of substructures - "up-hill" and "down-hill" transfers, respectively - (Ref. 32 and 33) were analyzed with this procedure. The technique was compared with a standard finite element modal analysis and demonstrated equivalent accuracy for decreased CPU time requirements.

One of the issues that arose in the generalization of these procedures was the determination of the specific nature of the force-type quantities introduced by masses in motion at their point of introduction between substructures. The Reissner based, combined finite element transfer matrix (FETM) formulation allowed consideration of both stress and force resultants as variables. Choices as to which of these to transfer between substructues can, then, be made. Numerical examples were run transferring displacements and tractions, as dictated by the standard transfer-matrix procedure, on the one hand; and transferring displacements and stresses, as possible in the pure mixed finite element formulation, on the other hand. As expected, both approaches converged to the correct answer. These numerical results also indicate that for a given mesh there is a slight loss in accuracy if tractions are transferred instead of stress components. However, the transfer of stress does entail additional numerical complications and complexities. Procedures for transferring just forces and displacements were formulated and implemented with some confidence that they would be simpler. This appears to lead to numerical conditioning problems in the final matrices.

Publications and presentations of these basic numerical analysis advances have been made as the results were developed (see Refs. 32 and 33) and a thesis is in preparation dealing with the last of the problems discussed here, namely numerical conditioning. Here again ARO support was considered to have moved the research sufficiently forward to allow other sources to continue it. Current research efforts are investigating means by which the numerical conditioning problems can be eliminated.

5.b.(2).(c) Helicopter Fuselage Shake-Testing Research
(Sr. Investigator: R. Bielawa)

This project was initiated late in 1985 with the objective of developing a dedicated experimental facility for shake-testing full scale helicopter airframe components. Because it was - and is - intended for use in basic helicopter vibrations research, its design emphasized characteristics which would allow accurately quantifying the dynamic characteristics of such components in a diagnostic manner. That is, the results of structural dynamics testing in this facility are intended to

increase understanding of the various phenomena involved so as to contribute to improved abilities to predict helicopter vibration.

An existing vibration isolation pad in the high bay area of Rensselaer's Jonsson Engineering Center was modified to accept rigid mounting of a "strong back" support structure. The design of this structure was the work of graduate student J. Gordis. Finite element (FEM) analysis using the mathematical model shown in Fig. 29 required several iterations before the strong back's lowest natural frequency could be made as high as 100 Hz. The completed strong-back, which was constructed of welded steel plate by an off-campus foundry/metal fabrication company, was delivered in January 1987. It is a four ton structure, fixed to the isolation pad at six points. The nature of these attachments was shown by the analysis to be critical to achieving the specification frequencies. An adapter ring makes it possible to mount various helicopter structures with a minimum of difficulty. A 7-1/2 ton travelling crane in the high-bay area facilitates movement and installation of test items and hanging or placing the larger electro-magnetic shakers. Random impact and "burst chirp" testing of the structure installed on its vibration isolation pad with no fuselage components installed (see Fig. 30) confirmed the FEM predictions of both its mode shape and frequency. This comparison is shown in Figs. 31a and b.

In early 1986, three helicopter tail cones were acquired for testing. Two are OH-58A tail cones, one metal monocoque, one composite, the third is an S-55 tail cone (metal monocoque). Both OH-58A tail cones, which include horizontal tail surfaces, were provided by the U. S. Army at Ft. Eustis. The S-55 was donated by the Sikorsky Aircraft Division of U.T.C. Another donation in 1987 by Rotorcraft Parts, Inc. of Sanford, Florida together with matching funds provided by Rensselaer made the corresponding tail rotor drive system parts available for the S-55 tail cone. Fig. 32 shows the full scale S-55 structure with drive system mounted on the strong-back.

A suitable IBM PC based finite element analysis was selected (COSMOS/M) and acquired in 1987 for accomplishing the finite element fuselage analysis tasks required to conduct research using this facility. The vibration testing equipment (ie shakers, sensors, data analysis systems, and recorders) listed in Table 18, Section 6 of this report, completed the remaining needs. Preliminary modal shake tests were conducted on the composite OH-58A tail cone, largely for facility familiarization purposes. At this point, the facility development is considered complete.

A first helicopter fuselage experimental research contract using the facility was awarded during the summer of 1987 with a start date of September 1, 1987. It is reasonable to expect that similarly useful projects will follow.

5.b.(2).(d) Generalized Analytical Testing Methodology
(Sr. Investigator: R. Bielawa)

A general methodology development was undertaken in the first half of 1986 to increase the efficiency of analyzing the effects of multidimensional changes to

airframes on their dynamic characteristics. Of particular interest was the result of such changes on frequency responses and/or mobilities. This new methodology was intended to allow modified flight responses (displacements, stresses, strains, etc.) due to complex mass or structural modifications to be calculated easily, to synthesize complete structures whose substructures have a variety of damping levels, to account for the addition of discrete vibration alleviation devices, and to be especially useful for interfacing structural components which are characterized using a mixture of analytical and experimental results. The approach formulated the method in the frequency domain and based it on a generalized substructuring scheme. Included in this study, which was the work of graduate student Bjorn Jetmundsen, are applications relating to vibration optimization and - because the methodology deals with strain distributions throughout the structure - criteria for fracture.

This research profited a great deal from the active and continual participation of Mr. William G. Flannelly of Kaman Aerospace and resulted in the doctoral thesis of B. Jetmundsen, listed in Appendix C. In addition to accomplishing all of the methodology formulation goals set for the project at its outset, a sample analysis was successfully performed using a 92 degree of freedom mathematical model of the AH-1G Bell Helicopter based on shake test results as supplied by Kaman. The new method was used to evaluate the effect of adding a heavy external store under the left (port) wing of the AH-1G aircraft attached by members that provided both stiffness and damping. The forced dynamic response of the entire airframe in a left rolling pull-out was calculated and compared with results for the helicopter without the external store. To make the analysis manageable within the time allotted, it was assumed that the applied loads were unaffected by adding the external store. The analysis results for vibratory response corresponded completely with those obtained in Ref. 34.

5.b.(3). Effect of Blade Construction Methods on Elasto Dynamics
(Sr. Investigator: R. G. Loewy)

A brief but fundamental examination of the way the structural dynamics of rotor blades is affected by typical construction techniques and the application of composite materials was conducted by a post-doctoral fellow, Dr. Gabriel Amazigo. In these analyses, a mathematical model was developed which includes three orthogonal components of extension (two in the plane of the blade cross-section), two orthogonal components of flexure, shear deformations and torsion. Pretwist was accounted for and the typical rotor blade cross-section profile was treated as a multiply-connected domain. The rotating, free-vibrations of a composite blade whose centroidal and elastic axes coincide, but whose center of mass is not coincident with them were examined with all rotary inertia effects included.

Numerical computations were performed using this mathematical model for several cases. The rotor blade example chosen has a blade length of 288 inches and chord of 21 inches. Its construction configuration was taken as similar to that used on the YAH-64 advanced attack helicopter main rotor blade. Leading and trailing edge caps, five internal tubular members and a Kevlar/graphite/Kevlar skin were assumed with typical stiffness and mass characteristics. Four uncoupled, free vibration cases were analyzed both non-rotating and rotating. In addition, these equations were also solved for cases with uniformly increasing rotational speeds, in which the degrees of freedom are coupled by time dependent-coefficients.

Although no particularly startling conclusions were drawn from the results of these studies of about 8 month's duration, they did produce one unexpected result; namely, that the elastic properties of rotor blade leading edge balance weights can be too influential to ignore.

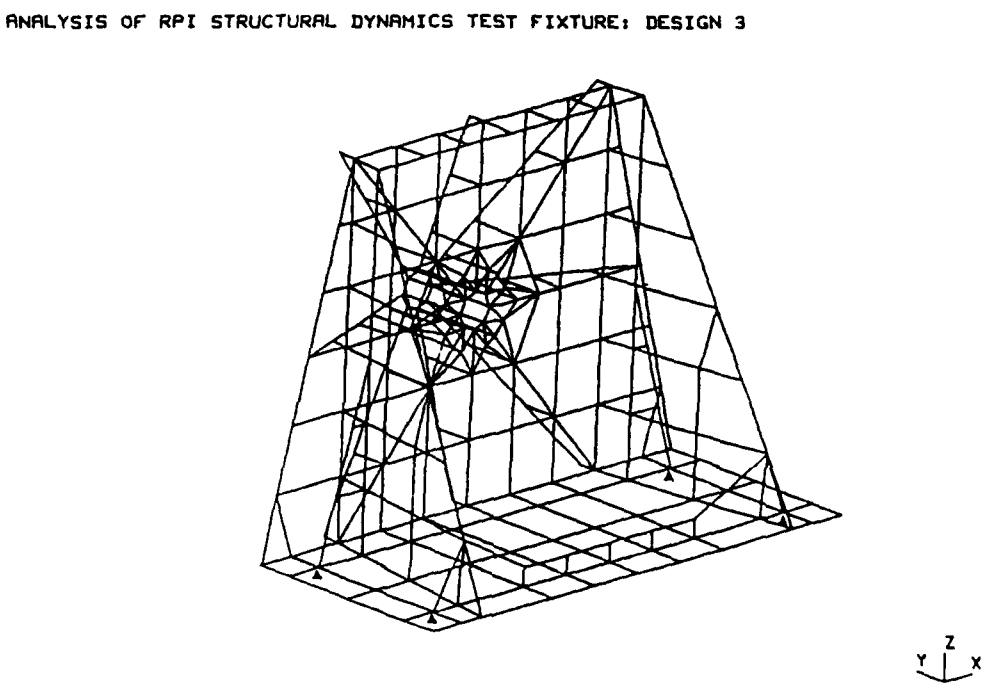

Fig. 29 - FEM Analysis Mesh for Fuselage Shake Test "Strong-Back" Design

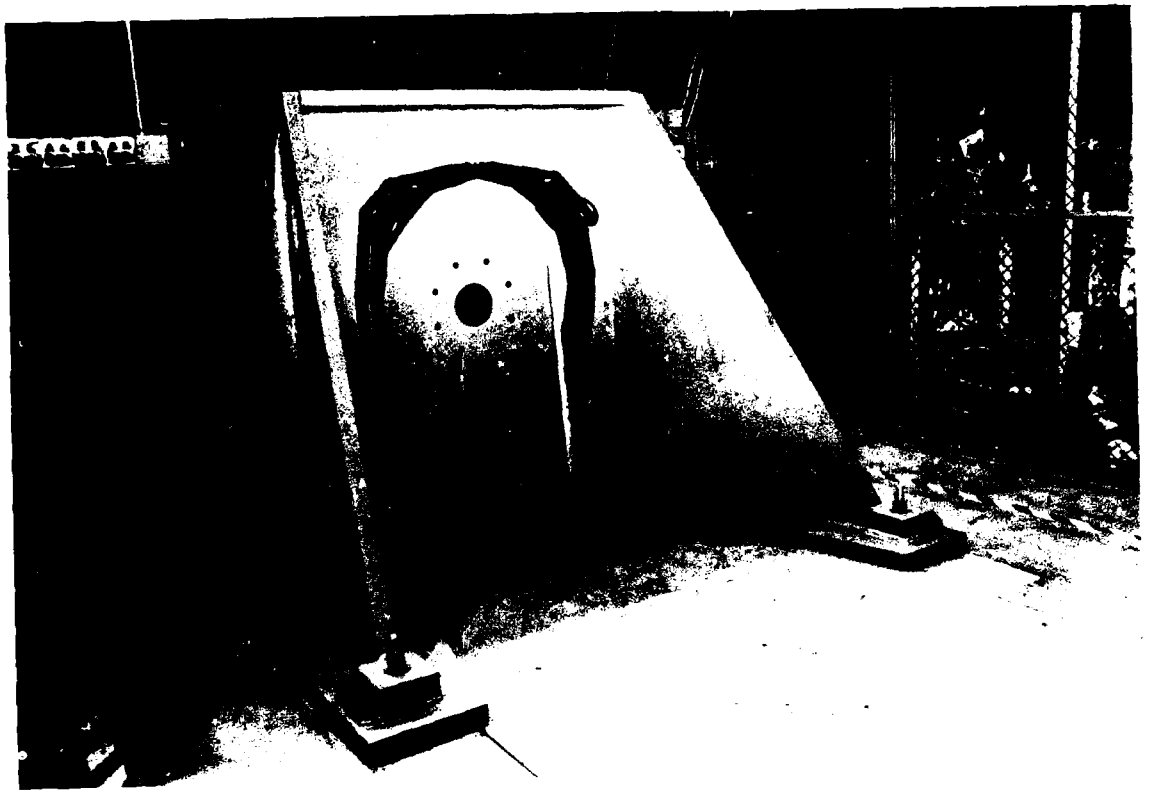

Fig. 30 - "Strong-Back" Structure Showing Attached Adapter Ring Structure for the S-55 Tail Cone

(a)

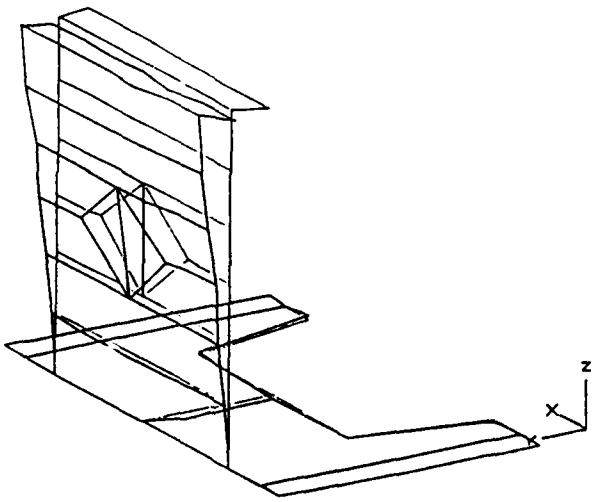

(b)

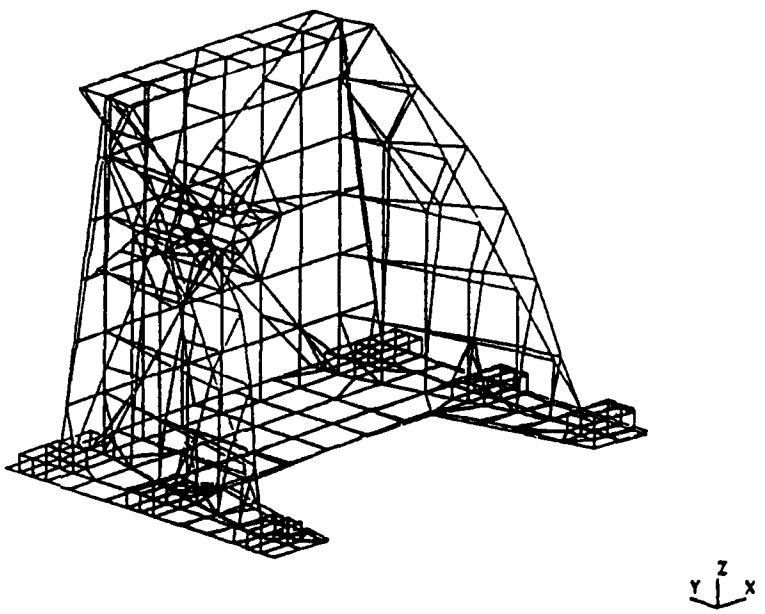

Fig. 31 - Comparison of Test and Analysis: First Free Vibration Modes and Frequencies for the Fuselage Shake-Test "Strong-Back"

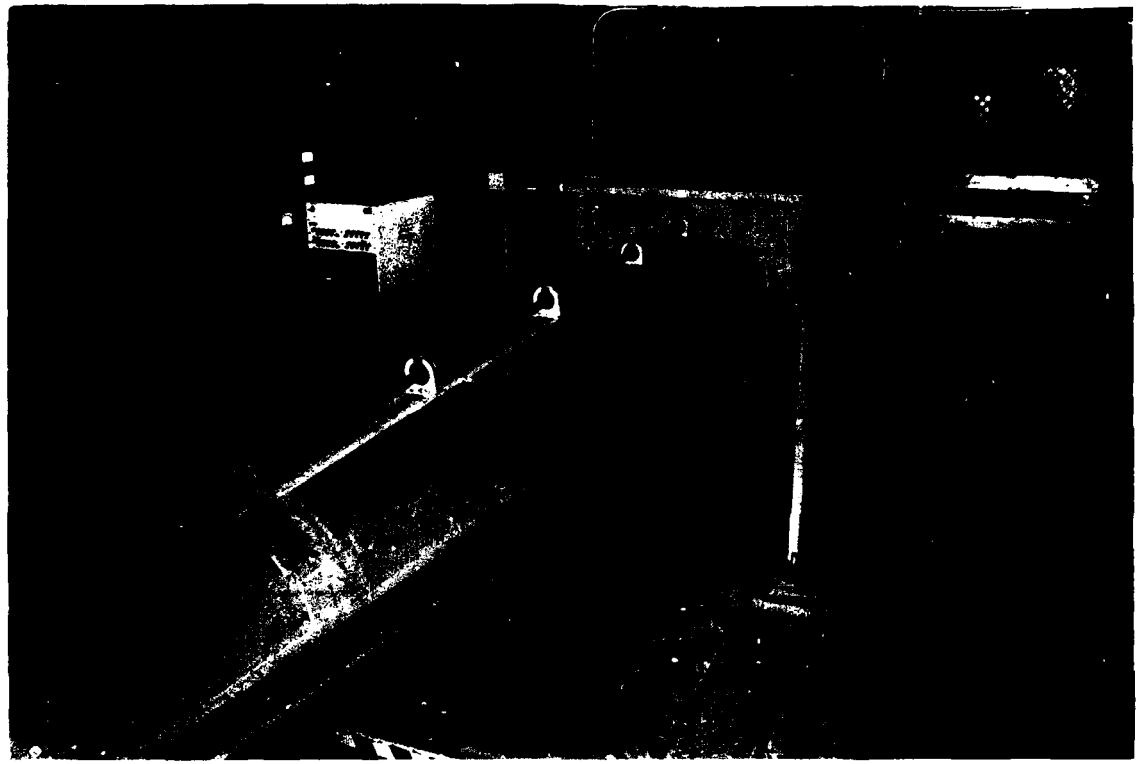

Fig. 32 - Full-Scale S-55 Helicopter Tail Cone Mounted on the Rensselaer RTC "Strong-Back" Structure

TABLE 14

Industrial Contacts for Helicopter Fuselage Analysis

Rensselaer RTC

(Circa '82-'83)

Bell Helicopter Company

Reese Allsmiller, ACAP Manager
William Alapic, Manager of Airframe Design
O.K. McCaskill, Chief of Airframe Structures Engineering

Boeing Helicopter Company

William Hardy, Technology Manager, Computing
Leonard Marchinksi, Chief of Structures Technology

McDonnell-Douglas Helicopter Company

Richard Crist, Airframe Structures Analysis Engineer

Sikorsky Aircraft Company

Richard Hayes, Manufacturing Engineering
Gary Jacuruso, Manufacturing Engineering

5.c. Unsteady Aerodynamics

5.c.(1). Passive Wave-Drag Reduction
(Sr. Investigator: H. Nagamatsu)

The intent of this research is to develop a passive shock-wave boundary layer control which will reduce impulsive in-plane blade loads, the power required and the rotor noise associated with transonic Mach numbers on the advancing blade tip in high speed forward flight.

At project initiation in July 1982, it seemed likely that this would be possible, since an investigation was conducted at Rensselaer under a grant from NASA Langley Research Center, concluded September 30, 1981, [Ref. 35] to study the application of passive shock wave-boundary layer control concepts to commercial and military fixed-wing aircraft. The objective in that work was to reduce the fuel consumed for long flights or carry more payload. The passive drag reduction concept was, in fact, to decrease appreciably the profile drag of biconvex and supercritical airfoils at transonic Mach numbers. [Refs. 36-38]

The major components of this passive system for alleviating wave drag are a porous surface under which lies an open cavity. These components are placed so as to coincide with the location of the terminating normal shock wave. The higher pressure behind the shock wave forces fluid from the boundary layer down through the pores at those chord stations into the cavity and back up through the pores at the relatively forward chordwise stations into the lower pressure supersonic region in front of the shock wave. This serves to deflect the flow slightly and cause an oblique shock wave to form ahead of the terminating normal shock wave. This oblique shock wave joins the normal shock wave at a fraction of the chord length above the airfoil surface, producing a lambda system as illustrated in Fig. 33. The effect of these flow changes is to reduce the severity of the velocity and pressure gradients across the terminating normal shock wave and to minimize the separation of the boundary layer. As a result, transonic drag is reduced by minimizing both boundary layer separation and the entropy increase which takes place across the shock waves. The major goals of the project were: 1) to determine the conditions which must exist for the passive drag reduction system to be effective for rotor blades; 2) to investigate system parameters important to optimal configurations; 3) to provide realistic estimates of the drag reduction possible; 4) to model free-flight conditions accurately through modifications of blow-down tunnel configurations and 5) to use computer codes for transonic flows as an adjunct of the experiments.

Since rotor advancing tip Mach numbers can approach sonic velocity, a 3x8-in. transonic wind tunnel was designed and constructed to operate over a Mach number range of 0.5 to 1.2 by utilizing the air dryer and an existing vacuum systems for Rensselaer's Mach 3 blow-down Wind Tunnel (Figs. 34). Following interchanges with rotorcraft community airfoil experts (Table 15) the decision was made to consider, as classical and representative rotor airfoils, the NACA 0012 and Bell FX 69-H-098 sections. These, it should be noted are thinner and have lower camber than the 14

percent thick supercritical airfoil studied in Refs. 36-38.

5.c.(1).(a). Steady Flow Conditions

Tests were conducted in two legs of the four-leg facility shown in Fig. 34. Two different test sections for the 3 x 15.4-inch leg were used; one to accommodate half-airfoil models on the tunnel floor and one to accommodate complete airfoil models. With the airfoils mounted on the bottom wall of the tunnel, the boundary layer ahead of the model was removed and split flow simulated by providing a stagnation point at the airfoil's leading edge (Fig. 35). A flexible ceiling was contoured to minimize the blockage effect and better simulate free flight conditions (Fig. 36). All tests were run in the 3 x 15.4-inch leg except for those on the Bell airfoil which was tested in the 3 x 8-inch transonic test section (Fig. 37). Thick lucite side walls are part of the test section structure to permit observation of shock waves and the flow over the models. Aluminum plates are fastened to the side walls, to minimize the wall deflection; they contain semicircular openings to accommodate Schlieren photography. Test Mach numbers were adjusted, in both tunnels, by using two flat plates, shown in Fig. 36 mounted in the aft-most portion of the test section. Hinged to the top and bottom walls, the deflections of these plates control the minimum throat area and thus, determine the freestream Mach number within the test section.

Constructing airfoil models required a computerized milling machine. The Bell model has a 4-inch chord, a cavity of 0.25 inches depth and an area of upper surface containing .025" holes, extending from approximately 33% to 90% chord $\frac{x}{c}$ = 0.33 to 0.90 in some cases and from 45% from 75% in others. In the latter case porosity was 3.26% of the total surface area. Sixteen static pressure taps were positioned along the centerline of the model's upper surface.

The full depth NACA 0012 airfoil model also has a chord of 4 inches and spanned the tunnel width (3 inches). Its surface has a porosity of 12.5% (based on total upper surface area) and extends from 33% to 94% chord. This porosity is also composed of 0.025 inch holes. Fourteen static pressure taps were placed on top and bottom surfaces 0.25 inches apart, on opposing sides of the centerline of the model; in addition, a stagnation tap was placed on the centerline of the leading edge.

Static pressure taps were also located throughout the test section and a total pressure probe in the settling chamber. The airfoil models' wake impact pressures were measured using a stainless steel total pressure rake located 1.75 in. behind the trailing edge of each model. These taps could be connected to 22 mercury filled U-tube manometers or silicon pressure transducers with a response time of 1 m.s. The outputs from these pressure gages were processed by A/D converters and the digitized outputs fed into a PC computer to analyze the data for pressure ratios and Mach numbers.

A single pass Schlieren optical system employing a zirconium light source, two

parabolic mirrors, two flat mirrors and an adjustable knife edge was used to reveal the shock waves on the airfoil. Pressure readings were analyzed using the basic compressible flow equations of steady, perfect, isentropic gas flow. The local static pressure, p, and freestream stagnation, pressure, p_o, are known, so that the local Mach number, M, can be obtained from

$$M = \left\{ \frac{2}{\gamma-1} \left[\left[\frac{p}{p_o} \right]^{\frac{1-\gamma}{\gamma}} - 1 \right] \right\}^{1/2}$$

where γ is the ratio of specific heats, equal to 1.4.

The local pressure coefficient can also be determined from:

$$C_p = \frac{2}{\gamma M_\infty^2} \left[\left[\frac{2+(\gamma-1)M^2}{2+(\gamma-1)M_\infty^2} \right]^{\frac{\gamma}{1-\gamma}} - 1 \right]$$

where M_∞ is the freestream Mach number.

To calculate the drag from experimental data, several relationships originally derived by Lock, Hilton and Goldstein [Ref. 39] were used. A "point drag coefficient" is determined at each probe of the rake by the following relation:

$$C_d' = 2 \left[\frac{P_o}{p_o} \right]^{\frac{\gamma-1}{\gamma}} \left[\frac{p/p_o}{P_\infty/p_o} \right]^{\frac{1}{\gamma}} \left\{ \frac{1 - \left[\frac{p/p_o}{P_o/p_o} \right]^{\frac{\gamma-1}{\gamma}}}{1 - \left[P_\infty/p_o \right]^{\frac{\gamma-1}{\gamma}}} \right\}^{1/2} \left\{ 1 - \left[\frac{1 - \left[\frac{P_\infty/p_o}{P_o/p_o} \right]^{\frac{\gamma-1}{\gamma}}}{1 - \left[P_\infty/p_o \right]^{\frac{\gamma-1}{\gamma}}} \right] \right\}^{1/2}$$

where P_o is the local stagnation pressure and P_∞ is the freestream static pressure.

The point drag coefficients are then integrated numerically across the wake region to determine the airfoil drag coefficient:

$$c_d = \frac{1}{c} \int_{wake} c_d' \, dy$$

where c is the chord length.

All testing involved careful evaluation of the flow fields in the test sections and adjustment of the variable top-wall insert so as to achieve the desired flow conditions, including simulation of free flight. The adjustable top-wall insert is composed of a 19 mil piece of stainless steel 17.5 inches long. There are six screws soldered to the steel which allow the curvature of the top-wall insert to be adjusted. Additionally, there are static pressure taps mounted along the centerline of the insert. This allows the measurement of local Mach number along the insert, necessary in the determination of the optimal contour. The insert is sketched in an optimal contour in Fig. 36 for the 3 x 8-in. test section.

Tunnel blockage effects using one-dimensional theory predicted maximum freestream Mach numbers which correlated well with measurements for simple tunnel configurations, but the total pressure rake behind the airfoil model produced minimum area directly behind the rake, limiting ability to control the location of the minimum area.

Despite these and other complications, such as the existence of a boundary layer along the top wall, it was possible to determine a contour that satisfied the free-flight conditions; namely, 1) the normal shock wave should be essentially vertical, 2) the flow behind the shock wave should be subsonic, and 3) the Mach number behind the airfoil model should be slightly less than the Mach number ahead of it. Knowledge of the probable shape of the streamlines at the top-wall location from CFD code calculations also aided in finding the optimal contour. The Schlieren photographs reproduced in Figs. 38-a and 38-b (in this case for the Bell airfoil) illustrate the test conditions achieved for solid airfoil contours.

During the course of this research the Bell and NACA 0017 airfoils were mounted on the bottom wall of the tunnel and a complete NACA 0012 airfoil was mounted in the center of the 3 x 15.4-in. tunnel test section both to confirm what was learned on the bottom-mounted specimens and to allow angle of attack variations. Certain general conclusions can be drawn from these experiments, which were all conducted under steady flow conditions; namely -

i) Satisfactory representation of free flight conditions required tunnel wall contouring

ii) The essentially normal shock structure on the aft portion of a helicopter type airfoil section at transonic Mach numbers can be changed to a lamda-type shock by means of properly sized and placed porosity over a cavity.

iii) Drag reduction through these passive means can be substantial; e.g. at the point of steep drag rise, M = 0.86 for the Bell airfoil drag is reduced by approximately 33%.

iv) Porosity should be beneath the normal shock position and extend forward to the desired position of the distributed lamda shock "legs"; e.g., from 45 to 75% chord on the Bell airfoil.

v) This passive drag control is relatively insensitive to cavity depth or shape and can easily be accommodated in normal rotorcraft airfoil depths to 75-85% chord.

vi) At low Mach numbers there is a slight increase in drag, primarily due to an increase in skin friction as a result of the porous surface, and the unnecessary recirculation of the boundary layer at these low Mach numbers. (It remains to be seen how this may be alleviated by "shutters".)

Evidence of these conclusions is contained in Figs. 39-a and 39-b, showing Schlieren photographs of the shock structure above a Bell airfoil upper surface contour, with and without the porous surface, respectively, at M = 0.86 and in Figs. 40, 41, and 42, which show local Mach Number distributions with chord, total pressure ratio (wake to free-stream) vs distance through the wake, and airfoil drag coefficient vs Mach Number, respectively, all for solid and porous airfoil aft upper surfaces.

As shown in Fig. 43, the solid surface Mach Number distributions on a 0012 airfoil is characterized by a sharp decrease in local Mach number at the location of the normal shock wave, whereas the Mach number distributions have a more gradual transition from supersonic to subsonic Mach number for the porous surface airfoil (x/c = 0.33 to 0.47). Similar results were found in the local pressure coefficient distributions.

Tests performed with the full 0012 airfoil model at an angle of attack of 4^{o} examined three different configurations of porosity; x/c = 0.33 to 0.47, x/c = 0.33 to 0.56 and x/c = 0.33 to 0.63. The drag coefficients were again calculated from wake pressure measurements for the solid and porous surfaces for a Mach number range of 0.60 to 0.81. These results are presented in Figs. 44-a, 44-b and 44-c. While some scatter is present in the data, it appears that the passive drag reduction scheme is effective over a larger range of transonic Mach Numbers when the porosity extends only to the 47% chord point. All of these results were reported in Refs. 40 through 43.

5.c.(1).(b). Unsteady Flow Conditions

Since rotor advancing tip transonic operation is a highly transient situation,

investigations into unsteady flow effects on the passive drag reduction concept were undertaken in the latter half of 1985. The flow Mach number in the test section of the 3 x 8-inch tunnel was fluctuated by oscillating a flow control wedge in the upper tunnel wall downstream of the test section, as shown in Fig. 36. This varied the minimum throat area for the tunnel. A variable speed d.c. electric motor actuates the wedge on the top wall with a cam. Small silicon resistance pressure transducers were used to measure the unsteady pressures in the test section, on the airfoil surface and in a wake impact probe. A 16 channel A/D converter processed and fed the unsteady pressure data to a PC computer for analysis and recording.

Preliminary unsteady flow results for solid and porous Bell airfoil models mounted in the floor of the 3 x 8-inch tunnel, have been obtained. The results for the flow over the airfoil with the porous plate and the cavity are presented in Fig. 45 for an oscillating frequency of 10.4 Hz. The locations of pressure taps on the airfoil and in the cavity are noted in the figure for porosity from x/c = .45 to .75 with a cavity depth of 0.25 inch. The flow Mach number 56% of chord in front of the model fluctuates between 0.43 to 0.83. Differences in cavity pressures sufficient to permit recirculation of the boundary layer downstream of the normal shock wave to the region upstream, i.e. in front of the shock wave, have been measured. Since all previous testing indicates that this is necessary to produce lambda shock waves with corresponding lower drags, the preliminary unsteady flow data promises drag improvements under transient conditions similar to those obtained in the static cases. These investigations are continuing. An important aspect is measurement of unsteady wake impact pressures downstream of the airfoil section to determine the unsteady profile drag. From these future experiments the most effective porous surface/cavity configurations for reducing transonic drag under unsteady flow conditions are expected to emerge.

5.c.(2). Blade Vortex Interactions

(Sr. Investigator: Prof. R. Mayle)

Situations in which a rotor blade encounters a vortex trailed or shed by a preceding blade or by itself in a previous revolution are common in rotorcraft operation. Close encounters or even intersections can occur on the main rotor of single rotor helicopters in high speed forward flight or in descents, and on the tail rotor or rear rotor of a tandem helicopter in a number of flight regimes, depending on specific aircraft geometries. High local velocities associated with vortices can be expected to influence blade aerodynamics profoundly, where such close encounters do occur. In fact, higher harmonic rotor loads, vibrations and impulsive blade noise are all thought to be adversely affected by blade vortex interactions.

Parameters affecting these interactions include the nature of the encounter (eg as illustrated in Fig. 46, for trailing vortices), the structure of the vortex (eg "rolled-up" or distributed, core size, etc.), and the way the airfoil reacts to the presence of the vortex. As regards the last point, an early investigator hypothesized that lift coefficient increments due to blade vortex interactions (BVI) could not exceed 0.3, based on experiments with 90^{o} vortex-blade intersections [Ref. 44].

Rensselaer initiated a project to examine in a fundamental way the interactions of vortices with lifting surfaces in July '82. It consisted of three parts: to develop facilities for appropriate experiments in a low speed wind tunnel, to conduct a series of careful tests which would provide insights at a basic level into the phenomena, and to perform theoretical analyses for correlative purposes.

5.c.(2).(a). Experimental Program

In keeping with the approach of maintaining simplicity, the concurrent or parallel leading edge intersection was chosen as the interaction configuration to be investigated. Accordingly a two-dimensional, BVI experimental set-up was developed in the form shown in Fig. 47. In this experimental system, the vortex is created by pitching a vortex generating airfoil five feet upstream and parallel to the instrumented test airfoil, which has an 18" chord and a .0012 section.

Since, to produce a concentrated vortex, the wing must be put abruptly into motion, a hydraulic system is used to drive it. Further, since inertial and aerodynamic loads are developed thereby, high stiffness is required to maintain a two-dimensional flow condition. The vortex-generating wing, which has a chord of 12", thus constructed with a foam core, fiberglas/epoxy skins and a spar with graphite cap strip fibers in the spanwise direction and web fibers $\pm 45^{o}$ to the vertical in the spanwise direction, for bending and shear stiffness, respectively. The hydraulic system consists of an accumulator fed from a reservoir which pressurizes two hydraulic cylinders, one at either end of the wing's span. Servos operate the control valves. Position and velocity transducers attached to the airfoil provide feedback signals to the control servos.

The vortex position and structure were found to be best measured by hot-wire anemometry. Since the flow is unsteady and turbulent, all measurements are ensemble averaged to provide the corresponding time-varying mean values. Typical results of measurements of the incident vortex are shown in Fig. 48 and compared with similar data from Ref. 45. The generated vortex was found to be virtually two-dimensional, had about 80% of the strength predicted, and had a core which is about one inch (or $^1/_{12}$ chord) in diameter at this position downstream, giving a vortex aspect ratio of about 60 to 1.

Interaction tests were conducted with both clockwise and counterclockwise rotating vortices made to pass above the symmetrical test airfoil which was set at zero angle of attack with respect to the free stream. Pressure transducers located inside the test airfoil and "polled" by a pressure driven, scanivalve system measured the steady and unsteady airfoil pressure distributions. (Fig. 47). Pressure coefficient histories at several chordal distances were thus recorded, and typical results are shown in Figs. 49 and 50 for the upper surfaces (C_{pu}). Corresponding data were obtained for the lower surfaces. Time histories of the lift, drag and moment coefficients were calculated from these measurements. Typical data are shown in Figs. 51 and 52. In each of the foregoing figures, Figs. 49 through 52, the experimental results are compared to predictions made in correlative analyses using the unsteady, discrete vortex potential flow theory discussed below.

5.c.(2).(b). Theoretical Analysis

The theoretical analysis portion of these studies modeled the two-dimensional interaction between a Joukowski airfoil and a vortex transported with the local airstream allowing for the appropriate deviations in the impinging vortex trajectories as well as in the trajectories of secondary vortices shed from the Joukowski airfoil as a result of changes in its induced lift.

The analysis, then, is based on an unsteady discrete free-vortex, classical potential flow theory. The generated, free vortex was modeled both as a single, concentrated vortex as shown in Fig. 53 and, for a close encounter, by a cluster of vortices with the same total strength as the concentrated vortex. The analysis allows for the airfoil to move either steadily or unsteadily through the fluid and allows for a freely convective wake. Comparisons of this nonlinear, unsteady analysis with linear airfoil theory for both periodic and transient airfoil problems and with advanced numerical methods for a two-dimensional parallel interaction problem showed the discrete free-vortex method to be not only accurate, but fast. Unsteady pressure distributions over the airfoil were also predicted as a result of this theory. Comparisons with the results of the linear theory of Theodorsen for an airfoil pitching and plunging sinusoidally showed good agreement except for very large amplitudes. Similar comparisons with Sears' linear results [Ref. 46] for a two-dimensional vortex-airfoil interaction showed good agreement except for close encounters. Since close vortex-airfoil encounters can be expected for a helicopter rotor in certain circumstances, the present theory is believed to be more appropriate. Numerous blade-vortex calculations were conducted. In particular, the initial vortex height

$(y/c)_o$ was varied from -1 to +1, nondimensionalized vortex strengths $\Gamma/U_\infty c$ from 0.1 to 0.4 were considered, and the angle of attack was varied from 0 to 4 degrees. (Here Γ is vortex strength, U_∞ free stream velocity and c the chord of the interacting lifting surface.) In each case, the lift, drag and moment coefficients C_L, C_D and C_M, respectively, were calculated. Representative results for zero angle of attack are shown in Figs. 54 and 55.

5.c.(2).(c). Correlation of Theory and Experiment

It was found that all of the calculated results displayed similar behavior and could be correlated by defining simple incremental lift, drag and moment coefficients which account for interactions at different heights, vortex strengths and airfoil angles of attack. A definition of total incremental lift coefficient, ΔC_L, and an incremental lift factor, Y, which relates initial lift change to total lift change, are shown in Fig. 56. In Fig. 57, the normalized incremental lift coefficient $\Delta C_L(U_\infty c/\Gamma)$ is plotted against the initial vortex height $(y/c)_o$ for various values of $\Gamma/U_\infty c$ and angles of attack.

All of the total incremental lift coefficient results are correlated quite well by the equation

$$\Delta C_L = 0.7 \frac{\Gamma}{U_\infty c \sqrt{|(y/c)_o|}} \; ; \; (y/c)_o \neq 0$$

Although not shown, the total incremental moment coefficient is correlated by the equations

$$\Delta C_M = \begin{cases} 0.18 \, |(y/c)_o|^{-0.45} \frac{\Gamma}{U_\infty c} \; ; \; (y/c)_o < 0 \\ 0.165 \, |(y/c)_o|^{-0.55} \frac{\Gamma}{U_\infty c} \; ; \; (y/c)_o > 0 \end{cases}$$

It was found that an incremental factor for the initial changes of both lift and moment can be well represented by

$$Y = 0.7 - 0.55 \, | \, (y/c)_o \, | + 0.2 \, (y/c)_o^2$$

Although the maximum incremental lift coefficient for a close encounter is about four times the dimensionless vortex strength $\Gamma/U_\infty c$, when calculated using the single vortex representation, this value drops to about one-third less when the tip vortex is modeled by a cluster of vortices. This is shown in Fig. 58. Comparisons with experimental results, Figs. 49 through 52, indicate that the effect is reduced further if the interaction causes flow over the airfoil to separate. Based on these results, we are lead to define three main regions of BVI, solely dictated by the initial height of the vortex

relative to the airfoil. These regions are shown in Fig. 59 and are defined as 1) the region of close encounters, $-0.15 < (y/c)_o < + 0.15$; 2) the region of forced airfoil separation, somewhere between $(y/c)_o = 0.1$ and 1.0; and 3) the region outside of these, where a simple inviscid theory, using a single vortex to represent the tip vortex, suffices to predict the interaction effect. Sears' theory, for example, [Ref. 46], as shown against experimental results in Figs. 51 and 52 predicts reasonable values even in the region of forced separation.

The non-linear theory predicted the pressure, lift, drag and moment histories for counter-clockwise vortex passage over the upper surface quite well, as shown in Figs. 49 and 51. The same theory, however, deviates more substantially from measured data for the clockwise vortex passage over the upper surface, as shown in Figs. 50 and 52. At this writing it appears that these differences in correlation are related to the separation of the flow over the upper surface of the airfoil where the clockwise rotating vortex severely retards this flow during the interaction. As a consequence, we conclude that inviscid theory is adequate when either the vortex passes far away from the airfoil or when the direction of the vortex is such as to accelerate the flow on the facing airfoil surface. It also appears that a BVI which tends to retard the flow on the facing airfoil surface can produce a large separation, as shown in these experiments, from which the airfoil does not recover until the vortex is well past the trailing edge.

Details of the research reported here may be found in Reference 47 and in the theses of R.A. Bergman, P. Renzoni and J. Straus in Appendix C.

5.c.(3). Unsteady Rotor Aerodynamic Coefficients in Forward Flight
(Sr. Investigator: Prof. R. Duffy)

Research into rotorcraft unsteady aerodynamics was initiated in the latter half of 1982 with the objective of making a more complete accounting for the complicated trailed and shed wakes behind and beneath oscillating blade segments. Most of the rotor dynamic codes to this time incorporate only quasi-static aerodynamic representations, Theodorsen fixed-wing type unsteady coefficients or, more recently, dynamic inflow effects (e.g. Ref. 48). The first of these neglects all wake vorticity, the second neglects three-dimensional effects and those due to other blades and what occurred in previous revolutions, and the last is appropriate only for relatively low frequency phenomena in which the gross effects of all blades are represented.

It was anticipated that in Rensselaer's approach a vortex lattice would be postulated for a particular radial segment of a rotor blade and at a particular azimuth, as shown in Fig. 60. The blade segment was pictured as oscillating through unit amplitude (either pitching or plunging) at a particular ratio of blade frequency to rotation speed; and at a particular advance ratio. As in most unsteady airfoil theories, the effect of uniform or nonuniform inflow on vortex vertical position would not be expected to be large, near the blade. These effects as well as the effect of displacements due to blade motion out of the plane of rotation would, therefore, not be included. Since a single blade segment at a particular radial station is to be considered in isolation, the concentrated vortices which trail from the radial boundaries of this segment of the vortex lattice would be representing a finite change in bound vorticity from the radial segment of interest to zero vorticity on either side. The velocities induced on all blade radial segments due to that particular vortex lattice were seen as being calculated and stored and the process repeated for a substantial number of azimuth locations and radial segments. Since this is a small disturbance, i.e. linear theory, the resulting induced downwash from one radial segment would be used to calculate forces and moments on all radial segments at the same and other azimuths where blade segments exist, based on unit motions of the reference radial segment. A superposition would then be made of the forces and moments generated when all blade segments are considered "reference segments", in proportion to their actual, rather than unit, motions.

5.c.(3).(a). Two- and Three-Dimensional Discrete Wake Studies

Both to provide insight into more complex behavior and to provide for efficient and accurate numerical analysis of what is a mathematically untractable problem, the simplest component situations were examined first, with the intent of building up to a complete representation. Accordingly, the Theodorsen problem, i.e. a two-dimensional airfoil in sinusoidal pitching and heaving motion in a uniform stream, was analyzed to arrive at the minimum 2-D discreet wake representation which appears to provide acceptably accurate predictions of oscillatory lift force and pitching moment, amplitude and phase. Sensitivity studies were carried out on combinations of heave and pitch oscillations to determine: optimum placement of the shed vortex nearest the airfoil, optimum shed vortex spacing, and required length of the

downstream vortex field for accurate prediction of Theodorsen's function. It was found that the first such shed vortex should be placed at one-half the distance that would be calculated based on the chosen time increment and reduced frequency $\frac{c\omega}{2V}$. This is the same result obtained in steady three-dimensional rotor aerodynamics analyses [Ref. 49]. The results of this phase of the research are reported in Ref. 50.

In a second step, investigations into the minimum wake needed to make similar predictions for a 3-D wing oscillating sinusoidally in a uniform stream were begun. The three dimensional, discrete vortex filament model developed for this work is shown in Fig. 61a together with the two-dimensional representation in Fig. 61b. The former model (i.e., Fig. 61a) was used to predict the Reissner functions for a rectangular wing oscillating in heave and pitch [Ref. 51 & 52].

5.c.(3).(b). Pulse Transfer Function and Application to Airfoils and Wings

At this point in the project, a postulated pulse excitation was found to be much more efficient in calculating non-steady aerodynamic characteristics than pure sinusoidal excitation for both heave and pitch. In this approach, the airfoil is subjected to a smooth pulse and the aerodynamic response calculated using rules developed for the discrete vortex filament model as to the position of shed circulation in the wake. Fast Fourier Transforms (FFT) are then used to invert the aerodynamic response, and the complete frequency response results. In other words, the time domain response to the smooth pulse forcing function is calculated followed by a reduction into its Fourier components. By choosing the forcing function to be non-zero over a small non-dimensional time interval, this technique is amenable to the FFT method. Because the full frequency spectrum is available from one run in time, this method is very efficient computationally. To obtain typical Theodorsen or Reissner functions using the pulse technique took only a fraction ($O[10^{-2}]$) of the computational time, compared to the sinusoidal discrete filament modeling approach.

The merit of the pulse transfer function (PTF) technique was demonstrated for unsteady transonic airfoil calculations by Batina [Ref. 53]. He chose an exponential pulse, as shown in Fig. 62a. By using the doublet-type pulse also shown in this figure, the response can be forced to zero in a much shorter time (Fig. 62-b). The benefit of this is explained in the following paragraphs. The choice of the exponential or doublet-type pulse does not affect the results of the PTF technique, as demonstrated by its use in calculating Theodorsen's function (Fig. 63). Since imposition of the Kutta condition (flow must always leave the trailing edge smoothly)is questionable at reduced frequencies, $k = \frac{\omega c}{2V}$ greater than 1.0 [Ref. 54], frequency domain results are only presented up to this point. Good agreement was also obtained in PTF applications to 3-D wings for Reissner function solutions (Fig. 64).

5.c.(3).(c). Application to Helicopter Rotors

As another step in increasing the complexity of the discrete wake model, the PTF technique was applied to the 2-dimensional rotary wing unsteady aerodynamic theory of Ref. 55. The rotary wing indicial response function developed by Venkatesan and Friedmann [Ref. 56] was used in conjunction with Duhamel's integral [See, for example, Ref. 57] to predict the response to an exponential pulse. The resulting lift deficiency function compared favorably with that provided by the [Ref. 56] polynomial approximation to Loewy's function [Ref. 55] from which the indicial response function was calculated.

Following this correlation, a discrete vortex model was set up to reproduce Loewy's function. The reference airfoil was modeled with a single bound vortex and control points at the 1/4-chord and 3/4-chord points, respectively. The shed and returning elements were located at 1/2 the distance traversed during the first time step and then continuing downstream at the freestream velocity. The lift deficiency functions resulting from the PTF analysis compared favorably with Loewy's function, with some underprediction of the real part and over-prediction of the imaginery part.

Continuing to the question of the influence of specific rotor wake geometry in forward flight, the issue of angularity of shed vorticity with respect to the blade trailing edge and curvatures of trailed vorticity were next addressed. As an approximation, a vortex model was postulated for calculating unsteady aerodynamic coefficients which includes the former and neglects the latter, as shown in Fig. 65. The strength of these wake vortices and their spacing, of course, reflect velocity variations with radius at a particular azimuthal location. Further, by neglecting wake distortion due to inflow, the skewed helical wake can be considered to be in the plane of the blade. Because this approximate vortex filament model neglects the curvature of the wake, only a short portion of the wake could be considered without introducing errors associated with such curvature. The doublet-type pulse was designed so as to wash-out all time domain effects in this region. The advantage of this model is, therefore, that the effects of forward speed are isolated at each azimuthal location.

The resulting lift deficiency functions for an aspect ratio 6 rotor blade, assuming a 20% blade cutout, are shown in Fig. 66-a through 66-d [Ref. 58]. The blade is modeled as having eight spanwise panels with bound vortex and tangency control points as shown in Fig. 61. From these results it is evident that the effect of three-dimensionality is to reduce the severity of the lift loss due to unsteady effects which would be calculated using Theodorsen's function. At an intermediate reduced frequency, the difference in the lift loss between that calculated using Theodorsen functions and the results presented here can be as much as 25%.

Imposing a limit on the reduced frequency ($k = 1.0$) due to uncertainties in the Kutta condition restricts the calculation of blade loads to only the first few harmonics for inboard portions of the retreating blade at high advance ratios. However, it is generally recognized that the greatest portion of the loading on a rotor blade occurs from the 50% radial position outward. In this range, most higher order frequencies of engineering interest are available from the results presented here.

5.c.(4). "Snap-Through" Airfoil Applications
(Sr. Investigator: Prof. R. Duffy)

Airfoil and composites research at RPI at the time of project initiation led to a concept that promised to allow rotor designers to make use of two-point camber airfoils. The approach is as follows: two airfoils are designed so that both have the same upper surface contour, but the lower surfaces differ. In one case a convex lower surface might minimize C_D and the concave lower surface maximize C_L. Such an arrangement would be aimed at performance increases. In another, the camber change might have maximum pitching moment change as an objective.

Lower surface contour changes, of course, would have to be compatable with the contour of the lower - aft limit of the portion of the structure acting as the "spar" and with the trailing edge. Further, the flexible portion of the lower surface responsible for changing contour might be made to be bistable as regards its position, to minimize actuator force requirements. Rensselaer composites research, in fact, showed that a plate for the lower surface could be made to have two stable positions, and be made to "snap through" from one contour to the other with very slight actuating pressure. This approach would use buckled modal shapes, however, with relatively high and constant axial loads imposed. Such would impose rather difficult rigidity constraints on the remainder of the airfoil section. It was, therefore, decided to use a simple $0\text{-}90^{\circ}$ layup for the "snap-through" segment; rotor blade dimensions are such that useful contour changes seemed possible with low actuating forces.

The steps taken to explore the potential of the snap-through airfoil concept as applied to helicopter rotors were, then, to:

i) Conduct wind tunnel tests to confirm the dynamic aerodynamic performance which could be obtained.

ii) Make theoretical correlative calculations to enhance understanding of the wind tunnel measurements and to allow interpolation/extrapolation to other flight conditions.

iii) Perform preliminary rotor aeroelastic analyses to determine how the concept would function in a realistic rotor design and operating environment.

5.c.(4).(a). Experimental Program

To explore the application potential of this concept, a full scale spanwise segment of a CH-47 "Chinook" helicopter rotor blade, which incorporates a VR-7 airfoil section, was obtained from Boeing Helicopter Company and the lower surface modified so as to incorporate a flexible graphite/epoxy skin. A pair of double-acting pneumatic cylinders coupled to a small scissors linkage were installed so as to "snap" this skin between stable inner and outer positions, thus changing the camber of the airfoil section. This has become known as the "snap-through airfoil section". Fig.

67 shows sketches of the original airfoil and as modified with snapped in and out lower panels. Note the trailing edge cusp, whose purpose is to reduce pitching moments.

The snap-through airfoil was installed in the RPI 4'x6' subsonic wind tunnel and a series of tests conducted. First, snap-through dynamic performance was evaluated with wind on, over a range of angles of attack. At low positive angles of attack, a set of small actuators could "snap" the airfoil at rates up to approximately four cycles per second. This is in the range of once per revolution frequencies for rotors the size of the CH-47. At high angles of attack, however, the increased positive pressure on the lower surface overpowered the actuators. A second set of high response actuators, capable of higher force levels were installed, and were found satisfactory as regards force output, but limited to somewhat lower cycling frequencies. The RPI wind tunnel six-component strain-gage balance system was also modified to record non-steady aerodynamic loads.

Wool tuft studies were also conducted under steady state conditions with the model in both the unsnapped and snapped-through positons, to confirm that no large scale separation occurs, as might be feared, at the relatively sharp chordwise slope discontinuity between the snap panel and the forward spar portion of the blade cross section. These studies showed that stall in the steady positive angle of attack regime occurs by trailing edge separation. At negative static angles, stall appears to be initiated by a separation bubble formed near the leading edge. Thus, the contour slope discontinuity appeared to be of no consequence.

Dynamic tests were conducted in the Reynolds number range from 1.27 to 1.8 million, based on chord, over an angle of attack range from -16^{o} to 20^{o}. The effect of "snapping" the airfoil was tested with repetition rates of up to 2.35 Hertz. Aerodynamic lift, drag, and pitching moments acting on the model were measured by three Lebow load cells. One cell measured lift directly while the two others were combined to measure drag and pitching moment. The test data was recorded on both a Honeywell 1508 Visicorder and interfaced for storage in an IBM PC/AT via a Metrabyte, Dash-16, A to D interface. The tunnel balance system was calibrated prior to each test. System cross-talk effects were measured and considered in the data reduction process. Aerodynamic lift and drag and pitching moment about the quarter-chord were reduced to coefficient form and then corrected for solid and wake blockage and tunnel wall effects using standard methodologies.

The resulting experimental unsteady lift and pitching moment data were reduced and compared. Moment response builds up twice as fast as the lift does. Lift coefficient changes were found to be about 0.05 and pitching moment changes (about the quarter chord) from .01 to .018. Response in both quantities is insensitive to angle of attack within linear portions of the lift curve slope.

These results are shown for the static case in Figs. 68 and 69. Note that the lift change is a small percentage of the operating value, but that the pitching moment change is increased by about 40%. (Drag is substantially unchanged over a lift coefficient range from about -0.3 to +1.0.)

Dynamic data for cycling at 1 and 2 Hz are shown for the lift coefficient in Fig. 70. A "wrong-direction" response to the first "snap", at zero time led to the discovery of actuator reactions being reflected in balance system measurements. Calibration runs with wind-off were then used to correct such dynamic data. Dynamic data thus corrected are shown in Fig. 72 for a single "snap" change.

5.c.(4).(b). Theoretical Correlation

The steady state lift and pitching moment coefficients of the snap-through airfoil in potential flow were found using a second order vortex panel method. The original FORTRAN computer language program may be found in Kuethe and Chow [Ref. 58] and was adapted for operation on an IBM PC/AT.

The coordinates of the airfoil were taken from direct measurements of the actual snap-through airfoil. They account for changes in shape of the upper surface near the trailing edge, which are due to removing considerable structure in modifying the VR-7 and installing the snap-through panel. The coordinates of the unmodified VR-7 were provided by Boeing Helicopter Co.

Pressure distributions over the unsnapped and snapped airfoil were calculated and, as expected, the effect of snapping the panel is to basically alter the pressure distribution over the aft portion of the lower surface, producing a higher $+\Delta C_p$ across the airfoil, and increasing lift and generating nose-down pitching moment.

To determine the difference in steady-state lift coefficient and pitching moment between the two snap-through states, the computer calculation was used to integrate the pressure coefficients over the airfoil surface through the angle of attack range from -2 deg. to 10 deg. Comparison with the experimental data showed good agreement.

An estimate of the aerodynamic response of the snap-through airfoil to a step snap was also calculated using an extension of the discrete vortex filament modeling methods for the non-steady aerodynamics of an airfoil section, described in Section 5.c.(3) of this report, above. For this purpose, the snap-through airfoil was assumed to have zero thickness, stationary leading and trailing edges and a mean line which can instantaneously change between two equilibrium shapes. Conservation of vorticity requires that time-varying vorticity be shed into the wake, resulting in a monatonic change with time during the snapping process of the aerodynamic lift and moment between two equilibrium sets of values corresponding to the two mean line shapes. The mean line shapes were determined from the surface coordinates of the airfoil obtained as described above in discussing the static calculations. Results of calculations for the response are shown in Fig. 71. The computed response is quite similar to the Wagner function for a flat plate airfoil [See, for example, Ref. 57] differing mainly in the zero time value, which is 0.5 for the Wagner case; i.e., a step function change in angle of attack. The computed response for the snap-through situation is compared with the experimental results in Fig. 72.

One further theoretical result requires mention, although no experimental data were available for correlation. Pressure coefficient distributions were examined as evidence of possible changes in critical Mach number as the airfoil changes shape. Typically, helicopter performance is limited by the onset of compressibility on the advancing blade tip. Any change in the free stream Mach number at which shock waves are formed would result in a degradation of performance. The variation in critical Mach number with C_ℓ was determined by calculating the minimum (most negative) pressure coefficient found on the airfoil and inferring the critical Mach numbers using the relations in Ref. 59. The results are graphed in Fig. 73. It appears that no adverse compressibility effects would be encountered.

5.c.(4).(c). Application Studies

A principal issue in applying the snap-through concept to rotor design is an aeroelastic issue. From wind tunnel theoretical studies as described above, it appears that blade lift would be changed slightly and blade pitching moment a lot on a structure which is quite limber in bending and torsion. That is, on a flexible blade, with differing response to excitation at different frequencies, the designer would have to consider whether changes in twist, due to blade elastic twist and pitching moment excitation would add to or subtract from, modify or negate the concommitant changes in blade lift.

To gain insight into this matter, a case study was conducted for the CH-47D "Chinook" rotor blade, using blade physical data, and loads provided for a forward flight speed of 62.8 kts ($\mu = 0.15$) and rotor lift of 20,932# by Boeing Helicopter Co. First, dynamic uncoupled twist response was calculated, with the snap-through sections statically at the "in" (higher nose-down pitching moment coefficient) position, for outboard blade sections beginning with 0.9 then 0.8, 0.7 and 0.6 of Radius. In all cases the pitching moment changes dominated lift changes in determining blade air load distributions. As a final investigation under the subject contract, a particular time-varying snap-through schedule was investigated for the case study conditions assuming, again, only torsion elastic response changes and that 2-D, quasi-static incremental lift and pitching moment changes are applicable. Changes in the dynamic vertical blade root forces as a function of azimuth calculated in this way are shown in Fig. 74. It appears that the concept can change rotor vibratory characteristics for frequencies up to 1Ω. Further work will be required to show what its potential is for applications like higher harmonic control, where frequencies is the $(N+1)\Omega$ ranges must be used (where N is the number of blades).

Details of the results of this research may be found in Refs. 50 and 60.

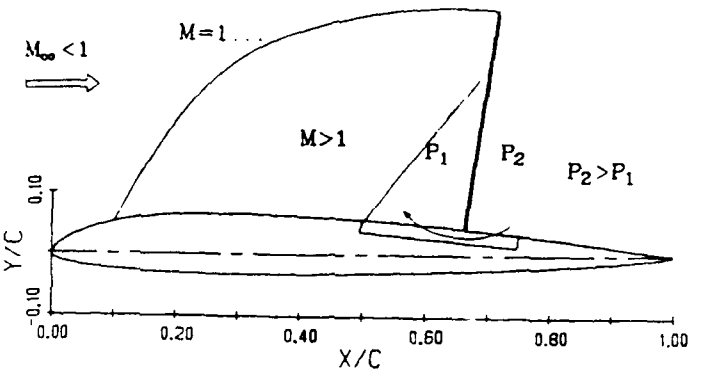

Fig. 33 - Lambda Shock System Produced by Passive Drag Reduction Concept

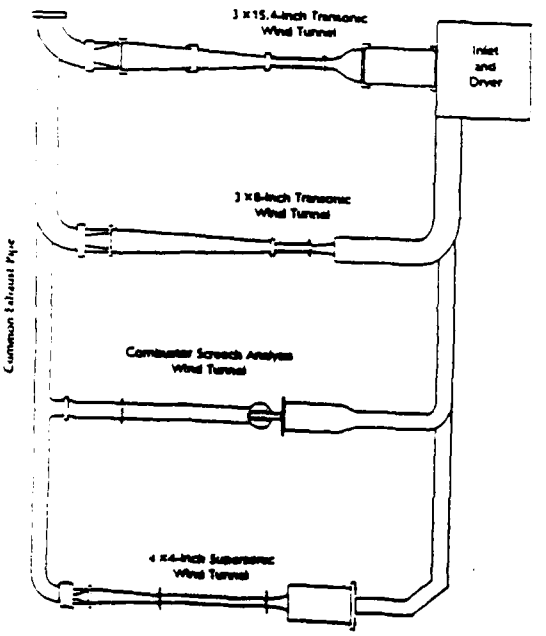

Fig. 34 - RPI Blow-Down Transonic Wind-Tunnel Facility

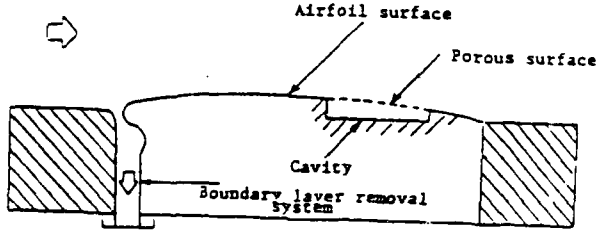

Fig. 35 - Schematic of Airfoil Model in Test Section

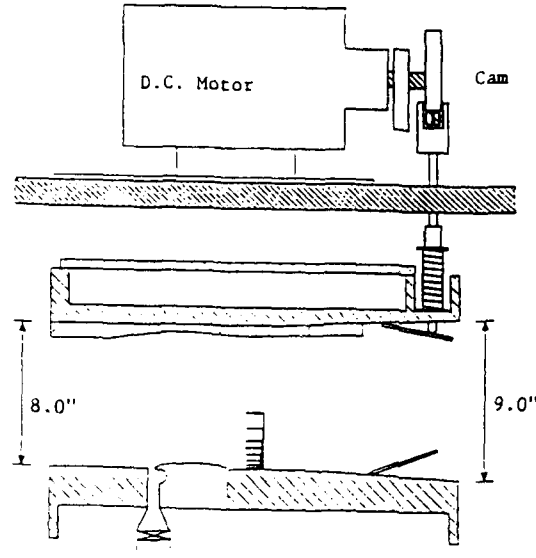

Fig. 36 - 3 × 8-in. Transonic Test Section with Contoured Ceiling and Oscillating Flow Control Wedge

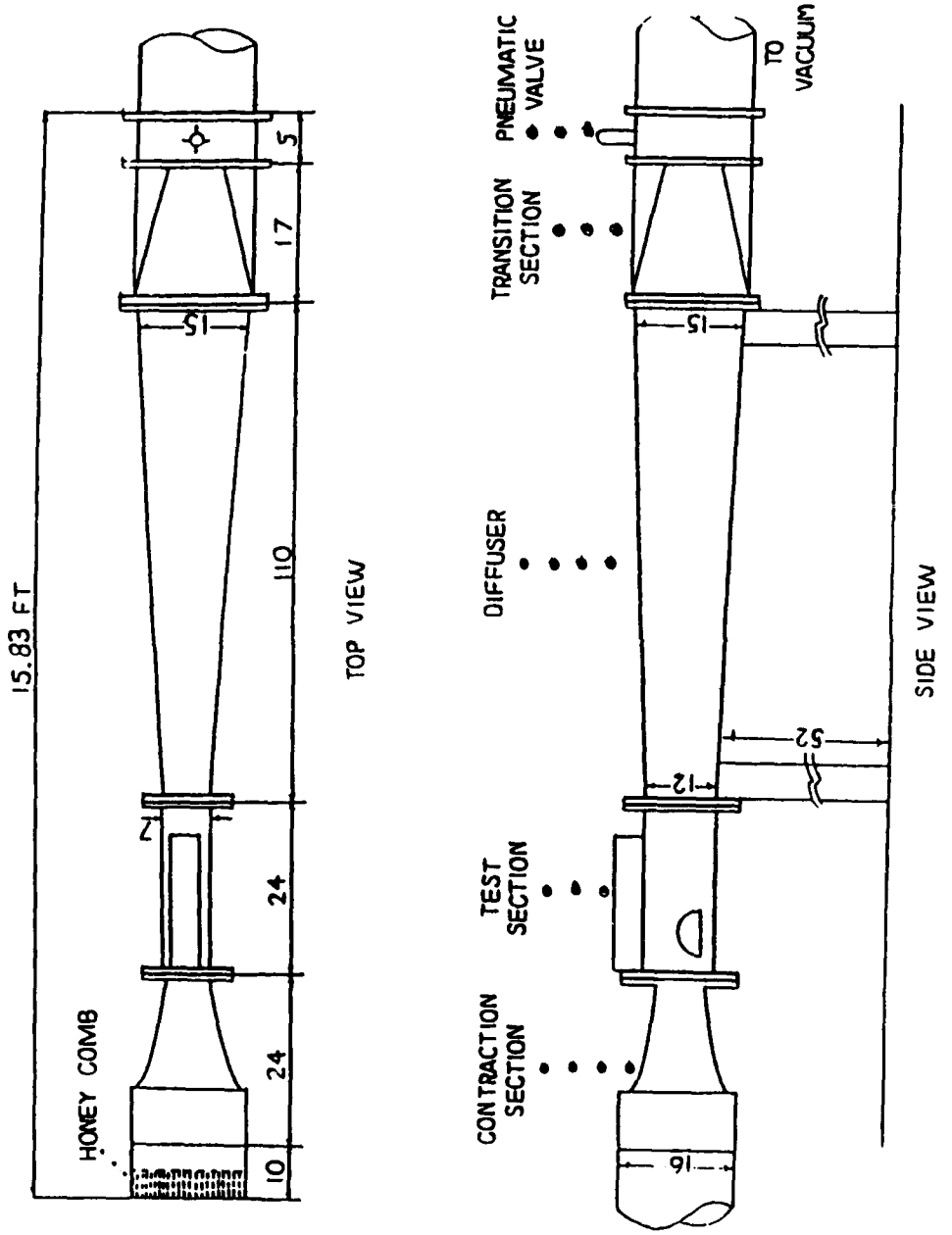

Fig. 37 - 3 x 8-in. Transonic Wind Tunnel

Fig. 38a - Schlieren Photograph of the Bell Airfoil with a Straight Top Wall at $M_\infty = 0.83$

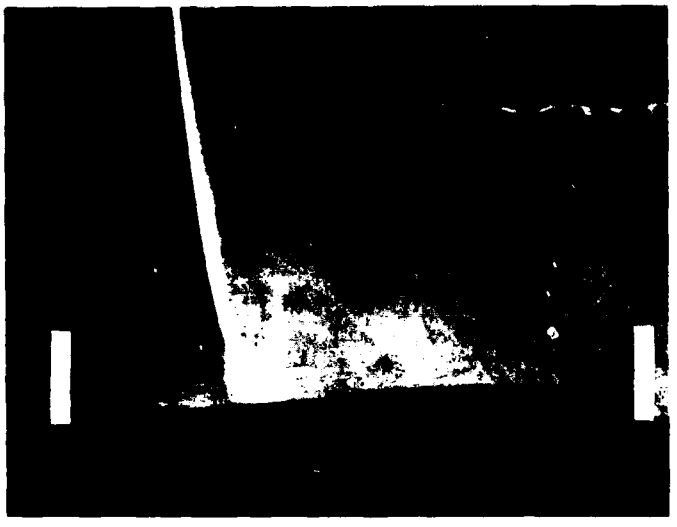

Fig. 38b - Schlieren Photograph of the Bell Airfoil with a Contoured Top Wall at $M_\infty = 0.866$

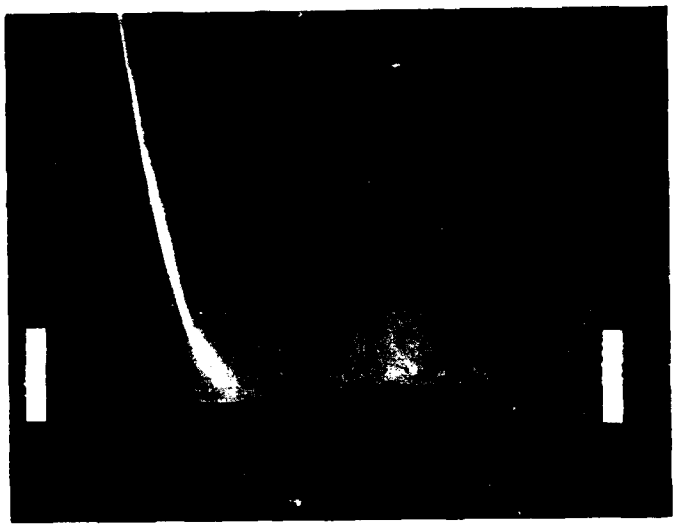

Fig. 39a - Schlieren Photograph of the Bell Airfoil with a Solid Surface at M_∞ - 0.86

Fig. 39b - Schlieren Photograph of the Bell Airfoil with a Porous Surface (45-75% x/c) at M_∞ = 0.86

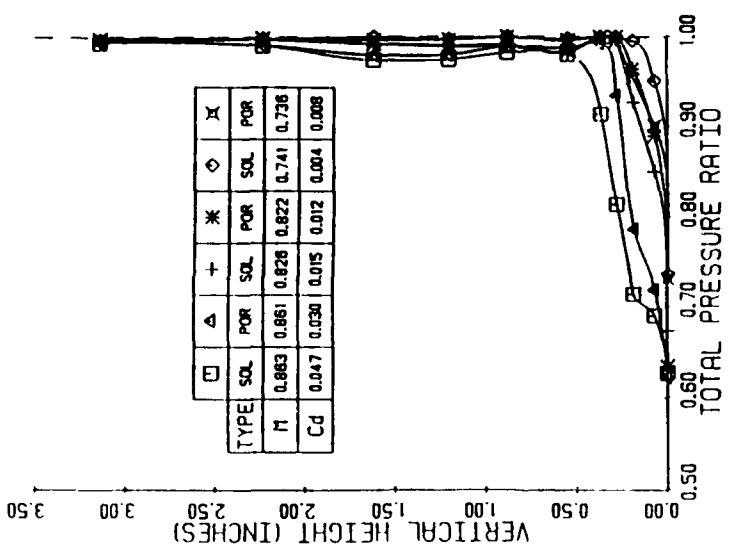

Fig. 41 - Wake Total Pressure Ratio Distributions for Solid and Porous Bell Airfoils M_∞ = 0.86, 0.82 and 0.74

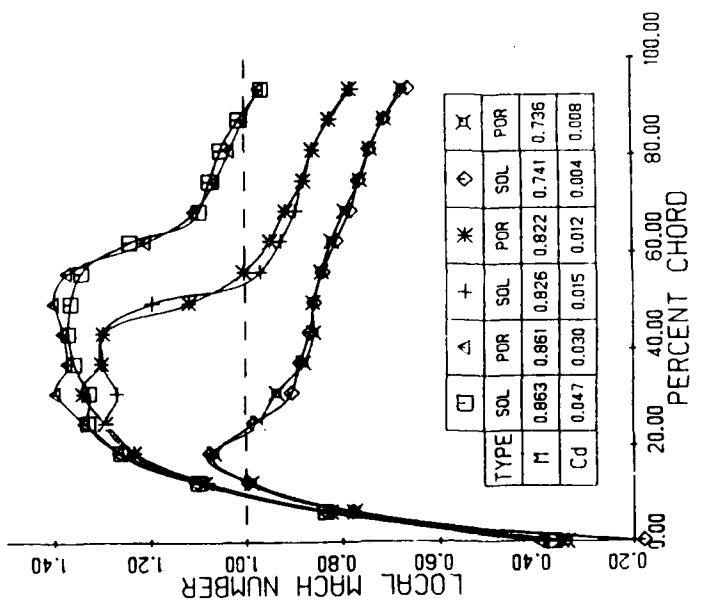

Fig. 40 - Mach Number Distributions Over the Bell Airfoil for Solid and Porous Cases at M_∞ = 0.86, 0.82 and 0.74

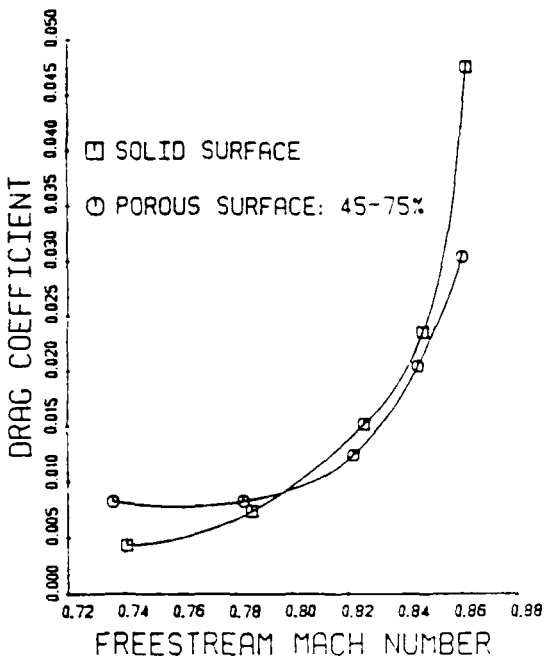

Fig. 42 - Drag Coefficient vs. Freestream Mach Number for Solid and Porous (45-75% x/c) Bell Airfoils

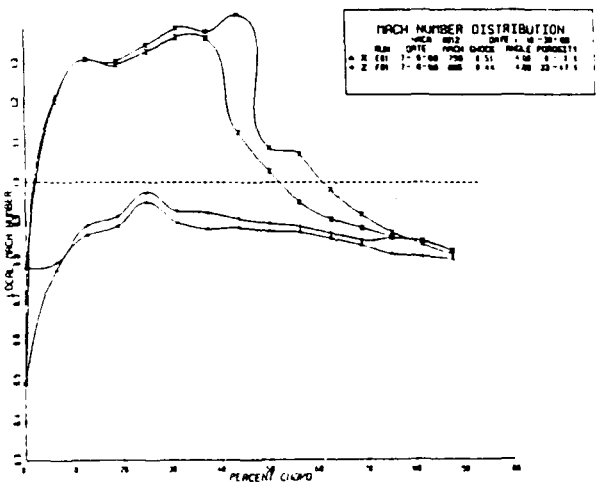

Fig. 43 - Mach Number Distribution for Solid and Porous 0012 Airfoils
$M_\infty = .80$, $\alpha = 4^o$

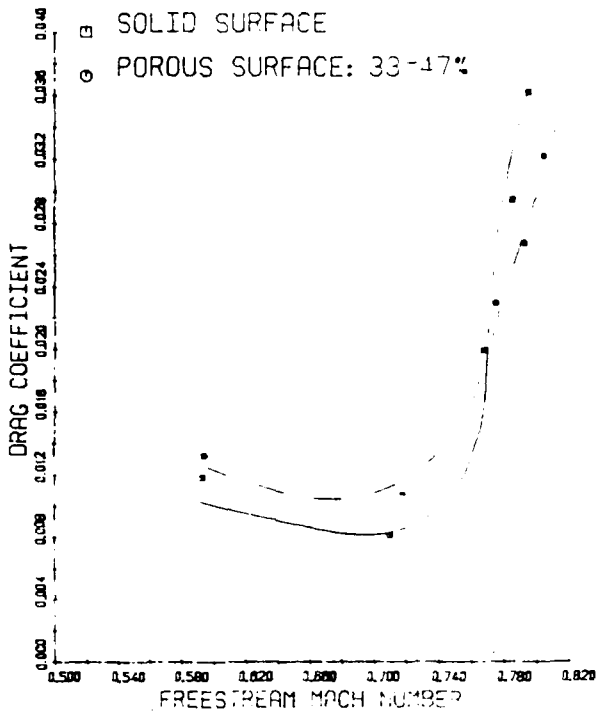

Fig. 44a - Drag Coefficient Variation with Mach Number for Solid and Porous (x/c = .33 to .47) 0012 Airfoils $\alpha = 4^{o}$

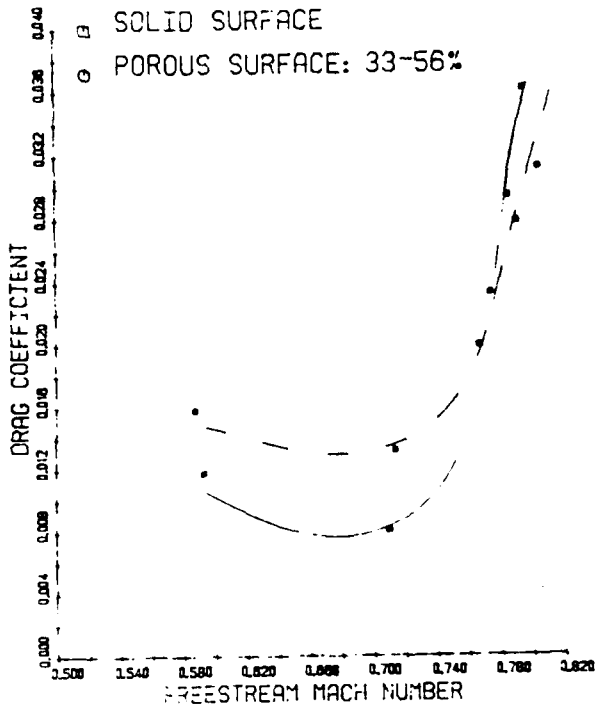

Fig. 44b - Drag Coefficient Variation with Mach Number for Solid and Porous (x/c = .33 to .56) 0012 Airfoils $\alpha = 4^{o}$

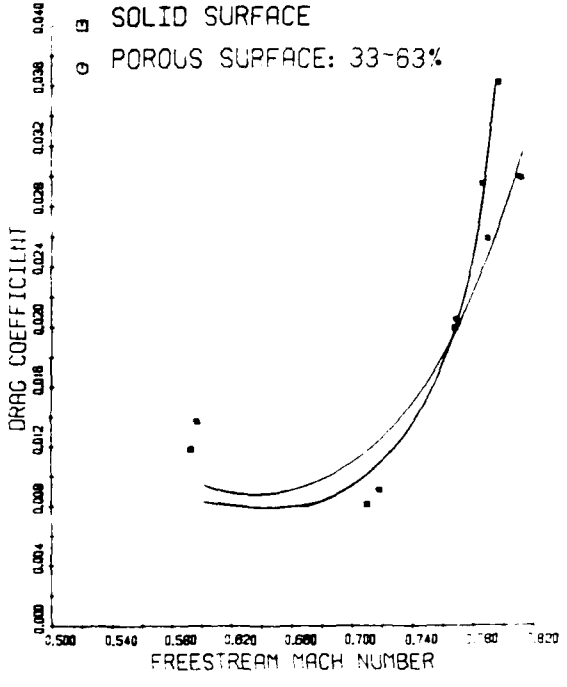

Fig. 44c - Drag Coefficient Variation with Mach Number for Solid and Porous (x/c = .33 to .63) 0012 Airfoils $\alpha = 4^{o}$

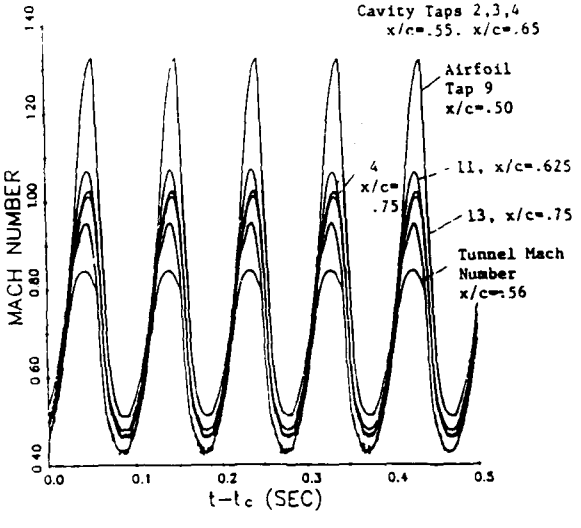

Fig. 45 - Unsteady Porous Bell Airfoil Surface/Cavity Pressure Survey Porosity (x/c = .45 to .75) Cavity Depth 1/4 Inch

Coincident L.E.

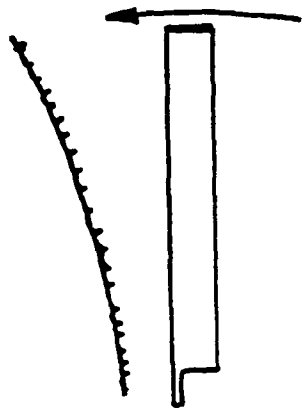

Travelling Radially

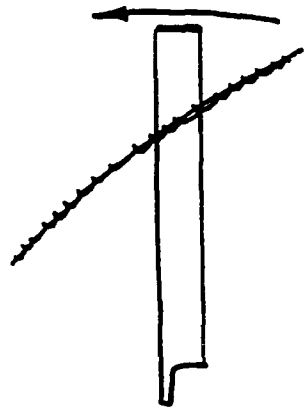

Vertical Slice

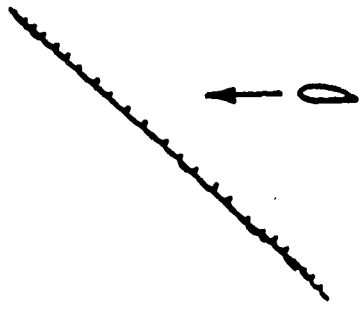

Fig. 46 - Trailing Vortex - Rotor Blade Intersection Patterns

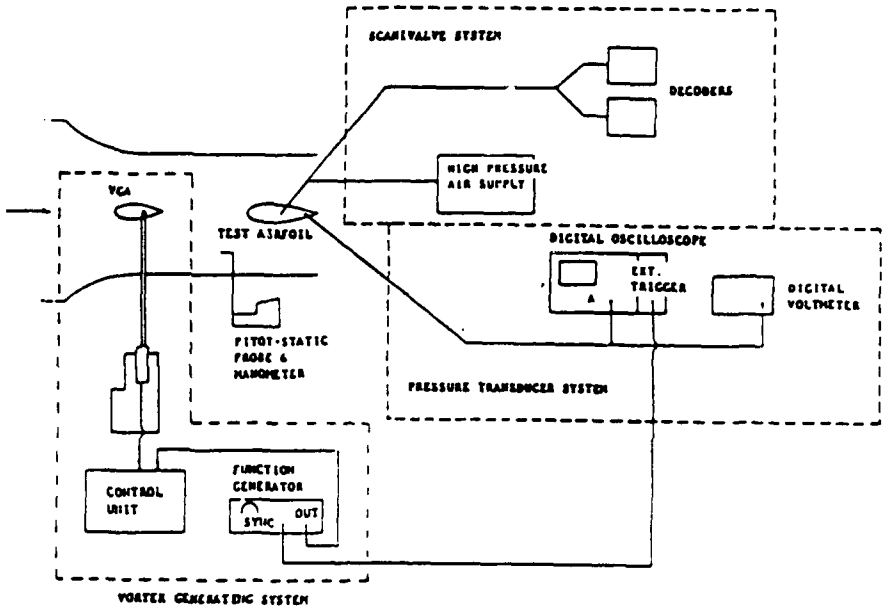

Fig. 47 - Blade-Vortex Experimental System Schematic

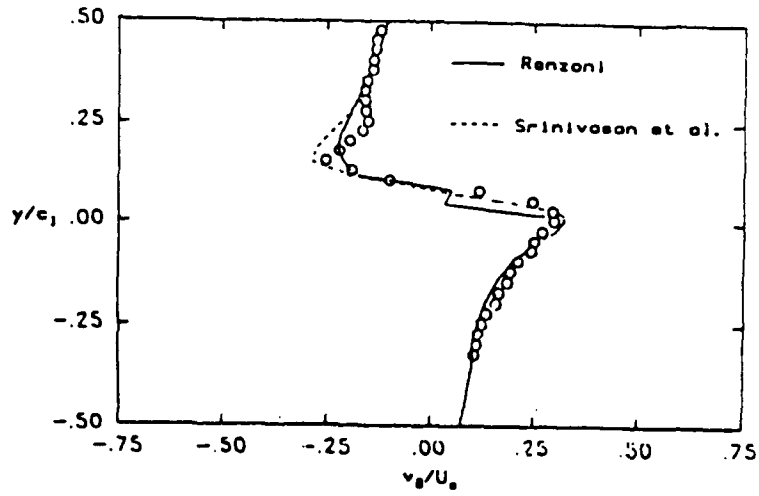

Fig. 48 - Measured and Calculated Velocity Distributions in Shed Vortex

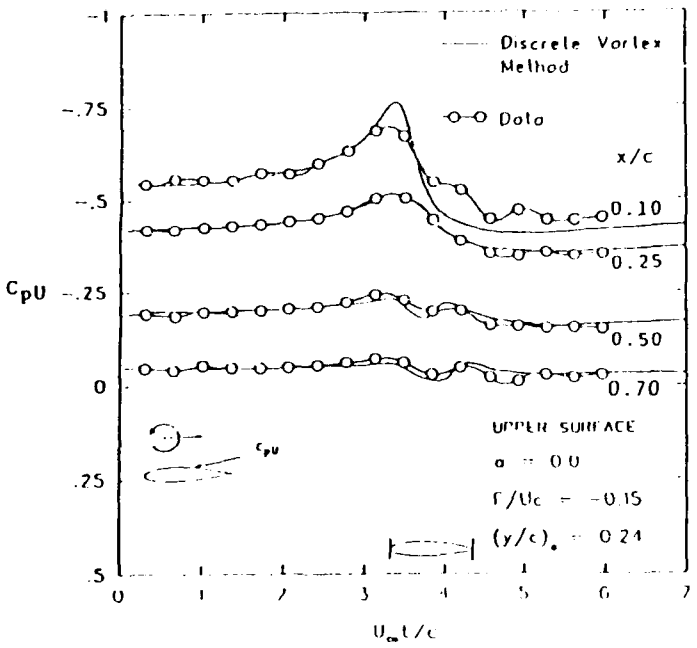

Fig. 49 - Measurements of Pressure-Time History for Upper Surface and Comparisons with Theory, Γ/Uc = 0.15

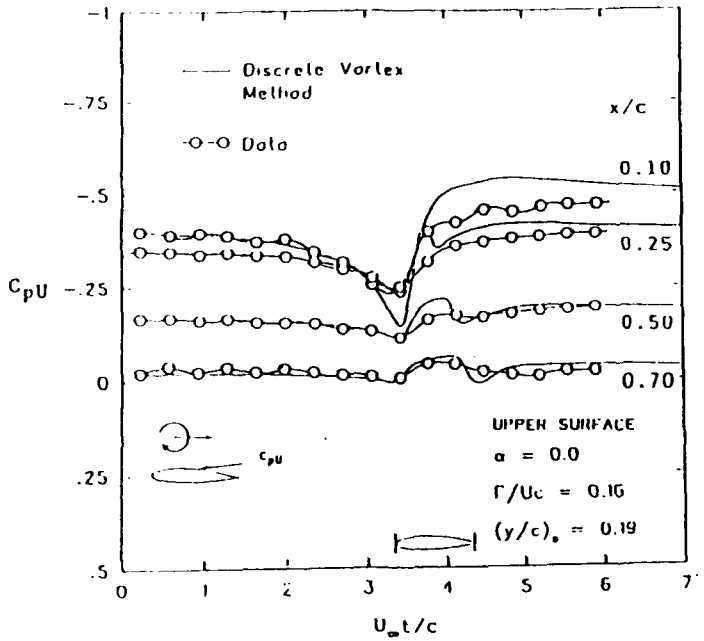

Fig. 50 - Measurements of Pressure-Time History for Upper Surface and Comparisons with Theory, Γ/Uc = 0.16

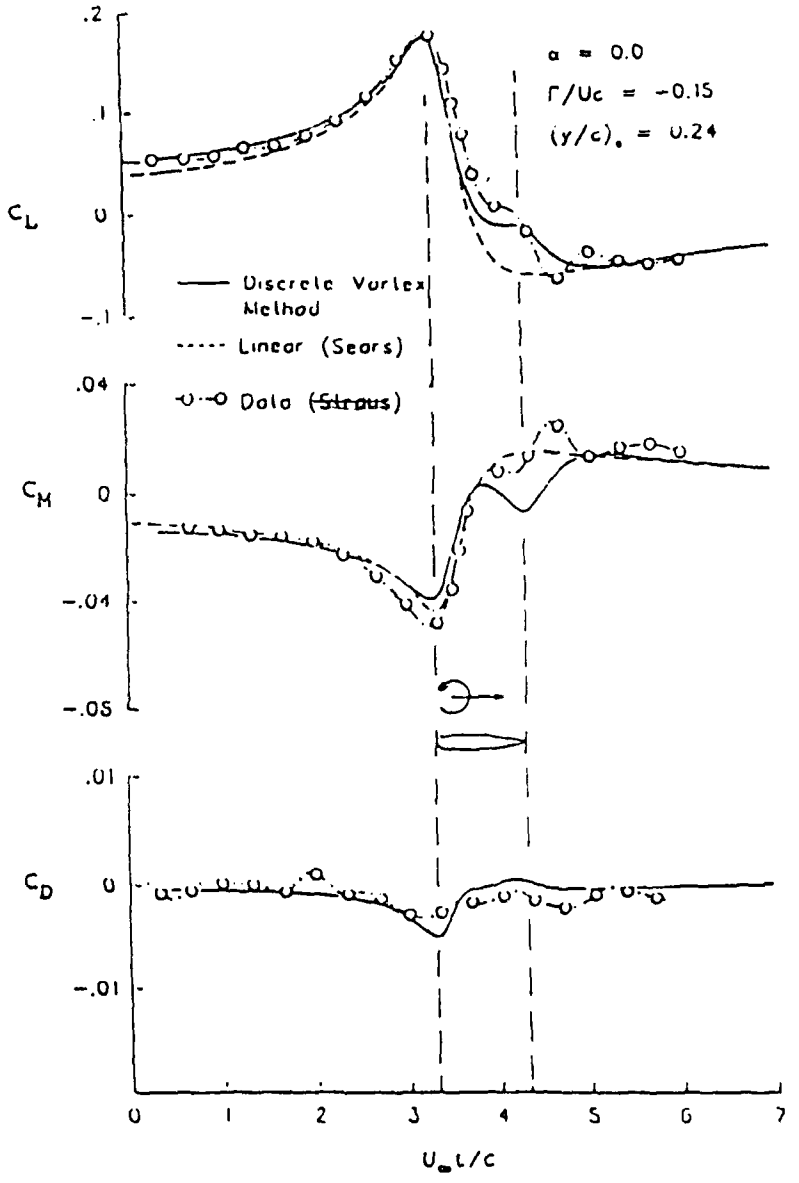

Fig. 51 - Temporal Variation in Lift, Moment and Drag Coefficients, Γ/Uc = 0.15

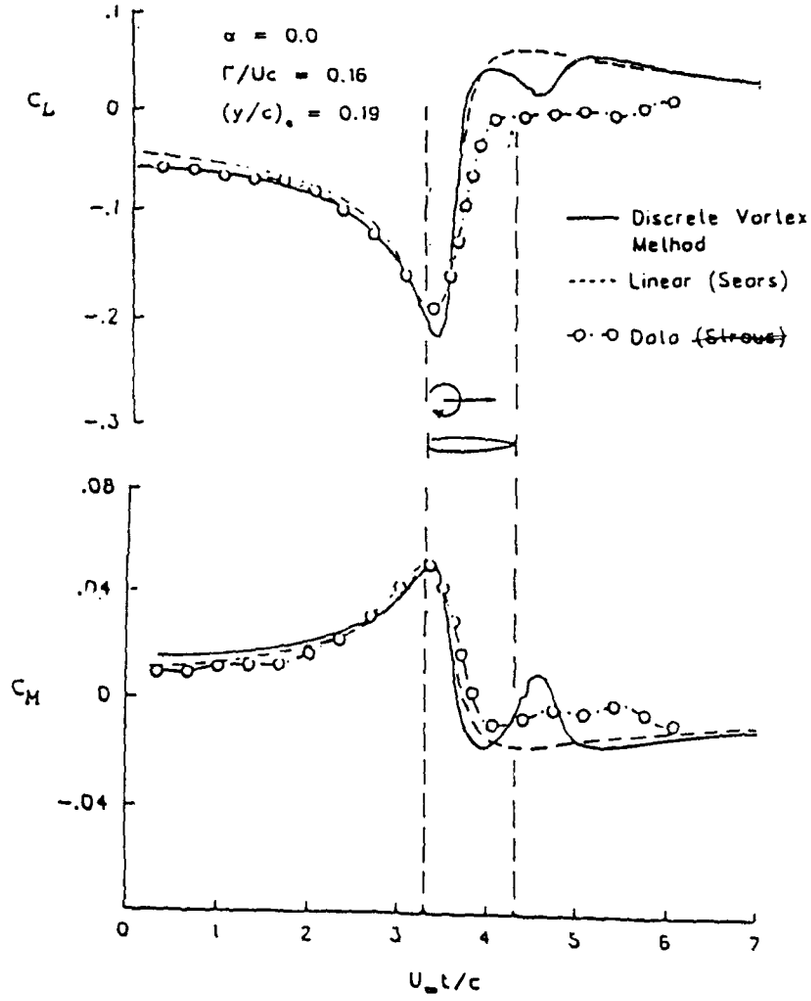

Fig. 52 - Temporal Variation of the Lift and Moment Coefficients, Γ/Uc = 0.16

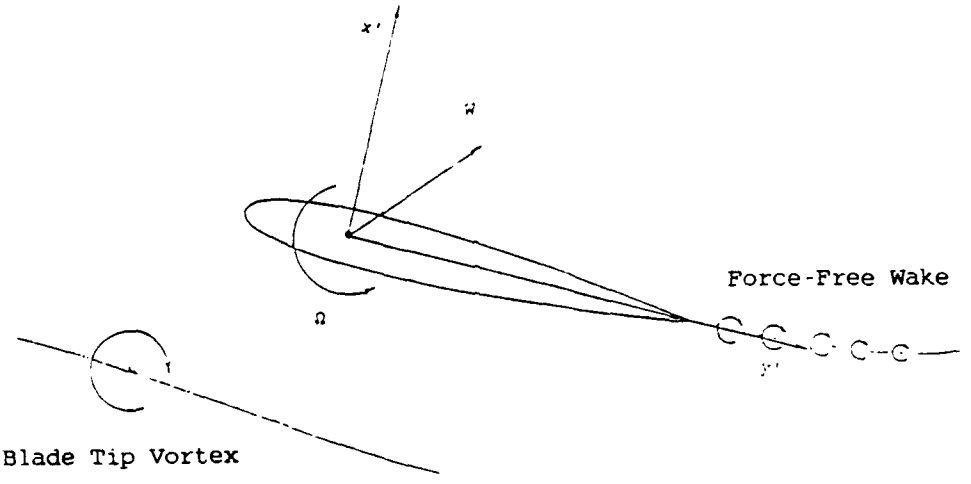

Fig. 53 - Theoretical Model for Blade-Vortex Interaction

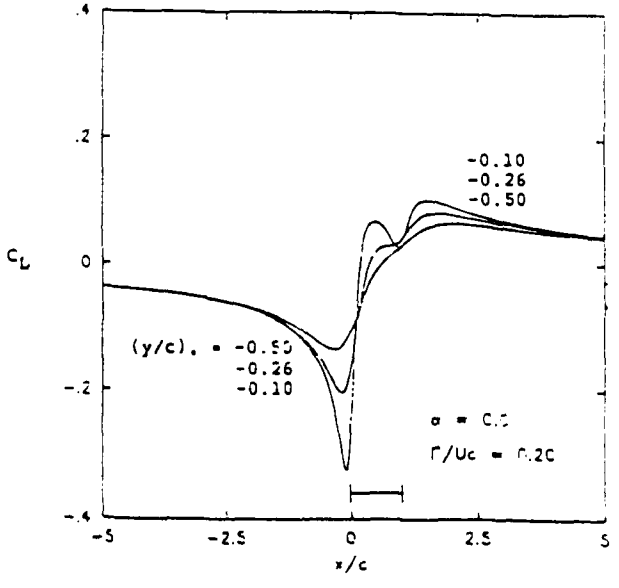

Fig. 54 - Effect of Initial Vortex Height on Lift Coefficient, $\Gamma/Uc_{\infty}c = 0.2$

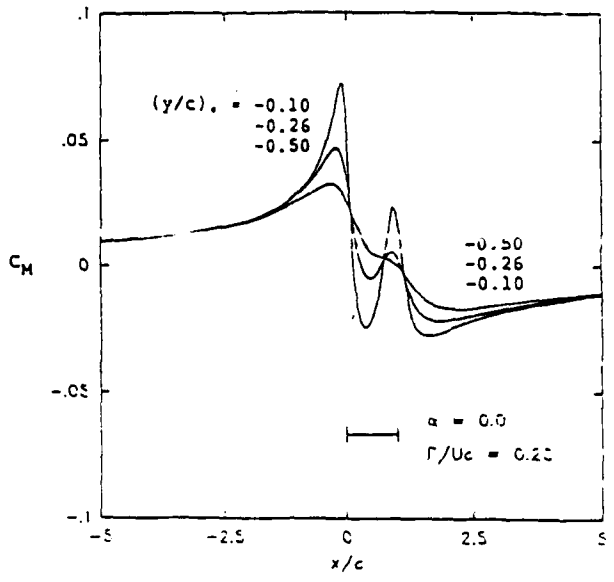

Fig. 55 - Effect of Initial Vortex Height on Moment Coefficient, $\Gamma/Uc_{\infty}c = 0.2$

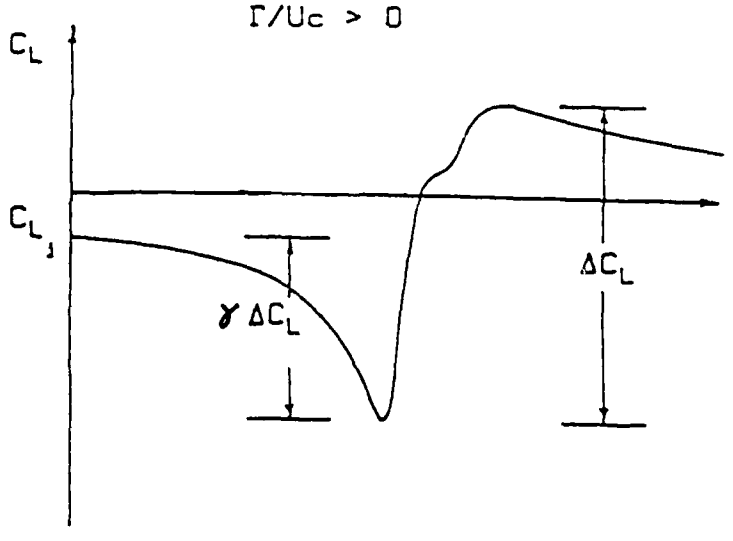

Fig. 56 - Definition of Incremental Lift Coefficients

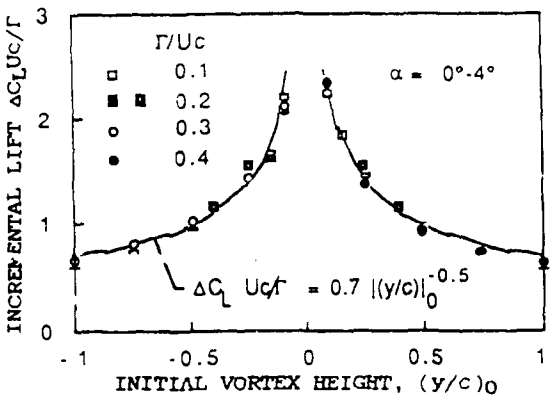

Fig. 57 - Correlation of the Incremental Lift Coefficient

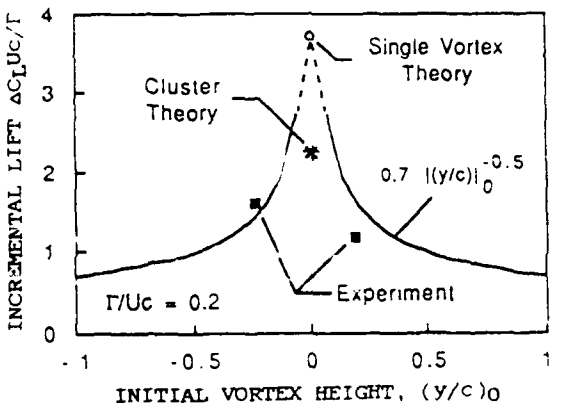

Fig. 58 - Incremental Lift Coefficient for a Close Encounter and Comparisons with Experiments

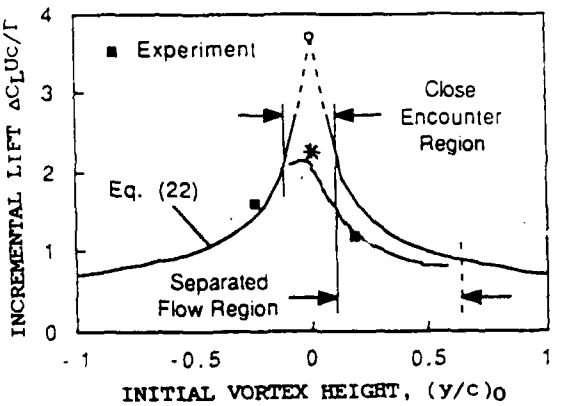

Fig. 59 - Blade-Vortex Interaction Regions

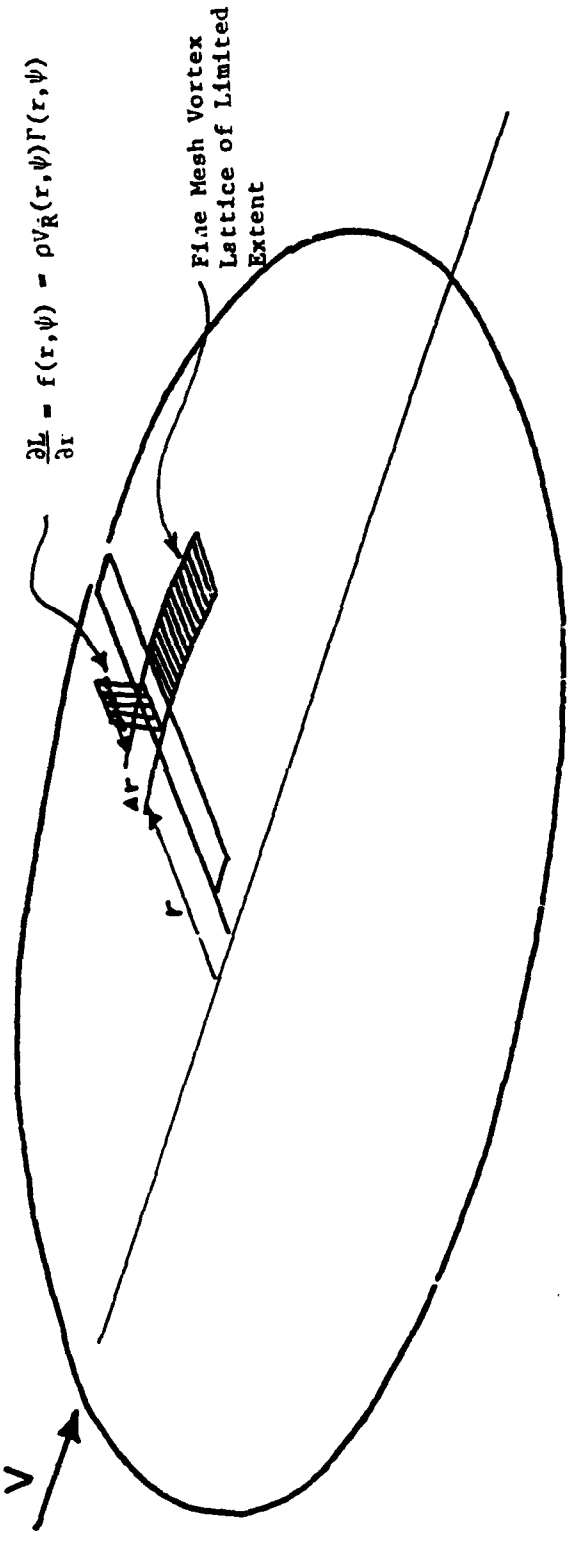

Fig. 60 - Vortex Lattice for 3-D Rotor Unsteady Aerodynamics Calculation

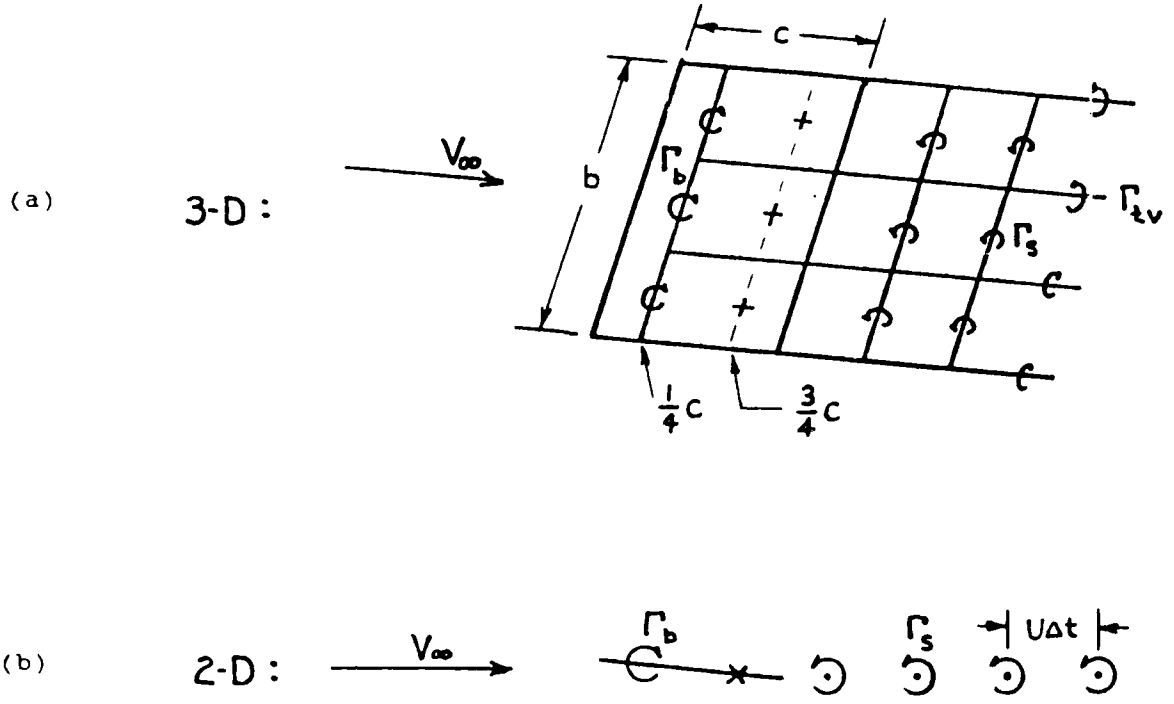

Fig. 61 - Discrete Vortex Models for Wings and Airfoils in Unsteady Uniform Flow

(a) PTF Pulses

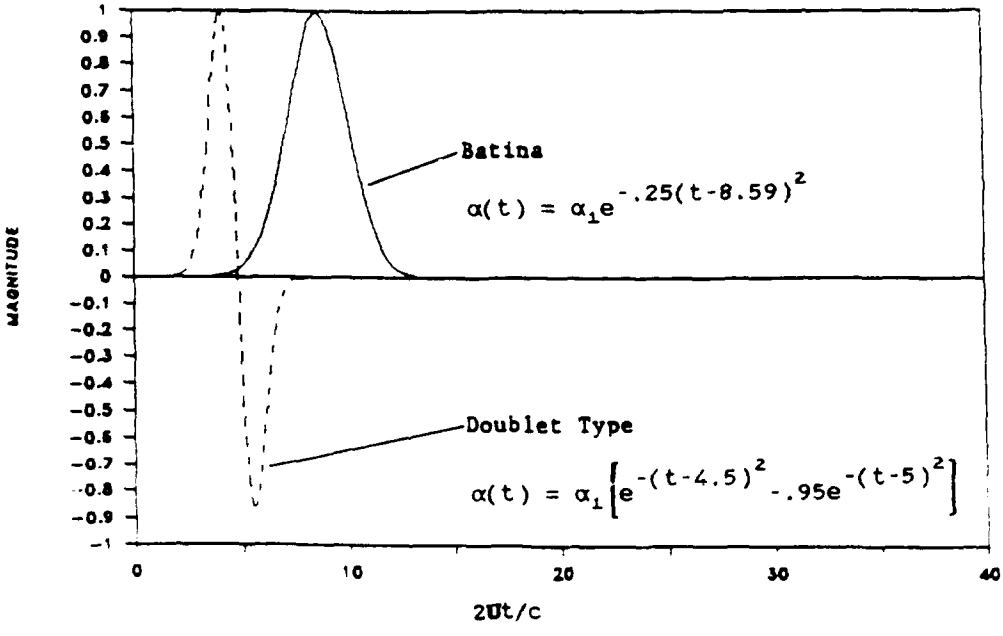

(b) PTF Pulse Responses

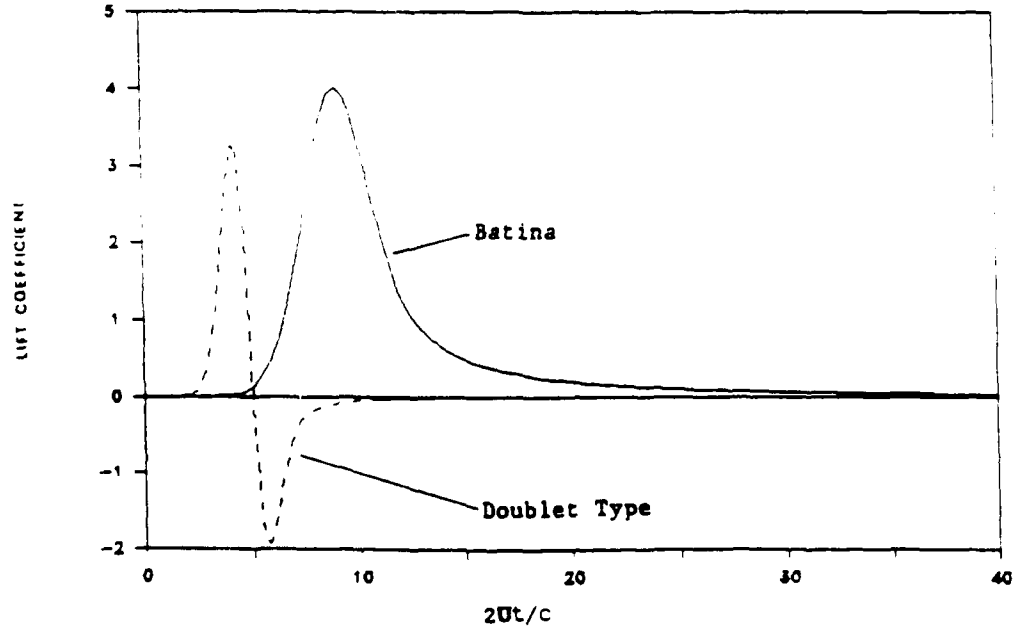

Fig. 62 - Pulse Disturbances and Aerodynamic Response

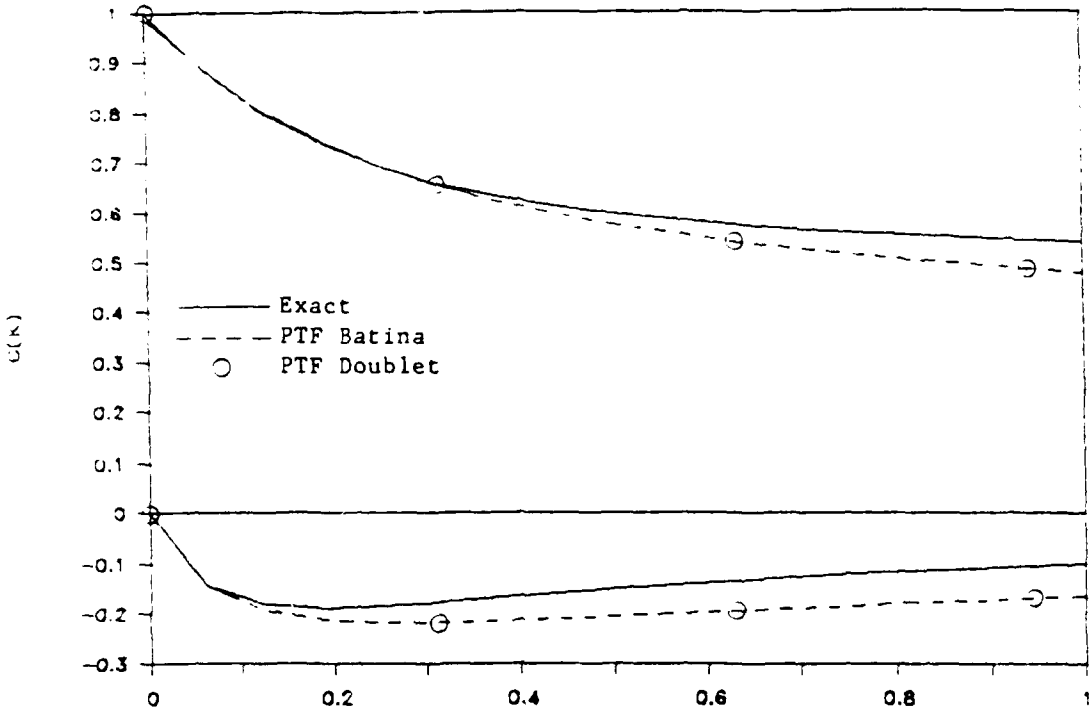

$$K = \frac{c\omega}{2V}$$

Fig. 63 - Comparison of PTF Results with Theodorsen's Function

AR=6 RECTANGULAR WING

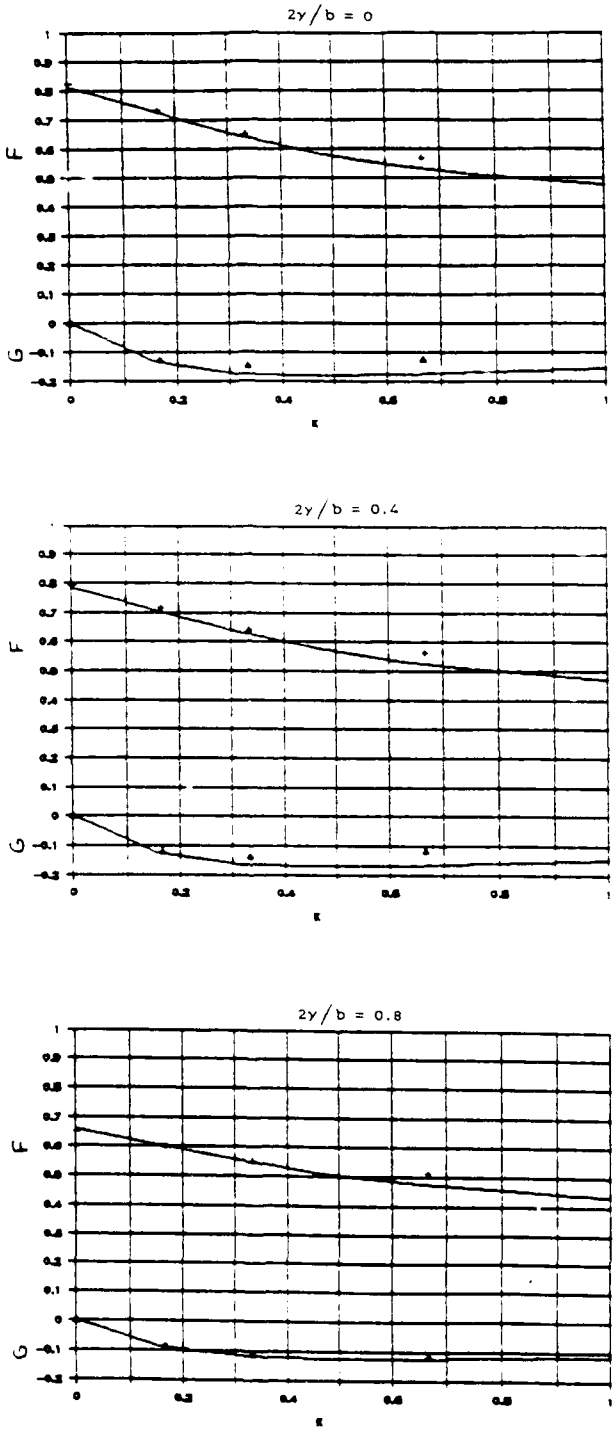

Reissner + , Δ

PTF ————

Fig. 64 - Comparison of PFT Results with Reissner's Solution
(Note: b = span; γ = circulation density)

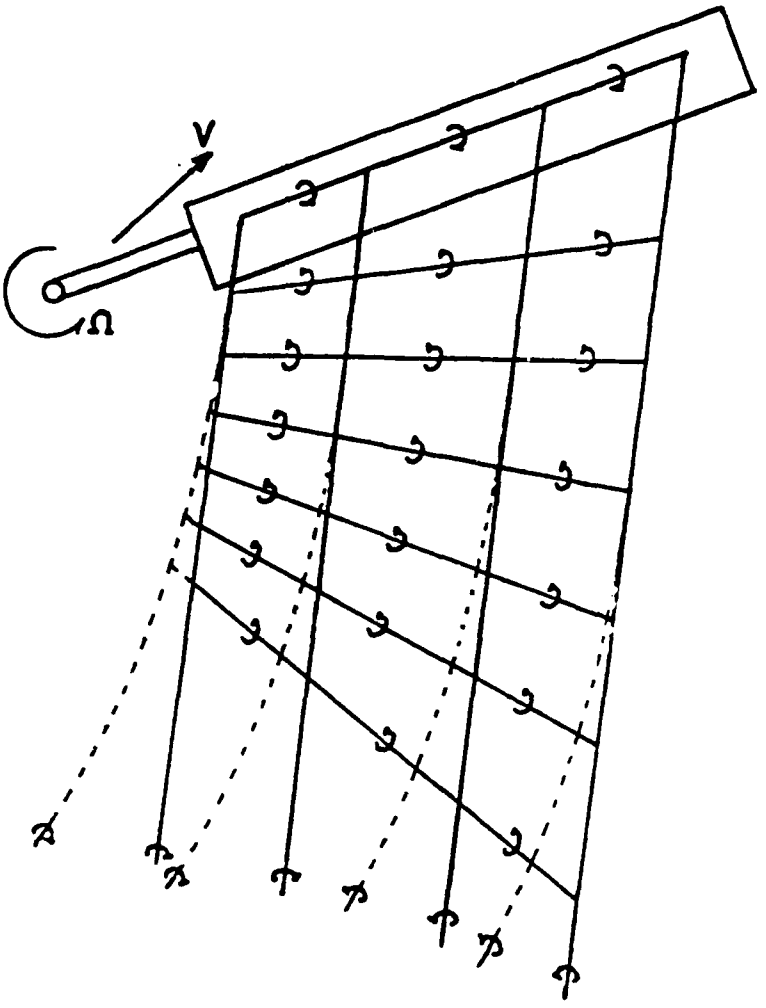

----- SKEWED HELICAL VORTEX POSITIONS
——— MODELED VORTEX POSITIONS

Fig. 65 - Discrete Vortex Model of a Rotor Blade in Forward Flight

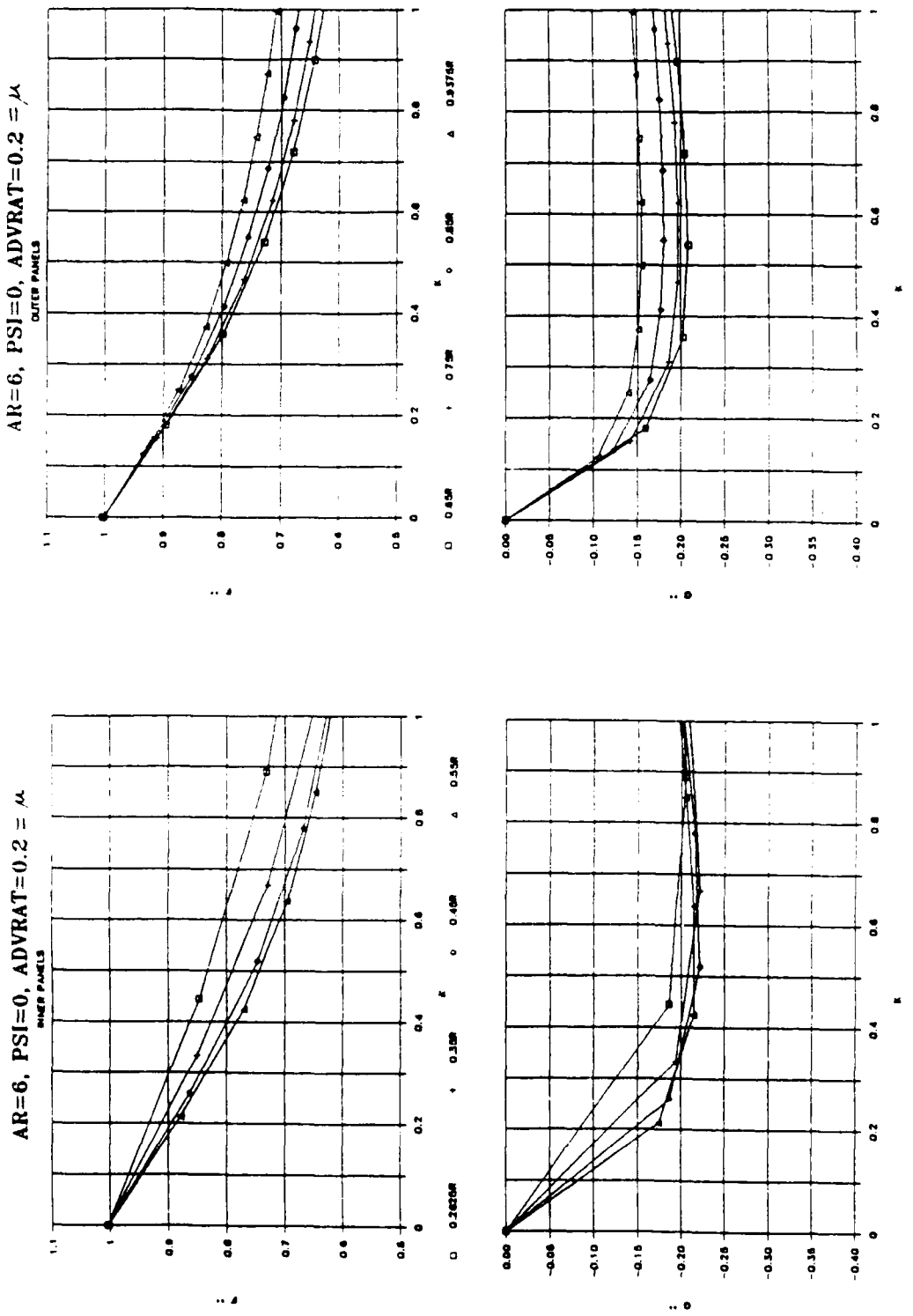

(a) PSI = 0

Fig. 56 Lift Deficiency Functions for an Aspect Ratio 6 Rotor Blade at an Advance Ratio of 0.20

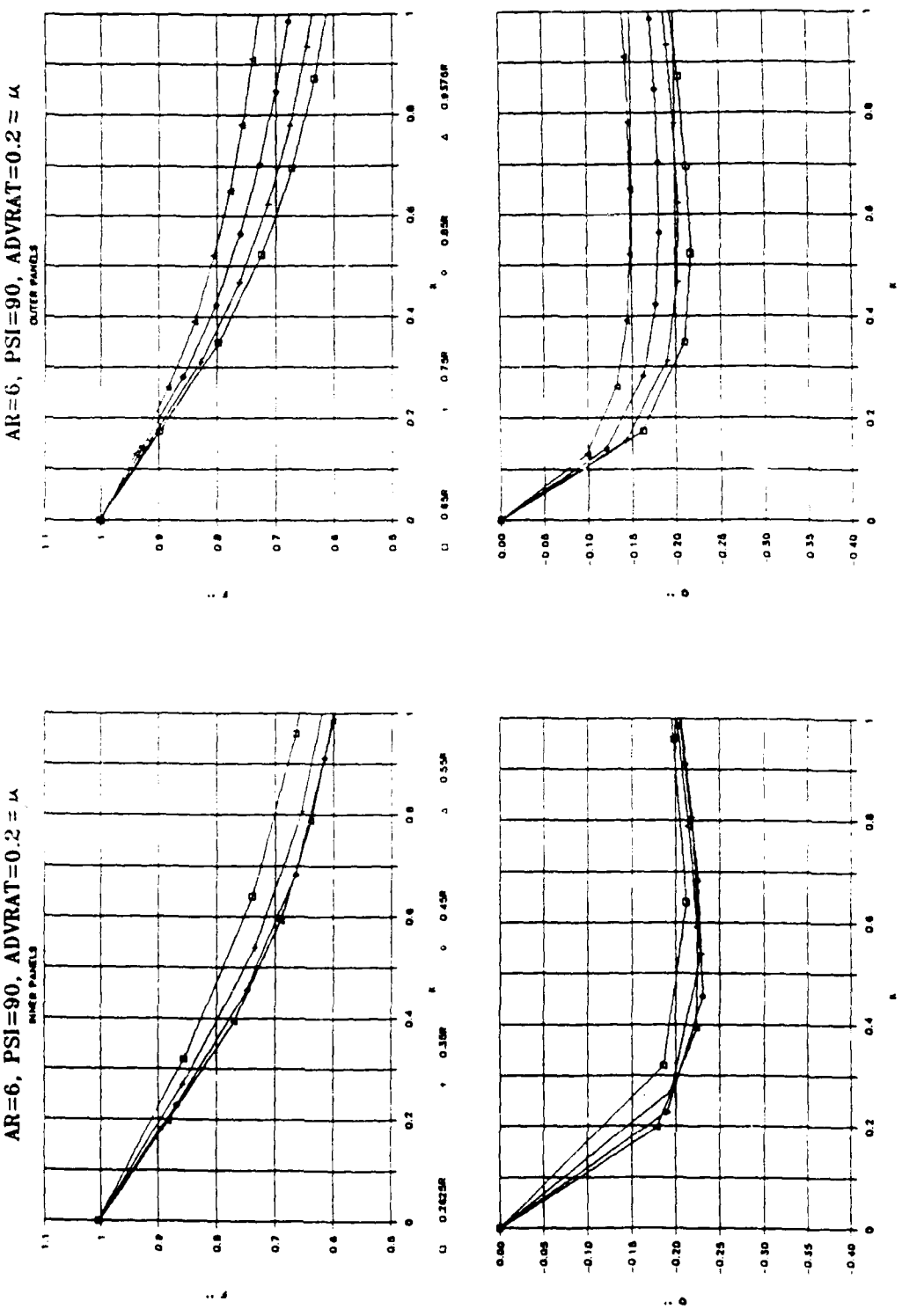
AR=6, PSI=90, ADVRAT=0.2 = μ
OUTER PANELS
AR=6, PSI=90, ADVRAT=0.2 = μ
INNER PANELS

(b) PSI = 90

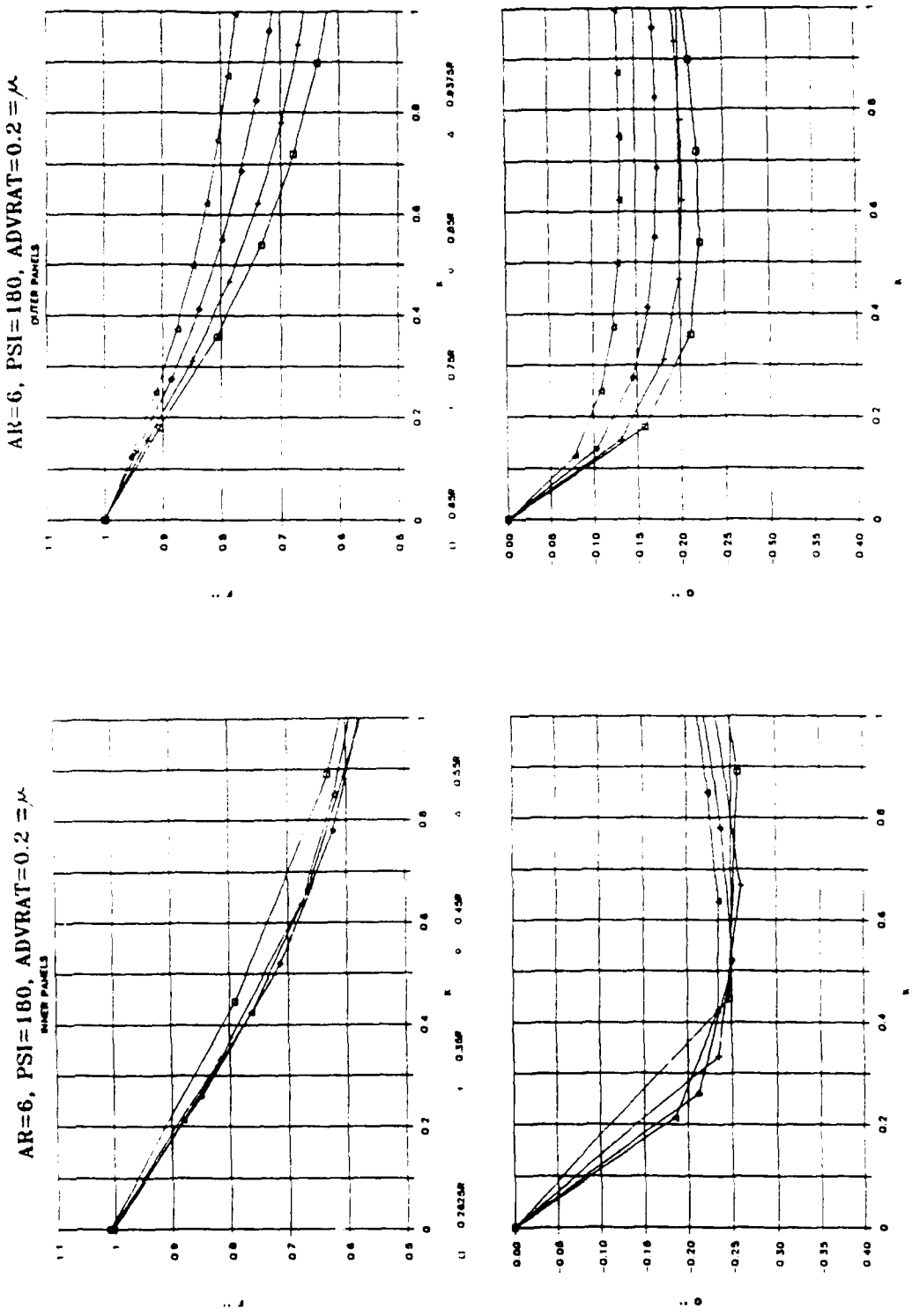
AR=6, PSI=180, ADVRAT=0.2 =μ
OUTER PANELS
AR=6, PSI=180, ADVRAT=0.2 =μ
INNER PANELS

(c) PSI = 180

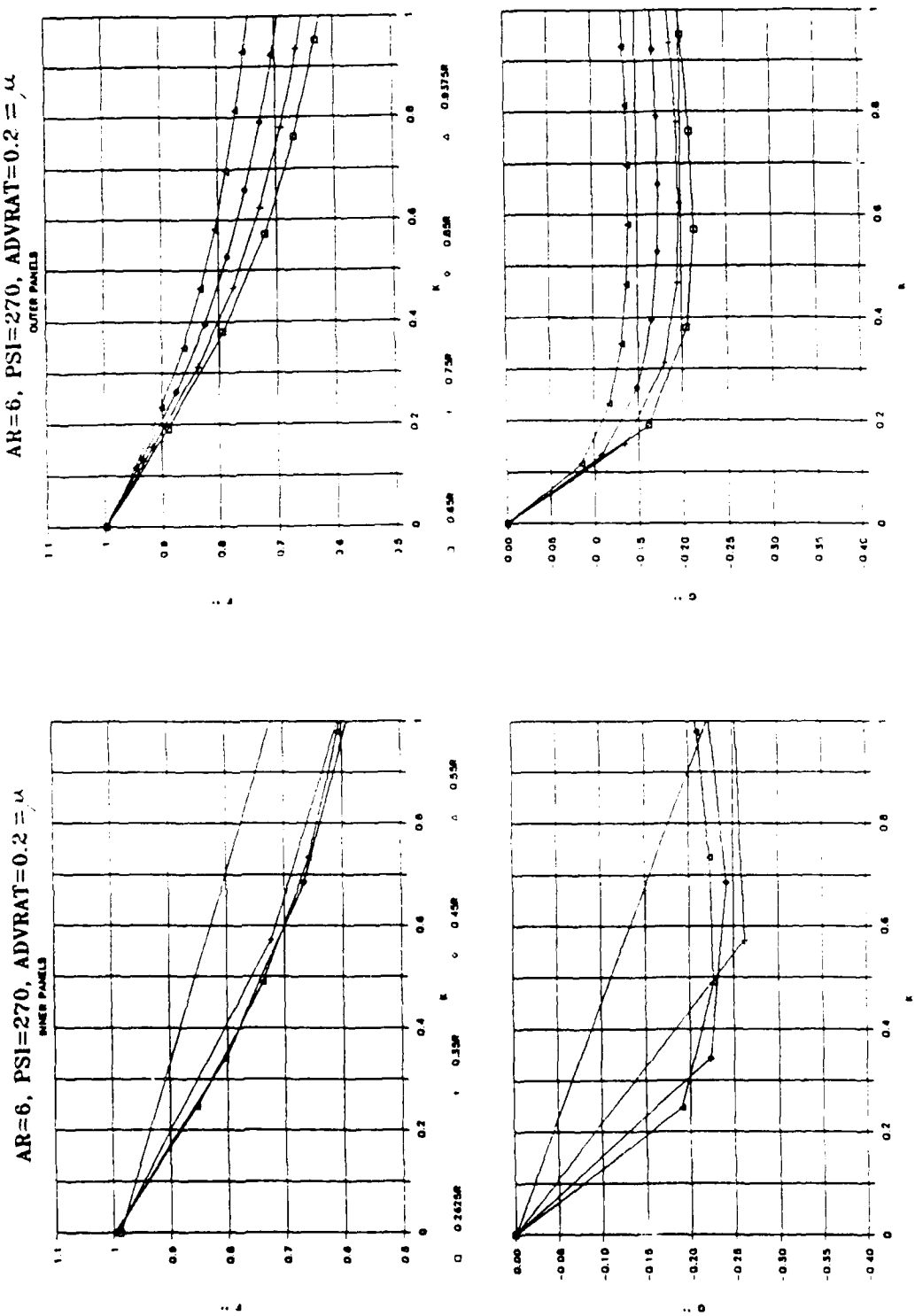
AR=6, PSI=270, ADVRAT=0.2
OUTER PANELS
AR=6, PSI=270, ADVRAT=0.2
INNER PANELS

(d) PSI = 270

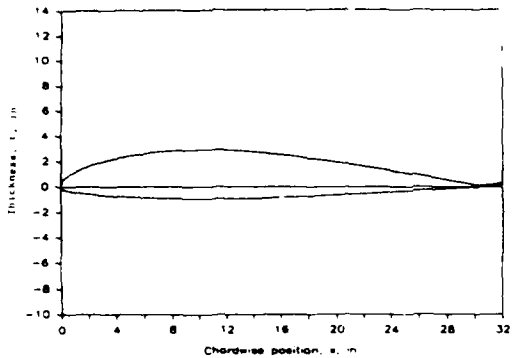

(a) Unmodified Boeing VR-7 Airfoil Section (- 3.1° Tab)

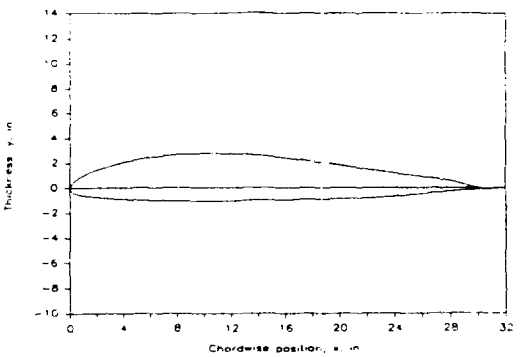

(b) Unsnapped Airfoil Geometry

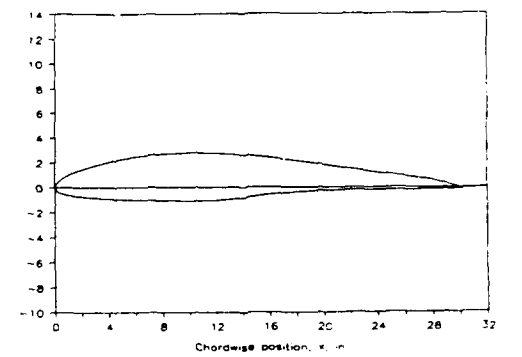

(c) Snapped-In Airfoil Geometry

Fig. 67 - Comparative Airfoil Shapes

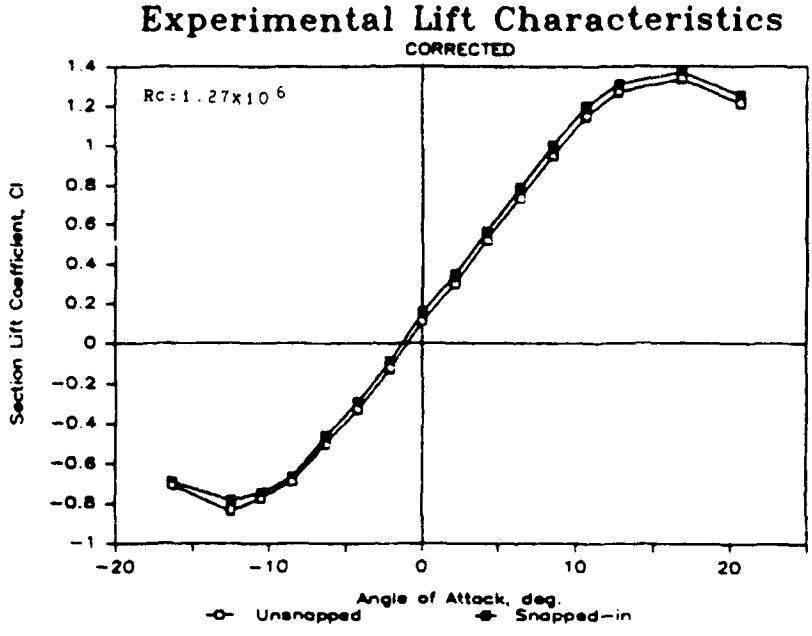

Fig. 68 - Experimental Steady-State Lift Coefficient

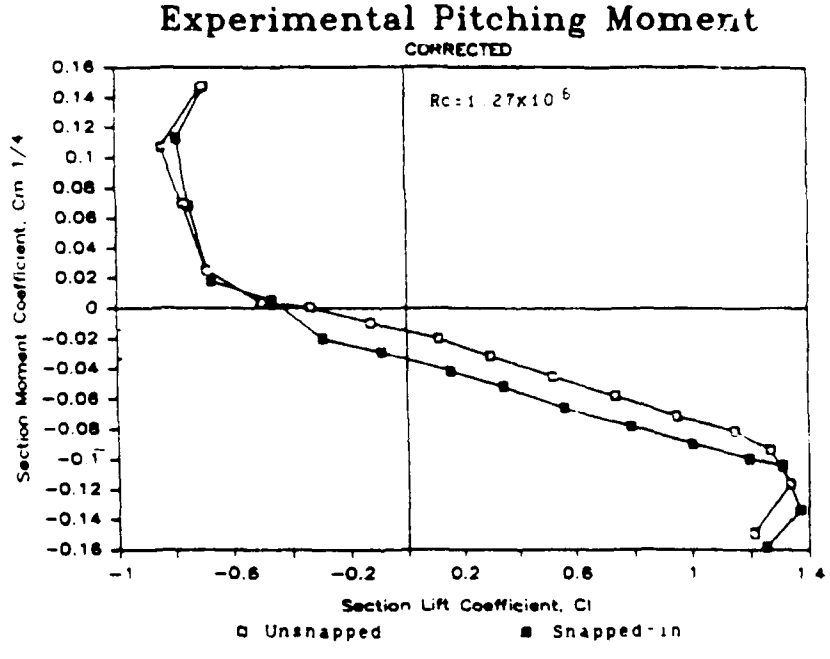

Fig. 69 Experimental Steady-State Pitching Moment Coefficient

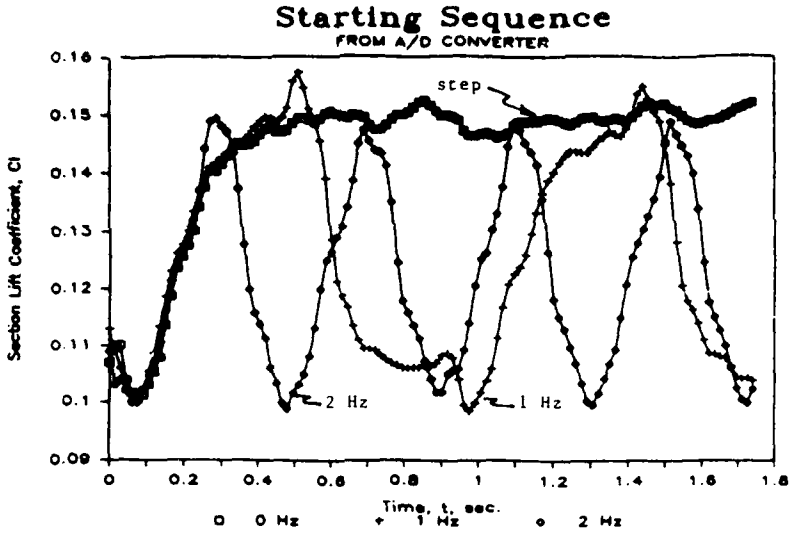

Fig. 70 - Aerodynamic Lift Response for the Step-Snap and Snapping Rates of Approximately One and Two Hertz

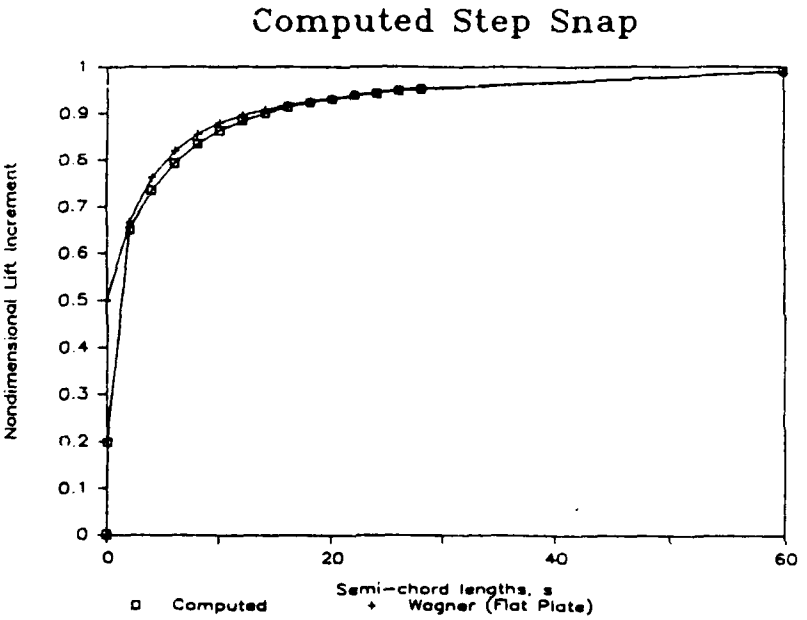

Fig. 71 - Computed Lift Response to Step Snap and Comparison with Wagner's Function

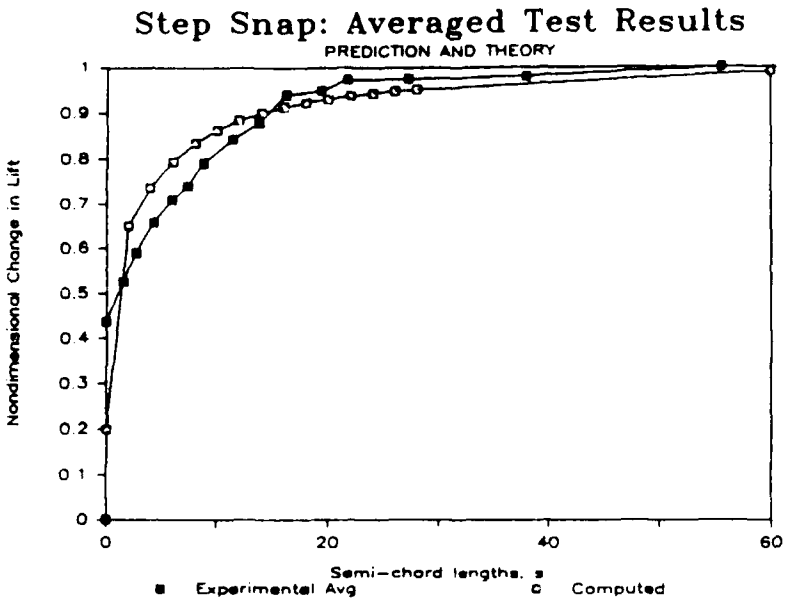

Fig. 72 - Comparison between Averaged Experiment Step-Snap Lift Response and Predicted Response

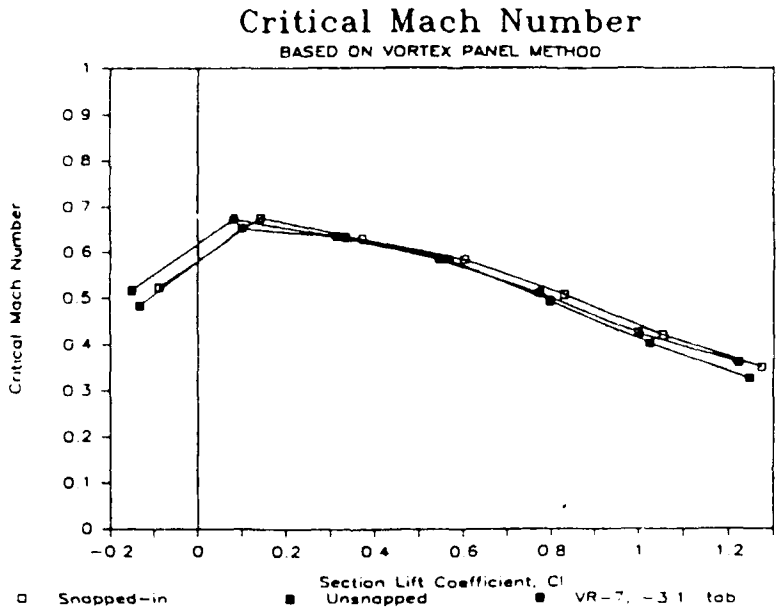

Fig. 73 - Vortex Panel Method Prediction of the Critical Mach Number

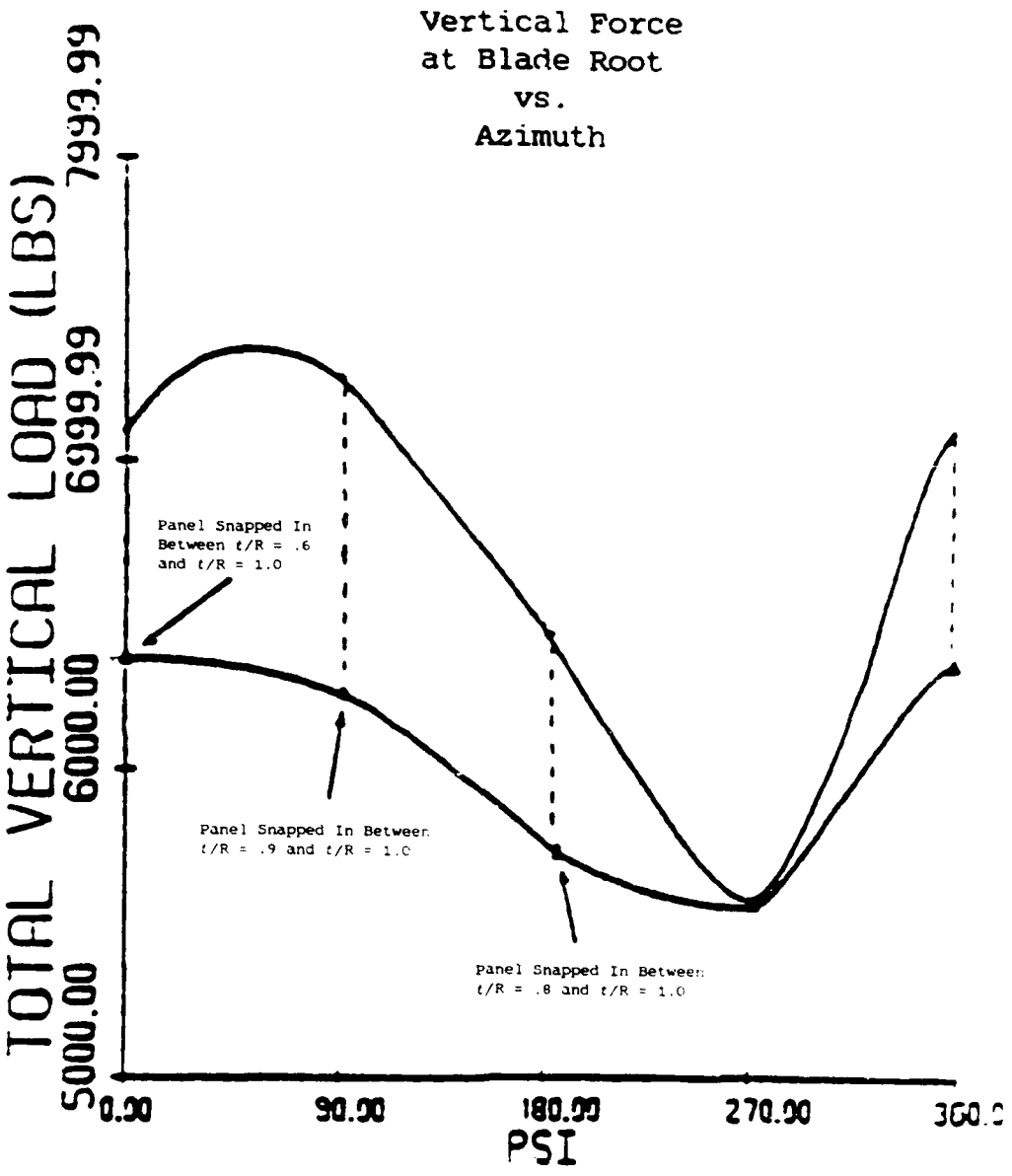

Fig. 74 - Total Vertical Shear at Hub vs Azimuth Angle for One Snap Panel Schedule

TABLE 15

Industrial Contacts and Sketches of Rotor Tip Airfoil Sections

Rensselaer RTC

Dr. W.J. McCroskey
Senior Staff Scientist
Department of the Army
Aeromechanics Laboratory
Ames Research Center

Mr. L.U. Dadone
Aerodynamics Group
Boeing Helicopter Company

Mr. G.J. Bingham
Aerospace Engineer
Department of the Army
Structures Laboratory
Langley Research Center

Mr. T.W. Sheehy
Chief of Aerodynamics
Sikorsky Aircraft Company

Dr. David Kocurek
Principal Engineer
Aerodynamics
Bell Helicopter Company

Mr. R.W. Prouty
Chief of Stability and Control
McDonnell-Douglas Helicopter Company

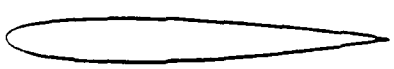

NACA 0012

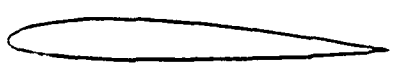

AMES-01

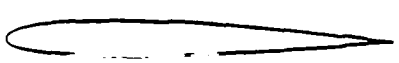

SIKORSKY SC-1095

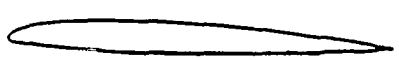

NLR-1

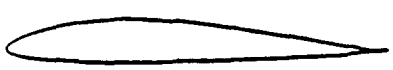

VERTOL VR-7

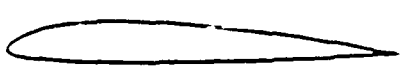

WORTMANN FX-098
BELL FX-69-H-098

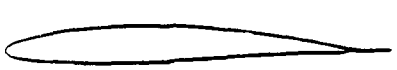

HUGHES HH-02

NLR-7301 SUPERCRITICAL

5.d. Aeroelasticity

Aeroelasticity is the discipline in which, for helicopter rotors, "it all comes together". Unsteady aerodynamics, elastic deformations, and inertial effects -- particularly those associated with rotational dynamics -- all interplay to determine equilibrium (trim), stability, and forced response. Of interest, ultimately, are the influences on performance, stability and control, blade structural integrity and the steady and vibratory loads transmitted to fuselage drive systems and controls. Because of its importance and inherent difficulty, three aeroelasticity research projects were initially undertaken under the aegis of the RRTC. By the close of the contract, five such projects were being pursued.

5.d.(1). Finite Element Approach to Rotor Dynamics

(Sr. Investigator: O. Bauchau)

Helicopter and tilt-rotor aircraft lifting rotors are becoming increasingly complex, when viewed as dynamic systems, due to a number of factors. New configurations are emerging, such as the bearingless main helicopter rotor; the constant speed joint, highly twisted, tilt rotor and the multiply ducted x-wing rotor. Further, more complex blade geometries are being introduced including swept tips, preconed or drooped blades, and flexbeam hub retentions with redundant load paths. Finally, composite materials are used more and more systematically at all levels in new blade designs. It follows, then, that increasingly capable, comprehensive analysis capabilities are needed as never before, requiring the development of new formulation and solution techniques.

The finite element method (FEM) is a well established technique for linear and nonlinear, static and dynamic analysis for a wide variety of structures. It is now gaining increasing popularity for dynamic rotor analysis. Finite element formulations offer major advantages in their ability to deal readily with complex geometries and redundant load paths, composite materials, and kinematic non-linearities. Computer codes based on finite elements existing at the initiation of this project were not well suited for rotor analysis. Plate and shell elements would have provided excellent accuracy, but the number of degrees of freedom involved in such a model would be prohibitive for analysis in support of design. On the other hand, existing beam elements would not have modeled accurately helicopter blade features such as pretwist or elastic coupling and the other deformation characteristics arising from the use of composite materials.

The goal of this research, therefore, was to develop a simple, yet accurate finite element for beamlike structures. The assumptions which formed the foundation for this analysis are:

i) The blade cross-section is assumed to be infinitely rigid in its own plane. Hence, applied loads induce only axial and shear strains in the walls of its load-carrying members.

ii) The displacement fields of the blade cross-sections have two components: they can undergo three (rigid) translations and three (rigid) rotations, and - in addition - deformations of the cross-sections out of their own plane. The rigid cross-section displacement components mentioned first correspond to the classical assumption that cross-sections remain plane. They need not, however, remain normal to the deformed axis of the blade; hence transverse shearing deformations are allowed. The out-of-plane cross-sectional deformations are restricted to the St. Venant warping deformations in bending and torsion. Such warping deformations are generally negligible for long, slender blades constructed using isotropic materials. These deformations, however, become much more pronounced when composite materials are used. Torsional warping deformations are particularly significant, and bending warping deformations are important when strong elastic coupling is present.

iii) Since structural integrity would require it, it was assumed that for any realistic design, deformations are limited to small strains. This allows linear stress-strain relations to be used. Within this assumption and the framework established by assumptions (i) & (ii), above, exact strain-displacement relationships were derived for arbitrarily large displacements and rotations. Euler angles were used to represent finite rotations.

iv) Three coefficients were defined and assumed to characterize the stiffness of the blade cross-section walls, assumed thin. These elastic coefficients are A_{nn} and A_{qq}, the Young's and shearing moduli, respectively, integrated through the wall thickness; and A_{nq}, the extension-shearing coefficient. Material properties were allowed to vary along the blade axis and over the cross-section. With isotropic materials, or for orthotropic materials when one axis of orthotropy is aligned with the axis of the blade, A_{nq} vanishes. If A_{nq} is non-zero, elastic coupling such as bending-twisting, or extension-twisting results.

v) While the kinematic descriptions chosen allow arbitrarily large displacements and rotations and complex geometries and configurations can be modeled, one more assumption must be made; namely

$$\sqrt{g} \triangleq 1 - \frac{t}{R_f} - \frac{c}{R_\ell} \approx 1$$

where, t is the thickness of the blade and c its chordlength; R_f and R_g the radii of curvature of the initial configuration of the blade in the flap and lag directions, respectively. For all practical helicopter configurations this condition is satisfied (actually $\sqrt{g} = 1$, exactly, for straight blades) so that this assumption does not seem to be a major restriction.

vi) In defining the kinetic energy of the system as a preliminary step in obtaining the dynamic characteristics of the blade, velocities associated with warping displacements were neglected. The blade was assumed to rotate at a constant, given angular velocity, Ω, with respect to an inertial frame, about a fixed hub. In calculating natural frequencies, i.e., the vibratory behavior of small perturbations, the resulting kinetic energy expression was linearized about a known equilibrium position of the blade. For dynamic response calculations, the full, i.e. nonlinear, expression for the kinetic energy was used.

The FEM for rotor blades which resulted, as noted above, allows accurate structural modelling through use of a new 3-D isoparametric beam element, including shear and cross-sectional warping effects, anisotropic material characteristics, and structural couplings. In addition, other advantages for this approach include the fact that the equations of motion need not be formally derived and the method can conveniently deal with configurational complexities such as precone, droop, sweep, torque offset, curved blades, and/or swept tips. Finally, the geometric non-linearities associated with large displacements and rotations are inherently included. Implementing the new method consists of the following steps; (a) the blade geometry is interpolated in its undeformed and deformed geometries, so that the displacement field can be found easily; (b) the standard FEM generates the stiffness matrix of a typical blade element; (c) three and four-noded elements are used with 3 translations and 3 rotations at each node and 1 degree of freedom per warping mode, the shapes for which are calculated in a separate program [Ref. 61, 62]; (d) equilibrium iteration is required since we are dealing with a non-linear problem in which the applied forces can be a function of the resulting displacements; that is the solution of the non-linear problem is found by solving a sequence of linearized problems using a modified Newton-Raphson iteration procedure; natural vibration frequencies and mode shapes are determined by solving a quadratic eigenvalue problem, which is done efficiently with a variant of the Lanczos Algorithm [Refs. 63].

To validate structural aspects of the theory which resulted from modeling actual cross sections, as discussed above, deformations theoretically predicted were compared with experimentally measured strain fields in a thin-walled composite beam. A straight box-beam with thin-walled rectangular cross-section to be subjected to a tip load was constructed and tested at Rensselaer, as the first such validation case. As shown in Ref. 64, the FEM theory results checked well with measured stress distributions in the composite cover plates of this beam when either bending or torsion loads were applied. Strain distributions were measured and compared with the results

of an analytical solution using Euler beam theory (no shear nor warping effects), the Saint-Venant beam theory, which includes shearing effects, and the present FEM solution. This comparison is shown in Fig. 75, where ϵ is normal strain, and γ is shear strain.

To verify the theory's accuracy when large deflections are encountered, a case reported in the literature [Ref. 65] was analyzed. This involved a slender beam with a solid aluminum rectangular cross-section subjected to a tip load which has a variable direction relative to the major axis of the cross-section. Excellent agreement was found between analytical and FEM results for static cases up to very large transverse displacements, of the order of the length of the beam. When the transverse tip load is small, transverse displacements are small and the FEM solution matches continuum mechanics predictions exactly. When the transverse load is increased enough, the nonlinear effects due to large transverse displacements become significant so that the continuum mechanics prediction becomes inaccurate. Excellent correlation between experiment and numerical results using the new FEM were exhibited in all cases. The slight discrepancy between the Ref. 66 solution and the present FEM solution was probably due to a modeling problem. The finite element program is formulated for thin-walled rectangular sections whose torsional and bending stiffnesses were matched to the corresponding stiffnesses of the actual beam. The inherent inaccuracies of this matching process are thought to be the cause of the slight discrepancies observed.

The experiments performed by Dowell, Traybar and Hodges [Ref. 66] involved frequency measurements on the slender aluminum beam of Ref. 64 described in the previous paragraph. The present FEM dynamic results were compared to these experimental measurements and with numerical predictions described in Section 5.d.(2) in this report. In this case, the measured frequencies correspond to small vibrations about the steady equilibrium position obtained by hanging the same dead load, P, at the tip of the cantilevered beam. The loading angle again is varied from 0^{o} to 90^{o}, and for each setting both in-plane and out-of-plane mode frequencies are measured. Figs. 76 and 77 show the variation of out-of-plane and in-plane frequencies, respectively, with this loading angle for a tip load, P = 2 lbs., which results in large displacements and rotations of the beam. Good correlation is shown for both bending frequencies.

The FEM computer code was also validated for the case of small vibrations of rotating beams by comparing its predictions with experimental data also in the literature [Ref. 67]. In this case, the dynamic characteristics of a torsionally soft, two-bladed, composite model helicopter rotor system was analyzed, and the predictions compared with experimental measurements. Fig. 78 shows a Southwell diagram for the 5 lowest predicted and measured natural vibration frequencies of the blades for five rotor speeds. The solid lines show the current FEM prediction and the symbols indicate experimentally measured frequencies. In this figure 1F, 2F and 3F stand for first, second, and third flap modes, respectively, 1E nd 1T for first lead lag and first torsion modes, respectively. Once again, good correlation was demonstrated. Furthermore, the blades were instrumented with strain gages, so that strain distributions in the natural vibration modes were measured as well. Figs. 79.a and 79.b show these various strain distributions at 0 and 1000 RPM, respectively. Both

experimental and predicted strains were normalized by the root strain value. The correlation is thus shown to be good for distributed modal characteristics as well as for eigen values.

The FEM code was subsequently generalized further to allow the analysis of nonlinear periodic systems. For this purpose a finite element in time (FET) technique was used. The first advantage of the FET approach is to allow periodic boundary conditions to be imposed on non-linear systems in a straightforward manner. This contrasts with time integration procedures that require initial conditions for start up and deal with periodic boundary conditions by iterating until convergence. The second advantage is that higher order integration schemes can be derived in a systematic fashion, simply by selecting different order polynomials for the time interpolation. Finally, the transition matrix, which is required for stability calculations based on Floquet theory, is a by-product of the solution procedure for the FET equations of the periodic response. Hence, the same solution algorithm can be used for both dynamic response and stability analysis.

As one example of non-linear response the harmonic response (HR) and super-harmonic response (SHR) of a clamped-clamped beam vibrating through large deflections was calculated using the new method. This example was analyzed by Tseng and Dugundji [Ref. 68]. The properties of the beam in question were:

Length (L) = 0.457m

Bending rigidity (EI) = $3.21 \times 10^{-2} Nm^2$

Mass per length = 5.19×10^{-2} kg/m.

An initial extensional strain of 5.76 μm/m was also assumed to be present. In applying the new FEM-FET method, two cubic elements were used to model the beam with four quartic elements in time. Fig. 80 compares the Ref. 68 experimental results and their analytical solutions with the present FET solutions. The normalized mid-span deflection, $\bar{w} = (w/h).(1/\bar{\omega})$, is plotted versus the normalized excitation frequency $\bar{\omega} = \omega_f/\omega_1$. Here w is the mid-span deflection, h the height of the beam, ω_f the excitation frequency. The analytical predictions of the Ref. 68 harmonic solution are shown to be in good agreement with the FET solution. Both solutions agree closely with the experimental results, except at large amplitudes, where theory slightly underpredicts mid-span displacements.

SHR can, in theory, occur around any integer values of the normalized excitation frequency, $\bar{\omega}$. Our analysis concentrated on the super-harmonic responses of order 2 and 3 (SHR2 and SHR3, respectively). Fig. 81 shows the detailed response around $\bar{\omega} = 1/3$, i.e. SHR3. This response consists of the superposition of vibrations at frequencies equal to ω_f and $3\omega_f$. Thus, the beam responds at the excitation frequency, but also at its own natural frequency $\omega_1 = 3\omega_f$. To capture the SHR3 response, it was necessary to increase the number of time nodes to 32 (eight quartic elements). The FET response was then analyzed using the Fast Fourier Transform to obtain the amplitudes of the various harmonics.

The FET method failed to detect any SHR2 response. On the other hand, the harmonic balance (HB) method predicts such response and is in close agreement with the observed experimental results. In a second attempt to obtain SHR2 response, the problem was analyzed after introducing an extremely small initial imperfection in the beam model, consisting of a sine-wave lateral deflection. It's maximum magnitude was set at 1/500 the thickness of the beam (i.e., 2.5×10^{-08} × length) at mid-span. Fig. 82 shows the experimental results for the SHR2 response, which agree closely with both the prediction of the HB method and the FET results for the beam with an initial imperfection. It is of interest that the initial imperfection also affects the first natural frequency of the beam, but this effect does not appear on a plot non-dimensionalized by frequency.

The second non-linear response example examined the stability of a beam subjected to a tip compressive follower force of magnitude P. The properties of the beam were the same as in the previous example. Two cubic elements were used to model the beam and 32 time nodes (eight quartic elements) to model one period. Solutions of this classical problem exist. Since the excitation does not vary in time, any period could be used for the FET model of this problem. In this example, the period of the lowest bending mode of the unloaded beam was selected.

A linearized stability analysis based on the eigenvalues of the transfer matrix was performed for various magnitudes of the follower force. Fig. 83 shows the two lowest bending frequencies of the system versus the non-dimensionalized follower force amplitude $\lambda = PL^2/EI$. The analytical solution and the FET predictions are essentially identical. Instability occurs at the frequency coalescence point, where one of the eigenvalues of the transfer matrix becomes larger than unity, indicating an exponentially growing solution. Fig. 84 compares this characteristic exponent, as predicted by the analytical solution, with that using the FET approach. Here again, excellent correlation is shown.

As a last example of the application of this FEM- FET method, the paramatric excitation of a beam under a pulsating load was investigated. This beam is clamped at one end; at the other end, the axial displacement is free but all other displacement components are constrained. Fig. 85 summarizes the results of stability analyses on a "q" versus "a" plot. Here

$$a = 4\,(\omega_1/\Omega)^2 \qquad\qquad q = {}^1/_2\, a\,(P/P\infty)$$

where Ω is the excitation frequency; ω, the first natural bending frequency; P the magnitude of the pulsating force; and $P\infty$ the Euler buckling load of the beam. The solid curves show analytical predictions of the stability boundaries based on a modal approximation followed by a perturbation solution of the resulting Mathieu equation. The symbols indicate FEM-FET predictions. Note that the stability boundaries are in close agreement.

As a result of this research, we have concluded that the finite element technique presents a unifying approach to the non-linear, structural dynamic/analysis of composite rotor blades. More specifically:

i) the complex structural behavior of composite blades is accurately modeled,

ii) the effects of shear and warping deformations, material anisotropy, and elastic couplings are included,

iii) arbitrarily large displacements and rotations are accounted for, within the limitations of small strains,

iv) no formal derivation of the non-linear equations of motion is required, eliminating a source of errors,

v) all non-linear terms are rationally taken into account, bypassing the need for ordering schemes,

vi) the FET approach provides a systematic approach for non-linear periodic response calculations, as well as linearized stability analysis.

Future work will concentrate on two aspects:

i) Derivation of a finite element based modal approximation to reduce the number of degrees of freedom in the analysis.

ii) Interfacing finite element structural models with aerodynamic load calculation programs to perform coupled aeroelastic analyses.

5.d.(2). Rotor Dynamic Analysis Using Generalized Coordinates
(Sr. Investigators: R. Loewy, A. Rosen)

The difficulty of predicting rotor blade forced response in helicopter forward flight motivated this project. Although the highly coupled nature of this problem (eg blade motion with aerodynamics, blade motion with hub, i.e. fuselage motion, etc) was well-appreciated, this particular research focused on several, much more restricted issues of rotor blade structural dynamics. Specifically, the research concentrated on the complexity of rotational dynamics effects, the non-linear aspects associated with large transverse deflections of rotor blades and the relative adequacy of truncated Fourier breakdown vis-a-vis finite increment, step-by-step time integration. The approach taken, from the outset, was to develop an analytical module which would be suitable for incorporation, subsequently, into a large comprehensive rotor analysis program (such as 2GCHAS). Furthermore, computational efficiency was also a goal from the start, since use as a design tool was envisaged. Because small changes in rotational speed and blade twist are such common design variables and relatively independent of blade structural design, it was decided to essentially eliminate the structural aspects by using a Galerkin method of solution. This method used the non-rotating, uncoupled - i.e. pure flap bending, lag bending and torsion, natural modes and frequencies of flat, i.e. untwisted blades (in a vacuum) as generalized coordinates. This research was performed by and resulted in the masters thesis written by Randall Smith and the doctoral thesis written by M. Bobby Mathew.

In order to ascertain the importance of the aspects enumerated above to rotor blade forced response in actual operation, a rotor blade typical of modern design practice and a realistic operating point were sought. Such were obtained from the Boeing Helicopter Company; namely, the YUH-61A ("UTTAS") helicopter rotor blade. This is a cantilever, psuedo-isotropic composite blade with conventional pitch bearings and tension-torsion strap. The flight condition chosen was cruise at 150 kts.

This blade had been analyzed extensively by Boeing, using the comprehensive computer program, C-60 [Ref. 69], whose structural dynamics modules make use of a transfer matrix analysis which couples out-of-plane bending and twist, but treats in-plane bending as uncoupled. For these purposes, the blade was mathematically modeled as twenty concentrated masses, each with appropriate mass moment of inertia characteristics, connected by massless, elastic members, inextensible, but with appropriate bending and torsional rigidities (EI & GJ, respectively). So that one-to-one comparisons of the results of the new method with those of Boeing's C-60 analysis could be made, we attempted to use an identical mathematical model. Because our intention was to study the effects of built-in, "pre-twist" and some comparison was desired for the new Galerkin method of solution making use of non-rotating, uncoupled natural modes and frequencies of the blades (in a vacuum) as generalized coordinates, a transfer-matrix analysis in which pretwist and its coupling of out-of-plane with in-plane bending was also programmed.

The generalized coordinate analysis described above for predicting rotating natural frequencies using non-rotating, uncoupled modes was completed and the results for the YUH-61A blade compared with those obtained using both C-60 and the transfer

matrix program programmed at RPI. All this was for coupled flap-bending torsion and uncoupled lag bending. Good correlation was obtained among all three methods. As shown in Table 16, this was accomplished with the new method using relatively few generalized coordinates. Furthermore, CPU-times were reduced by a factor of about 20 relative to the transfer matrix method.

With this success, a second step in analysis development was undertaken; namely to extend the generalized coordinate methodology to allow for the effects of blade pre-twist, as for example, in coupling in-plane and out-of-plane bending. For pretwisted blades, a system based on the principal axes of the airfoil cross-sections yields a curvilinear, non-orthogonal system of coordinates. Unlike the case of untwisted blades, then, coupling exists between bending motions in the two principal directions. As a result of this research it was shown [Ref. 70] that a new system of coordinates can be defined in which bending motions in two directions are mathematically uncoupled one from the other. As a result of using this system, the so-called "principal curvature transformation", the structural terms are simplified considerably. Moreover, by combining this new system of coordinates with a generalized coordinate technique, and using the modes of vibration of the same untwisted blade as generalized coordinates, the system stiffness matrix is obtained without direct structural modeling of the pretwisted blade; i.e., without EI or GJ entering the calculation explicitly. Thus, rotating (or for that matter, non-rotating) coupled in- and out-of-plane bending natural modes and frequencies of pretwisted blades can be calculated based only on their mass properties, and the non-rotating modes and frequencies of flat (i.e. untwisted) blades. Here again, excellent correlation was obtained with the results of the RPI-programmed transfer matrix analysis, and again CPU-times were reduced by factors of about 20. Still greater efficiency increases are attained if several twist distributions are to be examined. These results were also reported in Reference 70.

Continuing along the same lines, a third analytical development was begun to account for large bending deflections. A principal concern was their influence, together with transverse loads, in causing coupling between bending and torsion. Thus, a non-linear theory which maintains small strain assumptions, but accounts for up to the third power of rotations, as they result from bending deflections and torsion, was derived. The theoretical results of this derivation are reported in Ref. 71.

It is well-known that non-linear differential equations cannot be solved, in general, using superposition methods. Since the "generalized coordinates" approach is fundamentally a superposition method, it was necessary at this point in the research to confirm the accuracy of the method by making comparisons with experimental and analytical results available in the literature, which were incontrovertibly in regimes in which non-linearities are important. Such cases included (a) deflections of long, slender beams under static tip loads at various angles to their cross-section principal axis, (b) natural frequencies of such beams with heavy tip mass whose cross-section principal axes are at various angles with respect to gravity, (c) buckling under axial and transverse loads, and (d) static deformation under centrifugal effects at various rotational speeds in the presence of preconing. Publications in which these earlier results appeared, respectively, are Refs. 65, 66, 72 and 73. Good agreement with

all these experiments, considerably improved over the theories published to that date was obtained as shown in Figs. 86 through 91 from Ref. 74 and 75. (Similar correlations using a new FEM are given in Section 5.d.(1), above, in this report.)

As regards the buckling problem, the effect of pretwist on buckling due to axial compressive loads [Ref. 72] was predicted very well using only three generalized coordinates, if the pretwist is under 90^{o}. Lateral buckling of flat rods may be considered a classical problem [Ref. 76], but - at least in 1984 - no research on the lateral buckling of twisted rods could be found in the literature. The new analysis methodology was successful in obtaining coupled bending-torsion buckling results for a twisted beam under lateral load. It was shown, for example, that for beams whose ratios of bending rigidity in the two principal axis directions are less than about 9, nonlinear effects are so significant that eigenvalue analysis does not yield a meaningful buckling load. Details are available in Ref. 77.

Since the newly-developed method using generalized coordinates and the principal curvature transformation had thus been shown to efficiently and accurately predict static deflections and natural frequencies of beams subject to large amplitude deflections, the question as to whether deflections such as are encountered in high speed forward flight can cause differences in (instantaneous) natural frequencies was examined through its use. Fully coupled YUH-61A blade natural frequencies were calculated, together with their modes as they would occur in small amplitude oscillations about four different deflection shapes. These shapes were taken as "frozen" at what is predicted to occur at 0, 90, 180 and 270^{o} positions of azimuth by C-60 for the configuration and operating conditions shown in Table 17. They are shown in Figs. 92, 93, 94 and 95 for the flap bending, lag bending and pitch angle deflections, respectively. Two pitch angle plots are shown, the second with root angle adjusted to facilitate comparison of the elastic twist. The resulting four natural frequency variations with rotor speed are shown in Figs. 96 and 97, for the first torsion and second lag bending frequencies. These natural frequencies were affected most by the nonlinearities associated with large initial deflections. Note that significant changes occur at normal operating RPM between 3 & 4Ω for torsion, and between 5 & 6Ω for lag bending.

Aerodynamic loads calculated for forward flight at 150 kts using the C-60 computer program, also provided by Boeing Helicopter Company, were ultimately used to predict forced response. This was carried out to four different levels of completeness as depicted graphically in Fig. 97. Of these, the completely linear and completely non-linear cases are clear. The partially linear and partially non-linear cases, however, both treat higher harmonic response as small perturbations about initially deflected positions as defined by the sum of zero and first harmonic rotor response. The partially linear case predicts the zero and first harmonic response by linear means, whereas the partially non-linear analysis predicts those initial conditions using a fully non-linear analysis. The fully linear case was first exercised, for comparison with C-60 results. Correlation for deflections and moments were surprisingly sensitive to seemingly minor representational differences. After these

were minimized, including accounting for a structural damping coefficient, g = 0.02, as was done in C-60, reasonably good agreement was obtained for the time histories around the azimuth. It was found that time integration in 5^{o} azimuthal steps, using the full time history of load, on the one hand, and superposition of responses to individual loading harmonics following Fourier decomposition, on the other hand, gave responses which were very close, so long as at least ten harmonics were included. Airloads predicted by C-60 show significant differences depending on whether 15^{o} azimuthal steps or 5^{o} azimuthal steps were used, and the corresponding responses were also different, but time stepping or Fourier analysis method gave substantially the same results in either loading case.

To facilitate the time-step integration solution, the transition matrix technique was used to calculate dynamic response. Widely different magnitudes of time steps were used in these calculations to bracket the range defining adequate accuracy and acceptable efficiency. While it is dangerous to generalize, it seems clear that 30^{o} azimuthal steps are too large, whereas a time step of 1^{o} is accurate enough to predict response up to the twenty-fifth harmonic. To further assess computing efficiency, a straight-forward integration scheme was used assuming zero initial conditions, rather than insuring periodicity by manipulating the transition matrix. In such a procedure the intregration must, in theory, be carried over several rotor revolutions until the results converge. In our non-linear calculations, however, the response failed to converge, despite the inclusion of artificial damping. All our forced response calculations, therefore, used the transition matrix.

Response calculations showing both blade tip deflections and root moments, in flap bending, lag bending and torsion, were calculated by the four different means depicted in Fig. 97 and compared. The results obtained thereby showed significant torsional moment differences when the initial deflections were taken into account, irrespective of how accurately such initial deflections are represented. In fact, for both out-of-plane bending and torsion, the last three analysis methods enumerated above all gave essentially the same results. Only the fully linear analysis had significant errors, compared to the fully nonlinear case. Lag bending moment, however, was shown to be significantly dependent on how accurately the initial deflections were represented. The results of fully nonlinear and partially non-linear methods were essentially the same, and different from the results of fully linear and partially linear methods. It is particularly noteworthy that among these results no consistent trend as to the errors being conservative (i.e. overestimating moments and/or torques) or unconservative could be inferred.

Curves of instantaneous value of natural frequency all aroud the azimuth were plotted, reflecting - as in the earlier 0, 90, 180 and 270^{o} calculations - the effects of changing initially deformed states. These were correlated with the differences in response predicted by the fully linear and the remaining three analyses, as one possible source of the differences. Such did appear to be the case for torsion, but not for lag bending, as shown by a comparison among Figs. 99, 100 and 101 which plot flap bending, lag bending and torsion tip deflection time histories; Figs. 102, 103 and 104, which plot the corresponding root moments; and Figs. 105, 106 and 107, which show how the natural frequencies for the first predominantly flap and lag

modes, the second lag mode and the first torsion mode vary with azimuth, as a result of the predeformation variation with azimuth.

To summarize, the conclusions reached during this research include the following:

- Use of the principal curvature transformation and a generalized coordinate approach allows non-linear rotor blade dynamics calculations to be formulated with a considerable reduction in algebraic manipulations and attendant errors; to be performed with reductions in CPU time compared to transfer matrix, FEM and even more standard Galerkin analyses by a factor of between about 6 and 20; to be run with no explicit involvement of rigidities, such as GJ & EI, so that experimental information (ie mass, natural frequencies & mode shapes) is all the "structural" input data needed; to be performed as design trend studies for a range of twist, chordwise CG offsets and RPM's, very efficiently, if uncoupled, non-rotating natural modes (of a flat blade with chordwise CG on the elastic axis) are used as the generalized coordinates.

- Only a very few modes are needed, in general, as generalized coordinates to achieve accurate results, as is shown by comparisons with a variety of experimental cases in the literature which involve tip deflections of the order of about ½ the beam length.

- Some of the lower mode, rotating natural frequencies of actual rotor blades are significantly changed, relative to successive integer multiples of rotor speed, by the kind of predeformations encountered in high speed forward flight.

- Airloads predicted by sophisticated programs such as C-60, (which account for trailed vortex wakes, unsteady stall, compressibility, trimmed steady hub forces and moments, etc.) change enough if 5^{o} azimuthal increments are used, rather than 15^{o} increments, so that significant differences in forced response result. On the other hand, given a set of airloads, a small-step time integration predicts the same dynamic response as a 10-harmonic Fourier decomposition analysis.

- To be assured of accurate peak-to-peak values of bending and torsion moment at helicopter cruise speeds (around 150 kts), full non-linear analyses such as were developed in this research (retaining all deflection and rotation terms below fourth power, but assuming small strains) must be used. If any aspect of the calculation is linearized, eg predeformation or perturbation calculations, one cannot be certain that the results will be either conservative or non-conservative. Some differences in the nonlinear from the nonlinear response might be inferred as resulting from changes in "instantaneous natural frequency" (the effect of predeformation on small, first-order free vibration characteristics). Others cannot, and would seem to be, therefore, a result of differences in effective coupling between the modal coordinates.

These results are presented in more detail in Refs. 78 and 79.

5.d.(3). Development of a Model Rotor Impedance Test Rig
(Sr. Investigator: R. Bielawa)

A number of rotorcraft problems involve coupled motion of the rotor (or rotors) and the fixed airplane components which support them. These include forced vibration of the fuselage by vibratory rotor forces and coupled rotor-fuselage aero-mechanical instabilities, such as ground/air resonance and coupled rotor-wing aeroelastic instabilities, such as whirl flutter.

Both fundamental understanding of such phenomena and the capability to quantitatively analyze them are usually enhanced by the, by now, classical "black box" viewpoint. That is, putting aside the details of what takes place within the rotor, "given a prescribed oscillatory motion of the rotor hub, what are the forces and moments that must be applied to the hub to maintain that motion?" And, putting aside the details of what takes place within the fixed (i.e., non-rotating) airframe, "given prescribed oscillatory forces and moments acting at the top of the rotor shaft(s), what motions will result throughout the fixed (i.e., nonrotating airframe) as a result of those forces and moments?" The former "black box" is the "rotor impedance", and the latter the fixed airframe "hub mobility". The "wiring together" of these two "black boxes" through their interdependent quantities of hub motions, forces and moments provides for their proper coupling.

For many important rotorcraft design points, particularly those associated with high speed flight, characterizing the rotor impedance is the more difficult of the two black box identification problems. All of the complexities of nonlinear aerodynamics (reverse flow, stall, compressibility), rotational dynamics (gyroscopic and coriolis moments and forces, respectively) and the nonlinear effects associated with large displacements and rotations come into play. The ability to measure rotor impedance is, therefore, highly desirable. To be most valuable, of course, this should be possible at the earliest design stage, thus calling for techniques using wind tunnels, whirl rigs and rotor models.

Rotor whirl rigs designed to operate in a wind tunnel must not involve unrealistically large support and drive systems, or they will produce large unwanted aerodynamic interference. Support and drive systems which are acceptable in this respect will, therefore, be flexible to some unavoidable degree. The vibratory forces and moments produced by the rotor undergoing tests will tend to move the hub in ways that are unlikely to be what is desired for the impedance test. Inherent in a successful impedance test, whirl rig is the capability, therefore, to sense the hub motion, calculate the forces and moments that should be applied to oppose or at least supplement the rotor force so as to produce the desired hub motion, and apply these forces and moments to the hub. Since this must be done in "real time", the higher the frequencies involved, the more difficult the impedance whirl rig design problem. Since full scale Mach numbers are desired in rotor development testing, the smaller the model, the higher the frequencies that will be dealt with.

From all this it should be clear why no feasible rotor impedance whirl test rig has yet been developed, and why its development has seemed a legitimate, basic

research task. At Rensselaer, the evolution of a promising concept in 1983 led to the definition of a set of specifications and both design and analysis of a system which seems capable of providing the desired characteristics. A summary of what has been done under this contract on this research is contained in the following paragraphs.

5.d.(3).(a). Establishing System Specifications

Based on both hardware and software aspects to be integrated into a total system, the impedance whirl rig was designed to have capabilities as described in the following paragraphs.

It is to be capable of measuring rotor impedance at model scale for rotor diameters ranging from 6 ft. to 9 ft. at Froude- and Mach-scaled test conditions. The apparatus should enable basic research testing of rotor hub loads and impedance in hover, forward flight and in a vacuum, using existing government and/or industry facilties with minimum disruption of these test sites. The drive power requirements, hub force and moment application actuator (shaker) capacities and real-time digital signal processing (DSP) system characteristics are to be compatable with:

i) Scaling a full-scale, four-bladed rotor of 50 ft. diameter with a tip speed, ΩR, of 750 ft/sec. to model size.

ii) Mach-scaling a configuration representative of contemporary rotors to a model rotor with a diameter of 9 ft. and operating at a maximum torque blade loading coefficient, C_Q/σ, of 0.009.

iii) Froude-scaling a conventional rotor having a radius of 24 ft. and a tip speed of 726.3 fps to model rotors with a range of diameters from 6 to 9 ft; the latter scaled the same as the Mach-scaled configuration.

iv) Maximum power deliverable to the rotor of 100 HP.

v) An approximate weight of the mass to be moved by the servo-actuators (shakers), including rotor and support hardware, and defined herein to be the "metric mass", of 50 lb. Note that the metric mass includes not only the rotor, but the upper shaft assembly (including bearing package, shafting, swash-plate and swash-plate control motors) as well. The design of this metric mass must necessarily be of light-weight construction to minimize the actuator loads.

vi) A range of frequencies to be from 0.1Ω to the highest blade passage frequency with an additional 10% margin.

The resulting apparatus should, furthermore, be such that accuracy of measurement is maximized. The need for minimum metric mass precludes use of conventional

relatively heavy, high-compliance balance systems for measuring hub loads. Thus, light-weight, low-compliance load cells mounted within the hub itself were the means chosen for loads measurement. For compatability with the test environment in which the whirl rig is operated, the vibratory base reaction loads resulting from operation of the facility must be minimized. Transmissibility along each of the base axes should be no more than approximately 0.1.

Anticipated industry/government facility occupancy prompted the requirement that the whirl rig support pylon have a floor-to-rotor height of no more than about 9 ft., to allow entry into major wind tunnel facilities. The pylon should, furthermore, have a lateral blockage signature of no more than approximately 10 inches. Finally, the drive motor should fit within the aerodynamic "shadow" of the support pylon.

5.d.(3).(b). Design/Development Challenges

Among the developmental considerations identified early as basic design drivers for this facility, in addition to feasibility, are cost and simplicity. Influencing those objectives are the following:

i) An important limitation on the performance of the facility is the upper frequency limit of the shakers. As defined by the nominal Mach-scaled configuration, the shaker frequency required for 4P excitation poses severe demands on existing servo-valves. Only with newly available high-performance servo-valves with suitable flow rate capabilities, could an upper limit for the shaker frequency as high as 120 Hz be established.

ii) Within this limit, the capabilities provided by a 100 HP power source used with Mach-scaled rotors were examined. Fig 108 presents the projected test envelope available for Mach-scaled rotor testing with this facility. Ranges of rotor speed and C_Q (based on 100 HP delivered to the rotor) are presented in this figure. Also shown is the design point corresponding to the selected nominal test configuration.

iii) The use of off-the-shelf components in all major subsystems is to be maximized. This is clearly necessary for sensors and actuators, but is of equal importance in the case of readily avaliable and easily programmable real-time computer systems and supporting D/A and A/D components.

iv) Where off-the-shelf items are not available, maximum use of proven conventional technology will be sought, particularly in mechanical components.

Consistent with these guidelines, a relatively low-cost, compact hydraulic motor and complementary power system were found which promise to meet rotor drive power requirements. The high torque, low rotational speed characteristics of such an

arrangement also allows low-cost, high torque pulley-belt drive systems to be used for rotor speed reductions and/or increases.

5.d.(3).(c). Overview of the Apparatus

The design which has been develcped for the impedance test rig includes mechanical components which are typical of existing conventional rotor rigs, with the exception of the hydraulic shakers. These shakers are to drive the rotor hub with appropriate values of each of the five components of hub loads so as to achieve, in turn, unit motion for each of the hub degrees of freedom while suppressing all other motions to zero. Such combinations of loads are, by definition, the columns of the impedance matrix. This concept of operation requires shaking the model rotor in a highly controlled manner, so as to achieve unit motions in each of the five degrees of freedom: three orthogonal (x-, y- and z-) translations and pitch and roll rotations. On the other hand there is no requirement for test stand rigidity, so long as the actuators have sufficient travel, force and frequency capabilities.

To achieve reasonably accurate impedance characteristics by these means requires a high degree of precision in the controller. Furthermore, to achieve a high degree of testing flexibility, the controller must be generally programmable, and must, therefore, be based on real-time digital computing functions. Consequently, the usual mechanical components (support, rotor control and rotational drive) are only one part of a much more complex system.

Figure 109 presents a schematic of this impedance test apparatus from a functional viewpoint. It is comprised of four major subsystems:

i) mechanical components: rotor, rotor controls, pylon, drive system, and hydraulic actuators [needed for shaking the rotor].

ii) the preprocessor (A/D) function,

iii) the postprocessor (D/A) function, and

iv) a host computer for controlling the experiments.

In the following material, each of the four subsystems identified above are described in more detail.

5.d.(3).(d). Mechanical Components

Figure 110 presents a pictorial layout (with cut-away view) of the design of the mechanical components of the test apparatus at this writing. They represent state-of-the-art technology for the most part, although certain features are new, having been dictated by the test capabilities and operational considerations defined above. These features include:

Servo-Actuators

Six degree-of-freedom sinusoidal excitation of the metric mass will be accomplished by six servo-actuators (shakers). They are not shown in Fig. 110 for clarity. These actuators are to be mounted between the metric mass and the support pylon in a "daisy-chained" manner to form an octahedral arrangement. We anticipate assembling servo-actuators with the required characteristics using miniature high-pressure-rated (5,000 psi) hydraulic cylinders, with effective areas of 0.41 in^2, mated with high-performance servo-valves having excellent frequency response characteristics at 120 Hz with flow rates up to 10 gpm at 4,000 psi.

Support and Isolation Systems

As shown in Fig. 110 the support pylon assembly will consist of two interconnecting structures. An inner part is essentially a large tube, cantilever-mounted to the floor, enclosing the motor/belt drive assembly substructure, the lower shaft section and slip-ring assembly, and the composite middle shaft. An outer part consists of a massive isolation system to which the hydraulic shakers are to be attached. This massive outer part (about 500#) is intended to absorb the high vibratory loads which the shakers will develop and thereby greatly reduce the vibration levels in the test site environment. This will be important in wind tunnel installations wherein high vibratory loads may not be tolerated. The reactive inertial mass will be depleted uranium to minimize volume. This metal is safe from a radioactive standpoint, approximately 50% more dense than lead, is a structural material, can be made environmentally safe (the metal is pyrophoric) by plating with cadmium, and is reasonably available. Not shown in Fig. 110 are the appropriately sized and positioned springs connecting the inner and outer support structures.

The design of the outer isolation structure is intended to provide isolation for all excitation components induced by the shakers. Two basic types of isolation systems are planned; the system for lateral, roll and pitch motion will rely on simple isolator principles, whereas the vertical system will make use of nodal isolation due to the requirement for low steady deflections under gravity and lift loads. Disconnection breaks are to be provided at appropriate points along the pipe length for servicing the flex-joints, bearings and slip-ring assembly. While the details of this design are at present preliminary, they do not appear to present any serious problems in design and/or fabrication.

The lateral directions will be provided with parallel linkages with suitable spherical rod ends for the necessary articulation. They will also be "focused" on the c.g. of the metric mass or bearing package. This form of isolation is a variant of the focused pylon system and will also isolate in a rotational sense, significantly decoupling lateral translational and rotational motions. Consequently, the lateral vibratory loads can be shown to be attentuated by simple mass isolator principles. Transmissibility then can readily be expressed by the following equation:

$$T = (\delta_D/\delta_S)\,(m_2/m_1)\,[(\omega_n/\omega)^2 - 1]^{-1}$$

where the first ratio is of that between the dynamic and static amplitudes, which can be expected to have an order of magnitude of approximately unity. By tuning the natural frequency, ω_n to be quite low relative to the excitation frequency, ω, and setting the ratio of isolator mass, m_2, to isolated (ie the metric mass), m_1, equal to 0.1, a ten to one lateral isolation can be achieved.

Vertical isolation, as shown in Fig. 111, is to be accomplished using the well-established nodal isolation techniques originally developed for isolating vertical vibrations on rotorcraft [Ref. 80]. To establish the basic operation of this isolation system, a simplified analysis was performed wherein a massless beam of constant EI was configured to act in the manner suggested in Reference 81. In this configuration, a massive mass, m_1, was placed at the middle of a beam which was itself suspended at or close to its two "nodal" points; and tuning weights of mass, m_2, were put at the ends of the beam. Note that since the beam is symmetric only one half of the beam need be analyzed.

The established formulations and results for such systems show that acceptable operation is achieved principally when the excitation frequency is above the natural frequency of the free-free configuration. Although nodal isolation can be achieved at excitation frequencies below this natural frequency, the off-tuned transmissibilities typically exceed unity.

The results of the simplified analysis, as presented in the following figures, is dimensionalized by a characteristic frequency parameter, W, defined as:

$$W = \left[\, EI/m_1 L_3^3 \,\right]^{\frac{1}{2}}$$

All the following results then depend on the mass ration, $R_m = m_2/m_1$, and the frequency ratio, R_f, = ω/W. Figure 112 shows how mass ratios must vary to achieve nodal isolation for various values of the ratio of beam length ratios, L_2 to L_3 (see Fig. 111) and excitation frequencies nondimensionalized by W.

Figure 113 indicates how the natural frequencies of the isolation system, as configured for those nodal pivot locations and mass ratios used in Fig. 112, vary with excitation frequency. These results show that in order to achieve good isolation with low transmissibilities for "off-tuned" conditions, values of the frequency ratio, R_f, in the range 7 to 10 should be used. For these values, excitation frequencies will be above and well-separated from natural frequencies, and good operation will thereby be achieved for the off-tuned conditions.

In order for the nodal isolation system to "work" for significant variations in excitation frequency, the isolator must be manually reconfigured by varying the mass, m_2, as the frequency is varied. Figure 114 shows the results of such an operating

strategy. The mass ratio, R_m, varied as follows: within each of the ranges indicated along the R_f axis, the indicated value of R_m has been taken from the curve in Fig. 112 corresponding to the value of R_f in the middle of each respective range. These values, of course, produce exact isolation at the integral values of R_f. Note that quite respectable transmissibilities are then achieved, especially for a L_2/L_3 ratio of (0.4), with mass ratio kept constant within each range of R_f, even in the off-tuned conditions. Preliminary analysis has shown that this isolation system can be designed with excellent static deflection and spring rate characteristics using standard steel construction and conventional bearings.

Finite element analysis will aid in the detailed design of the actual cruciform two-beam structure shown pictorially in Fig. 111, including the ring-like portion for providing clearance for the inner steel pylon structure. The exact "fine-tuned" values of the incremental masses needed for total isolation at the chosen discrete frequencies will oe determined experimentally.

Hub and Load Instrumentation

A distinctive feature of the hub design is the load cell assembly incorporated so as to measure hub forces and moments at and about the exact point of reference, ie the center of the hub, and in the push-rods, as shown in the Figure 115. With this arrangement, the measured loads define directly the dynamic system whose impedance is to be measured; no dynamic tares are required to account for structural flexibilities of nonessential intervening components. This arrangement does, however, require that load and acceleration measurements be made in the rotating system. Consequently, trigonometric resolution is needed to obtain the appropriate quantities in the fixed system.

Thus, the mP (nonrotating coordinate system) test frequency sinusoidal responses of interest are seen in the rotating (hub) coordinate system as mP responses for the "collective" responses (i.e., vertical loads and accelerations) ans as 1P, (m-1)P and (m+1)P responses for the "cyclic" responses (i.e., lateral forces and loads and the pitch and roll quantities). This requirement complicates the data acquisition process.

A detailed design of a titanium rotor hub for the apparatus has been completed. Details, including finite element analysis results, are given in Ref. 82. Some of its features are shown in Fig. 116. Criteria to which it was designed are as follows:

i) It should accommodate the existing set of bearingless type model rotor blades committed by NASA for use in this facility, and also be able to accommodate other bearingless rotor models as well.

ii) Construction should be of sandwich type, with two sets of load cells [(4) Kistler model 9251A, 3-axis piezo-electric units, and (4) Entran model ELF-319/1250-500 miniature single axis piezo-resistive units, respectively] mounted in series and structurally enclosed between the upper and lower plate parts (see Fig. 115).

iii) The lower hub plate should form the structural link between load cells and the remainder of the rotor (whose impedance is being measured). This lower plate must accommodate (4) Entran EGA-2-C miniature biaxial acceleratometers in a compact attachment scheme.

iv) The upper hub plate should form the structural link between the load cells and the upper drive shaft and provide a mounting place for the (8) B & K model 2644, line-drive charge amplifiers needed for the piezo-electric load cells. Attachment to the shaft should be accomplished using a 30^{o}, 20-tooth involute spline to allow mating the upper drive shaft with existing model rotor hubs.

The resulting hub design is estimated to weigh approximately 6 lb. (.9 lb. for the titanium plates and 5.1 for the load cells, accelerometers, titanium bolts and miscellaneous parts).

While the combined electrical charge outputs from the (4) 3-axis load cells would normally be twelve in number, two of the outputs of each load cell are combined with those of other load cells to form eight composite signals. The installation scheme selected for these load cells is somewhat unorthodox, but conveniently maintains polar symmetry. It is shown in Figure 117.

Power Drive System

The traditional use of high density, high speed, water-cooled variable speed DC electric motors was rejected on the basis of expense. A hydraulic motor and supporting power supply were found to be suitable alternative power sources. Such motors actually have ideal application to rotor testing by virtue of their better match in rotor speeds. This eliminates use of expensive gear-driven speed reduction units and simplifies the test environment; ie only one system is needed - hydraulic power lines. Because of the vibratory loadings present, special design practices will have to be observed to minimize the potential lateral play in the bearings.

5.d.(3).(e) Preprocessor

The preprocessor subsystem converts selected analog signals from the instrumentation transducers (mainly those at the hub) to digital form in an appropriate format and sends them to the host computer. A (programmable) digital implementation was selected for this basic function, principally because it offers the greatest degree of tasking flexibility and stable, accurate control.

The specific functions assigned to the preprocessor are:

i) demodulating the narrow band harmonic responses of the hub (accelerations and loads) at the test frequency, mP, to determine amplitude and phase of the signals (using a discrete Fourier analysis, DFA),

ii) detecting rogue transient response (at some frequency, nP, distinct from mP, using Fast Fourier Transform, FFT, techniques) as one of the bases for implementing a facility "health" monitoring capability, and

iii) demodulating the rogue responses, once detected, at the non-test frequency, nP, again using a DFA.

Digital implementation of DFA and FFT calculations requires both efficient algorithms and the use of a suitable fast and programmable microprocessor to produce accurate calculations in real-time. The DFA algorithm selection was made on the basis of optimizing both speed and accuracy. Means by which the required integrals are to be evaluated were selected on the basis of an index consisting effectively of a multiplication of CPU time with computational error, for a series of synthesized signals whose Fourier coefficients are specified. The resulting integrals were formed using simple numerical integration formulae wherein the time period of integration, T_C, was divided by (2^n) into exact fractions. The results of varying this power, n, showed that, for present purposes the optimal division of T_C, is into eighths. On the basis of this abbreviated theoretical development, the specific functionality of the preprocessor subsystem was schematically summarized as in Fig. 118.

A suitable microcomputer was identified in the Texas Instruments TMS320 family of digital signal processors. This is a 16/32-bit high-performance microprocessor optimized for signal processing operation. The SKY-Challenger board, configured with two onboard TMS32020 microprocessors in master-slave configuration and developed for operation within a VME-bus mini-computer environment, was selected for implementing the above algorithms. A/D conversions and low-pass and band-pass filtering will be accomplished using ICS-100 digital signal processing boards. Lastly, provision is being made for including anti-aliasing filtering of the analog signals prior to input to the ICS-100 boards. This filtering has the requirement of being programmable (to allow for variable frequency, mP) and should be achievable using available DSP technology.

The preprocessor development was guided by the following standards:

i) analog signal preprocessing, from analog data to Fourier coefficients in host computer memory in digital form, must occur within an 833 microsecond window.

ii) Fourier component accuracy must be with 0.5%.

These goals were successfully met during Phase I implementation tests of the algorithms on a TMS32010 within an IBM PC host computer environment. It appears that the preprocessor will more than adequately satisfy all requirements set for it.

5.d.(3).(f) Postprocessor

The three functions of the postprocessor are to command (1) the trim-producing swash-plate control angles; (2) the hydraulic (shaker) servo-actuators; and (3) the (user-defined) emergency shutdown procedures (when required).

The swash-plate is to be controlled by direct linear motion motors [(3) Compumotor AX57-55-R units]. These units offer excellent load capability, have precise motion control and are digitally controllable by the host computer using a single RS-232C port.

Servo-actuator (shaker) activation requires generating six independent precision analog sine wave voltages, i.e., each with the same prescribed frequency, but with separate amplitudes and phase angles. Fig. 119 illustrates a typical shaker control unit which has at its core a Natel HCDX-3106 Solid State Control Differential Transmitter. This component receives analog inputs of the form A*sinθ and A*cosθ, and generates the amplitudes and phase angles of the output signals using these values. Tests with an interim implementation within an IBM PC host computer environment demonstrated specified sine-wave analog voltages with errors of no more than 0.94%. This is well within expectations for the servo system.

5.d.(3).(g) Host Computer

The host computer controller shown in Figure 109 (Subsystem 4) must perform the following tasks:

i) synchronize operations of the preprocessor and postprocessor subsystems.

ii) trim aerodynamic forces and moments and control shaker actuation (forces). These define the principal controller operation.

iii) monitor facility "health"

iv) control data acquisition

v) perform pre-test check-out.

Achieving these functions in a real-time environment, with a minimum of system development, called for a well-developed computer architecture. Evaluation of the systems available led to selection of a Mizar system.

The timing functions for multi-rate sampling; 8P, 8mP, 8(m+1)P, 8(m-1)P, and 8nP (for the preprocessor), JmP (for postprocessor), and KP (for the programmable anti-aliasing analog filters), must be controlled by the host computer to achieve subsystem synchronization. This function will be provided by a dedicated VME-bus timing control module.

Typical (linear) control systems with plant and controller subsystems can be expressed in the following state-space form:

$$\{\dot{X}(t)\} = [A]\{X(t)\} + [B]\{u(t)\}$$

$$\{u(t)\} = -[F]\{X(t)\} + \{R(t)\}$$

where A and B are plant description matrices, R(t) is the reference input vector and u(t) and X(t) are the input and output vectors, respectively, of the plant.

The objective of the controller design is to determine an appropriate controller function, F. While several methods could be used to obtain this controller function, the LQR theory and adaptive control theory have been successfully implemented in similar applications and are thus likely candidates for this system. A schematic diagram of the planned controller operation is shown in Fig. 120. The output of the plant {X}, shown in Fig. 120, represents the vibratory responses and the hub loads processed by the preprocessor. the controller input, {e} is the difference of {X} and $\{X_r\}$, representing the reference vibratory responses and trim loads, respectively. The controller command {u} can control both the swash-plate mechanism and sine wave generator (servo-actuators) to achieve desired trim conditions and shaker activation.

5.d.(3).(h) Health Monitoring and Emergency Procedures

These monitoring tasks include:

i) activating the FFT calculation;

ii) selecting the critical response frequency (nP);

iii) monitoring nP response values;

iv) monitoring drive system status and other mechanical parts;

v) evaluating "health" parameters; and

vi) activating the predetermined emergency shutdown scenario.

The emergency shutdown function is initiated by health assessment algorithms monitored within the host computer. Implementation is performed by the post-processor in the form of a VME-bus module card configured with 32 mercury-wetted relays [VMIC model VMIVME- 2200]. This switching capability will provide for a wide variety of host computer programmable emergency shut-down scenarios.

All data, both the subset needed directly for feed-back control and all the

remainder are to be stored in a suitable FM waveform recorder (for analog signals) and hard disk within the Mizar system (for digital signals). The selected FM recorder is a Kyowa Dengyo model RTP-650A. An FM cassette recorder with prerecorded signals will be used to input the instrumentation amplifiers, prefilters and A/D converters so as to conduct efficient pre-test check-out.

5.d.(3).(i) Status at Contract Closure

After four years of developmental studies and design, construction of the RPI Model Rotor Impedance Test Facility is now underway. Hardware for three of the four major subsystems (the preprocessor, postprocessor and real-time VME-bus mini-computer portions) has been selected and purchased. Assembly and check-out are targeted for third quarter of 1988. Elements of the support pylon and isolation systems are in preliminary design state. The titanium hub is being fabricated. More details as to current status are contained in Ref. 83.

The development of the facility to this date is seen to have brought together many of the technologies of current interest to the existing technology base. Component identification, detailed design of and funding for the remaining mechanical components are incomplete. With the completion of this subject ARO contract, the rotor impedance rig project is seen as having met the original ARO objectives, and no further funding for this facility development will be provided by ARO. In view of the importance of the problem and promise of the facility, we are confident of sufficient support from other sources to bring this research to a conclusion useful to the rotorcraft technology community.

5.d.(4) Ground/Air Resonance with Flexible Rotor Shafts
(Sr. Investigator: R. Loewy)

5.d.(4).(a). Background

One of the earliest instabilities encountered by helicopters was "ground resonance". Although these often-destructive oscillations were experienced prior to that time, Robert Coleman was successful in identifying the basic mechanism for this type of instability [Ref. 84] in 1942. He showed that the phenomenon was essentially mechanical, involving a transfer of the rotor's energy of rotation into oscillations at frequencies close to the blades' lag natural frequency, phased among the blades so as to be seen as regressive in the nonrotating system. The phenomena of "air resonance" did not, for the most part, appear until the advent of hingeless rotor blades in the mid 1960's [Ref. 85]. The term "resonance" is a misnomer in both instances, since the resulting motions are self-excited and not due to external forcing functions ie they are true instabilities (see, for example, Ref. 86).

Like most multimode instabilities, ground/air "resonance" involves the coalescence of two natural frequencies, usually fuselage/hub motion and the regressive in-plane blade motion. Study of these instabilities continues today, since avoiding them is a fundamental tenet of rotorcraft design and many aspects of the problem have not been completely resolved (see, for example, Ref. 87). The present study seeks to extend those conducted to date by determining the possible effects of rotor shaft flexibility on these two types of instability. Shaft flexibilities between the plane of the swashplate or "spider" (ie the point at which nonrotating controls join rotating controls) and the individual blades' pitch arm or pitch "horn" (ie where the rotating upper controls join each blade) are analyzed for possible kinematic coupling between blade pitch motion and other blade or hub motions. Some helicopters are designed with significant shaft flexibility (eg Ref. 88) and certain recent hub additions, such as "mast mounted sights", can lower the natural frequencies of associated modes to regimes in which ground/air resonance can be affected. Accordingly, study of this problem was begun in the Spring of 1986.

5.d.(4).(b) Analytical Approach

A simple linearized model of a helicopter which assumes a rigid fuselage and rigid, hinged (ie fully articulated) blades is assumed, but with a flexible rotor shaft. The blades are spring restrained about coincident flap-lag hinges and are modelled as long, thin cylinders with equal inertias in flap and lag. Blade preconing and steady geometric pitch are taken as zero. Fuselage degrees of freedom include lateral and longitudinal translations and pitch and roll rotations about the aircraft center of gravity, taken as level with the contact points of the four springs that represent the landing gear stiffness. The fuselage is not free to translate in the vertical direction or rotate about the vertical axis (ie to yaw). Rotor shaft flexibility allows displacements and rotations of the hub mass similar to the four degrees of freedom of the fuselage, but kinematic couplings involving blade pitch (ie shaft-pitch coupling) are included within the context of the linearity assumption and specific hub designs.

Two dimensional strip theory is the basis for the aerodynamic forces included (see, for example, Ref. 89.)

Note that these assumptions do not lead to a mathematical model of completeness, generality or accuracy. They are, however, reasonable in a first attempt to ascertain the possible effects of rotor shaft flexibility, if any, on ground/air resonance.

5.d.(4).(c) Status

The, by now, well-known equations of motion for helicopters with rigid rotor shafts have been re-derived, in the process of accounting for shaft flexibility. These equations have been validated by comparison with published results, setting shaft and control spring rigidities to values approaching infinity. To properly introduce shaft-pitch coupling into the system of equations of motion, the blades' pitch degree of freedom has been added. Initial stability analyses have been performed using the new model over a range of shaft flexibilities and the results compared with some available in the literature.

It should be noted that adding four more hub degrees of freedom to include shaft flexibility effects and an additional pitch/torsion degree of freedom for each blade complicates the derivation of governing equations substantially. Rensselaer's Symbolic Computation Laboratory, with computers that run MACSYMA software, was used to derive the equations of motion including expressions for transformation matrices, position vectors and aerodynamic forces and carrying out the necessary time derivatives, integrations, multiblade coordinate transformations and steps required by Lagrange's equations.

The sources of kinematic coupling due to shaft flexibility are shown in Figs. 121 through 123 and give rise to the relations shown in Figs. 122 and 123. In those expressions ΔP is the change in blade pitch angle due to those couplings. The resulting equations of motion, as developed using MACSYMA, are as follows:

β_c equation

$$\ddot{\beta}_c - \left(\frac{e\sigma}{I_b} + 1\right)(\ddot{\theta}_F + \ddot{\theta}_S) + \frac{\gamma\Omega}{24}(3 + 4\bar{e})(\dot{\beta}_c + \Omega\beta_s) + 2\Omega\dot{\beta}_s$$

$$+ \frac{\gamma\Omega}{12}[2\phi_i - \theta_p(3 + 4\bar{e})](\dot{\zeta}_c + \Omega\zeta_s) - \frac{\gamma\Omega}{24}(3 + 8\bar{e} + 6\bar{e}^2)(\dot{\theta}_F + \dot{\theta}_S)$$

$$+ \frac{\gamma\Omega}{12R}[3\phi_i - \theta_p(4 + 6\bar{e})](\dot{v}_F + \dot{v}_S - h\dot{\phi}_F) + 2\Omega\left(\frac{e\sigma}{I_b} + 1\right)(\dot{\phi}_F + \dot{\phi}_S)$$

$$+ \left(\frac{e\,\sigma\,\Omega^2}{I_b} + \frac{K_\beta}{I_b}\right)\beta_c + \frac{\gamma\Omega^2}{24}(3 + 8\bar{e} + 6\bar{e}^2)(\phi_S - \eta\theta_S - \tan\delta_3\beta_c) = 0$$

β_s equation

$$\ddot{\beta}_s + \left(\frac{e\sigma}{I_b} + 1\right)(\ddot{\phi}_F + \ddot{\phi}_S) - 2\Omega\dot{\beta}_c + \frac{\gamma\Omega}{24}(3 + 4\bar{e})(\dot{\beta}_s - \Omega\beta_c)$$

$$+ \frac{\gamma\Omega}{12}[2\phi_i - \theta_p(3 + 4\bar{e})](\dot{\zeta}_s - \Omega\zeta_c) + \frac{\gamma\Omega}{24}(3 + 8\bar{e} + 6\bar{e}^2)(\dot{\phi}_F + \dot{\phi}_S)$$

$$- \frac{\gamma\Omega}{12R}[3\phi_i - \theta_p(4 + 6\bar{e})](\dot{u}_F + \dot{u}_S + h\dot{\theta}_F) + 2\Omega\left(\frac{e\sigma}{I_b} + 1\right)(\dot{\theta}_F + \dot{\theta}_S)$$

$$+ \left(\frac{e\,\sigma\,\Omega^2}{I_b} + \frac{K_\beta}{I_b}\right)\beta_s + \frac{\gamma\Omega^2}{24}(3 + 8\bar{e} + 6\bar{e}^2)(\eta\phi_S + \theta_S - \tan\delta_3\beta_s) = 0$$

ζ_c equation

$$\ddot{\zeta}_c + \frac{\sigma}{I_b}(\ddot{v}_F + \ddot{v}_S - h\ddot{\phi}_F) - \frac{\gamma\Omega}{24}[8\phi_i - \theta_p(3 + 4\bar{e})](\dot{\beta}_c + \Omega\beta_s) + 2\Omega\dot{\zeta}_s$$

$$+ \frac{\gamma\Omega}{12}\left[\left(2\theta_p\phi_i + \frac{C_{d_o}}{a}(3 + 4\bar{e})\right) + \frac{C_\zeta}{I_b}\right](\dot{\zeta}_c + \Omega\zeta_s)$$

$$+ \frac{\gamma\Omega}{24}[(8 + 12\bar{e})\phi_i - \theta_p(3 + 8\bar{e} + 6\bar{e}^2)](\dot{\theta}_F + \dot{\theta}_S)$$

$$+ \frac{\gamma\Omega}{12R}\left[3\theta_p\phi_i + \frac{C_{d_o}}{a}(4 + 6\bar{e})\right](\dot{v}_F + \dot{v}_S - h\dot{\phi}_F)$$

$$+ \left(\frac{e\,\sigma\,\Omega^2}{I_b} + \Omega^2 + \frac{K_\zeta}{I_b}\right)\zeta_c + \frac{\gamma\Omega^2\phi_i}{12}(2 + 3\bar{e})(\eta\theta_S - \phi_S + \tan\delta_3\beta_c) = 0$$

ζ_s equation

$$\ddot{\zeta}_s - \frac{\sigma}{I_b}(\ddot{u}_F + \ddot{u}_S + h\ddot{\theta}_F) - \frac{\gamma\Omega}{24}[8\phi_i - \theta_p(3 + 4\bar{e})](\dot{\beta}_s - \Omega\beta_c) - 2\Omega\dot{\zeta}_c$$

$$+ \frac{\gamma\Omega}{12}\left[\left(2\theta_p\phi_i + \frac{C_{d_o}}{a}(3 + 4\bar{e})\right) + \frac{C_\zeta}{I_b}\right](\zeta_s - \Omega\zeta_c)$$

$$- \frac{\gamma\Omega}{12R}\left[3\theta_p\phi_i + \frac{C_{d_o}}{a}(4 + 6\bar{e})\right](\dot{u}_F + \dot{u}_S + h\dot{\theta}_F)$$

$$- \frac{\gamma\Omega}{24}[(8 + 12\bar{e})\phi_i - \theta_p(3 + 8\bar{e} + 6\bar{e}^2)](\dot{\phi}_F + \dot{\phi}_S)$$

$$+ \frac{\gamma\Omega^2\phi_i}{12}(2 + 3\bar{e})(\tan\delta_3\beta_s - \theta_S - \eta\phi_S) + \left(\frac{e\,\sigma\,\Omega^2}{I_b} + \Omega^2 + \frac{K_\zeta}{I_b}\right)\zeta_s = 0$$

θ_F equation

$$-\left(\frac{e\sigma}{I_b}+1\right)\ddot{\beta}_c-\left(\frac{h\sigma}{I_b}\right)\ddot{\zeta}_s+\left(\frac{2I_{\theta_F}}{bI_b}\right)\ddot{\theta}_F$$

$$+\frac{2}{bI_b}[(h_m+h)m_m+bhm_b+hm_h](\ddot{u}_F+\ddot{u}_S+h\ddot{\theta}_F)$$

$$+\frac{2}{bI_b}\left(be\sigma+(h_m^2+hh_m)m_m+\frac{1}{2}be^2m_b+\frac{1}{2}bI_b+I_{H_\theta}+I_{M_\theta}\right)(\ddot{\theta}_F+\ddot{\theta}_S)$$

$$-\frac{\gamma\Omega}{24}(3+8\bar{e}+6\bar{e}^2)(\dot{\beta}_c+\Omega\beta_s)+\frac{\hbar\gamma\Omega}{12}[6\phi_i-\theta_p(2+3\bar{e})](\dot{\beta}_s-\Omega\beta_c)$$

$$-2\Omega\left(\frac{e\sigma}{I_b}+1\right)\dot{\beta}_s-\frac{\gamma\Omega}{12}[(2+3\bar{e})\phi_i-\theta_p(3+8\bar{e}+6\bar{e}^2)](\dot{\zeta}_c+\Omega\zeta_s)$$

$$-\frac{\hbar\gamma\Omega}{12}\left[3\theta_p\phi_i+\frac{C_{d_o}}{a}(4+6\bar{e})\right](\dot{\zeta}_s-\Omega\zeta_c)+\left(\frac{2C_zd_\theta^2}{bI_b}\right)\dot{\theta}_F$$

$$+\frac{\gamma\Omega}{8}(1+4\bar{e}+6\bar{e}^2+4\bar{e}^3)(\dot{\theta}_F+\dot{\theta}_S)$$

$$+\frac{\hbar\gamma\Omega}{2R}\left[\theta_p\phi_i+\frac{C_{d_o}}{a}(1+2\bar{e})\right](\dot{u}_F+\dot{u}_S+h\dot{\theta}_F)$$

$$+\frac{\hbar\gamma\Omega}{4}[(3+6\bar{e})\phi_i-\theta_p(2+6\bar{e}+6\bar{e}^2)]\dot{\phi}_F$$

$$-\frac{2\Omega}{I_b}(2e\sigma+e^2m_b+I_b)(\dot{\phi}_F+\dot{\phi}_S)$$

$$+\frac{\hbar\gamma\Omega}{6}[(3+6\bar{e})\phi_i-\theta_p(1+3\bar{e}+3\bar{e}^2)]\dot{\phi}_S$$

$$-\frac{\gamma\Omega}{12R}[(3+6\bar{e})\phi_i-\theta_p(4+12\bar{e}+12\bar{e}^2)](\dot{v}_F+\dot{v}_S)$$

$$+\frac{\gamma\Omega^2}{8}(1+4\bar{e}+6\bar{e}^2+4\bar{e}^3)(\tan\delta_3\beta_c+\eta\theta_S-\phi_S)$$

$$+\frac{\hbar\gamma\Omega^2\phi_i}{4}(1+2\bar{e})(\eta\phi_S+\theta_S-\tan\delta_3\beta_s)+\left(\frac{2d_\theta^2K_z}{bI_b}\right)\theta_F \qquad =0$$

ϕ_F equation

$$\left(\frac{e\sigma}{I_b}+1\right)\ddot{\beta}_s-\left(\frac{h\sigma}{I_b}\right)\ddot{\zeta}_c+\left(\frac{2I_{\theta_F}}{bI_b}\right)\ddot{\phi}_F$$

$$+\frac{2}{bI_b}[(h_m+h)m_m+bhm_b+hm_h](h\ddot{\phi}_F-\ddot{v}_F-\ddot{v}_S)$$

$$+\frac{2}{bI_b}\left(be\sigma+(h_m^2+hh_m)m_m+\frac{1}{2}be^2m_b+\frac{1}{2}bI_b+I_{H_\phi}+I_{M_\phi}\right)(\ddot{\phi}_F+\ddot{\phi}_S)$$

$$+\frac{\gamma\Omega}{24}(3+8\bar{e}+6\bar{e}^2)(\dot{\beta}_s-\Omega\beta_c)+\frac{\bar{h}\gamma\Omega}{12}[6\phi_i-\theta_p(2+3\bar{e})](\dot{\beta}_c+\Omega\beta_s)$$

$$-2\Omega\left(\frac{e\sigma}{I_b}+1\right)\dot{\beta}_c+\frac{\gamma\Omega}{12}[(2+3\bar{e})\phi_i-\theta_p(3+8\bar{e}+6\bar{e}^2)](\dot{\zeta}_s-\Omega\zeta_c)$$

$$-\frac{\bar{h}\gamma\Omega}{12}\left[3\theta_p\phi_i+\frac{C_{d_o}}{a}(4+6\bar{e})\right](\dot{\zeta}_c+\Omega\zeta_s)+\left(\frac{2C_zd_\theta^2}{bI_b}\right)\dot{\phi}_F$$

$$+\frac{\gamma\Omega}{8}(1+4\bar{e}+6\bar{e}^2+4\bar{e}^3)(\dot{\phi}_F+\dot{\phi}_S)$$

$$-\frac{\bar{h}\gamma\Omega}{2R}\left[\theta_p\phi_i+\frac{C_{d_o}}{a}(1+2\bar{e})\right](\dot{v}_F+\dot{v}_F-h\dot{\phi}_F)$$

$$-\frac{\bar{h}\gamma\Omega}{4}[(3+6\bar{e})\phi_i-\theta_p(2+6\bar{e}+6\bar{e}^2)]\dot{\theta}_F$$

$$+\frac{2\Omega}{I_b}(2e\sigma+e^2m_b+I_b)(\dot{\theta}_F+\dot{\theta}_S)$$

$$-\frac{\bar{h}\gamma\Omega}{6}[(3+6\bar{e})\phi_i-\theta_p(1+3\bar{e}+3\bar{e}^2)]\dot{\theta}_S$$

$$-\frac{\gamma\Omega}{12R}[(3+6\bar{e})\phi_i-\theta_p(4+12\bar{e}+12\bar{e}^2)](\dot{u}_F+\dot{u}_S)$$

$$+\frac{\gamma\Omega^2}{8}(1+4\bar{e}+6\bar{e}^2+4\bar{e}^3)(\theta_S+\eta\phi_S-\tan\delta_3\beta_s)$$

$$+\frac{\bar{h}\gamma\Omega^2\phi_i}{4}(1+2\bar{e})(\phi_S-\eta\theta_S-\tan\delta_3\beta_c)+\left(\frac{2d_\phi^2K_z}{bI_b}\right)\phi_F \qquad =0$$

u_F equation

$$-\left(\frac{\sigma}{I_b}\right)\ddot{\zeta}_s + \frac{2}{bI_b}[m_m + bm_b + m_h](\ddot{u}_F + \ddot{u}_S + h\ddot{\theta}_F) + \left(\frac{2h_m m_m}{bI_b}\right)(\ddot{\theta}_F + \ddot{\theta}_S)$$

$$+\left(\frac{2m_f}{bI_b}\right)\ddot{u}_F + \frac{\gamma\Omega}{12R}[6\phi_i - \theta_p(2 + 3\bar{e})](\dot{\beta}_s - \Omega\beta_c)$$

$$-\frac{\gamma\Omega}{12R}\left[3\theta_p\phi_i + \frac{C_{d_o}}{a}(4 + 6\bar{e})\right](\dot{\zeta}_s - \Omega\zeta_c)$$

$$+\frac{\gamma\Omega}{2R^2}\left[\theta_p\phi_i + \frac{C_{d_o}}{a}(1 + 2\bar{e})\right](\dot{u}_F + \dot{u}_S + h\dot{\theta}_F)$$

$$+\frac{\gamma\Omega}{6R}[(3 + 6\bar{e})\phi_i - \theta_p(1 + 3\bar{e} + 3\bar{e}^2)](\dot{\phi}_F + \dot{\phi}_S)$$

$$+\frac{\gamma\Omega^2\phi_i}{4R}(1 + 2\bar{e})(\eta\phi_S + \theta_S - \tan\delta_3\beta_s) + \left(\frac{8K_x}{bI_b}\right)u_F = 0$$

v_F equation

$$\left(\frac{\sigma}{I_b}\right)\ddot{\zeta}_c + \frac{2}{bI_b}[m_m + bm_b + m_h](\ddot{v}_F + \ddot{v}_S - h\ddot{\phi}_F) - \left(\frac{2h_m m_m}{bI_b}\right)(\ddot{\phi}_F + \ddot{\phi}_S)$$

$$+\left(\frac{2m_f}{bI_b}\right)\ddot{v}_F - \frac{\gamma\Omega}{12R}[6\phi_i - \theta_p(2 + 3\bar{e})](\dot{\beta}_c + \Omega\beta_s)$$

$$+\frac{\gamma\Omega}{12R}\left[3\theta_p\phi_i + \frac{C_{d_o}}{a}(4 + 6\bar{e})\right](\dot{\zeta}_c + \Omega\zeta_s)$$

$$+\frac{\gamma\Omega}{2R^2}\left[\theta_p\phi_i + \frac{C_{d_o}}{a}(1 + 2\bar{e})\right](\dot{v}_F + \dot{v}_S - h\dot{\phi}_F)$$

$$+\frac{\gamma\Omega}{6R}[(3 + 6\bar{e})\phi_i - \theta_p(1 + 3\bar{e} + 3\bar{e}^2)](\dot{\theta}_F + \dot{\theta}_S)$$

$$+\frac{\gamma\Omega^2\phi_i}{4R}(1 + 2\bar{e})(\eta\theta_S - \phi_S + \tan\delta_3\beta_c) + \frac{8K_y}{bI_b} = 0$$

θ_S equation

$$
\begin{aligned}
&-\left(\frac{e\sigma}{I_b}+1\right)\ddot{\beta}_c+\left(\frac{2h_m m_m}{bI_b}\right)(\ddot{u}_F+\ddot{u}_S+h\ddot{\theta}_F)\\
&+\frac{2}{bI_b}\left(be\sigma+h_m^2 m_m+\frac{1}{2}be^2 m_b+\frac{1}{2}bI_b+I_{H_s}+I_{M_s}\right)(\ddot{\theta}_F+\ddot{\theta}_S)\\
&-\frac{\gamma\Omega}{24}(3+8\bar{e}+6\bar{e}^2)(\dot{\beta}_c+\Omega\beta_s)-2\Omega\left(\frac{e\sigma}{I_b}+1\right)\dot{\beta}_s\\
&-\frac{\gamma\Omega}{12}[(2+3\bar{e})\phi_i-\theta_p(3+8e+6\bar{e}^2)](\dot{\zeta}_c+\Omega\zeta_s)\\
&+\frac{\gamma\Omega}{8}(1+4\bar{e}+6\bar{e}^2+4\bar{e}^3)(\dot{\theta}_F+\dot{\theta}_S)\\
&-\frac{2\Omega}{I_b}(2e\sigma+e^2 m_b+I_b)(\dot{\phi}_F+\dot{\phi}_S)\\
&+\frac{\gamma\Omega}{12R}[(3+6\bar{e})\phi_i-\theta_p(4+12\bar{e}+12\bar{e}^2)](h\dot{\phi}_F-\dot{v}_P-\dot{v}_S)\\
&+\frac{\gamma\Omega^2}{8}(1+4\bar{e}+6\bar{e}^2+4\bar{e}^3)(\tan\delta_3\beta_c+\eta\theta_S-\phi_S)\\
&+\left(\frac{8EI}{LbI_b}\right)v_S-\left(\frac{12EI}{LbI_b}\right)u_S \qquad\qquad = 0
\end{aligned}
$$

ϕ_S equation

$$\left(\frac{e\sigma}{I_b}+1\right)\ddot{\beta}_c-\left(\frac{2h_m m_m}{bI_b}\right)(\ddot{v}_F+\ddot{v}_S-h\ddot{\phi}_F)$$

$$+\frac{2}{bI_b}\left(be\sigma+h_m^2 m_m+\frac{1}{2}be^2 m_b+\frac{1}{2}bI_b+I_{H_\phi}+I_{M_\phi}\right)(\ddot{\phi}_F+\ddot{\phi}_S)$$

$$+\frac{\gamma\Omega}{24}(3+8\bar{e}+6\bar{e}^2)(\dot{\beta}_s-\Omega\beta_c)-2\Omega\left(\frac{e\sigma}{I_b}+1\right)\dot{\beta}_c$$

$$+\frac{\gamma\Omega}{12}[(2+3\bar{e})\phi_i-\theta_p(3+8\bar{e}+6\bar{e}^2)](\dot{\zeta}_s-\Omega\zeta_c)$$

$$+\frac{\gamma\Omega}{8}(1+4\bar{e}+6\bar{e}^2+4\bar{e}^3)(\dot{\phi}_F+\dot{\phi}_S)$$

$$+\frac{2\Omega}{I_b}(2e\sigma+e^2 m_b+I_b)(\dot{\theta}_F+\dot{\theta}_S)$$

$$-\frac{\gamma\Omega}{12R}[(3+6\bar{e})\phi_i-\theta_p(4+12\bar{e}+12\bar{e}^2)](\dot{u}_F+\dot{u}_S+h\dot{\theta}_F)$$

$$+\frac{\gamma\Omega^2}{8}(1+4\bar{e}+6\bar{e}^2+4\bar{e}^3)(\theta_S+\eta\phi_S-\tan\delta_3\beta_s)$$

$$+\left(\frac{8EI}{LbI_b}\right)\phi_S+\left(\frac{12EI}{LbI_b}\right)v_S \qquad =0$$

u_S equation

$$-\left(\frac{\sigma}{I_b}\right)\ddot{\zeta}_s + \frac{2}{bI_b}[m_m + bm_b + m_h](\ddot{u}_F + \ddot{u}_S + h\ddot{\theta}_F) + \left(\frac{2h_m m_m}{bI_b}\right)(\ddot{\theta}_F + \ddot{\theta}_S)$$

$$+ \frac{\gamma\Omega}{12R}[6\phi_i - \theta_p(2 + 3\bar{e})](\dot{\beta}_s - \Omega\beta_c)$$

$$- \frac{\gamma\Omega}{12R}\left[3\theta_p\phi_i + \frac{C_{d_o}}{a}(4 + 6\bar{e})\right](\dot{\zeta}_s - \Omega\zeta_c)$$

$$+ \frac{\gamma\Omega}{2R^2}\left[\theta_p\phi_i + \frac{C_{d_o}}{a}(1 + 2\bar{e})\right](\dot{u}_F + \dot{u}_S + h\dot{\theta}_F)$$

$$+ \frac{\gamma\Omega}{6R}[(3 + 6\bar{e})\phi_i - \theta_p(1 + 3\bar{e} + 3\bar{e}^2)](\dot{\phi}_F + \dot{\phi}_S)$$

$$+ \frac{\gamma\Omega^2\phi_i}{4R}(1 + 2\bar{e})(\eta\phi_S + \theta_S - \tan\delta_3\beta_s) - \left(\frac{12EI}{L^2bI_b}\right)\theta_s + \left(\frac{24EI}{L^3bI_b}\right)u_S = 0$$

v_S equation

$$\left(\frac{\sigma}{I_b}\right)\ddot{\zeta}_c + \frac{2}{bI_b}[m_m + bm_b + m_h](\ddot{v}_F + \ddot{v}_S - h\ddot{\phi}_F) - \left(\frac{2h_m m_m}{bI_b}\right)(\ddot{\phi}_F + \ddot{\phi}_S)$$

$$- \frac{\gamma\Omega}{12R}[6\phi_i - \theta_p(2 + 3\bar{e})](\dot{\beta}_c + \Omega\beta_s)$$

$$+ \frac{\gamma\Omega}{12R}\left[3\theta_p\phi_i + \frac{C_{d_o}}{a}(4 + 6\bar{e})\right](\dot{\zeta}_c + \Omega\zeta_s)$$

$$+ \frac{\gamma\Omega}{2R^2}\left[\theta_p\phi_i + \frac{C_{d_o}}{a}(1 + 2\bar{e})\right](\dot{v}_F + \dot{v}_S - h\dot{\phi}_F)$$

$$+ \frac{\gamma\Omega}{6R}[(3 + 6\bar{e})\phi_i - \theta_p(1 + 3\bar{e} + 3\bar{e}^2)](\dot{\theta}_F + \dot{\theta}_S)$$

$$+ \frac{\gamma\Omega^2\phi_i}{4R}(1 + 2\bar{e})(\eta\theta_S - \phi_S + \tan\delta_3\beta_c) + \left(\frac{12EI}{L^2bI_b}\right)\phi_S + \left(\frac{24EI}{L^3bI_b}\right)v_S = 0$$

In these equations the following definitions apply:

a	=	blade-airfoil-section lift-curve slope, rad^{-1}
b	=	number of blades
c	=	blade chord, ft
c_{d_o}	=	blade-airfoil profile drag coefficient
C_ζ	=	blade root lead-lag damping coefficient, slug·ft^2·radians/sec
d_θ	=	longitudinal distance between K_z contact points, ft
d_ϕ	=	lateral distance between K_z contact points, ft
e	=	blade root offset, ft
e	=	e/R
E	=	Young's modulus, lb/ft^2
h	=	distance from body cg to rotor hub, ft
h	=	h/R
h_m	=	distance from hub to cg of mast mounted component, ft
I_b	=	blade inertia about flap and lead-lag hinges, 1/3 $m_b R^2$, slug·ft^2
I_{F_θ}	=	fuselage pitch inertia about body cg, slug·ft^2
I_{F_ϕ}	=	fuselage roll inertia about body cg, slug·ft^2
I_{h_θ}	=	hub pitch inertia about body cg, slug·ft^2
I_{h_ϕ}	=	hub roll inertia about body cg, slug·ft^2
I_{m_θ}	=	mast mounted component pitch inertia about body cg, slug·ft^2
I_{m_ϕ}	=	mast mounted component roll inertia about body cg, slug·ft^2
K_x	=	equivalent longitudinal landing-gear spring constants, lb/ft
K_y	=	equivalent lateral landing-gear spring constants, lb/ft
K_z	=	equivalent vertical landing-gear spring constants, lb/ft
K_β	=	flap spring rates at blade root, ft·lb/rad
K_ζ	=	lead-lag spring rates at blade root, ft·lb/rad
l	=	shaft length from swash plate to hub, ft
m_b	=	blade mass, slug
m_h	=	hub mass, slug
m_f	=	fuselage mass, slug
m_m	=	mast mounted component mass, slug
R	=	blade radius less root offset (e), ft

u_F = longitudinal translation of the fuselage (in x direction), ft

u_S = translation of the hub (in x direction) due to shaft bending, ft

v_F = lateral translation of the fuselage (in y direction), ft

v_i = induced velocity, ft/sec

v_S = translation of the hub (in y direction) due to shaft bending, ft

β_c, β_s = cosine and sine components of cyclic multiblade coordinates for blade flap deflections, rad

γ = blade Locke number, $\rho a c R^4 / I_b$

η = kinematic coupling parameter, $(e_r - e_l)/e_p$

ζ_c, ζ_s = cosine and sine components of cyclic multiblade coordinates for blade lead-lag deflections, rad

θ_c = fuselage pitch about body y-axis, rad

θ_p = rotor-blade collective pitch angle, rad

θ_s = shaft angular deflection about body y-axis, rad

ρ = air density, slug/ft^3

σ = blade first moment of inertia, 1/2 $m_b R$, slug·ft

ϕ_F = fuselage roll about body x-axis, rad

ϕ_i = inflow ratio, $v_i/\Omega R$

ϕ_S = shaft angular deflection about body y-axis, rad

Ω = rotor angular velocity, rad/sec

Note that these equations are not written in the standard form in which, for example, all terms multiplying a given derivative of a variable such as $\ddot{\theta}_F$ or $\dot{\theta}_F$ have been gathered together. Rather some multipliers of the same quantities, say $\ddot{\theta}_F$ or $\dot{\theta}_F$, have been kept separate in favor of grouping terms such as $\ddot{\theta}_F$ and $\ddot{\theta}_S$ or $\dot{\theta}_F$ and $\dot{\theta}_S$ where these terms have the same multipliers. In this form it is more obvious where fuselage and shaft degrees of freedom give rise to the same or similar effects, and where they do not. In the β_C and β_S equations, for example $\ddot{\theta}$ and $\ddot{\phi}$ terms and $\dot{\theta}$ and $\dot{\phi}$ terms have the same multipliers, whether they have F (fuselage) or S (shaft) subscripts. In the ζ_C and ζ_S equations, to the contrary, there is no shaft counterpart for the terms $h\dot{\phi}_F$ and $h\dot{\theta}_F$, since h represents the height of the rotor above the fuselage CG, and ϕ_S and θ_S are defined as measured at the hub center.

Computer program check-out was validated for the rigid shaft model replicating "Coleman diagrams" for aeromechanical instabilities and comparing them to the results presented in Ref. 90. The model used in the earlier study is a soft-inplane (.7Ω), 1.62 meter diameter rotor model with a flex strap retention system. Coleman frequency plots and modal damping variations with rotor speed for this model are given in Fig. 124 nd 125, respectively, as calculated by the Rensselaer program. These check very closely with the results of Ref. 90, confirming the accuracy of the rigid shaft portion of the aeromechanical instability code for cases of zero pitch-lag and flap-pitch coupling.

The example chosen to assess the effects of shaft flexibility is the OH-58D helicopter, Ref. 88. The basic mass, stiffness and dimensional data used in the Rensselaer parametric analyses can be deduced from this reference. Shaft and upper control element characteristics are the parameters varied to investigate trends in these studies. Of major interest are the borderline values of shaft flexibility at which ground/air resonance behavior just begins to be influenced by the shaft-pitch coupling effects. At this writing computational results are just beginning to be accumulated.

5.d.(5) Modal Dynamics of Composite Blades
(Sr. Investigator: R. Loewy)

A generalized coordinate analysis of rotor blades making use of the principal curvature transformation (Section 5.d.(2). of this report) has been shown to be accurate and efficient in predicting the natural frequencies of small amplitude free vibrations of rotor blades about predeformed (stressed and unstressed) states and for their non-linear response, limited to small strains, to known forcing functions. The analyses conducted to date, however, have been conceived largely for metal or psuedo isotropic composite blades. The substantial transverse shear deflections and elastic tailoring possible with composite blades whose construction allows shear-dominated matrix behavior have not been included. Because of the promising possibilities foreseen for such blade characteristics (Refs. 9, 91 & 97) it, therefore, seemed reasonable to extend the earlier analyses to include the heretofore neglected effects.

In principle, what must be done to extend the earlier analysis, are the following:

i) include in the strain energy expression an accounting for transverse shear displacements, cross-sections being free to warp, and the cross-coupling terms among out-of-plane bending, in-plane bending and torsion

ii) provide generalized coordinates (eg non-rotating or rotating natural free-vibration mode shapes) which either contain transverse shear deformation and cross-sectional warping information, or as an alternative, independent modal information of that kind as additional generalized coordinates.

Such analyses were initiated in September of 87 and amount, to some extent, to a combination of the separate analyses of Refs. 64 and 71. At the present writing, some of the additional contributions to strain energy have been incorporated, others remain to be completed, and initial attempts have begun to assemble data for the additional shear-dominated deflections to be used as generalized coordinates appropriate for typical blade designs.

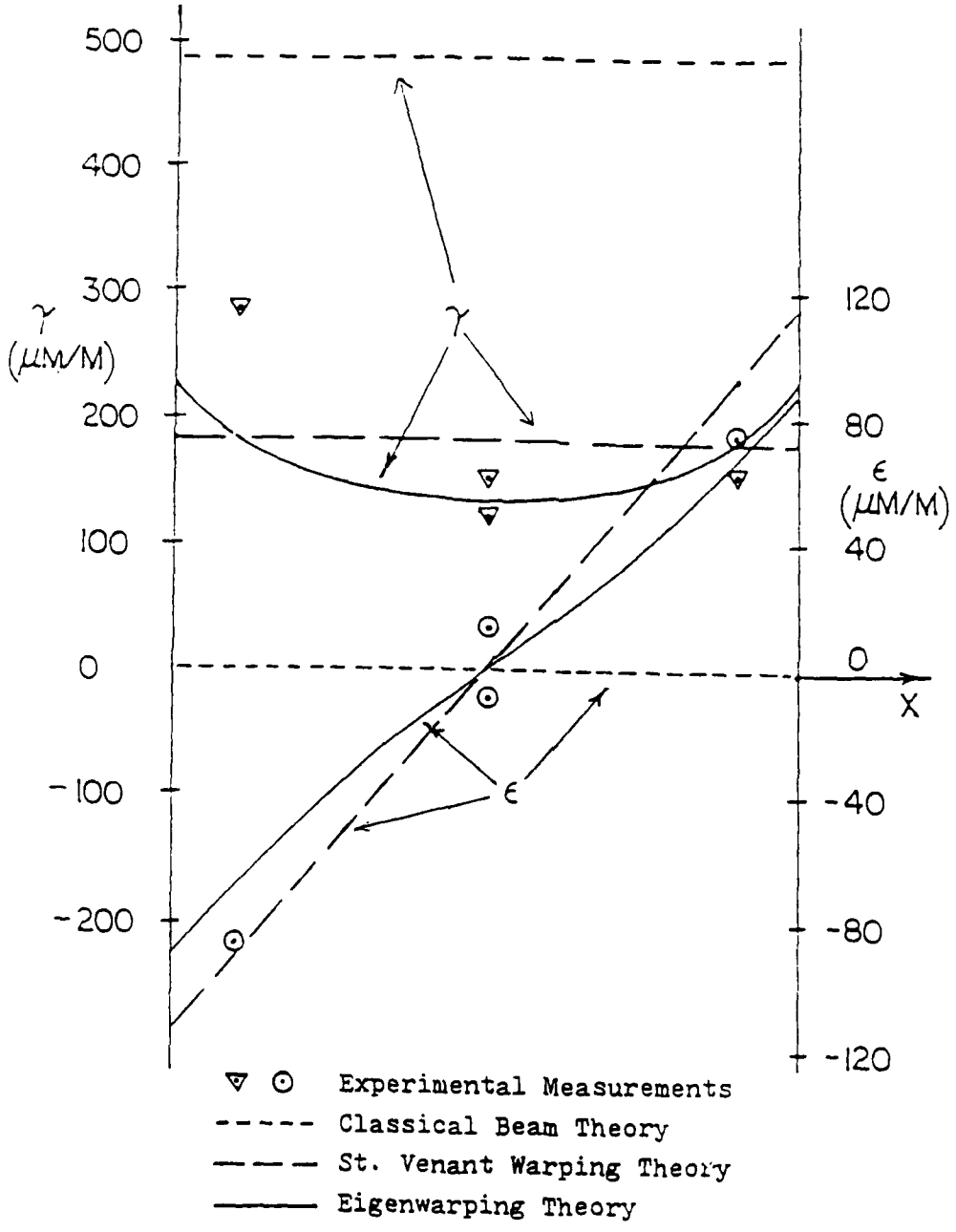

Fig. 75 - Strain Distributions in the Upper Skin of the Balance Beam, at 45% Span

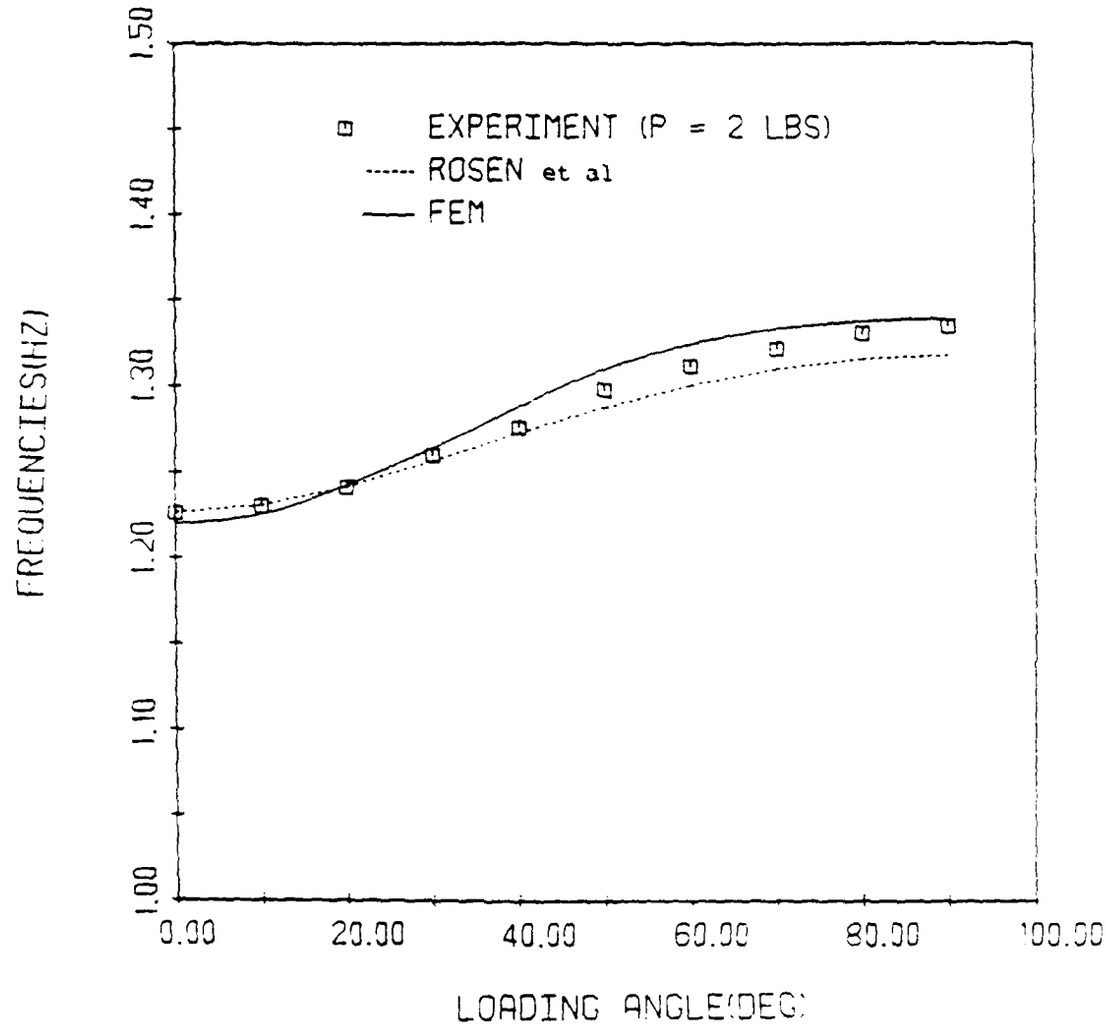

Fig. 76 - First Natural Out-of-Plane Bending Frequency vs. Loading Angle

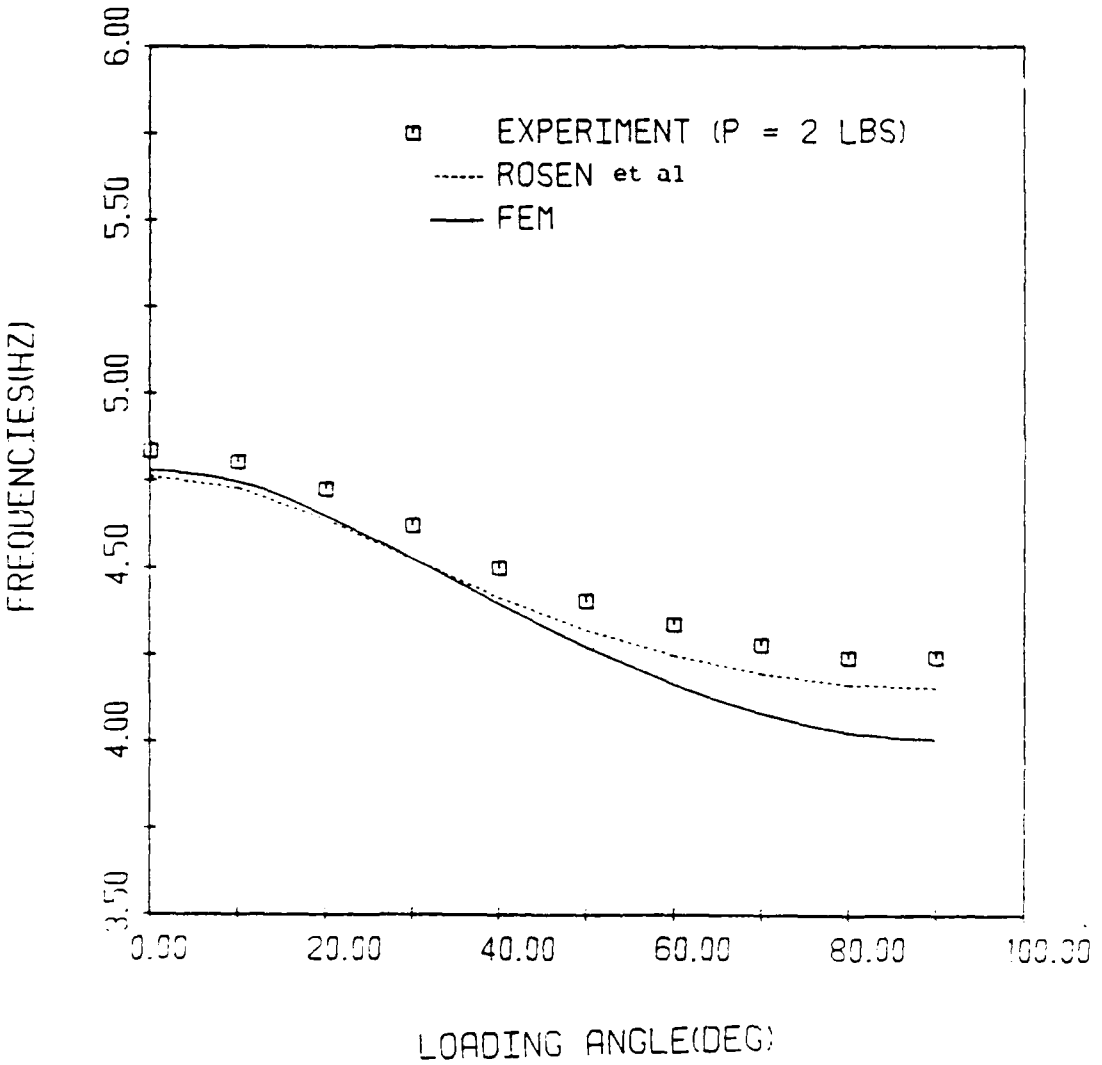

Fig. 77 - First Natural In-Plane Bending Frequency vs. Loading Angle

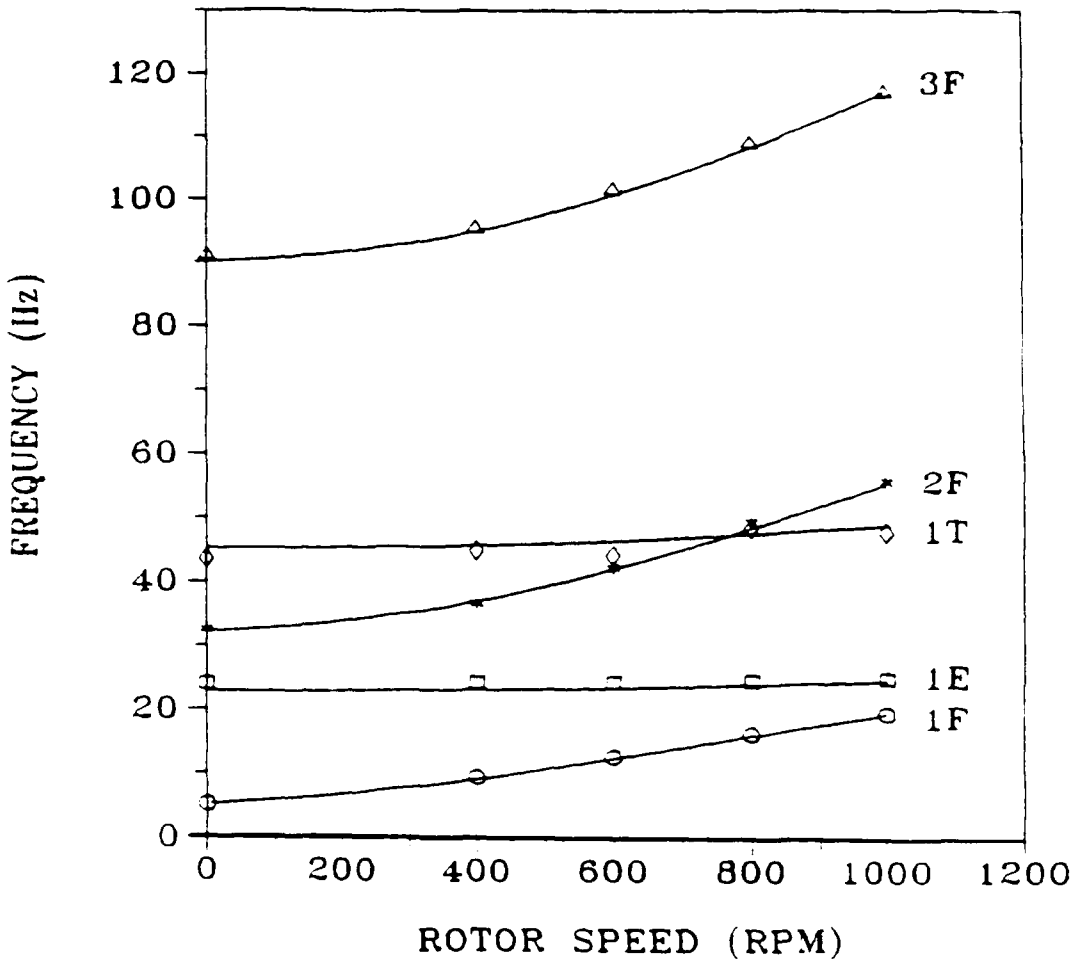

Fig. 78 - Effect of Rotor Speed on the Modal Frequencies for Rotor Configuration 1 (Symbols are experimental measurements, and solid curves are the FEM predictions)

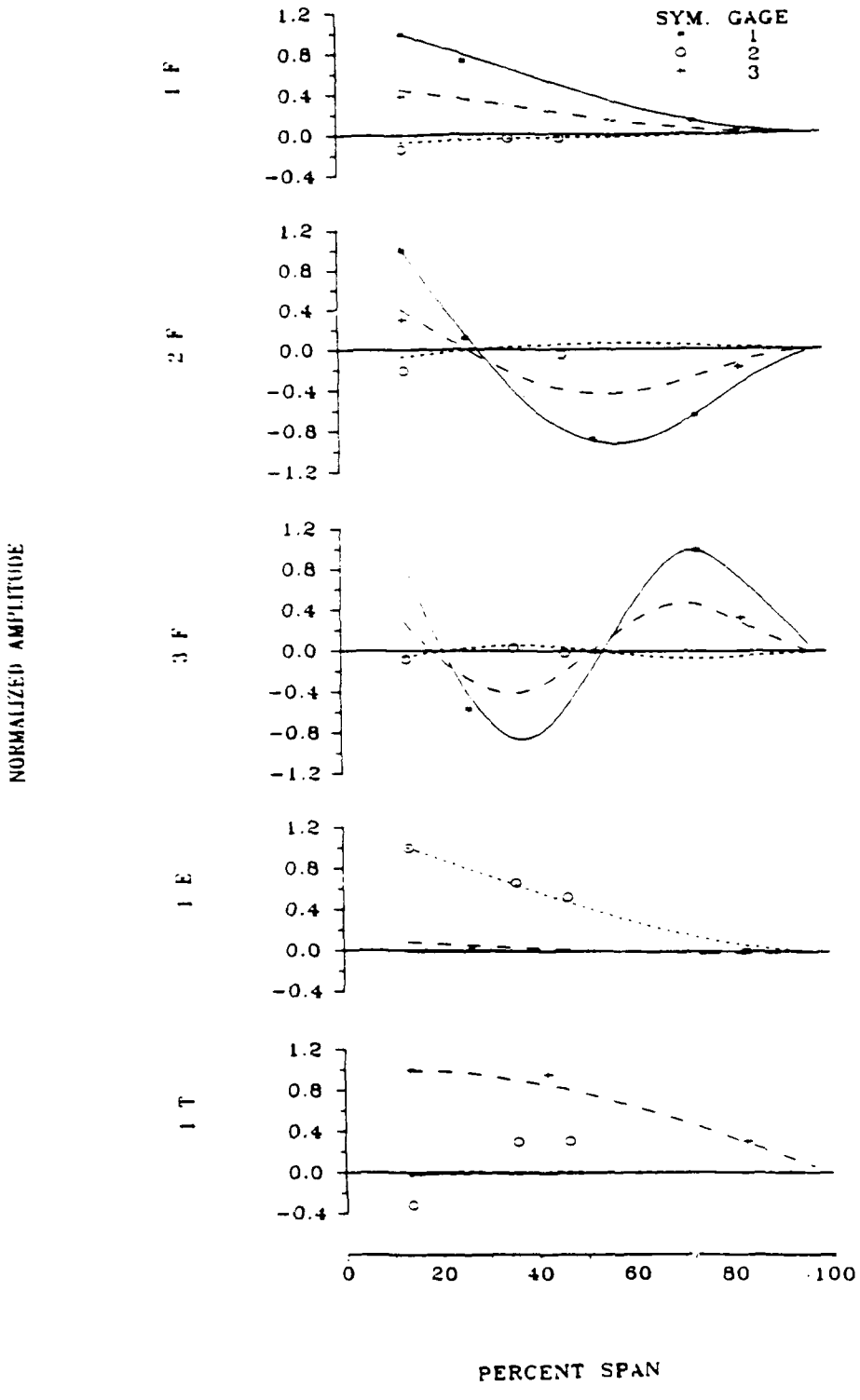

Fig. 79a - Comparison of Modal Amplitudes for Rotor Configuration 1 at 0 RPM

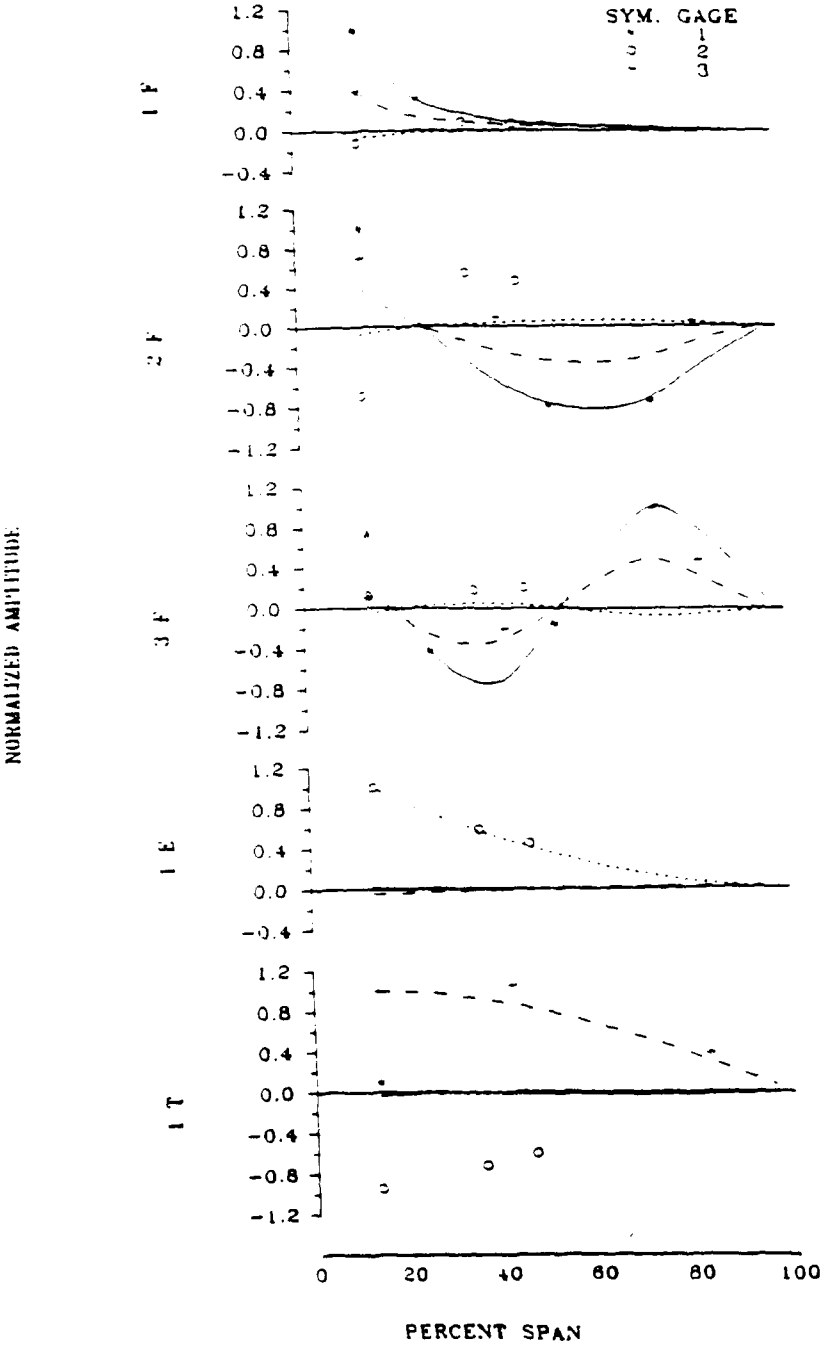

Fig. 79b - Comparison of Modal Amplitudes for Rotor Configuration 1 at 1000 RPM

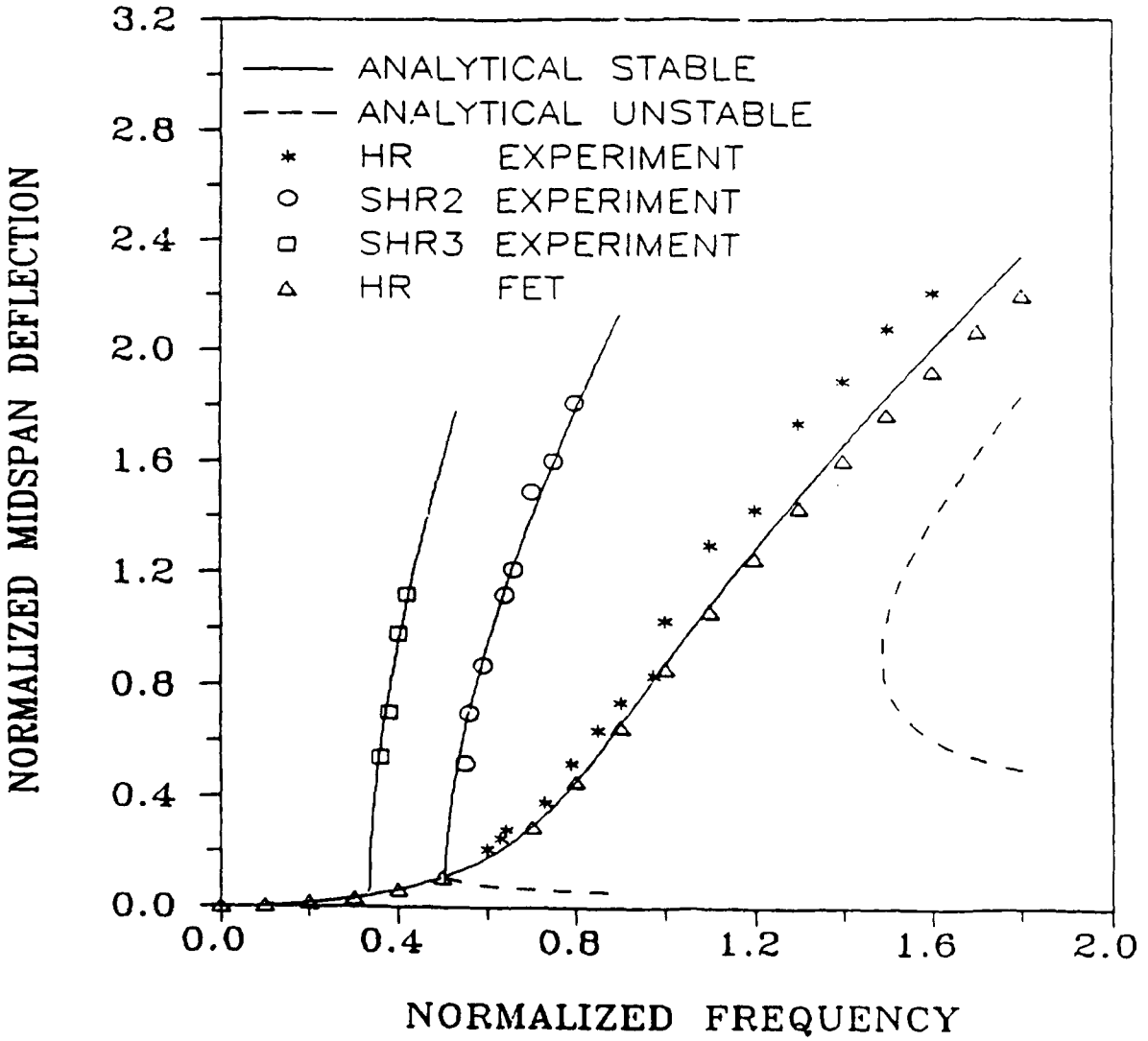

Fig. 80 - Harmonic and Super-Harmonic Response of a Clamped-Clamped Beam

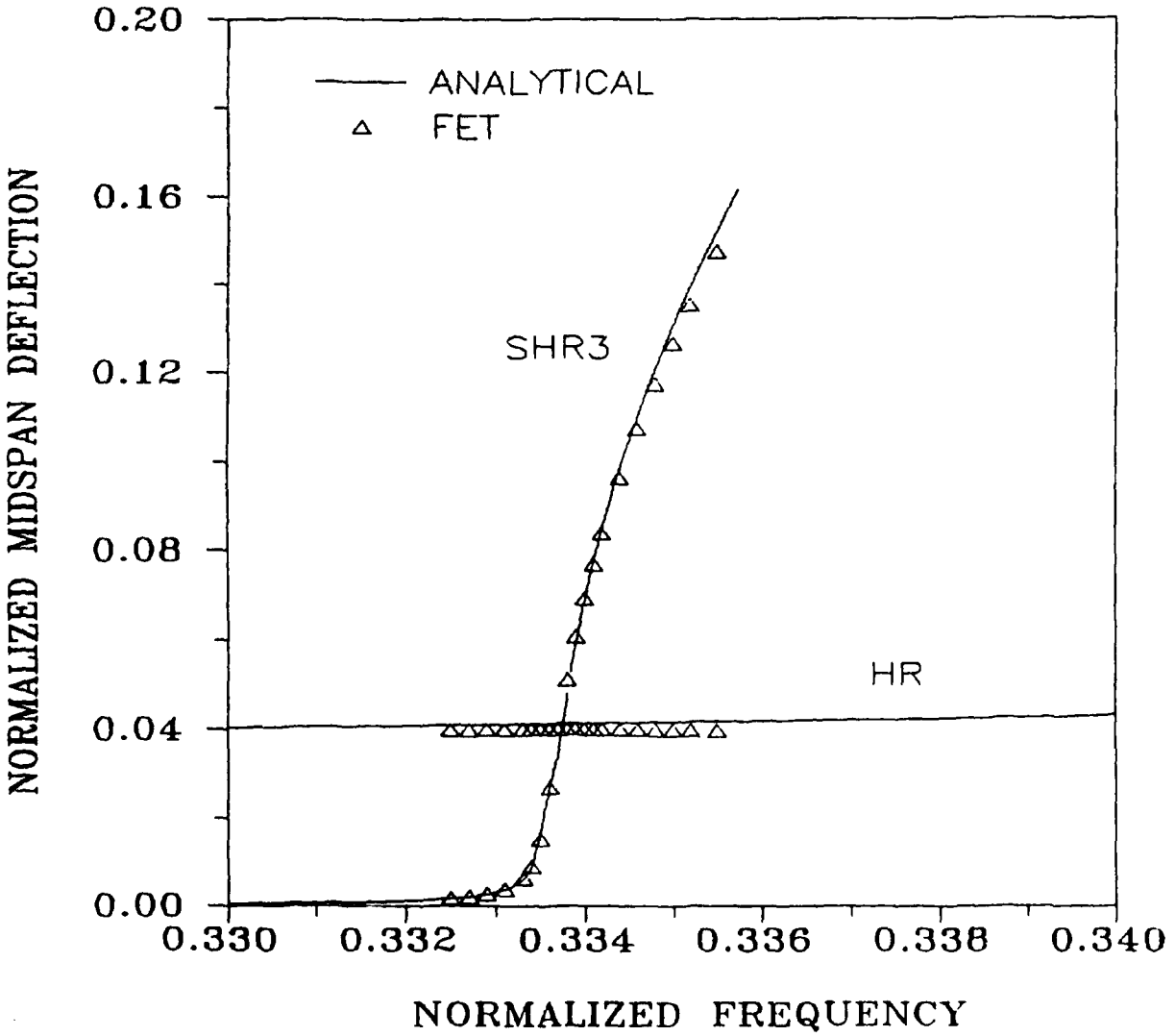

Fig. 81 - Detail of the Super-Harmonic Response SHR3

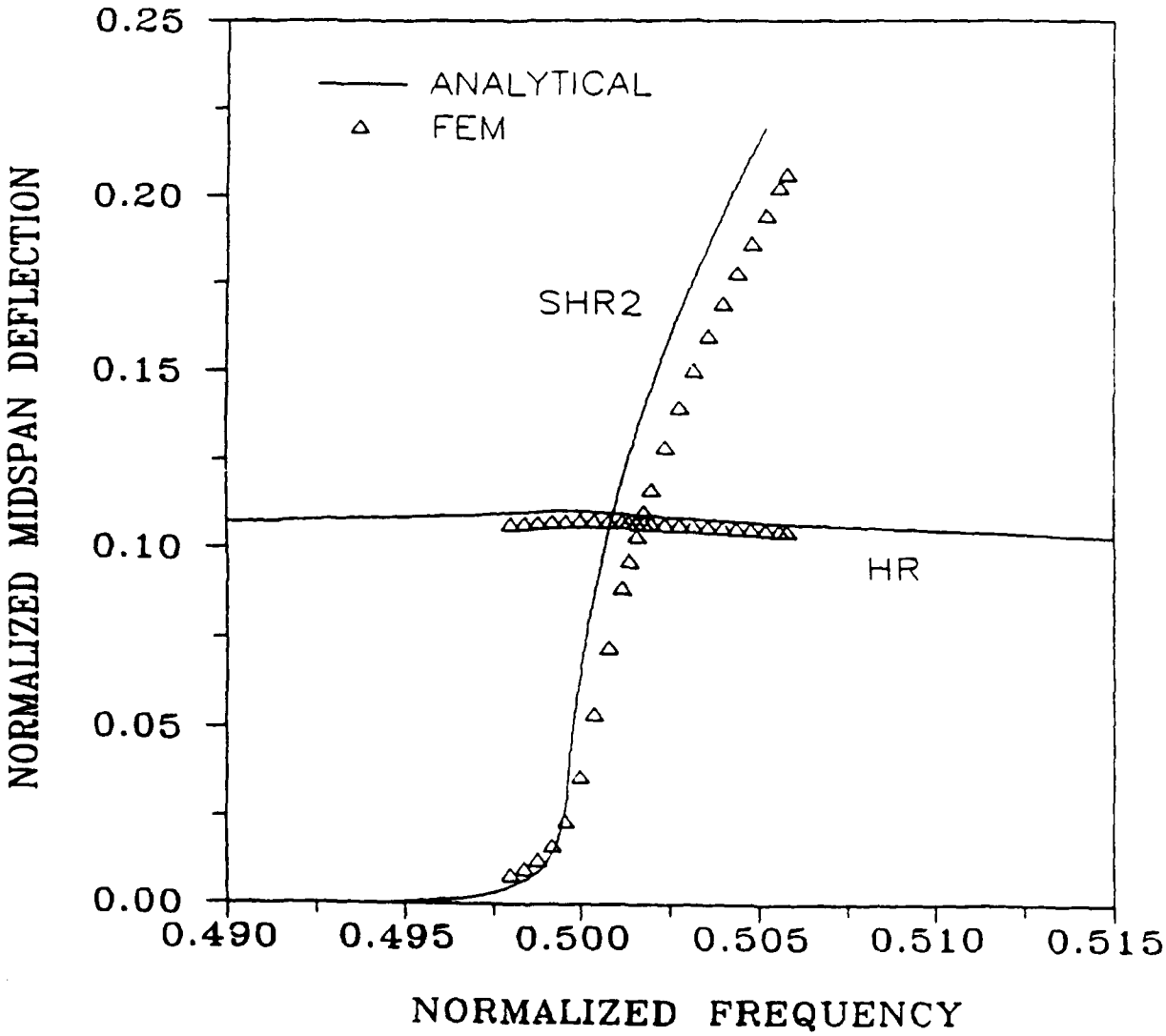

Fig. 82 - Detail of the Super-Harmonic Response SHR2 (The FET results were obtained for a beam with an initial imperfection.)

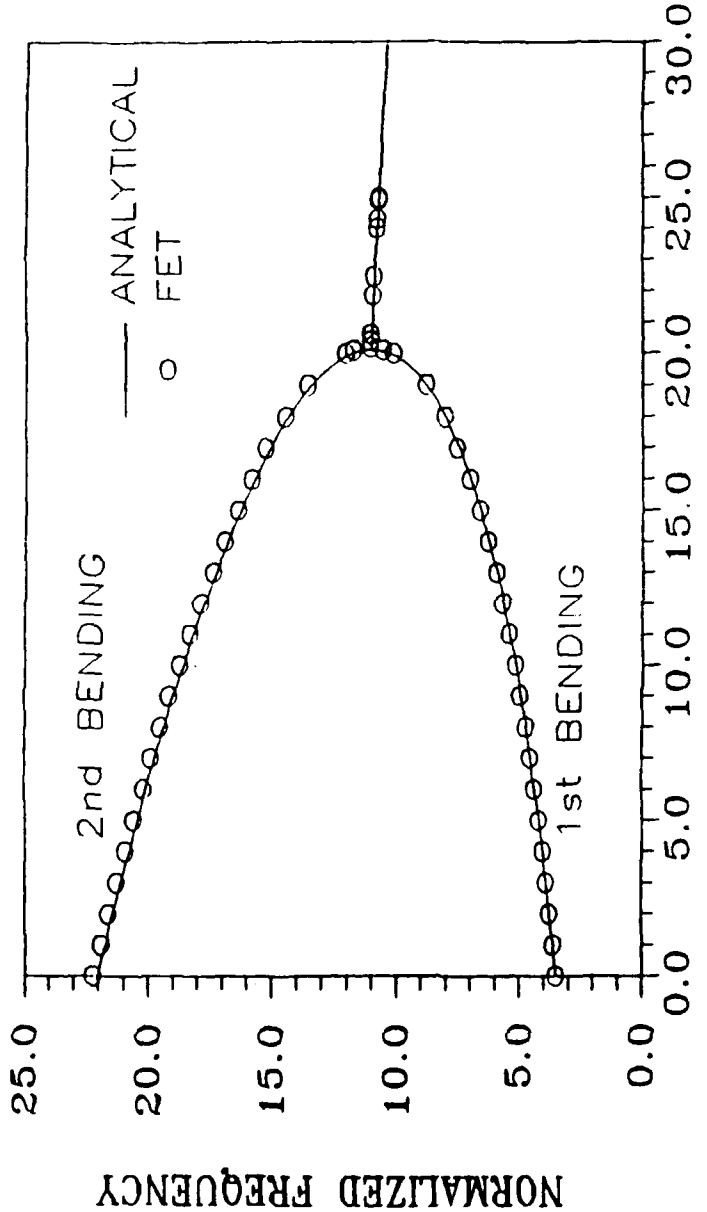

Fig. 83 - Linearized Stability Analysis of a Cantilevered Beam under a Tip Follower Force. Two Lowest Bending Frequencies of the Beam vs the Normalized Follower Force λ

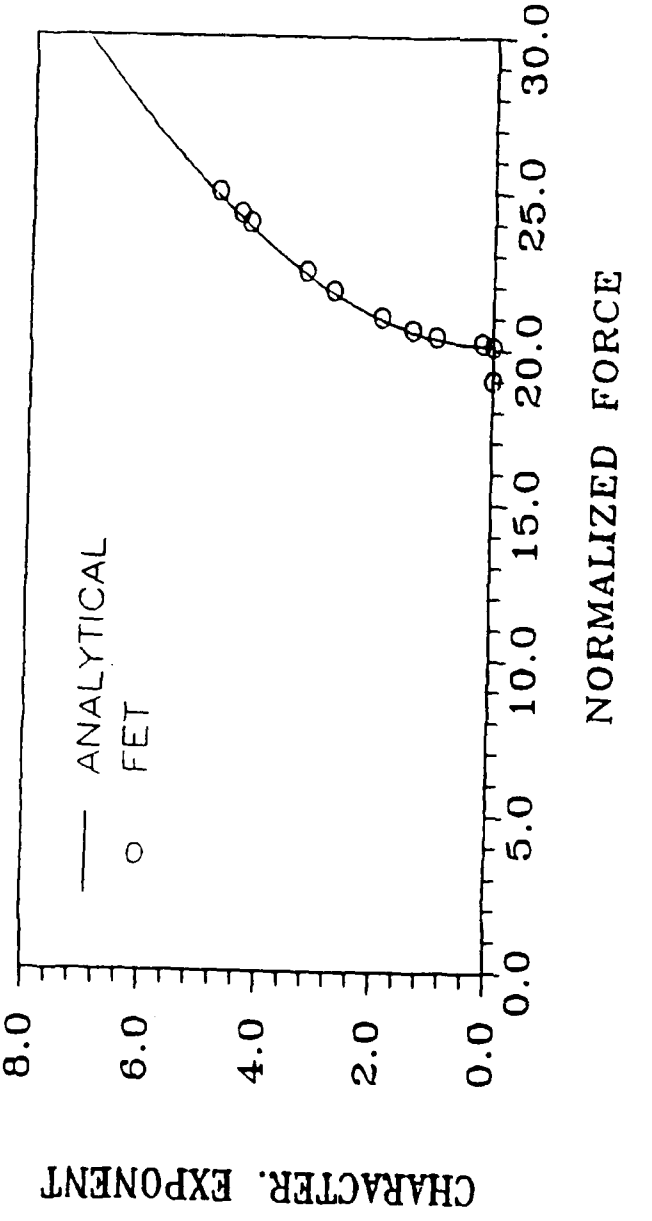

Fig. 84 - Linearized Stability Analysis of a Cantilevered Beam under a Tip Follower Force. Characteristic Exponent of the System vs the Normalized Follower Force λ

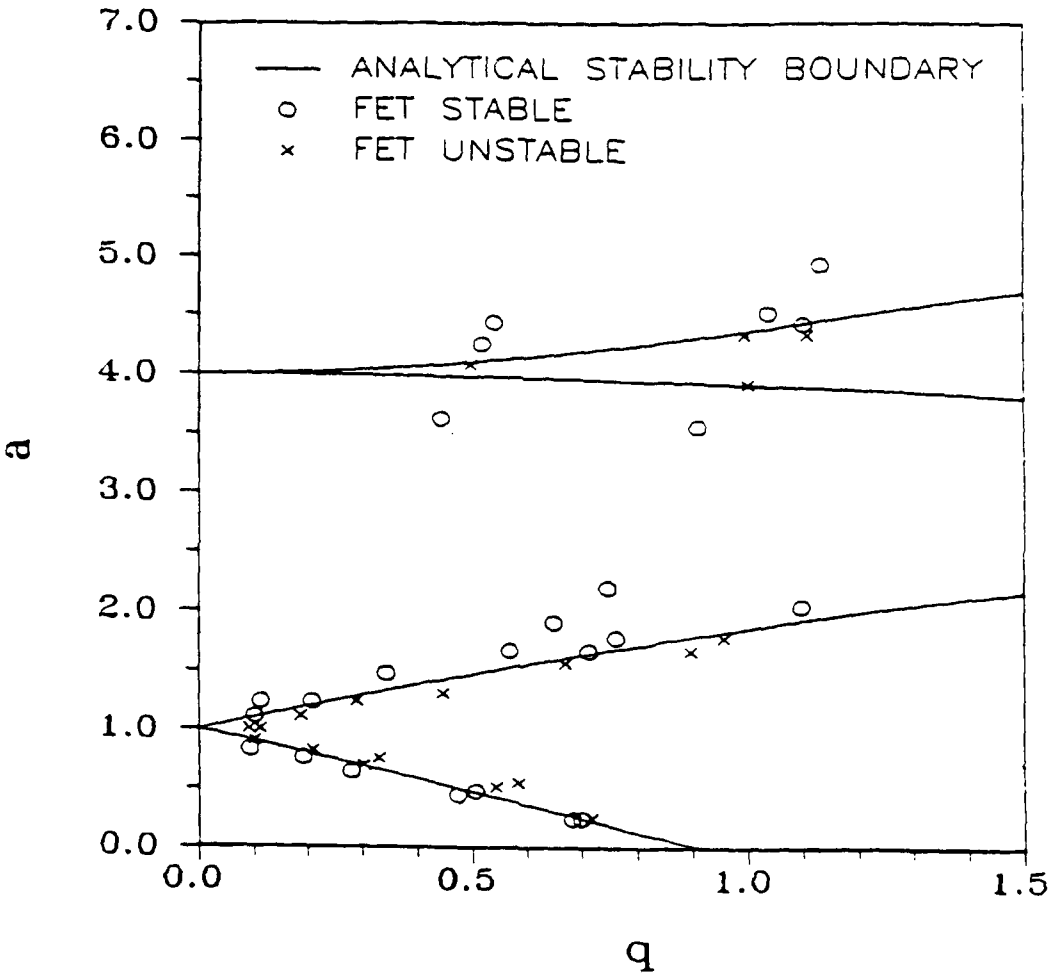

Fig. 85 - Stability Boundaries for the Parametrically Excited Undamped Beam

THEORY

—— Present Method (Model D)
---- Theoretical Results of Refs. 65, 66

EXPERIMENT

Load, P = 13.344 N (3 lbs)
Load, P = 8.896 N (2 lbs)
Load, P = 4.448 N (1 lbs)

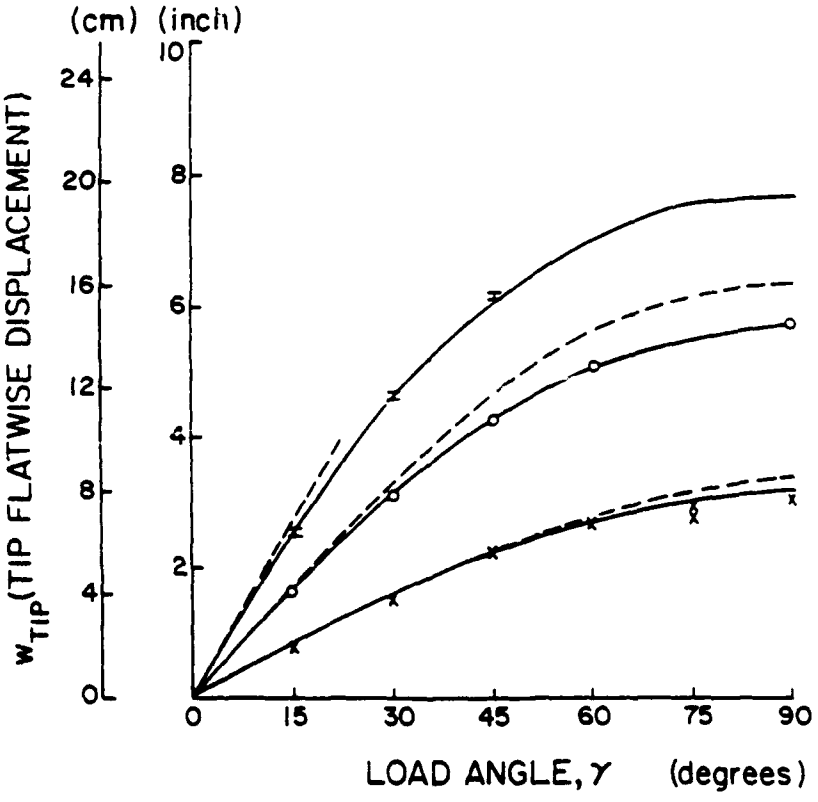

Fig. 86 - Comparison Between the Calculated and Experimental Results of the Flatwise Component of the Tip Displacement

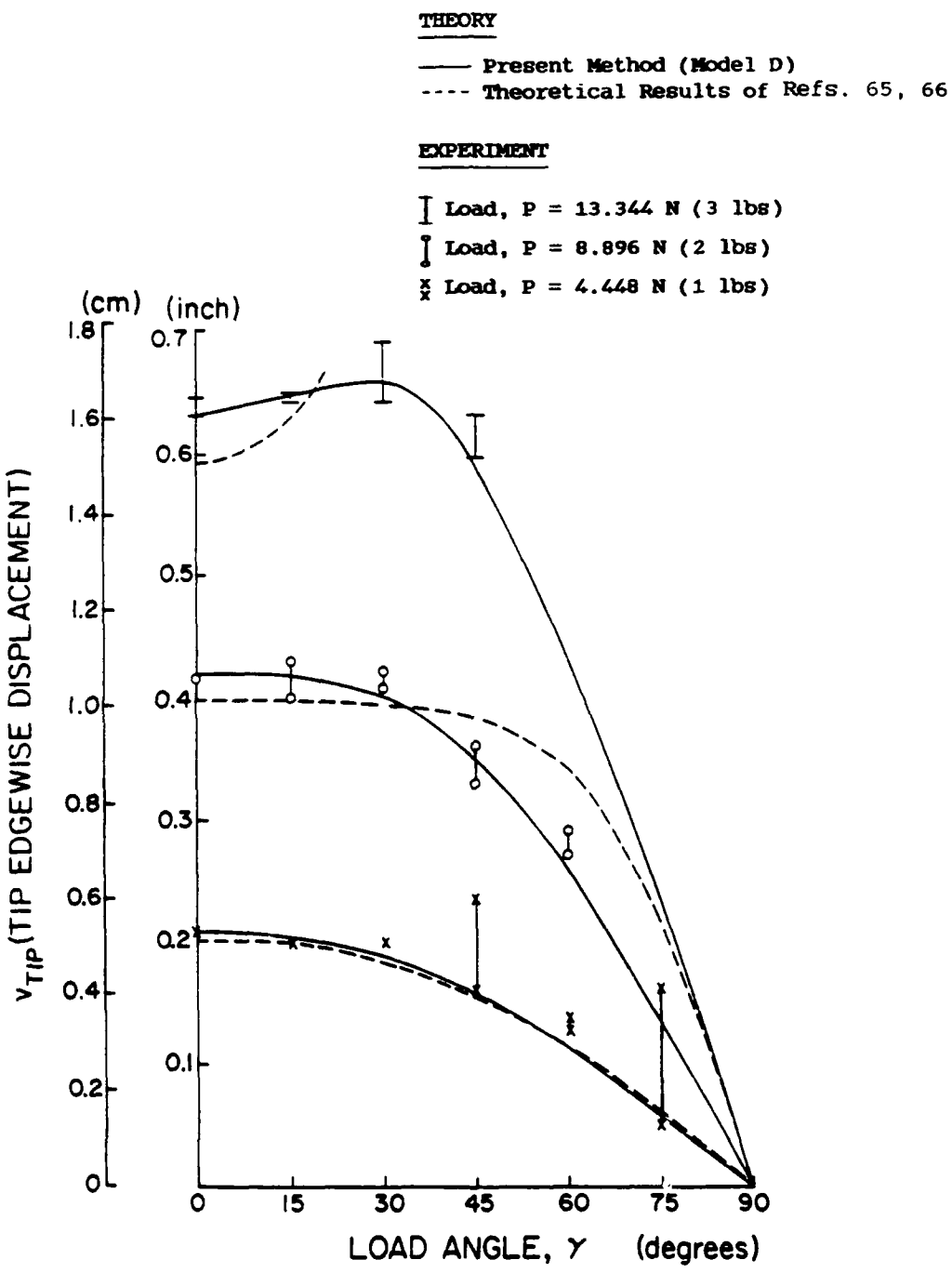

Fig. 87 - Comparison Between the Calculated and Experimental Results of the Edgewise Component of the Tip Displacement

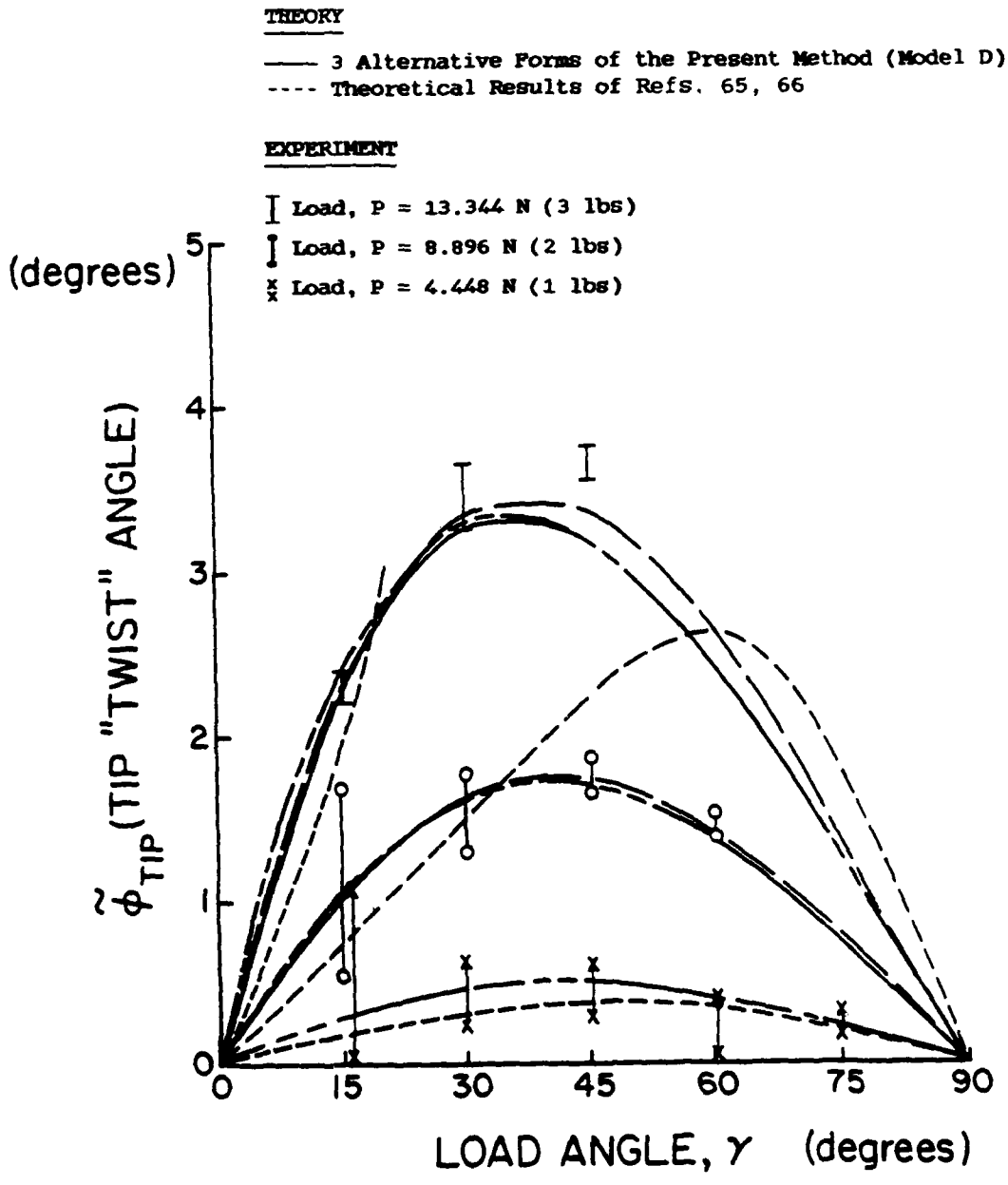

Fig. 88 - Comparison Between the Calculated and Experimental Results of the Tip "Twist Angle"

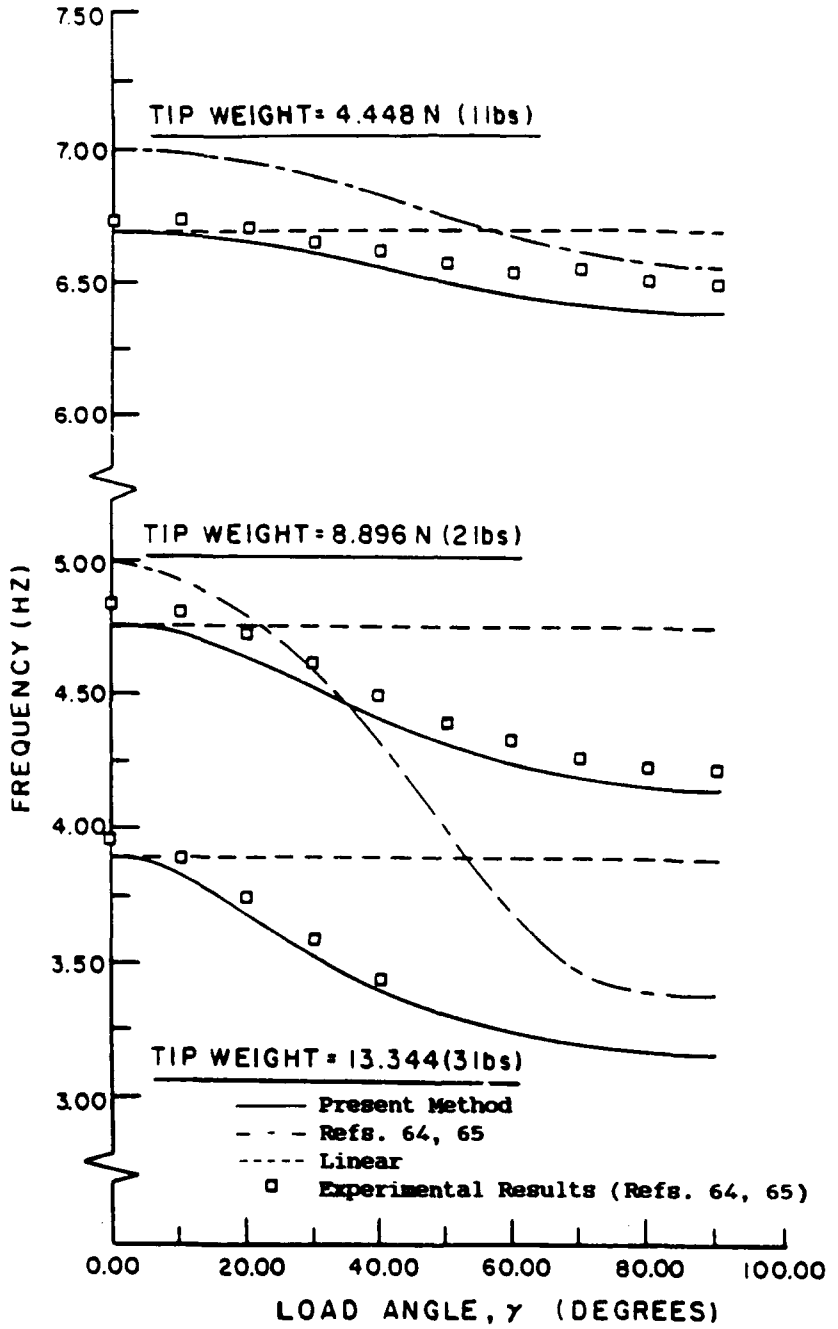

Fig. 89 - Nonrotating Beam - The First Flatwise Natural Frequency

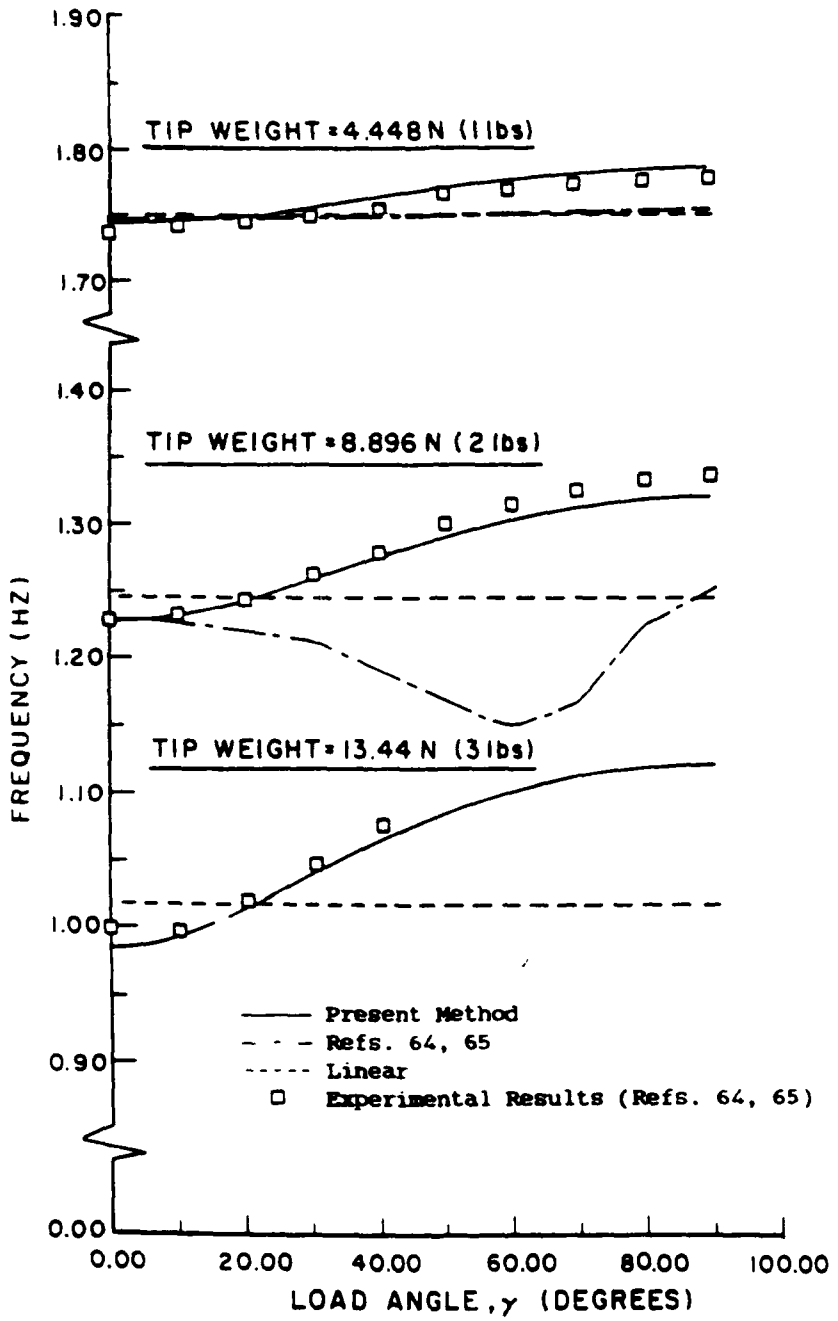

Fig. 90 - Nonrotating Beam - The First Edgewise Natural Frequency

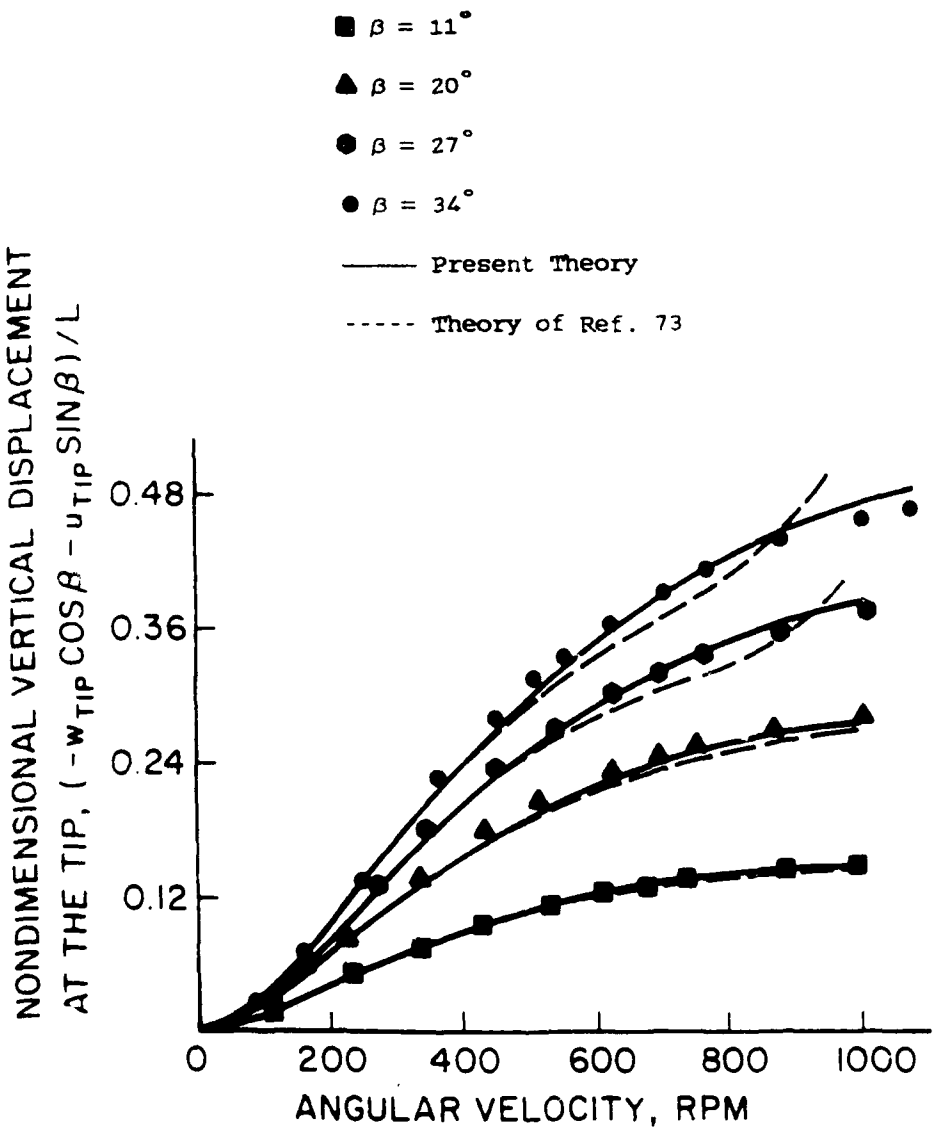

Fig. 91 - Experimental Results (Ref. 73)

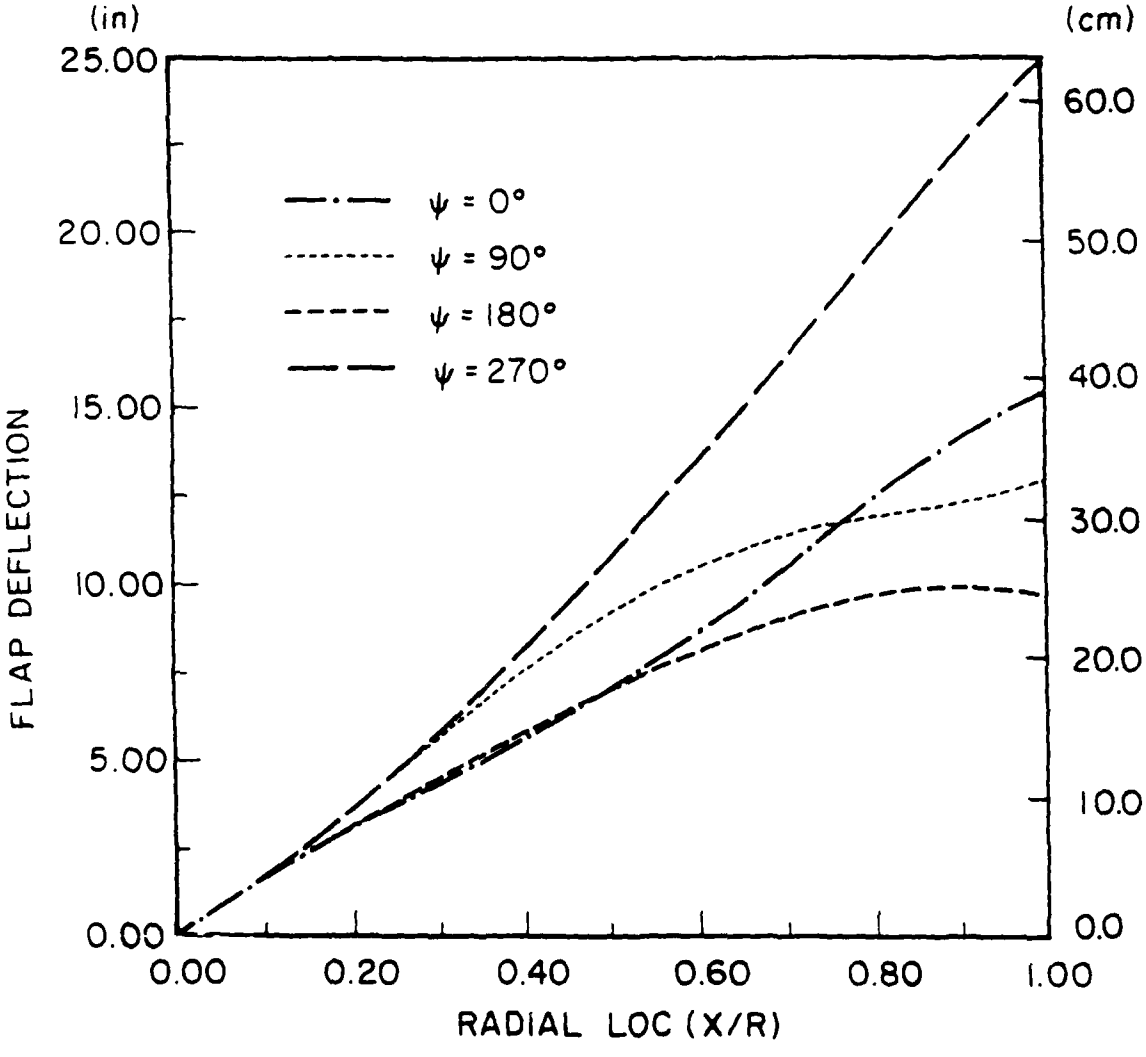

Fig. 92 - Instantaneous Deflection of the UH-61A Rotor Blade at Normal Operating RPM of 150 Knots in Four Azimuthal Locations: Flap Bending

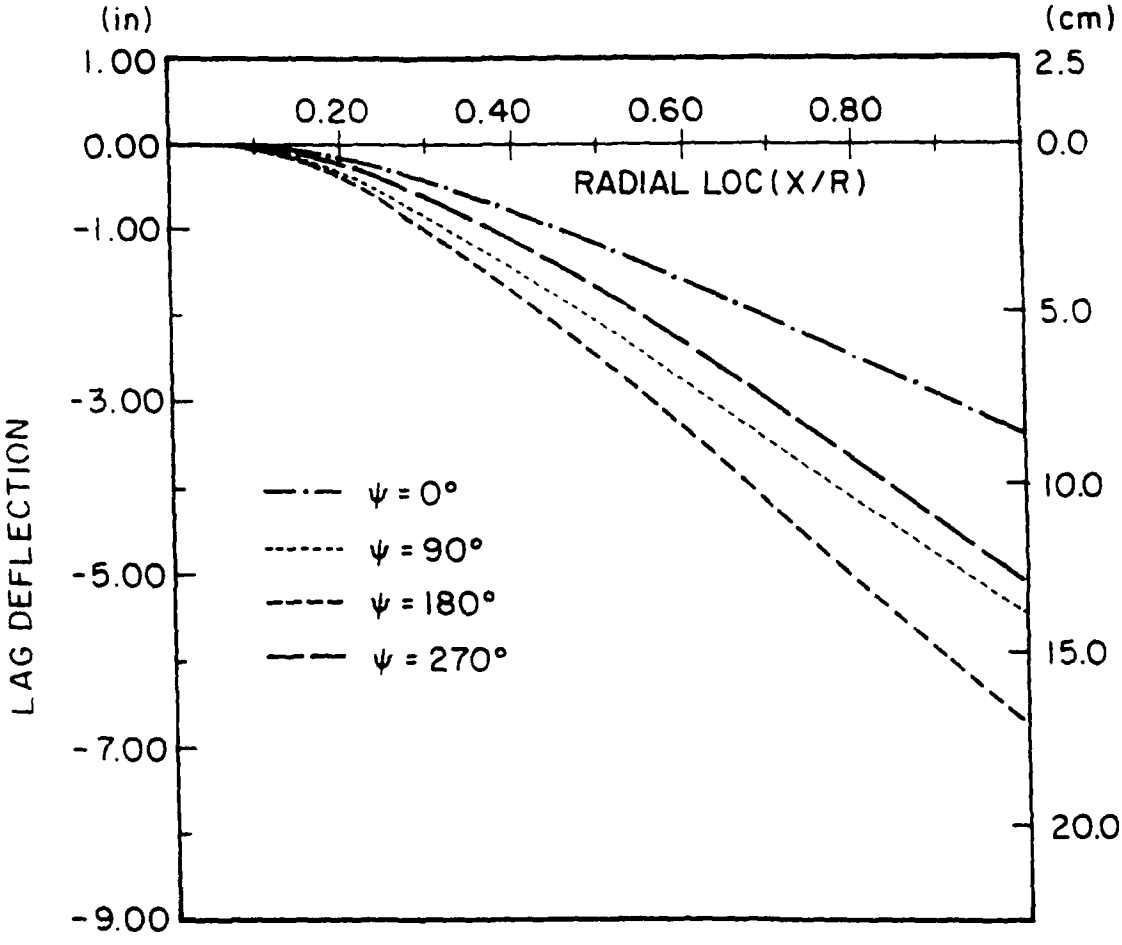

Fig. 93 - Instantaneous Deflection of the UH-61A Rotor Blade at Normal Operating RPM of 150 Knots in Four Azimuthal Locations: Lag Bending

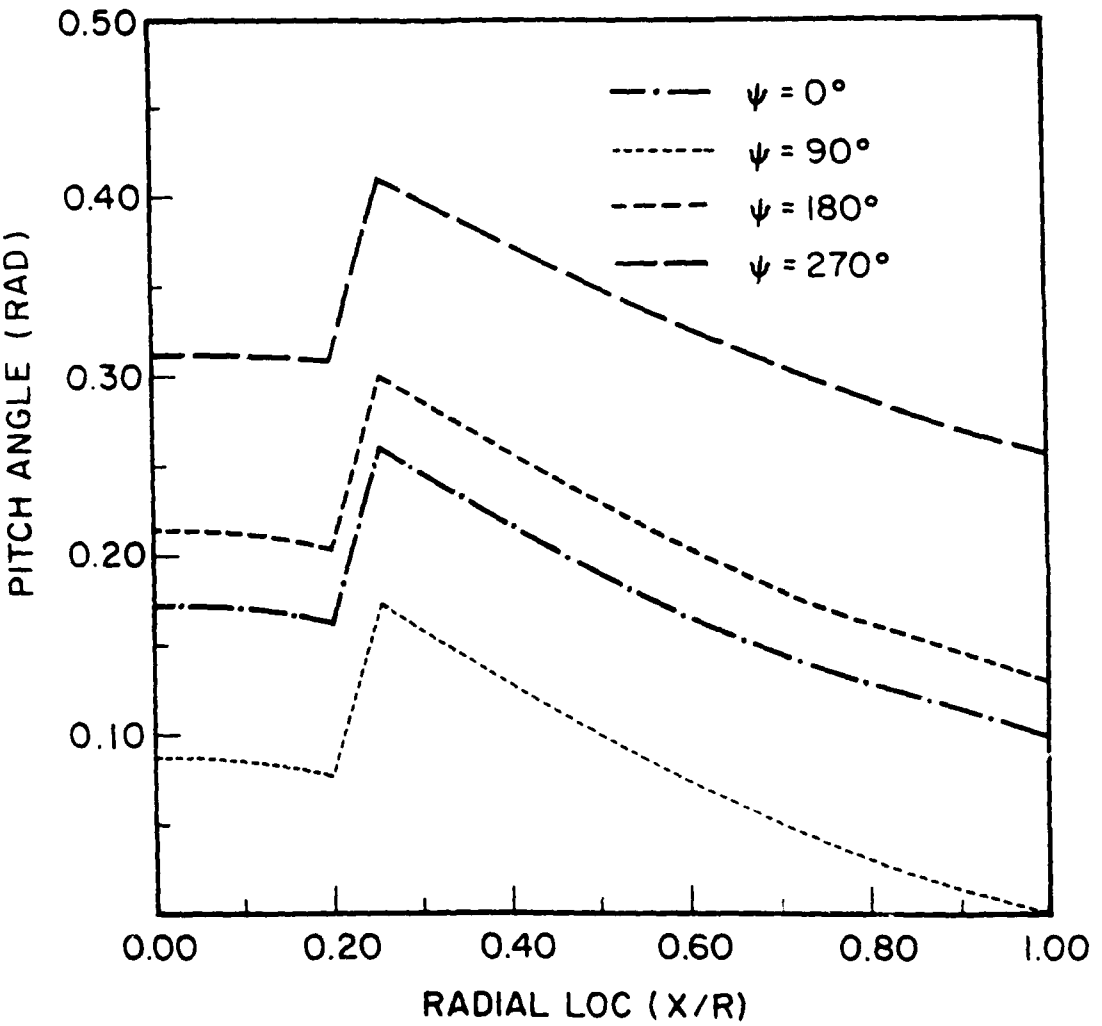

Fig. 94 - Instantaneous Deflection of the UH-61A Rotor Blade at Normal Operating RPM of 150 Knots in Four Azimuthal Locations: Pitch Angle

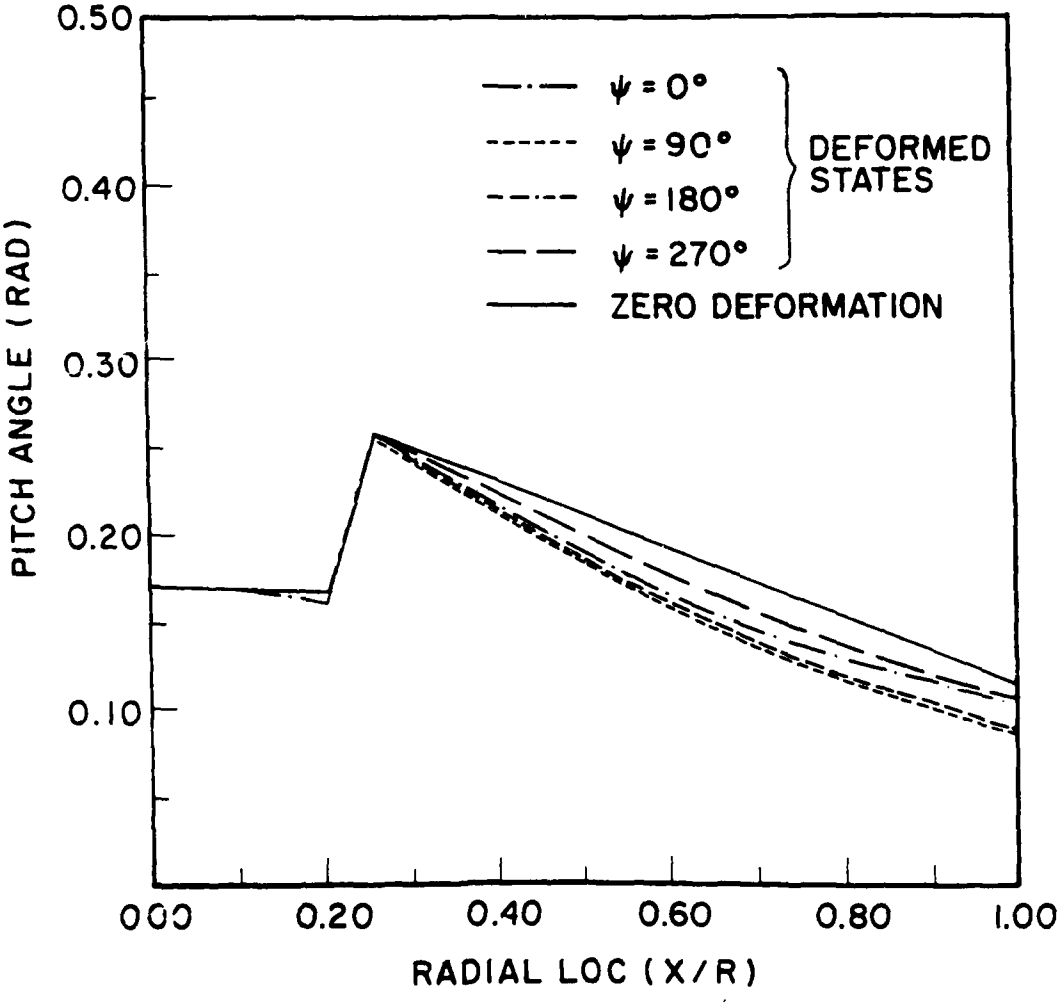

Fig. 95 - Instantaneous Deflection of the UH-61A Rotor Blade at Normal Operating RPM of 150 Knots in Four Azimuthal Locations: Pitch Angle, Adjusted

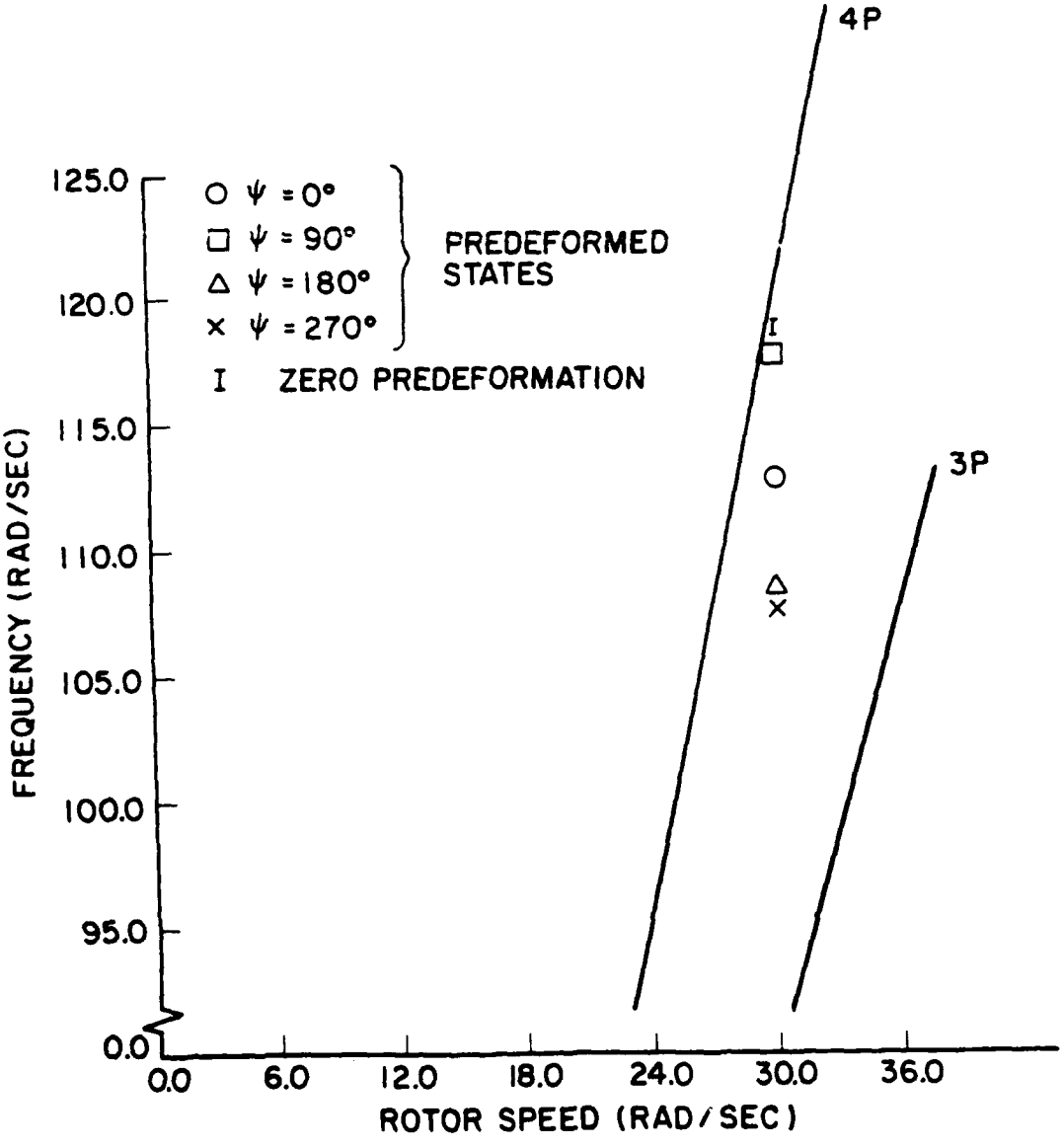

Fig. 96 - Portion of Campbell Diagram for UH-61A Blade Showing Natural Frequency Variations Resulting from Predeformed States: First Torsion

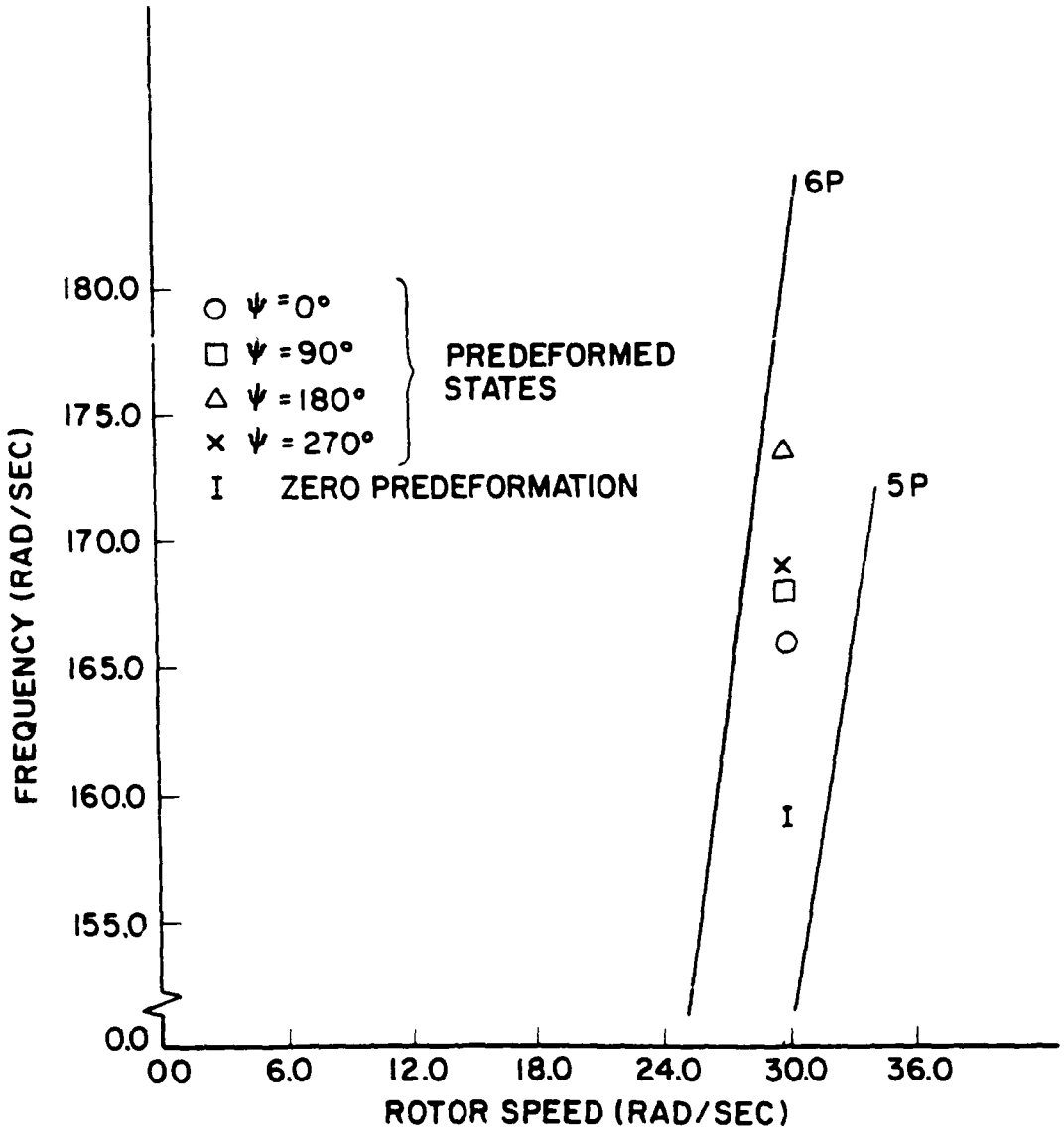

Fig. 97 - Portion of Campbell Diagram for UH-61A Blade Showing Natural Frequency Variations Resulting from Predeformed States: Second Lag Bending

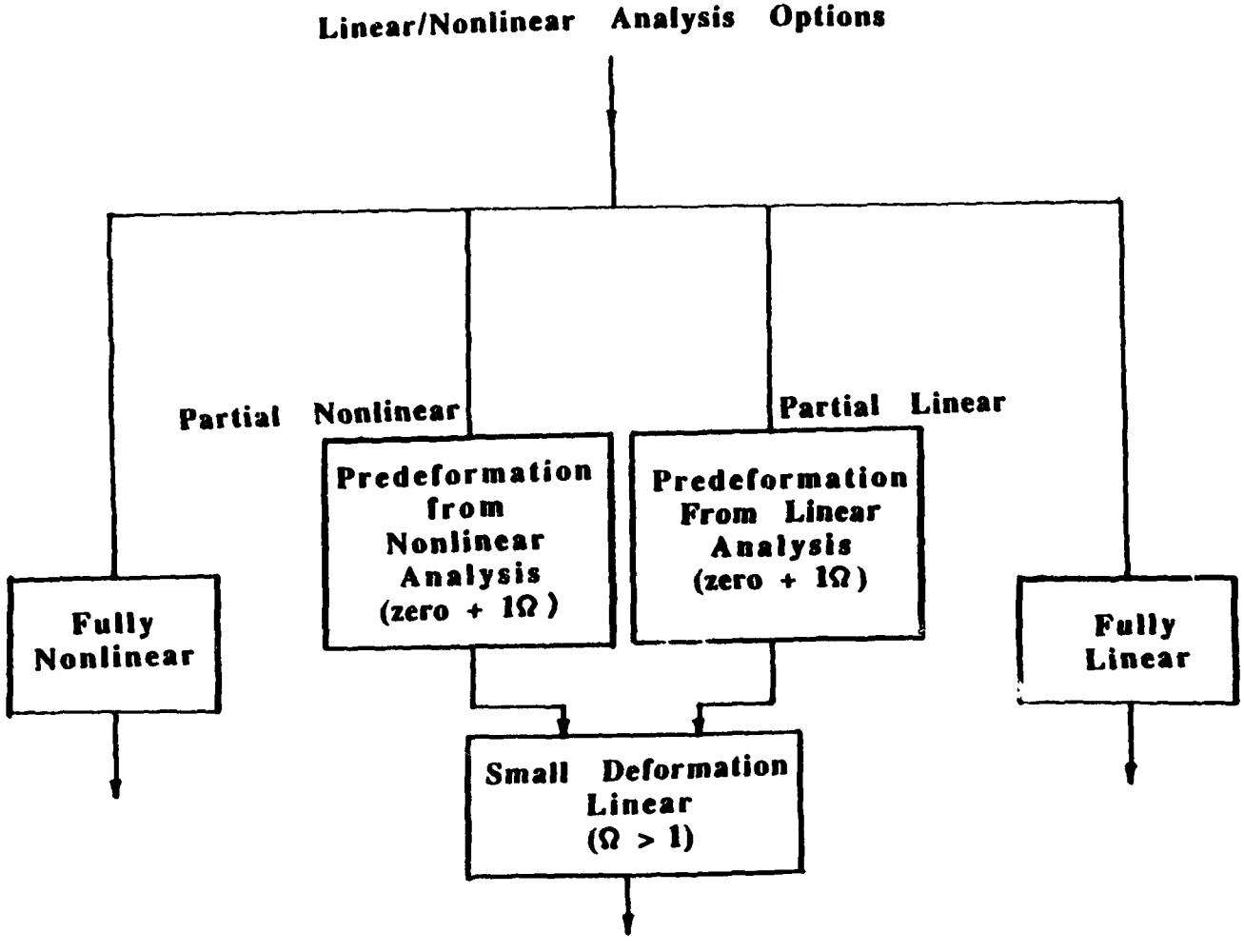

Fig. 98 - Linear/Nonlinear Analysis Options

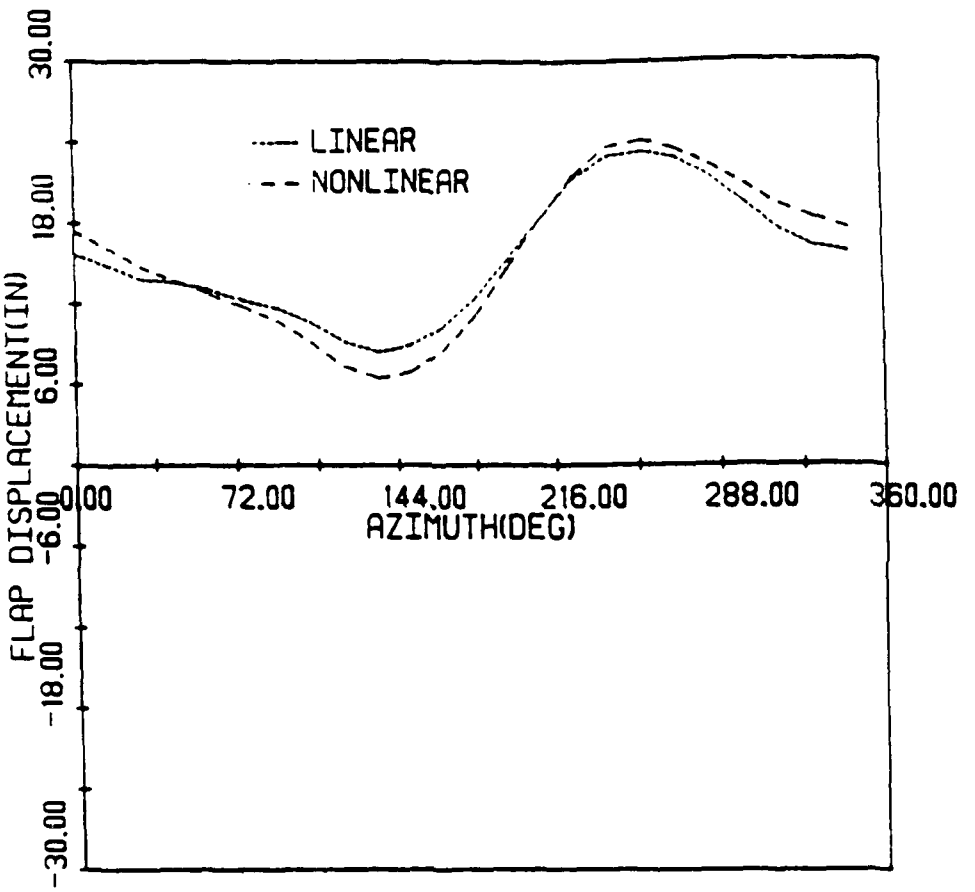

Fig. 99 - Comparison of Linear and Nonlinear Analysis Flap Displacement at the Tip

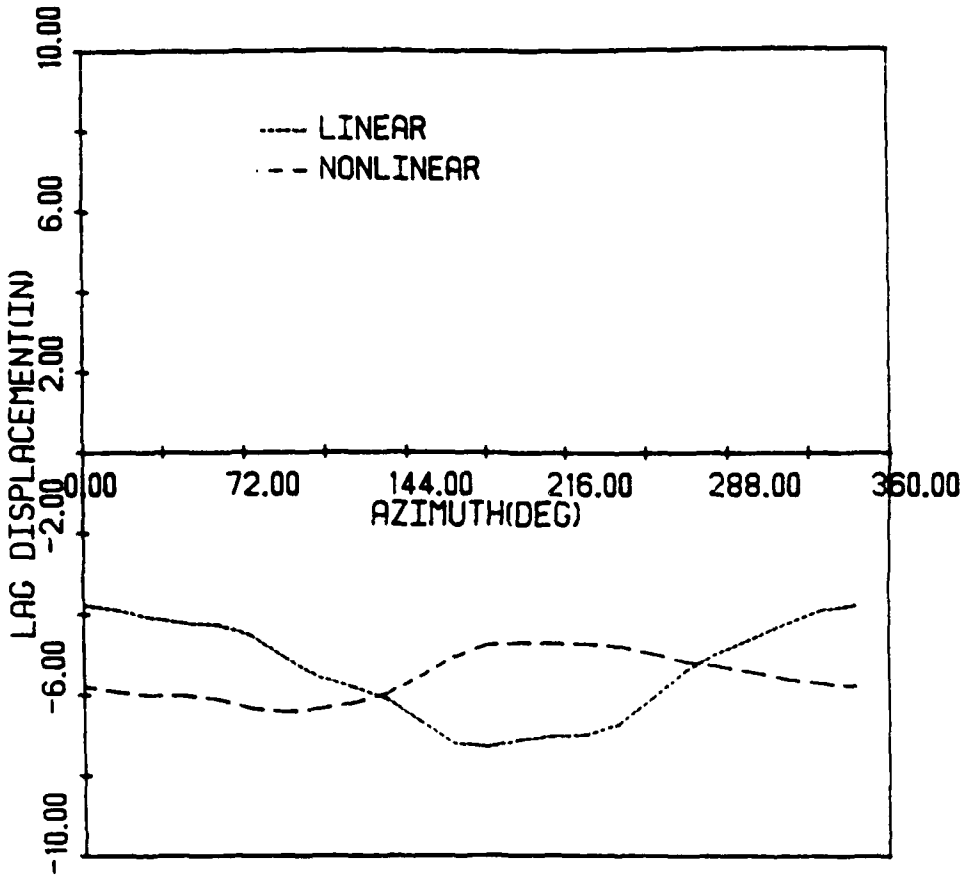

Fig. 100 - Comparison of Linear and Nonlinear Analysis Lag Displacement at the Tip

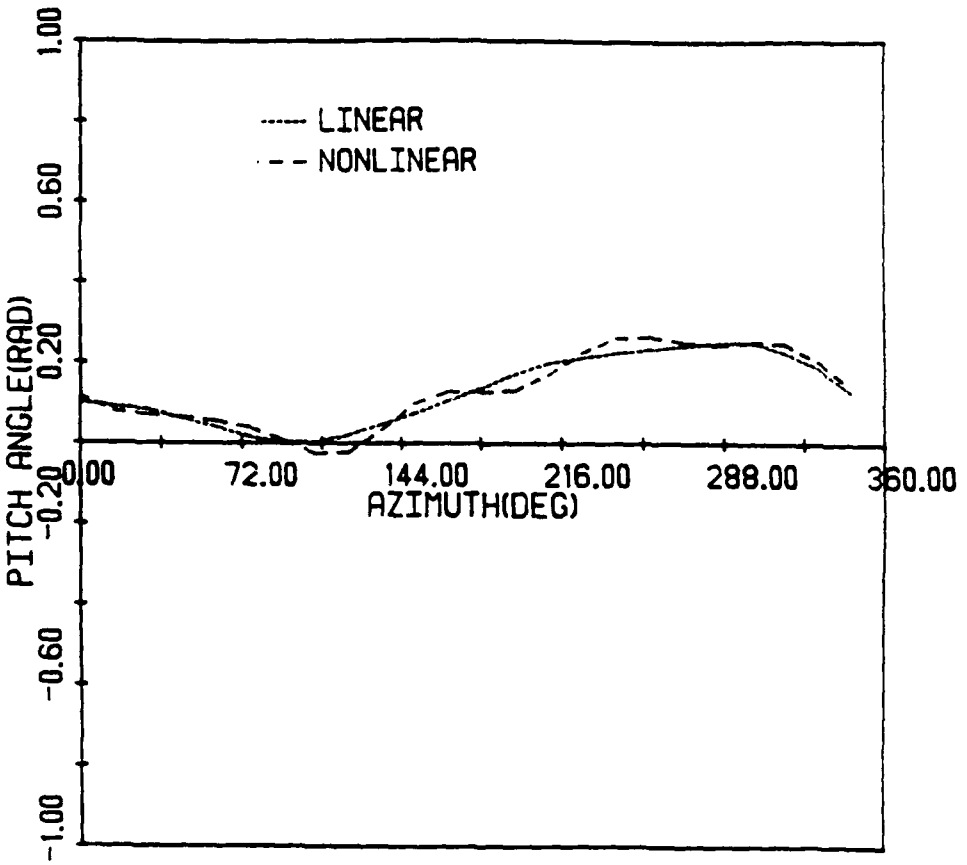

Fig. 101 - Comparison of Linear and Nonlinear Analysis Pitch Angle at the Tip

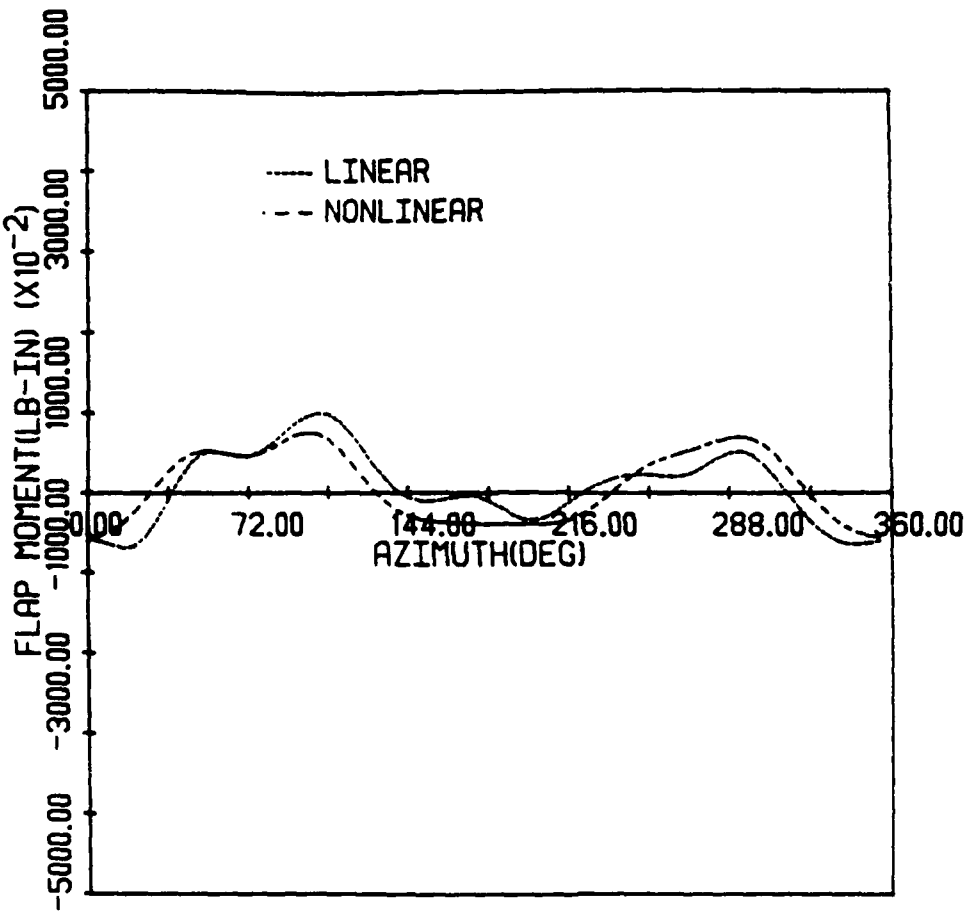

Fig. 102 - Comparison of the Resultant Flap Bending Moment at the Root Between Linear and Nonlinear Analysis

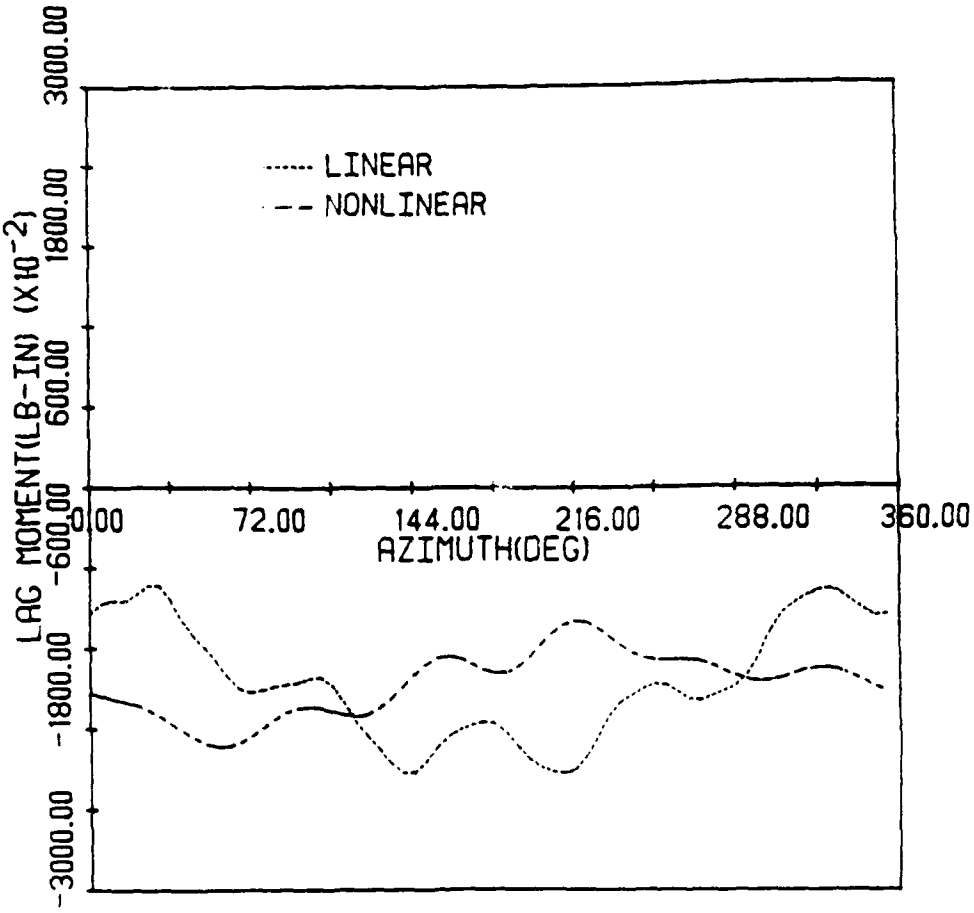

Fig. 103 - Comparison of the Resultant Lag Bending Moment at the Root Between Linear and Nonlinear Analysis

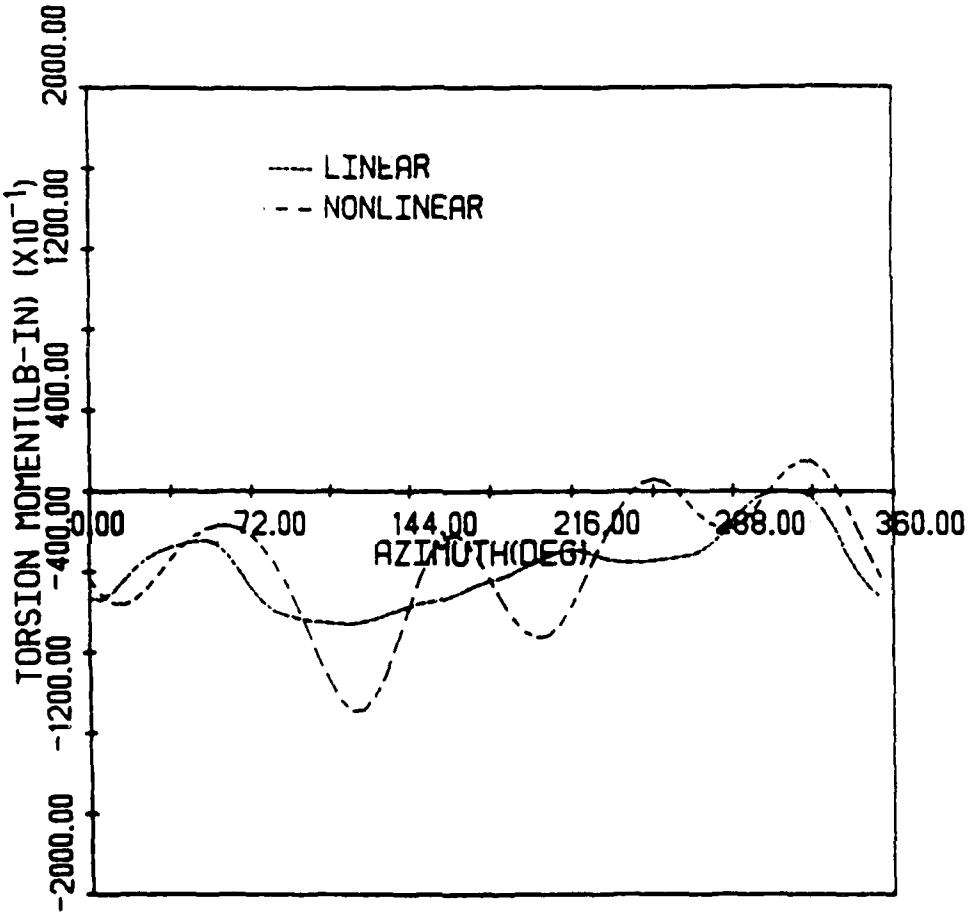

Fig. 104 - Comparison of the Resultant Torsional Moment at 20% Radius Between Linear and Nonlinear Analysis

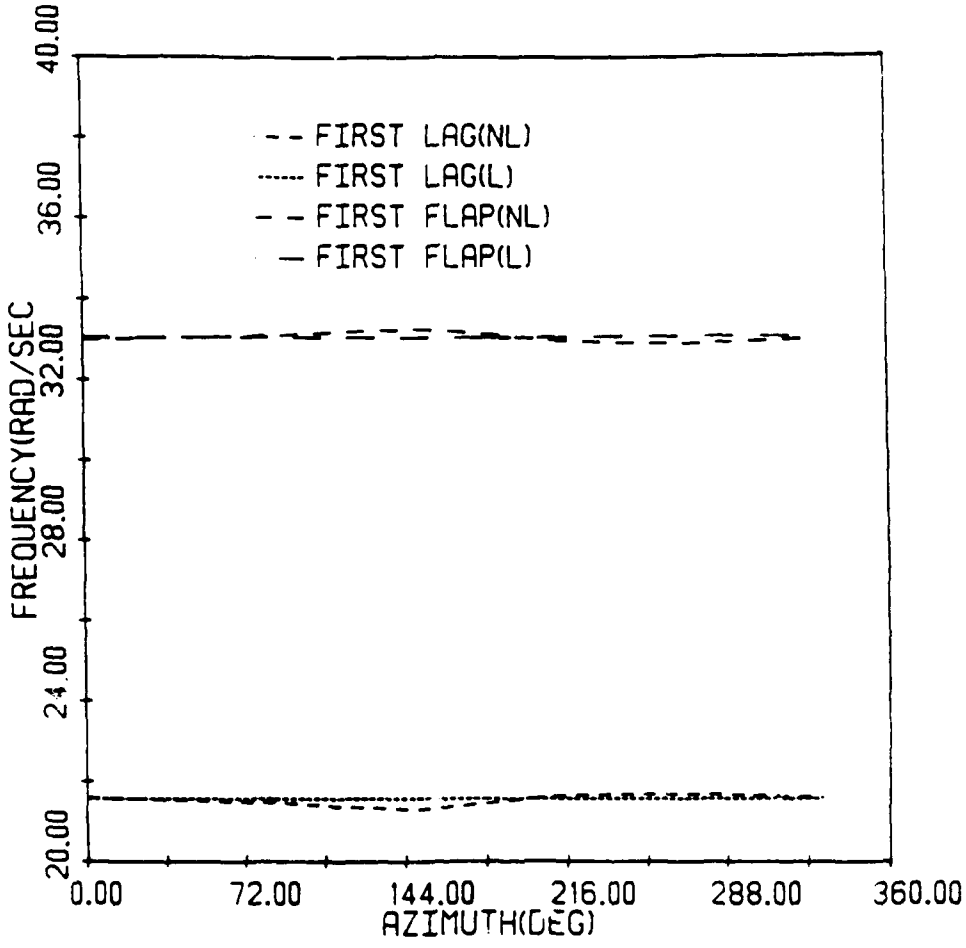

Fig. 105 - Variation of the First Predominantly Flap and Lag Frequencies with Azimuth

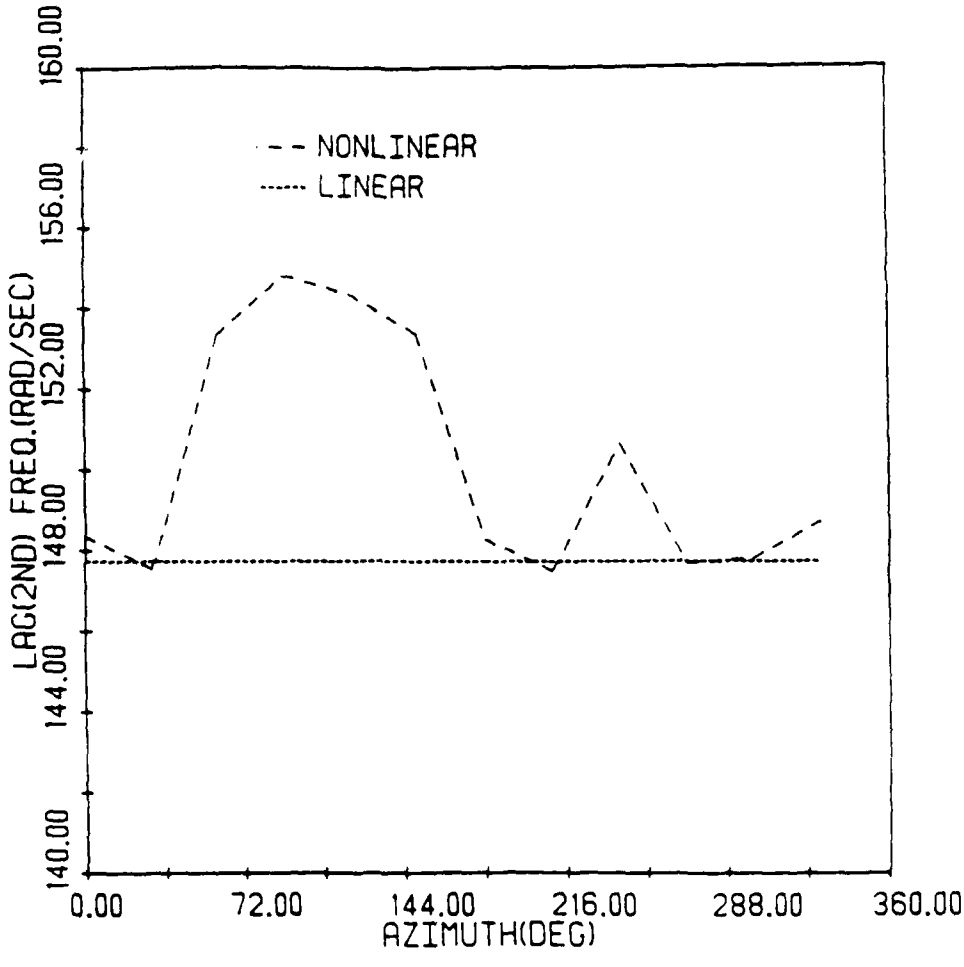

Fig. 106 - Variation of the Second Predominantly Lag Frequency with Azimuth

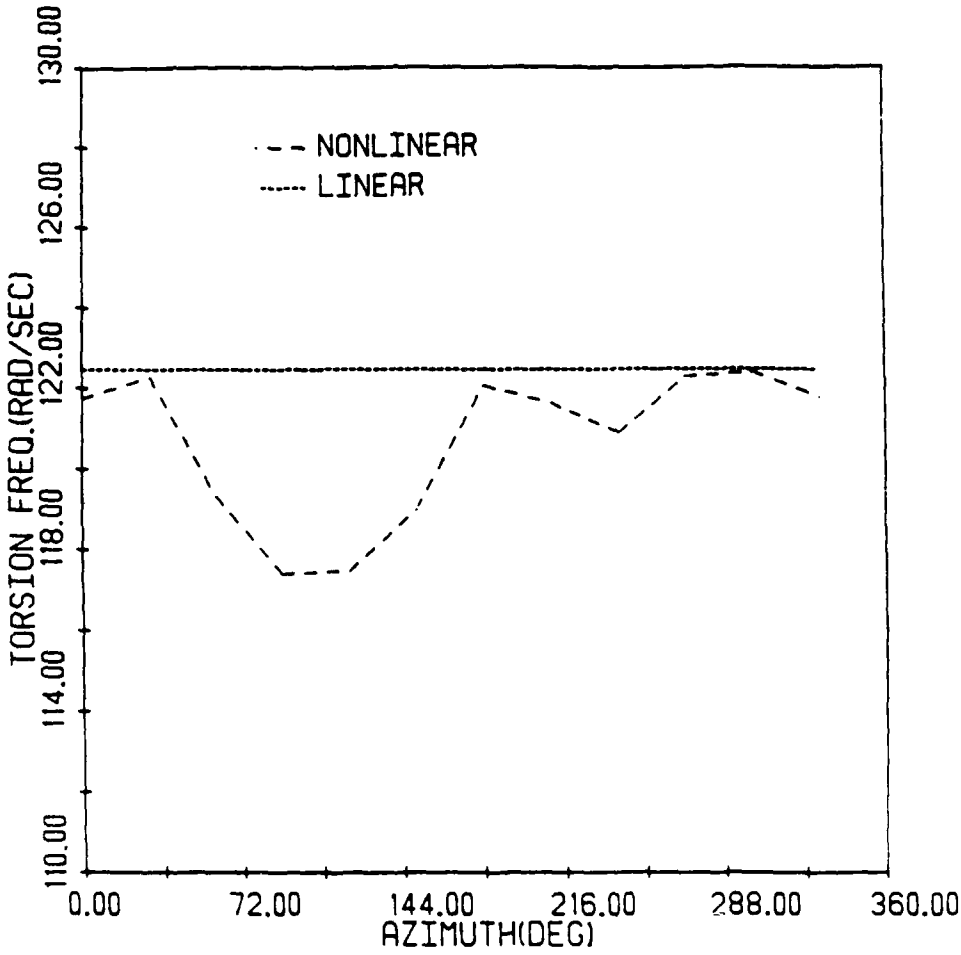

Fig. 107 - Variation of the First Predominantly Torsional Frequency with Azimuth

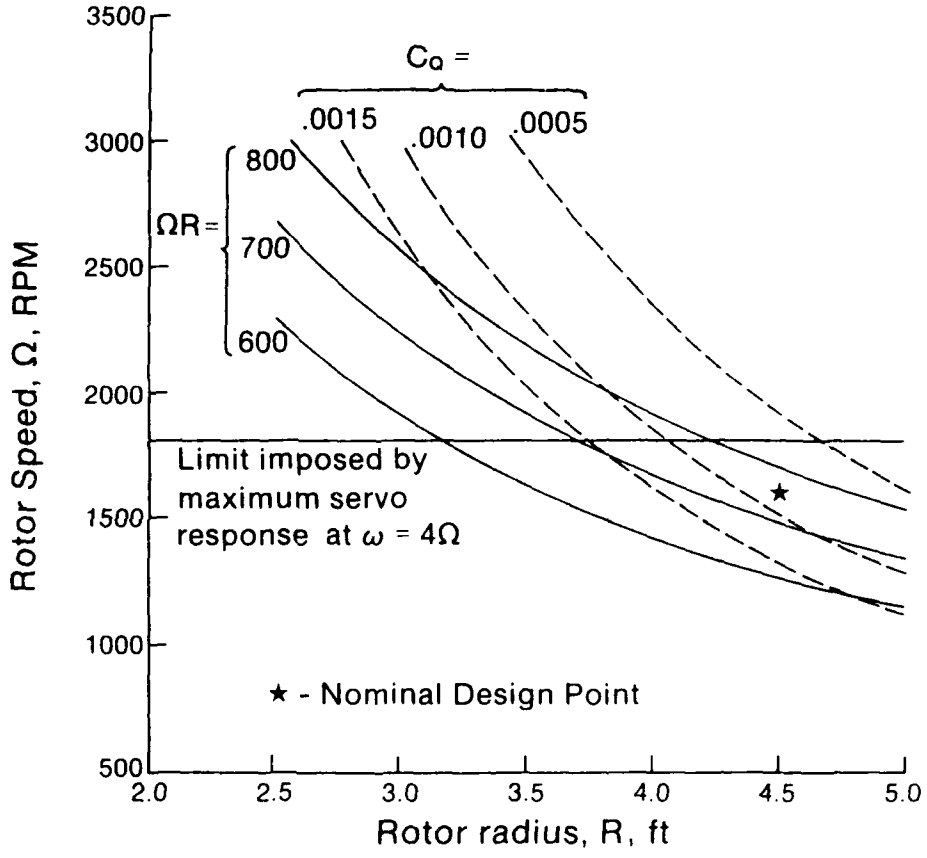

Fig. 108 - Available Test Envelope for Mach-Scaled Rotors, 100 HP Maximum Delivered Rotor Power

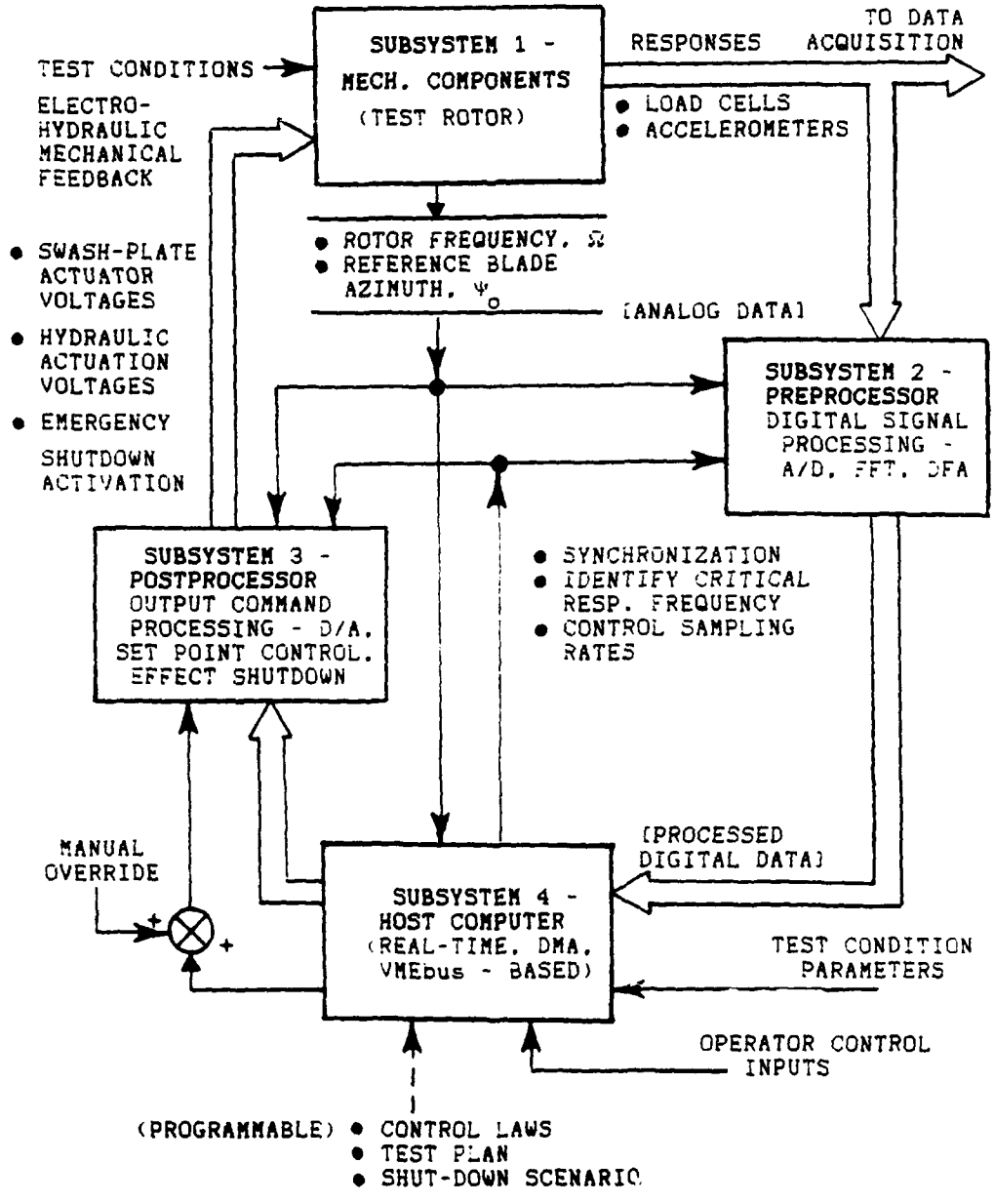

Fig. 109 - Schematic Representation of RPI Model Rotor Impedance Test Facility Showing Major Subsystems

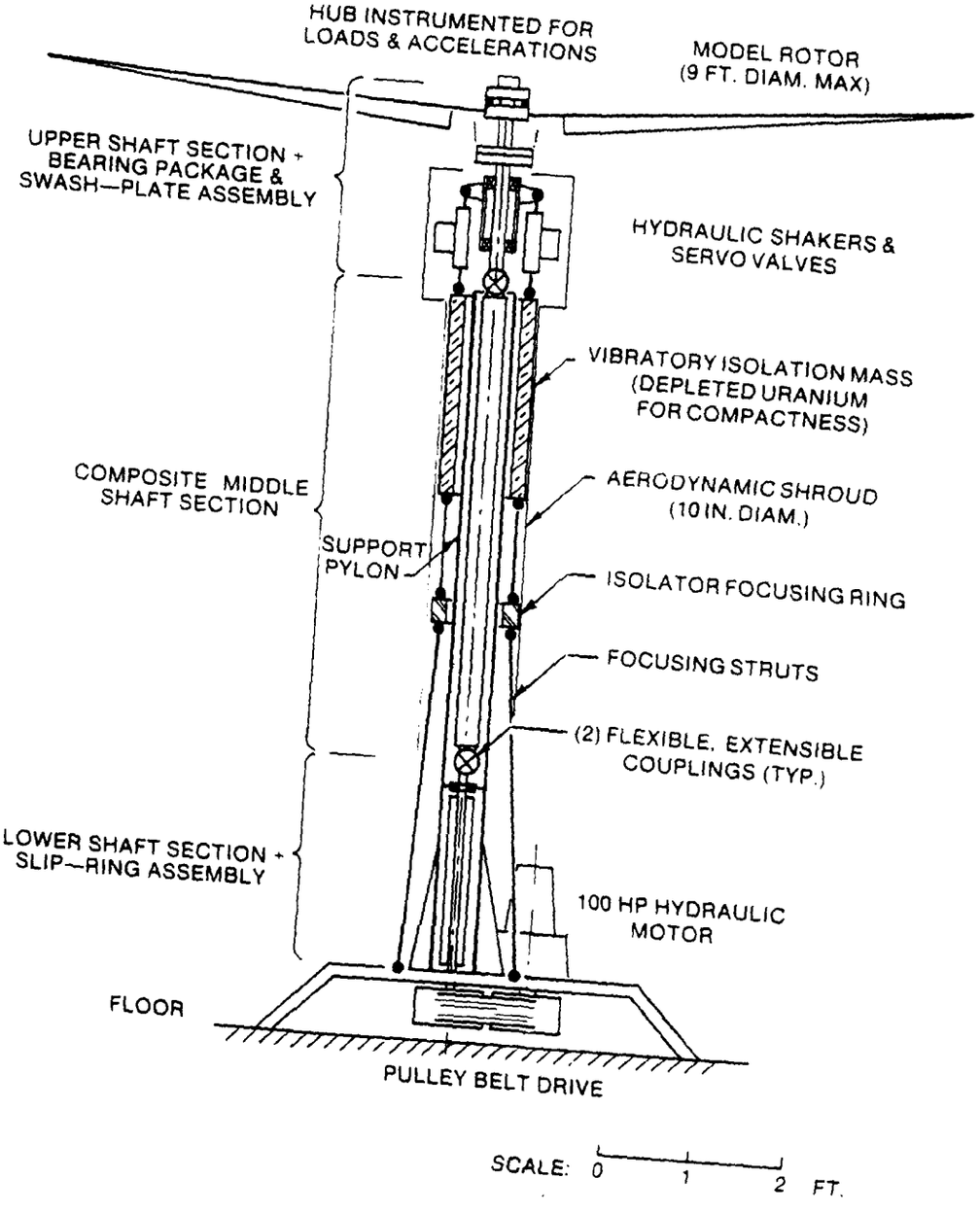

Fig. 110 - Pictorial Layout (with cut-away view) of the Mechanical Components of the RPI Model Rotor Impedance Test Facility

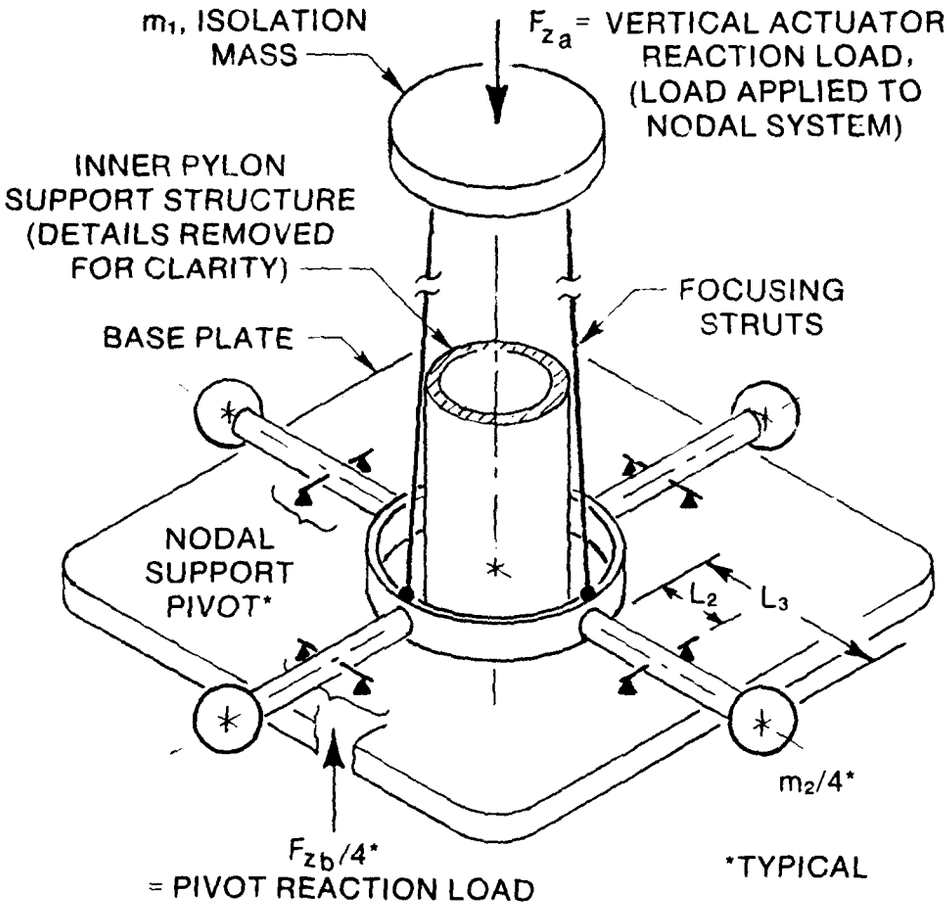

Fig. 111 - Isolation System Elements

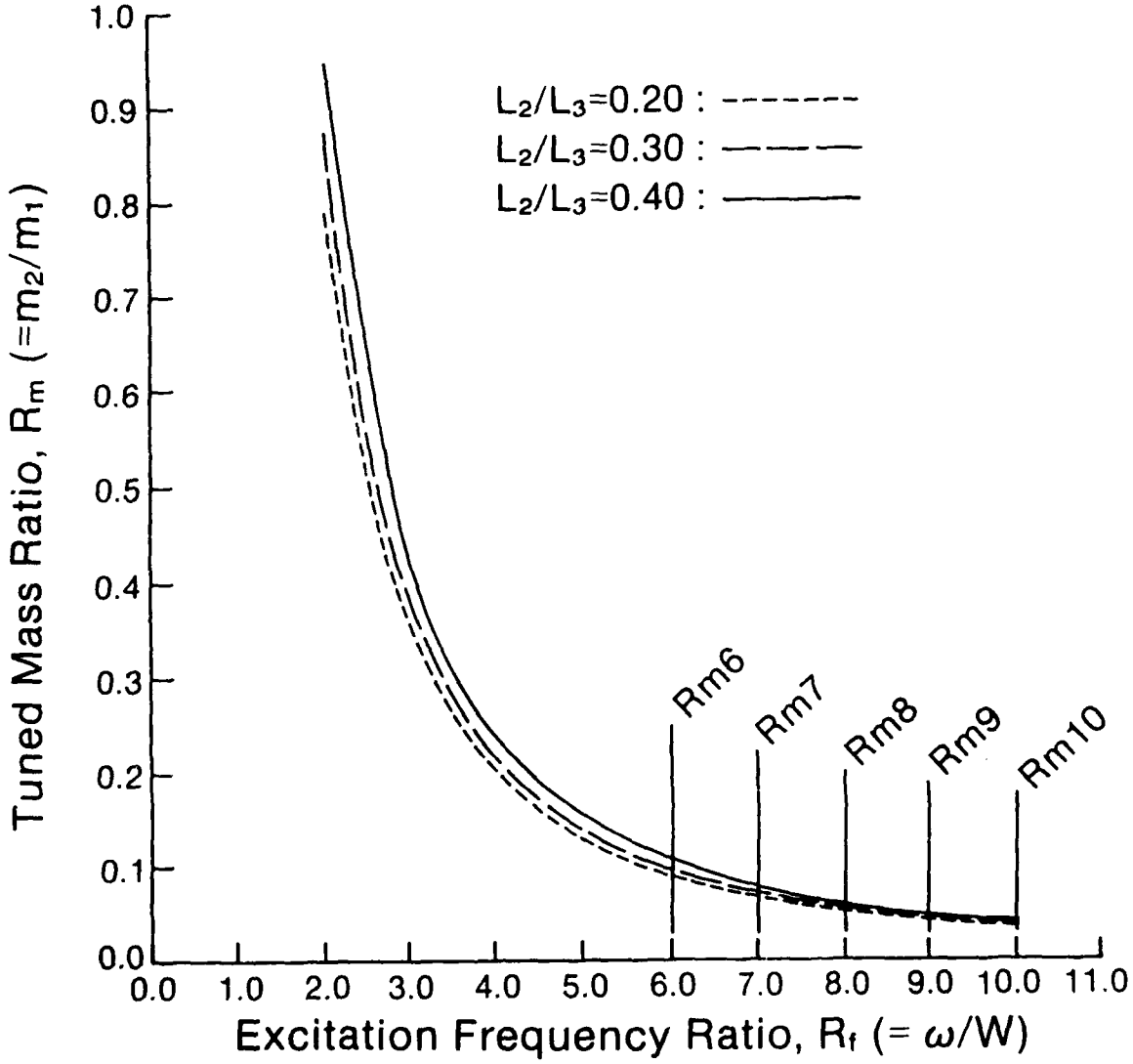

Fig. 112 - Variation of Mass Ratio Needed to Achieve Nodal Isolation at Various Nodal Pivot Locations

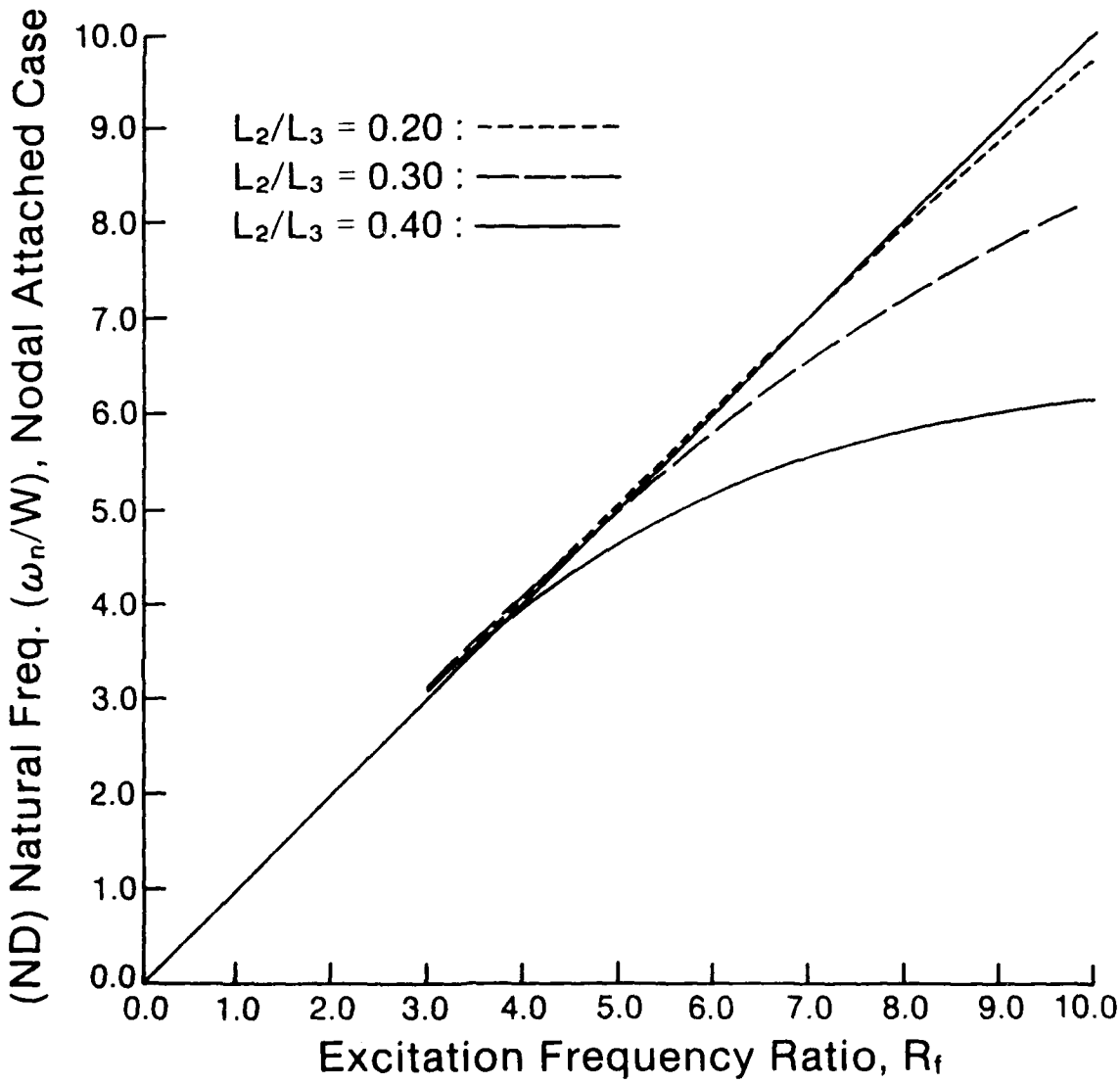

Fig. 113 - Natural Frequency Variations with Variations in Excitation Frequency Ratio

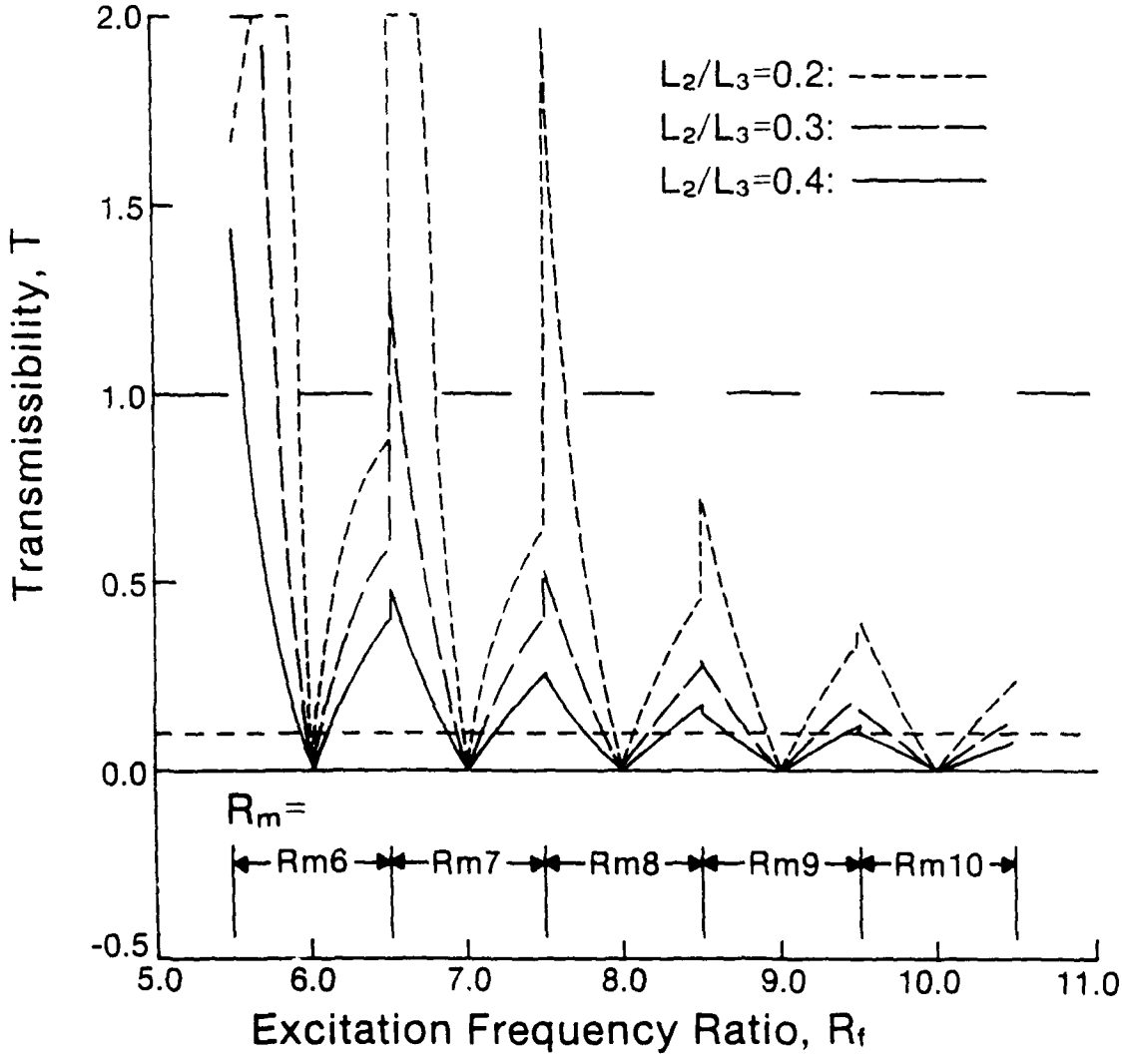

Fig. 114 - Variation of Transmissibilities with Excitation Frequency Ratio for Discrete Variations in Mass Ratio

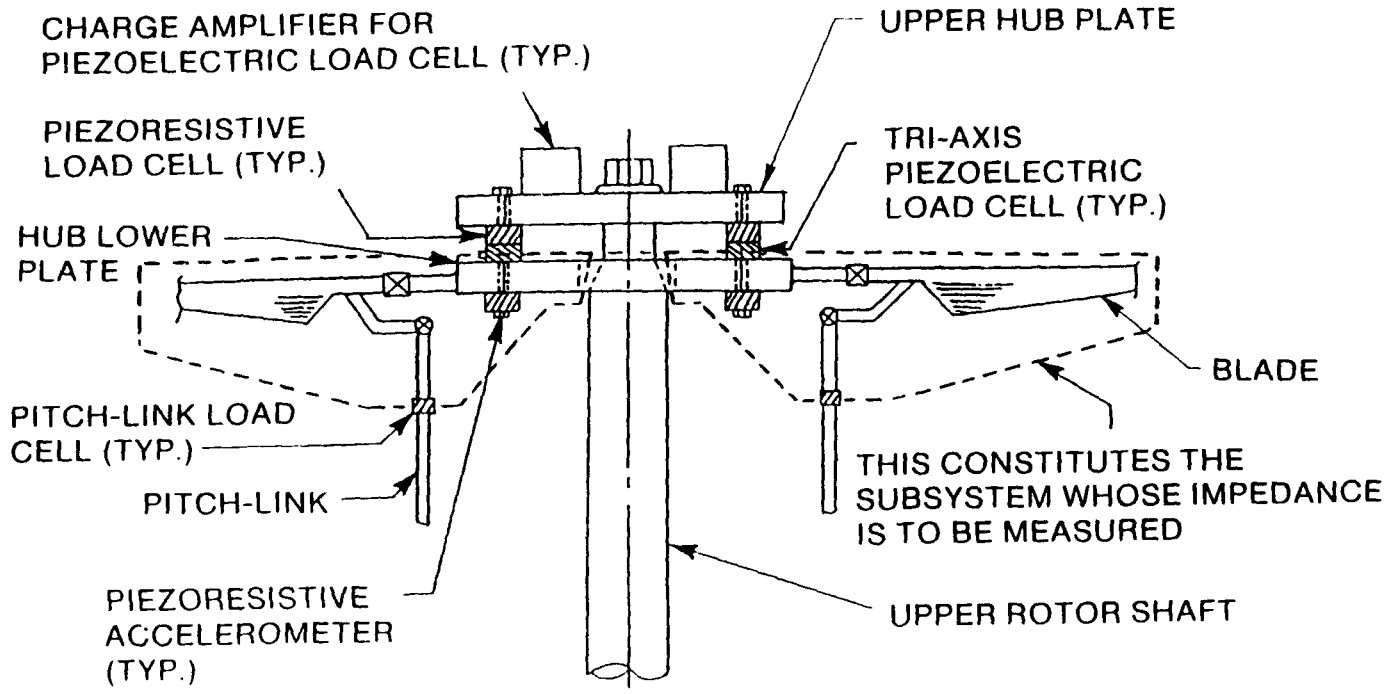

Fig. 115 - Schematic of Transducer Locations Illustrating Method for Measuring Hub Loads and Motion

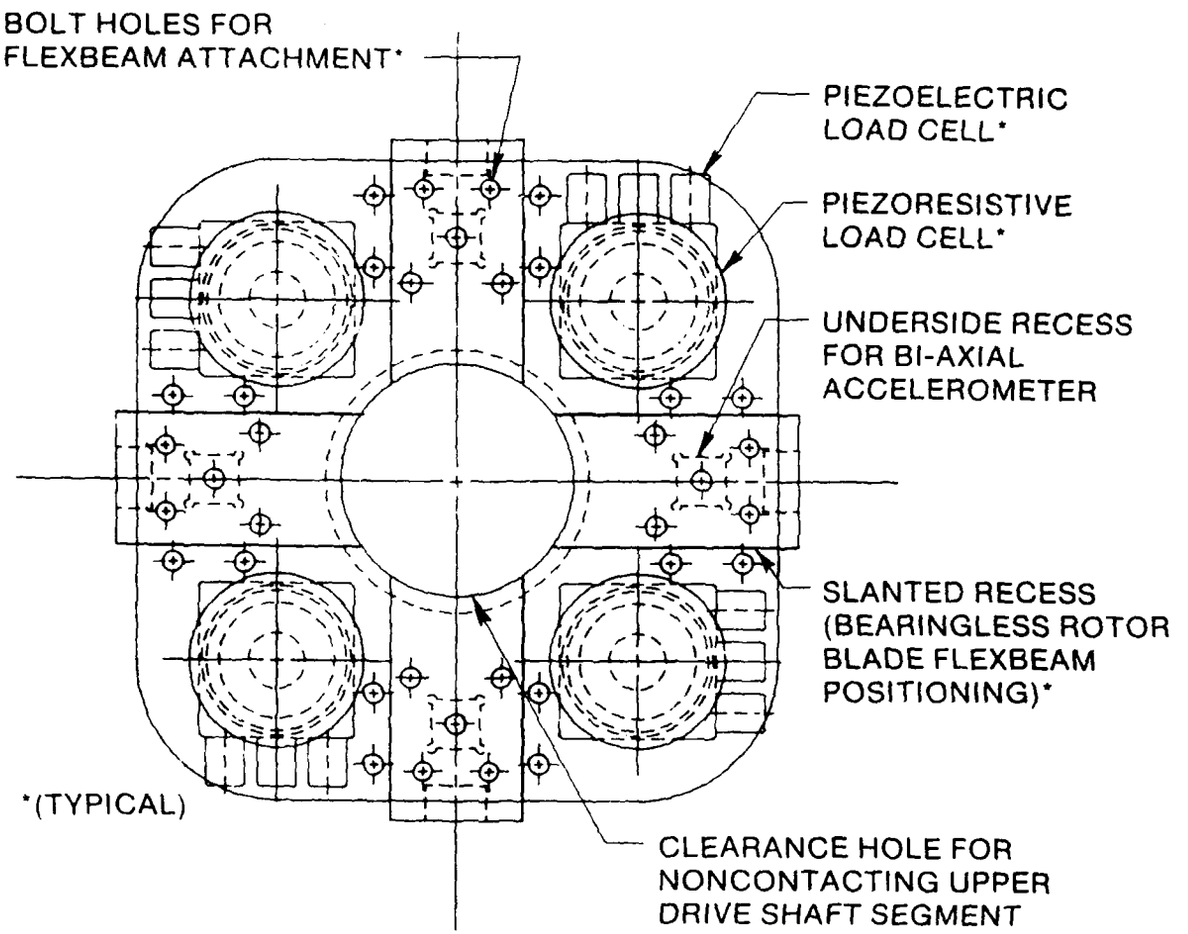

Fig. 116 - Titanium Hub Design - Lower Plate with Installation of Load Cells

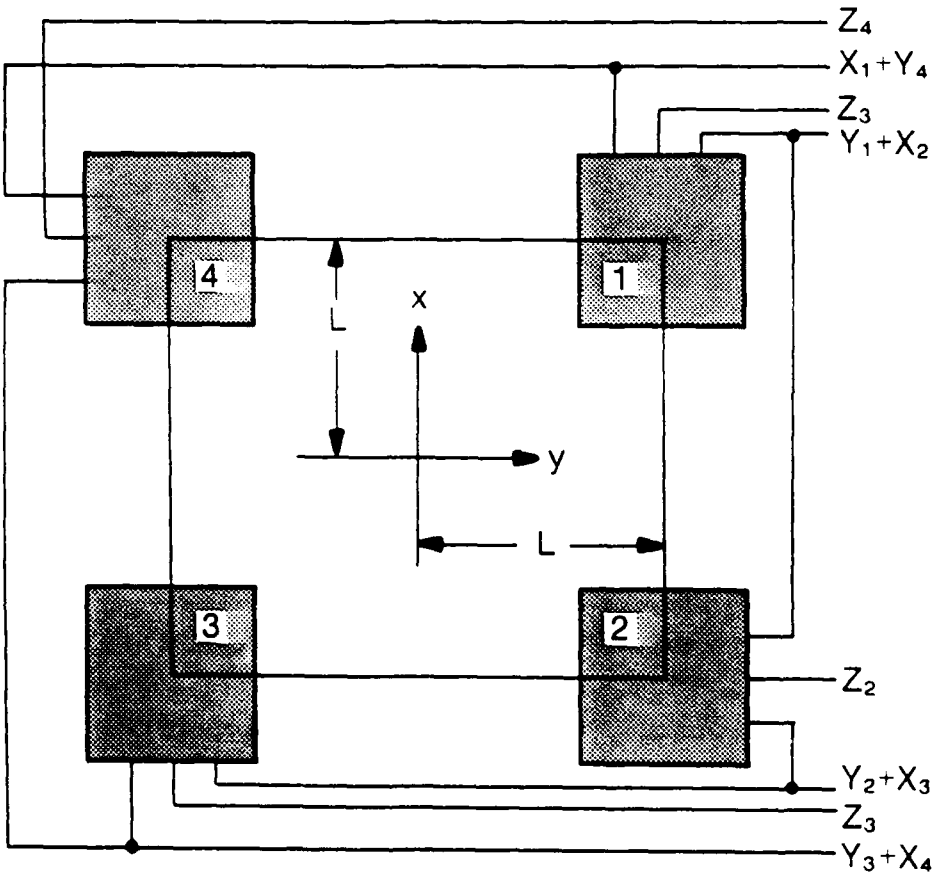

Note: z-axis is into page

Fig. 117 - Electrical Installation Scheme for Piezo-Electric Load Cells

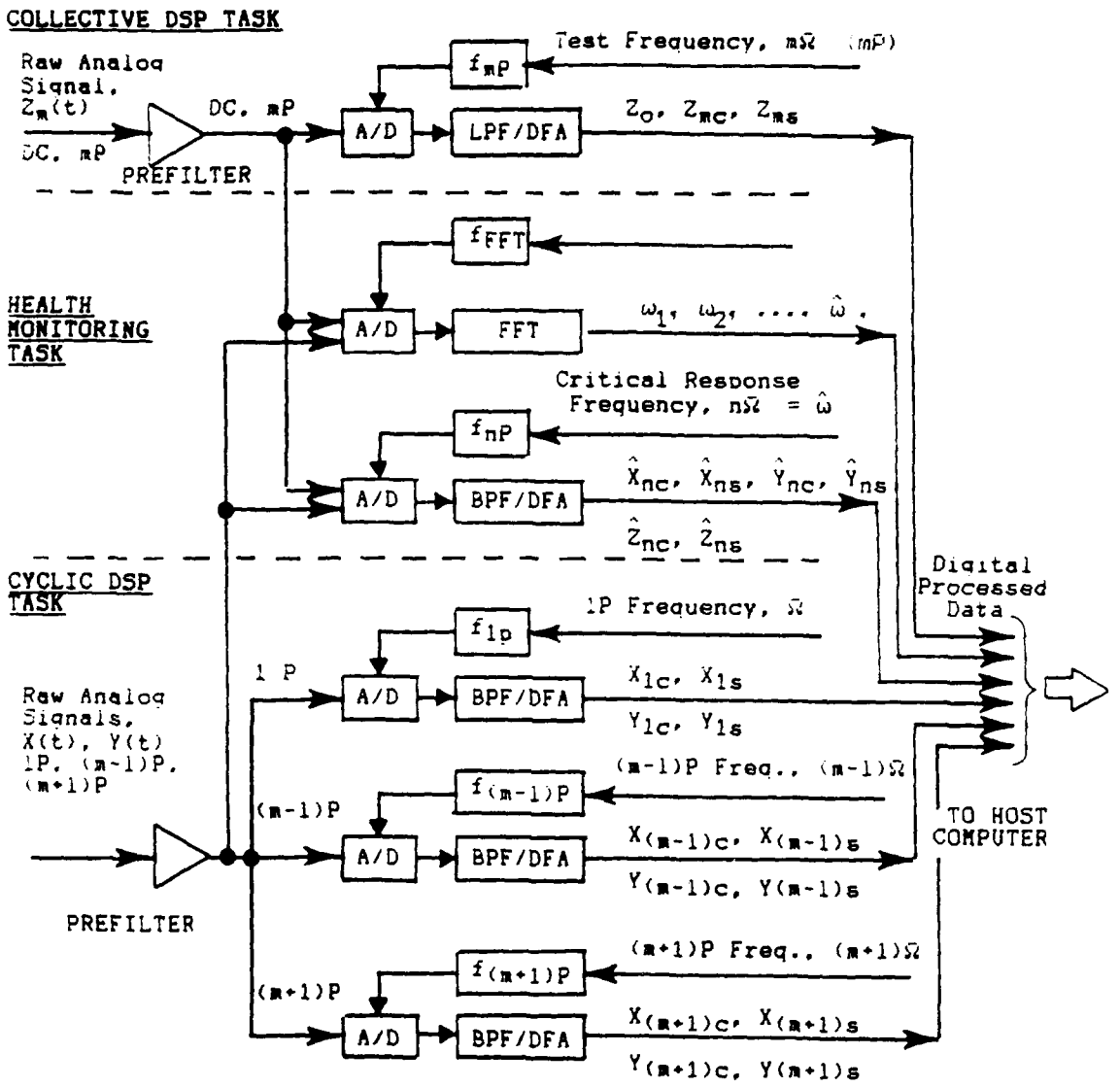

X(t), Y(t), Z(t) : REPRESENT LINEAR ACCELERATION, FORCE, ANGULAR ACCELERATION AND/OR MOMENT

m : TEST FREQUENCY FACTOR
Ω : ROTOR ROTATIONAL FREQUENCY
ω : FFT DETECTED RESPONSE FREQUENCY
f : SAMPLING RATE

FFT : FAST FOURIER TRANSFORM
DFA : DISCRETE FOURIER ANALYSIS
LPF : DIGITAL LOWPASS FILTER
BPF : DIGITAL BANDPASS FILTER

Fig. 118 - Schematic Representation of Required Functions for Preprocessor Subsystem

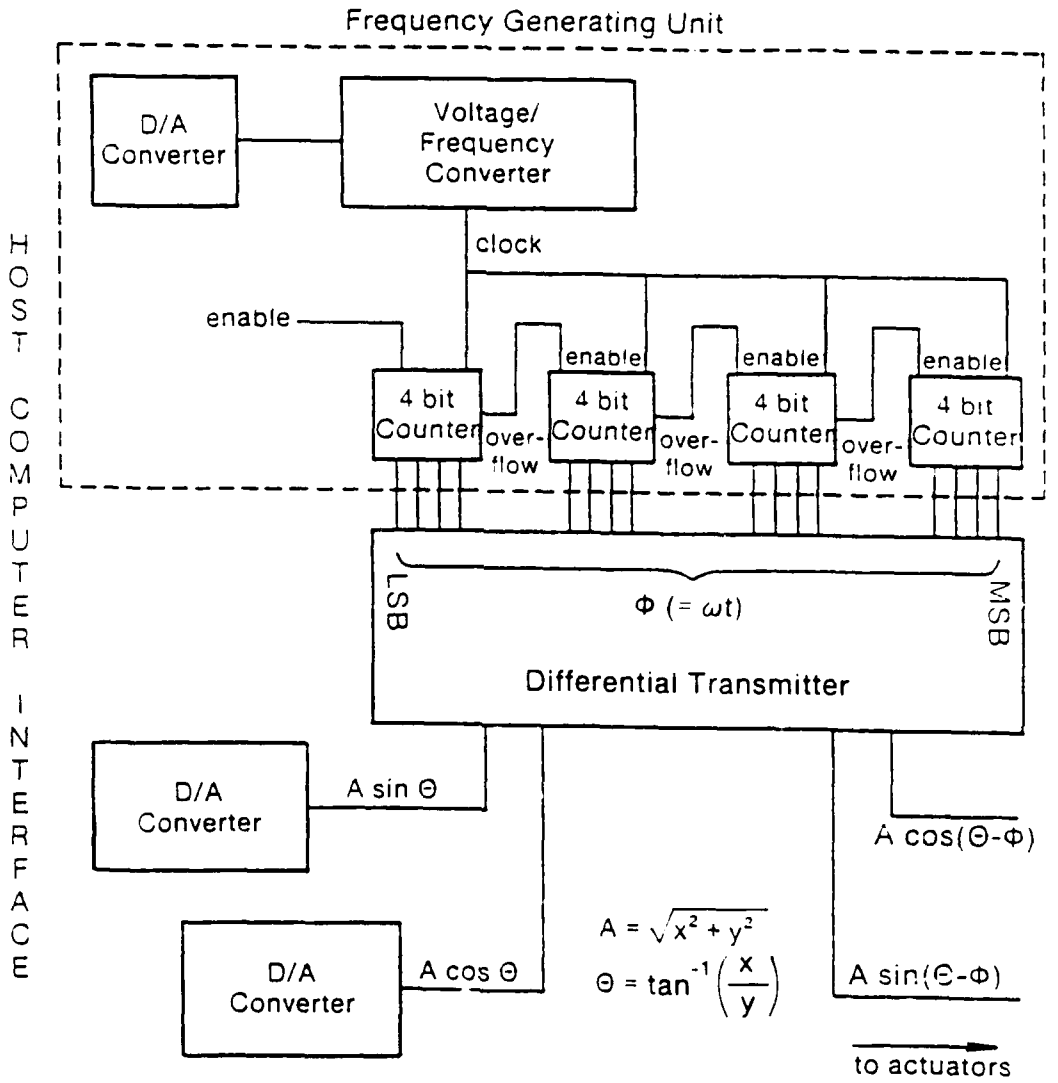

Fig. 119 - Implementation Details of the Postprocessor Precision Sine Wave Generator

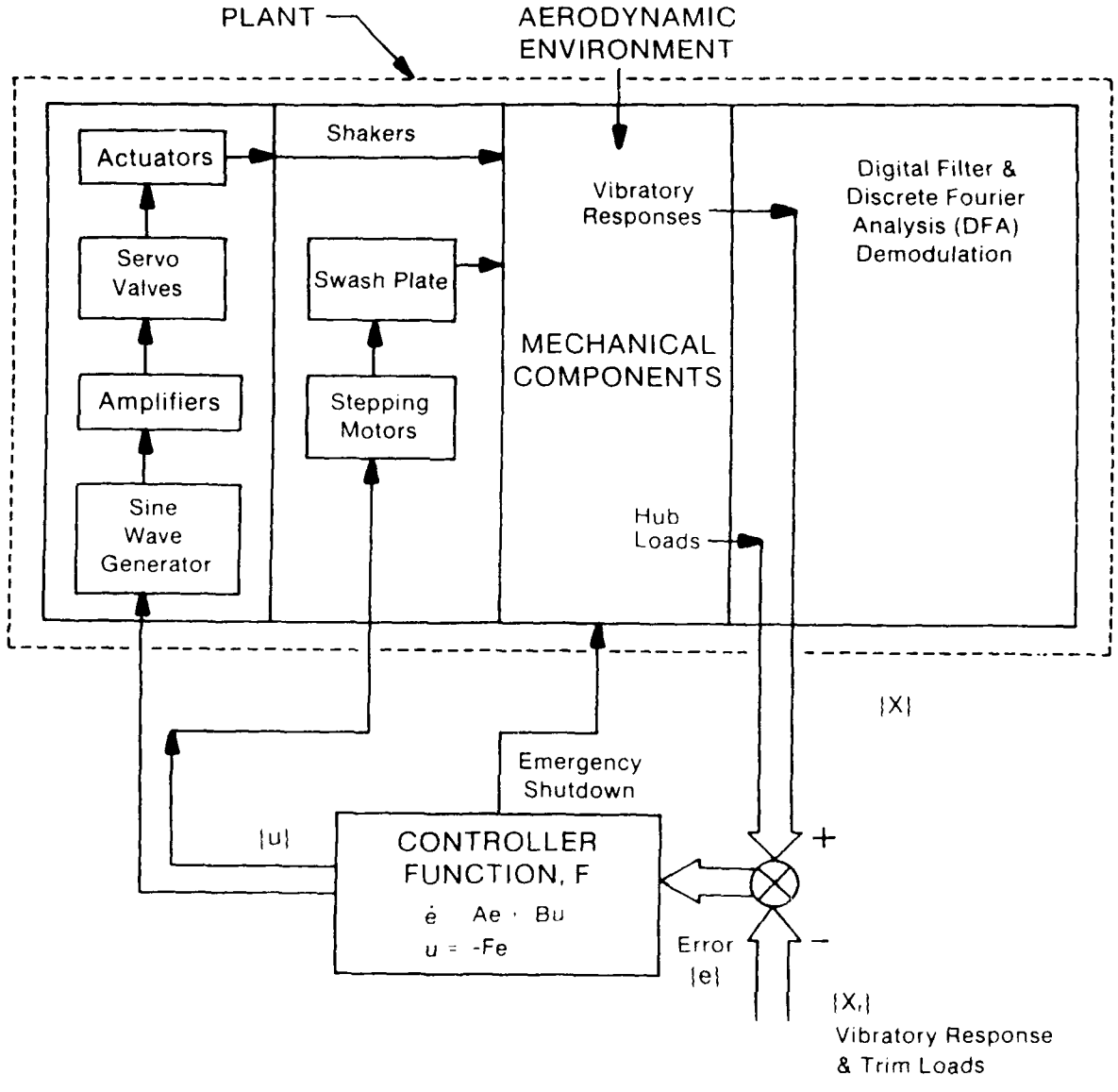

Fig. 120 - Schematic of the Planned Controller Operation

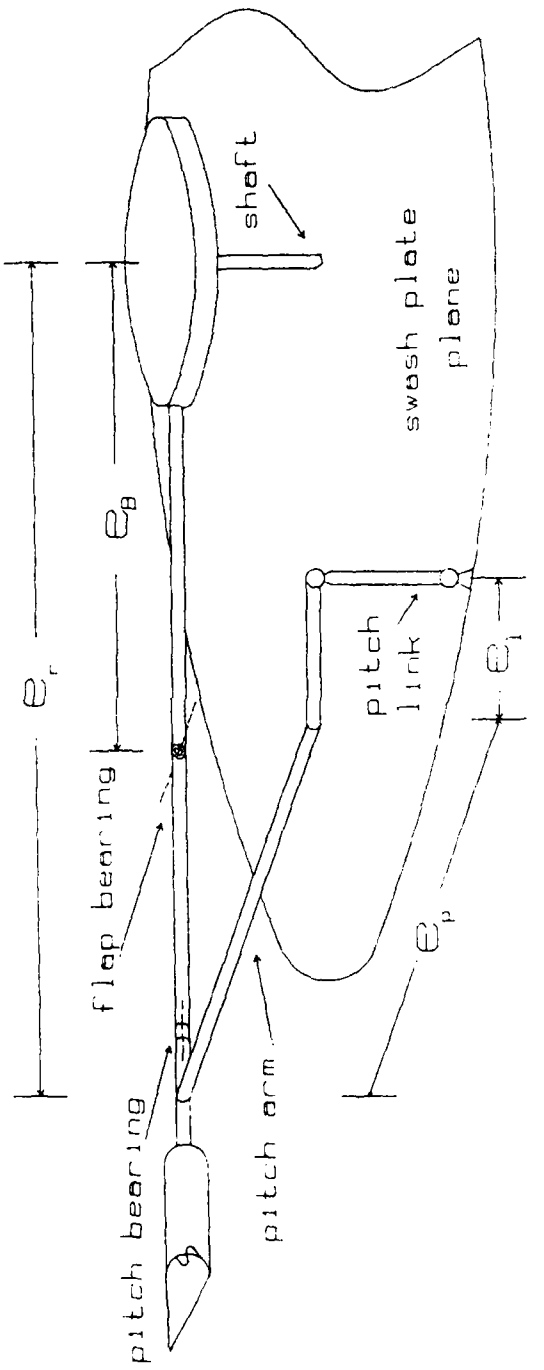

Fig. 121 - Reference Schematic of Upper Control Components

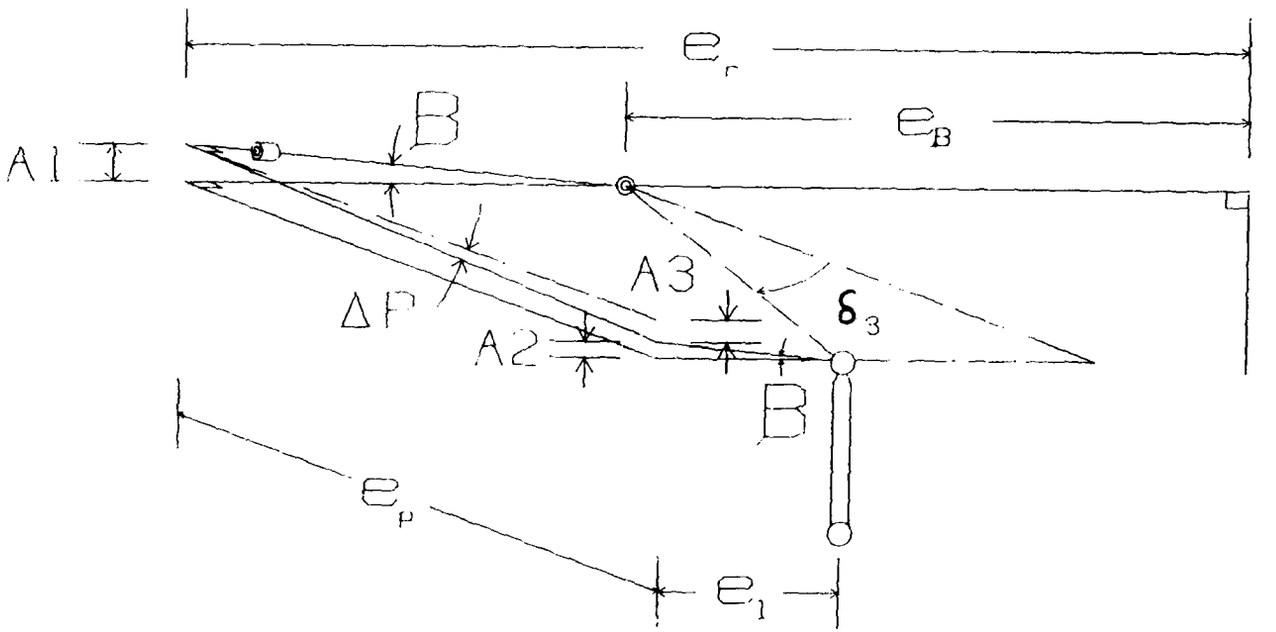

$$\Delta P = -\left[\frac{e_r - e_\beta - e_l}{e_p}\right]\beta$$

$$\triangleq -\tan \delta_3 \, \beta$$

Fig. 122 - Typical δ_3 Kinematic Coupling for Leading Edge Pitch Arm

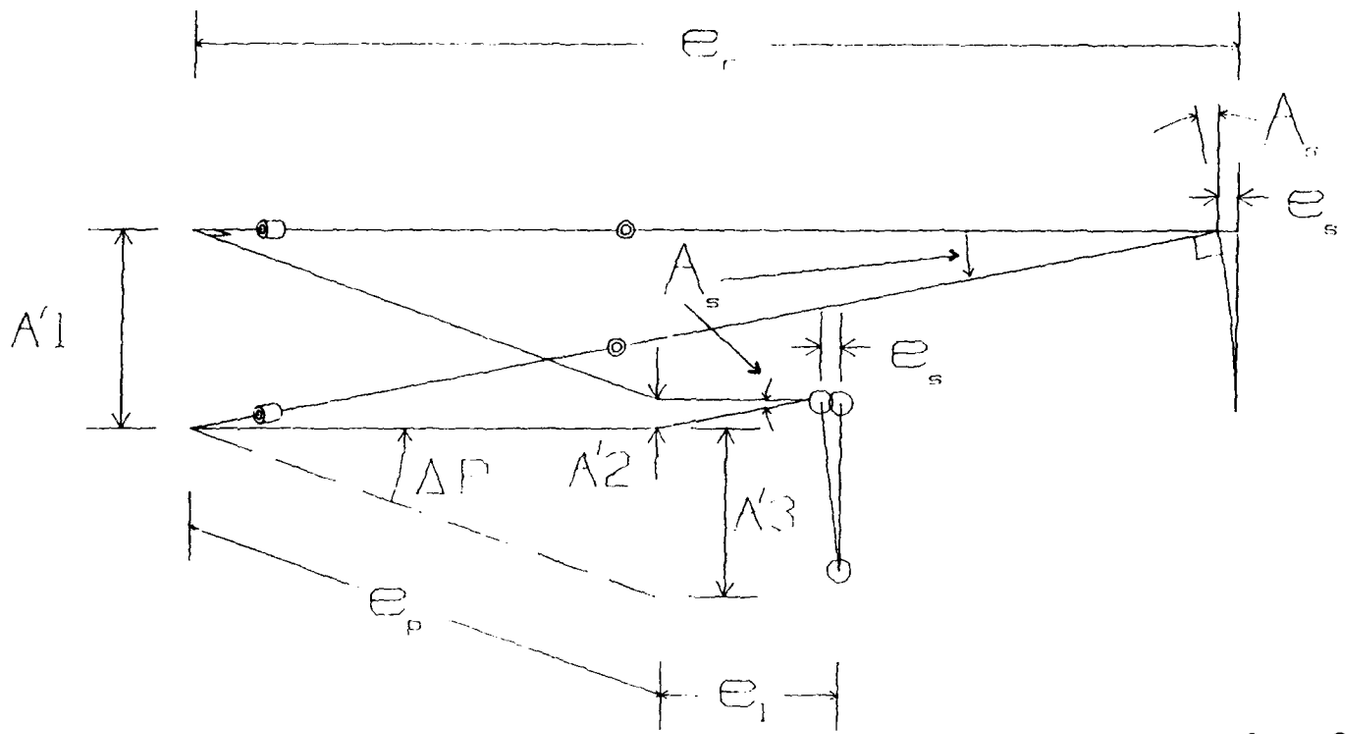

$$\Delta P = \left\{ \frac{e_r - e_l}{e_p} \right\} A_s$$

$$\triangleq \eta A_s$$

Fig. 123 - Kinematic Coupling of Shaft Deflection and Change in Pitch for Blade with Leading Edge Pitch Arm

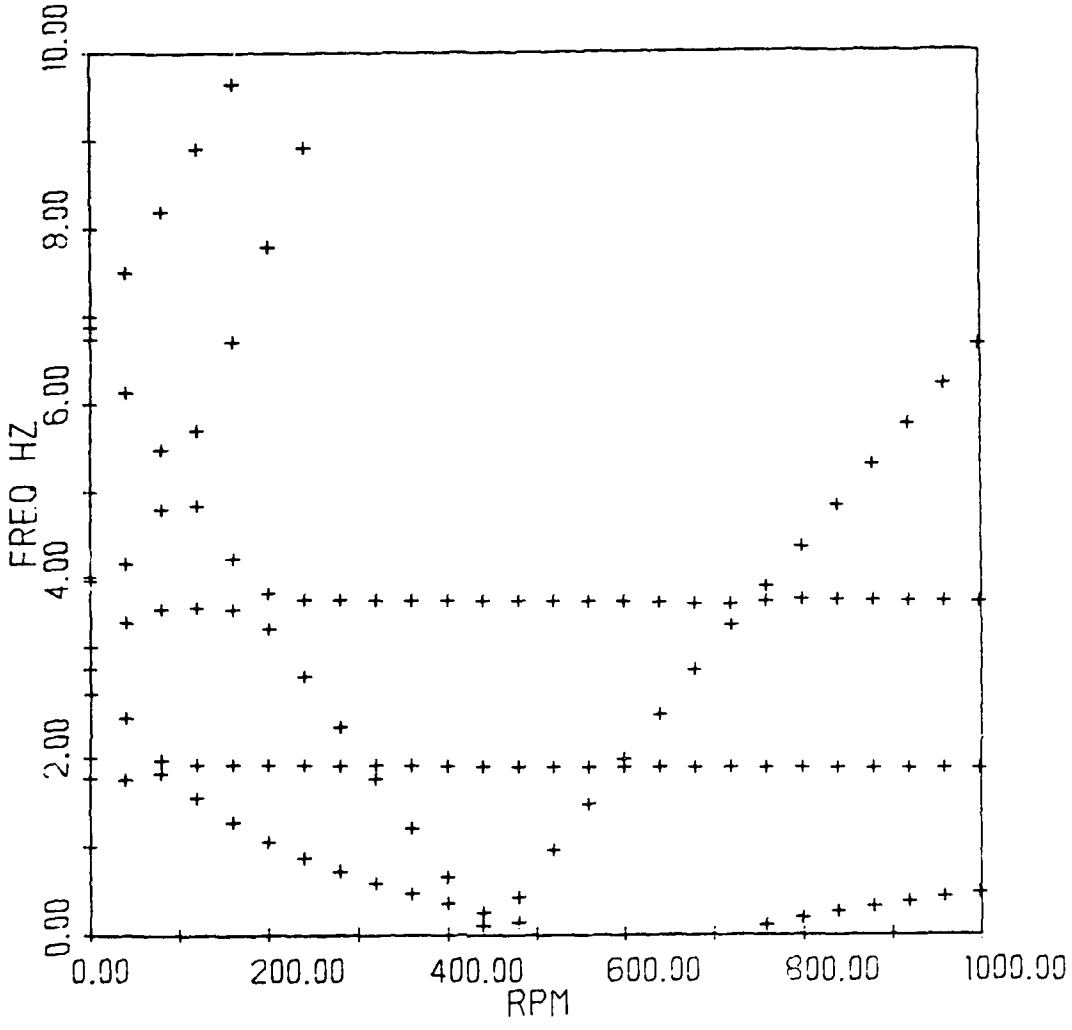

Fig. 124 - Rensselaer Calculation of the Coleman Frequency Diagram for Aeromechanical Instability of the Model of Ref. 90 (zero pitch-flap, pitch lag coupling and low structural damping - i.e., less than 0.5%)

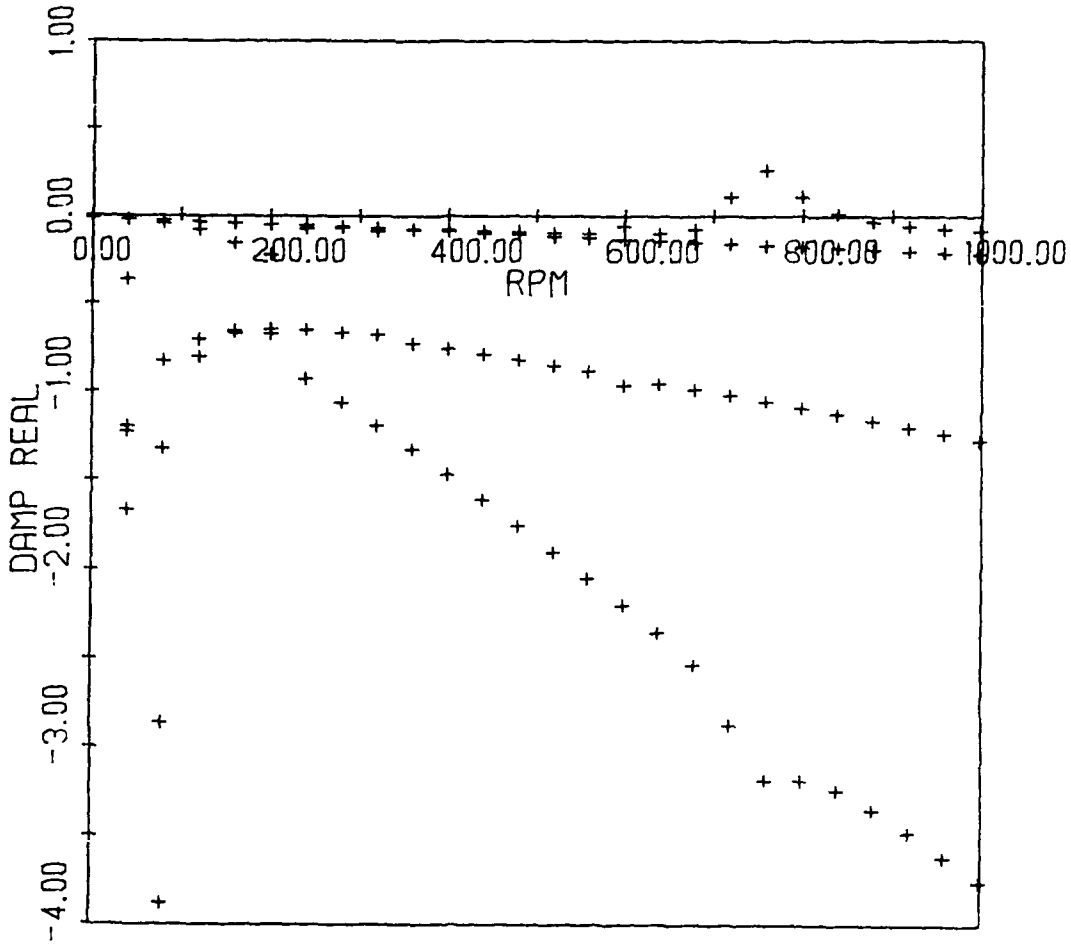

Fig. 125 - Rensselaer Calculation of the Real Part of the Eigenvalues for Aeromechanical Instability of the Model of Ref. 90 (zero pitch-flap, pitch lag coupling and low structural damping - i.e., less than 0.5%)

TABLE 16

Rotating Natural Frequency Predictions

(in Rads/Sec)

(Ω = 286 RPM)

Modal Types \ # of Modes Used	Rensselaer Results										B-V* Results
	1	2	3	4	5	6	7	8	9	10	
	35.765	34.847	34.512	34.490	34.303	34.244	34.195	34.195	34.195	34.195	34.293
		82.346	82.223	81.830	81.559	81.390	81.224	81.224	81.224	81.224	81.97
Coupled				122.937	122.776	122.769	122.758	122.758	122.758	122.758	123.258
Flap-Bending			164.005	168.792	168.762	168.633	168.566	168.566	168.566	168.566	173.130
Torsion					269.373	269.280	269.278	269.278	269.278	269.278	278.680
						368.775	339.639	339.639	339.639	339.639	335.526
							394.810	394.810	394.810	394.810	410.191
Uncoupled								22.556	22.395	22.296	22.462
Lag									148.462	148.462	148.986
Bending										422.863	424.626

*BOEING-VERTOL CALCULATION RESULTS
(C-60 Program; 20 Mass Stations)

TABLE 17

YUH - 61A Main Rotor Blade

(Boeing Vertol Uttas Rotor Blade)

- Flight Conditions

  Flight Speed = 150 Knots

  Thrust = 17000 lbs

  Rotor Speed = 286 RPM

- Rotor/Blade Geometry

  Radius = 24.5 ft

  Pretwist = -8°

  Chord = 23 inches

  Number of Blades = 4

  Blade Segmented into 20 Sections

6. Developing New National Resources

University facilities, with rare exceptions such as particle physics accelerators, are not impressive when compared to those of government laboratories or industry. University budgets generally are not such as to support the development, maintenance or even use of major research facilities. While some universities have quite respectable wind tunnels, for example, and conduct programs in them which are quite useful, few would argue that unique university capabilities of that kind exist, compared to NASA's resources or those in some of the largest aircraft companies. Cases do exist, however, in which research equipment is assembled in unusual ways or basic improvements made as part of research on a university campus. In those instances, the facility's development usually constitutes, in itself, fundamental research. That research is undertaken precisely because the capabilities which are sought do not exist and, in fact, the feasibility of the technique has not been proven beforehand. Such capabilities, when developed on a campus, are then not only useful in their application, but perhaps more importantly in demonstrating feasibility, so that other developers with greater resources can move ahead in that same area, using the university-developed technique.

Several undertakings of this kind were initiated as part of the RRTC's program. The rotor impedance test rig discussed in Section 5.d.(3) is clearly an instance of research attempting to establish the feasibility of an experimental technique where past efforts have been largely unsuccessful. Furthermore, the specific apparatus is being sized so as to be suitable for conducting tests in a number of government and industry wind tunnels, as has also been noted in that section of this report. Should the development of this facility be carried to a successful conclusion, there is every reason to believe that it will both be used itself in programs of advanced rotor dynamics and aeroelastic research and also lead to later generations of similar rotor testing apparatus being developed and built elsewhere.

A second facility with unusual capabilities is the sub-scale, super-critical shaft testing set-up described in Section 5.b.(1). When this apparatus is fully developed it will allow confirmation of the dynamic characteristics of advanced composite - and other - drive shaft systems at model scale. Through its use, increased confidence can be gained regarding the behavior of drive systems which may represent substantial departures from past practice, without the major expense of building and testing the full-scale system. It is expected that this facility will prove useful not only for Rensselaer's RTC program of optimized drive system research, but for others in this field as well.

The full-scale helicopter fuselage component shake testing facility developed under the subject contract and described in Section 5.b.(3) is a third example of what may be considered a new national resource. While certainly not unique, since fuselage shake testing is done routinely at all helicopter companies and several government laboratories, the RRTC capabilities have several unusual and desirable aspects. The "back-stop", for example, has been carefully designed to have high natural frequencies. Shake testing is often done with the entire fuselage soft-suspended, to simulate free flight. A relatively rigid back-stop has advantages, however, when

dealing with component structures, since "cantilever" attachment among components occurs when such components are assembled. Further, the RRTC facility is a dedicated facility, so that test initiation and execution can be done expeditiously. A helicopter fuselage shake-testing research project with sponsorship external to this university and beyond the ARO COE program has already been awarded and is being conducted in this facility. We anticipate that its use for the benefit of programs conducted on behalf of or even by off-campus organizations will continue to justify the investment of effort, funds and equipment expended to bring it to its current operational state.

In addition to the specific new facilities discussed above, substantial new and advanced equipment was acquired during the period of the subject contract. The existence of Rensselaer's RTC, designated as an ARO Center of Excellence and with its active program of advanced rotorcraft technology research helped convince sponsors of equipment grants and the Rensselaer Polytechnic Institute administration that such equipment would be put to good use and, therefore, justify the expenditures involved. Table 18 summarizes research equipment acquisitions applicable to rotorcraft technology over the contract period. The improved experimental capabilities represented in Table 18 should also be considered available, with the proper arrangements, to the wider rotorcraft research and development community.

TABLE 18

Major Equipment Acquisitions

Related to the Rensselaer RTC Program

(Page 1 of 2)

ITEM	COST	SOURCE
Four-Beam, Two-Color Laser Doppler Velocimeter System	90,000 39,445	DoD RPI
	129,445	Total
Load Cells, Pressure Transducers and Associated Amplifier	29,000	ARO Contract
Chemical Vapor Deposition Facility	125,250 41,750	DoD RPI
	167,000	Total
Three-Axis, Computer-Controlled Pilament Winding Machine	65,000 28,800 6,200	DoD RPI ARO Contract
	100,000	Total
44-Spindle Braider (Tubular Structures)	14,000	Faculty/Students*
Autoclave (Mini-Bonder)	30,000 10,000	ARO Contract Faculty/Students*
	40,000	Total
Computer-Controlled Mechanical Tester (Student Use)	50,000	INSTRON CO.
Servo Hydraulic Mechanical Tester (Fatigue: 10^{-8} Torr 2,000°f)	200,000	DARPA/ONR

TABLE 18 (Cont'd.)

(Page 2 of 2)

ITEM	COST	SOURCE
Servo Mechanical Tester for Ceramics (Ultra Precise Loading Rate; 1700°C in air)	150,000	DARPA/ONR
General Purpose Mechanical Tester	70,000	DARPA/ONR
Two-Shaker, Ten-Channel Structural Dynamic Excitation & Analysis System	150,000 50,000	DoD RPI
	200,000	Total
Supercritical, Scaled Shaft Dynamic Test Rig (Dynamometer, Transducers, Data Processing)	58,520	ARO Contract
Real Time Computer Feedback Control for Rotor Impedance Testing	112,768 37,589	DoD RPI
	150,357	Total
Symbolic Computation Laboratory Equipment	85,000 59,000 33,000 63,000	ARO/NASA NSF RPI Manufacturers
	240,000	Total

ARO - COE Contract	$ 123,720
RPI (Cost Matching)	230,584
Other (DoD, NSF, Manufacturers)	1,233,018
Grand Total	$1,598,322

* Through special arrangement with the DuPont Company

7. Technology Transfer

The research results generated on a campus wil' be considerably less likely to be useful if the faculty conducting that research are not continuously aware of the programs being undertaken and problems encountered by both researchers and practitioners in industry and government. Similarly, the most potentially useful university research result will lie fallow unless that same research, development, and user community beyond the campus is informed of the advances made on the campus in a timely manner. Both aspects call for technology transfer activities.

The former objectives have been furthered under the subject contract by faculty, staff and student attendance at professional society meetings and visits to government and industry sites, and by seminars on rotorcraft related subjects given on our campus on the part of members of government, industry and the faculties of other universities. Summaries of attendance at professional society meetings at national or international level, associated with Rensselaer RTC program objectives, is given in Table 19 and of RRTC visits to rotorcraft community organizations beyond the campus in Table 20. A similar summary of pertinent seminars given on our campus is contained in Table 21.

The latter objective, that is, transfer from the Rensselaer RTC to members of the rotorcraft technology community beyond the campus, is done in many ways. Among them are presentations made, papers published and presented, technical discussions held on and off campus, special courses offered for other than Rensselaer students (usually summer "short courses" as part of a continuing education program) individual faculty consulting and service on government advisory committess, and -- the most effective all-around measure -- placement of Rensselaer RTC graduates in rotorcraft technology organizations beyond the campus.

Table 22 lists papers published reporting results of the Rensselaer RTC program. This list includes those in refereed journals, proceedings of major professional society meetings, and the special Rensselaer RTC reports distributed to pertinent members of the rotorcraft community. Table 23 summarizes presentations made of similar results which have come about through the activities of the Center. Note that many of these presentations have been indicated in the listing of professional society meetings attended in Table 19. A listing of technical discussions held with members of the rotorcraft community from beyond the campus is given in Table 24, whether held off- or on-campus.

Special short courses were given both on campus and off, in two technology areas within which the Center has concentrated its research. These were "Advanced Composite Materials & Structures" and "Rotor Structural Dynamics, Aeroelasticity and Vibration". A summary of the dates of these offerings, where they took place, the faculty involved and some statistics of the attendees is given in Table 25.

On Sept. 10 and 11, 1987 an international workshop on composite materials & structures for rotorcraft was held on the RPI campus. This meeting was organized and run by the Center, with the assistance of the steering committee shown in Table 26. General Chairman for the meeting was Dr. R. J. Diefendorf. Attendance was by

invitation only, and 60 participants attended representing 22 companies, 19 universities, 10 different U.S. government agencies, and 6 different countries. All of the major U.S. helicopter manufacturers were represented. The success of this workshop was such that the majority of participants recommended that it be repeated every few years.

Placement of graduates from the inception of the Rensselaer Rotorcraft Technology Center program to the end date of the current contract are as shown in Table 27.

Table 19

Summary of Pertinent Professional Meetings Attended

Rensselaer RTC

Date	Meeting	RRTC Personnel
2/2-4/83	NASA Workshop on PEM Modelling of of Rotorcraft Structure - Langley Research Center	M. Shephard*
3/30-4/1/8	AHS Specialists Meeting - Composites Philadelphia, Pa.	J. Diefendorf D. Goetschel R. Loewy* V. Paedelt
4/11-14/83	56th Structures & Materials Panel of AGARD, Specialists Meetings, London, England	R. Loewy
5/9/83	39th AHS Annual Forum, St. Louis	J. Diefendorf R. Loewy H. Nagamatsu V. Paedelt
6/6-9/83	ASTM/NASA International Meeting on Composites - Langley Research Center	J. Diefendorf
2/23-25/84	Industry, Government Conference on Uses of Kevlar in Aircraft, St. Thomas, V.I.	J. Diefendorf*
3/5-7/84	AIAA 13th Aerodynamic Testing Conference, San Diego, Ca.	R. Duffy*
3/20-25/84	Rotor Flight Experiments Workshop NASA Ames Research Center, Moffett Field, Ca.	R. Bielawa
4/2-6/84	58th Mtg of the Structures & Materials Panel of AGARD, Siena, Italy	R. Loewy*

* Session Chairman or Speaker

Date	Meeting	RRTC Personnel
5/16-18/84	40th AHS Annual Forum Crystal City, Va.	R. Bielawa J. Diefendorf R. Loewy* H. Nagamatsu V. Paedelt S. Winckler** R. Zinner**
6/24-28/84	92nd Annual Conference American Society for Engineering Education Salt Lake City, Utah	R. Loewy*
7/28-8/4/84	Annual Meeting, Experimental Aircraft Association, Oshkosh, Wi.	J. Diefendorf*
8/13-16/84	NASA Composite Materials & Structures Review - A/C Energy Efficiency Program, Seattle, Washington.	R. Loewy
8/28-31/84	10th European Rotorcraft Forum, The Hague, Netherlands	R. Bielawa
9/24-28/84	CAMP '84 - Computer Graphics for Management and Productivity, Berlin, East Germany	M. Shephard
10/16-18/84	AHS Midwest Region Helicopter Patigue Specialist's Mtg, St. Louis	E. Krempl
10/22-25/84	NASA Symposium on Advances and Trends in Structures and Dynamics, Washington, D.C.	M. Shephard
10/29-31/84	Workshop on Blade Vortex Interaction NASA Ames Research Center, Moffett Field, Ca.	R. Mayle*
11/7-9/84	2nd Decennial Specialists Mtg on Rotorcraft Dynamics, Moffett Field, Ca.	R. Loewy R. Bielawa
1/14-17/85	23rd AIAA Aerospace Sciences Mtg, Reno, NV	H. Nagamatsu*

* Session Chairman or Speaker
** Student

Date	Meeting	RRTC Personnel
2/19-21/85	1st ARO International Conf. on Rotorcraft Basic Research, Research Triangle Park, N.C.	R. Bielawa M. Darlow R. Loewy* A. Rosen S. Winckler***
4/15-17/85	26th AIAA Structures, Struc. Dyn. & Materials Conf., Orlando, FL	M. Darlow* O. Bauchau
4/21-26/85	60th AGARD Structures & Materials Panel Mtg, San Antonio, TX	R. Loewy
5/3/85	8th International UPEM Symposium, Storrs, CT	M. Shephard*
5/6-9/85	AGARD Unsteady Aerodynamics Workshop, Göttingen, W. Germany	R. Mayle
5/13-16/85	3rd Army Conf. on Applied Math & Computing, Atlanta, GA	M. Sutcu**
5/14-17/85	41st AHS Annual Forum, Ft. Worth, TX	R. Bielawa J. Diefendorf R. Loewy V. Paedelt D. Radford** S. Winckler***
7/30-8/1/85	International Conference on Composite Materials V, San Diego, CA.	J. Diefendorf
9/9-12/85	NSF Workshop on Composite Mfg., Gaithersburg, MD.	J. Diefendorf
9/10-13/85	ASME Vibrations Conference, Cincinnati, OH.	M. Darlow
10/1-3/85	2nd Meeting on Design Analysis Methods for Vibrations (DAMVIBS) NASA Langley	R. Bielawa

* Session Chairman or Speaker
** Student
*** ARO Distinguished Fellow

Date	Meeting	RRTC Personnel
10/21-25/85	SAMPE National Technical Mtg., Kiamesha Lake, NY	R. Kraus*** D. Radford** S. Winckler***
11/17-22/85	ASME Winter Annual Mtg, Miami, FL	E. Degen**
11/6-8/85	AHS/NAI International Mtg on Theoretical Basis of Helicopter Technology, Nanjing, P.R.C.	R. Loewy*
12/4-5/85	ARO & Georgia Tech. Workshop on Rotor Dynamics, Atlanta, GA	R. Bielawa* R. Loewy* O. Bauchau*
12/16-20/85	2nd Int'l Conf. on Biaxial/Multiaxial Fatigue, Sheffield, United Kingdom	E. Krempl*
1/6-9/86	AIAA Aerospace Science Mtg, Reno, NV	H. Nagamatsu*
4/8/86	3rd Annual Materials Technology Center Conference, Carbondale, IL	J. Diefendorf*
4/16/86	CIEM Symposium, U. of Tenn.	M. Shephard*
4/21-23/86	Government/Industry Working Group for 2GCHAS Program Mtg, NASA Ames Res. Center, Moffett Field, CA	R. Bielawa
5/13-14/86	ASM Symposium on Advanced Composite Materials, Schenectady, NY	M. Darlow
5/19-21/86	27th Annual Structures, Dynamics & Materials Conference, San Antonio, TX	R. Loewy*
6/2-4/86	AIAA/ASME 4th Joint Thermophysics & Heat Transfer Conf, Boston, MA.	H. Nagamatsu*

* Session Chairman or Speaker
** Student
*** ARO Distinguished Fellow

Date	Meeting	RRTC Personnel
6/2-5/86	42nd Annual Forum, Washington, DC	R. Bielawa J. Gordis** R. Halvorson*** C. Jaran*** R. Kraus*** R. Loewy R. Martin*** V. Paedelt P. Renzoni** J. Straus*** A. Trainer** S. Winckler***
7/9-10/86	Int'l. Conf. on Reliability of Methods for Engineering Analysis, Swansee, U.K.	M. Shephard
9/9-11/86	NASA Technical Summary Review NASA AMes Res. Ctr.	R. Bielawa
9/22-25/86	Twelfth European Rotorcraft Forum, Garmisch-Partenkirchen, FRG	R. Bielawa*
9/22-25/86	First World Congress on Computational Mechanics, Austin, Texas	M. Shephard
10/21-22/86	AIAA/AHS/ASEE Design Meeting, Dayton, Ohio	R. Loewy*
12/1-4/86	DAMVIBS Workshop at NASA Langley Res. Ctr., Hampton, VA.	R. Bielawa*
1/12-15/87	AIAA Aerospace Sciences Conf.,	H. Nagamatsu* T. Mitty** G. Nyberg**
3/10-12/87	MSC World Users Conference, Los Angeles, CA	M. Shephard*
3/17-19/87	NASA/Army Rotorcraft Technology Mtg., Ames Res. Ctr., CA.	R. Loewy

* Session Chairman or Speaker
** Student
*** ARO Distinguished Fellow

Date	Meeting	RRTC Personnel
4/28-5/1/87	The Mathematics of Finite Elements and Applications, West London, UK	M. Shephard
5/18-21/87	43rd AHS Annual Forum, St. Louis, MO	R. Bielawa M. Darlow* J. Diefendorf R. Loewy V. Paedelt S. Winckler
4/6-7/87	28th Annual SDM Conf., Monterey, CA.	R. Loewy
6/8-10/87	AIAA Fluid Dynamics and Plasma Conf., Honolulu, Hawaii	H. Nagamatsu*
11/18-20/87	2nd Technical Workshop on Dynamics and Aeroelastic Stability Modeling of Rotorcraft Systems, Boca Raton, FL	R. Loewy* O. Bauchau* M. Crespo da Silva*
12/7/87	Composites in Manufacturing Meeting Society of Manufacturing Eng's, Long Beach, CA.	R. Loewy

* Session Chairman or Speaker

Table 20

Summary of Visits to Rotorcraft Technology Organizations

Rensselaer RTC

Date	Purpose of Visit	Place	RRTC Personnel
1/27/83	General Familiarization Plant Tour	Sikorsky Div., U.T.C., Stratford, CT.	J. Diefendorf R. Duffy D. Goetschel 18 AHS Student Members
1/28/83	Discussion on Engineering Mechanics and Solid Modelling	General Motors Res. Labs, Warren, MI.	M. Shephard
5/24-26/83	Workshop on Tough Composites	NASA Langley Res. Ctr.	J. Diefendorf
6/6/83	Discussion of Composite "Scissors"	Sikorsky Div., U.T.C., Stratford, CT.	D. Goetschel M. Niederer*
6/20/83	Discussion of Composite Manufacturing Problems	Sikorsky Div., U.T.C., Stratford, CT.	M. Shephard M. Yerry*
7/29/83	Progress Report Presentation of I.T. R. Subcontract	Boeing-Vertol	R. Loewy
8/18/83	Seminar on Passive Drag Control at Transonic Mach Numbers	U.S. Army RTL, Ames Res. Ctr.	H. Nagamatsu
8/19/83	Discuss Transonic Rotor Airfoil Phenomena	U.S. Army RTL, Ames Res. Ctr.	H. Nagamatsu
8/29-31/83	"Peer Review" of Rotor Aeroelasticity Program	NASA Langley Res. Ctr.	R. Loewy (with R. Huston, NASA J. Drees, Bell R. Ormiston, AVRADCOM)

* Student

Date	Purpose of Visit	Place	RRTC Personnel
9/26/83	Review of ARO-C.O.E.'s in Rotorcraft Technology	U of Md	R. Loewy (with A. Gessow, U of Md., R. Gray, GIT)
11/16/83	Review of ARO-C.O.E.'s in Rotorcraft Technology	G.I.T.	R. Loewy (with R. Gray, GIT)
3/13-15/84	Review of IRAD	Hughes Helicopter Phoenix, Az	J. Diefendorf
3/26/84	Plant Trip & Technical Discussion	Agusta Helicopter Group, Malpensa, Italy	R. Loewy
5/15/84	Review of JVX Rotor Aeroelastic Stability	Bell Helicopter, Ft. Worth, TX	R. Loewy
7/30/84	Discussion of Impedance Test Rig Project	Boeing-Vertol Essington, PA.	R. Bielawa
7/31/84	To Discuss D-400 Development	NASA Langley USA RTL	R. Bielawa
8/9/84	Discussion of Research on the Heavy Lift Research Vehicle (HLH)	NASA Hq Washington, DC	R. Loewy
8/28/84	Gave Seminar on Composite Materials	Lord Corp., Erie, PA	J. Diefendorf
9/8/84	28th Annual AHS Northeast Regional Clambake	Wallingford, CT	10 Student members of the RPI AHS Chapter
9/14/84	Discussion of Hybrid LTA - Rotorcraft Heavy Lift Systems	DARPA Roslin, VA	R. Loewy
3/6/85	Technical Briefing on Rotor Impedance Test Rig	U.T.R.C. E. Hartford, CT	R. Bielawa S. Garing* K. Hsueh* P. Singh*

* Student

Date	Purpose of Visit	Place	RRTC Personnel
3/13/85	Plant Visit	Sikorsky Aircraft Stratford, CT	V. Paedelt S. Winckler*
4/23/85	Review; Research on NDE for Composite and Metal Rotor Components	Southwest Res. Institute, San Antonio, TX	R. Loewy
5/8/85	Tour of Blade Vortex Interaction Facility	Max Planck Inst. Göttingen, FRG	R. Mayle
5/14/85	Plant Visit	Bell Helicopter Ft. Worth, TX	J. Diefendorf V. Paedelt D. Radford* S. Winckler*
6/5/85	Discussion of On-Site Special courses on Composite Materials & Structures	Sikorsky Aircraft Stratford, CT	O. Bauchau J. Diefendorf
7/29/85	Discussion of Passive Transonic Drag Reduction & Aero-acoustics of Helicopter Rotors	US Army Aero-Mechanics Lab. NASA Ames	H. Nagamatsu
8/22/85	Discussion of Research & Long Range Planning	Research Triangle Park, Durham, NC	R. Loewy
11/21/85	Review of Rotorcraft Research Program	US Army ATL Ft. Eustis, VA	R. Loewy
12/10-11/85	Review of V-22 Osprey Program	Bell Helicopter Ft. Worth, TX	R. Loewy
1/10/86	Discussion of Shake Test Facility	Sikorsky Div., U.T.R.C., Stratford, CT.	O. Bauchau R. Bielawa J. Gordis*
1/30/86	Tour of Composite Blade Mfg. Facility	Kaman Aerospace, Bloomfield, CT.	R. Loewy

* Student

Date	Purpose of Visit	Place	RRTC Personnel
3/10/86	Discussion of Passive Drag Reduction Concept for Helicopter Rotor-Tip Airfoils	Boeing-Vertol Essington, PA.	H. Nagamatsu
3/14/86	Discussed Filament Winding of Complex Parts	General Motors, Detroit, MI.	J. Diefendorf
3/18/86	Reviewed Program of The Center for Composite Materials	U. Of Delaware, Newark DE.	R. Loewy
4/30/86	Discussed Filament Winding of Complex Parts	General Motors, Detroit, MI.	J. Diefendorf
5/29/86	Facilities Tour and Technical Discussion	Kaman Aerospace, Bloomfield, CT.	M. Darlow R. Kraus*
6/6/86	Discussion of RTC's Shake Test & Rotor Impedance Test Facilities	NASA/US Army Lab's, Langley Res. Ctr.	R. Bielawa
6/6/86	Discussion of Direction of RPI's RTC	Army Research Office, Durham, NC.	R. Loewy
7/15-86	Discussion of Blackhawk Helicopter Rotor test Plans	NASA Ames Res. Ctr	R. Bielawa R. Loewy
7/16/86	Discussion of FEM Rotor Analysis Programs	USAAR&T Ames Res. Ctr.	O. Bauchau
8/5/86	Facilities Tour and Technology Developments Discussion	McDonnell-Douglas Helicopter Co., Mesa, AZ.	R. Loewy
10/30/86	Discussion of Rotor Aerodynamics	Boeing-Vertol Essington, PA.	R. Mayle
11/17/86	Presentation on COE's to Director, Chief Scientist, Dr. R. Singleton and Dr.G. Anderson	Army Research Office, Durham, NC	R. Loewy (with A. Gessow, U Md, D. Schrage, G.I.T.

* Student

Date	Purpose of Visit	Place	RRTC Personnel
1/12/87	Discussion of V-22 Tilt Aeroelastic Problems	U.S. Navy Air Systems Command, Crystal City, VA.	R. Loewy
1/29/87	Discussion of Modeling and Analysis Requirements	Hughes Aircraft, Los Angeles, CA.	M. Shephard
4/3/87	Discussion of Rotor Dynamics and Wind Tunnel Testing	U.S. Army RTL, Ames Res. Ctr.	R. Loewy
4/10/87	Discussion of Research in Rotorcraft Technology	U.S. Army Research Office, Durham, NC	R. Loewy
5/19/87	Gave Seminar "Finite Element Modeling of Composite Helicopter Blades"	U.T.R.C., Hartford, CT	O. Bauchau
6/9/87	Discussion of Status of RPI Rotorcraft Research	NASA Langley Res. Ctr.	R. Bielawa K. Hsueh* S. Winckler

* Student

Table 21

Seminars By "Outside" Speakers on Rotorcraft Technology Topics

Given at the

Rensselaer RTC

Date	Subject	Speaker
12/8/82	Formulation and Solution of Rotary-Wing Aeroelastic Stability & Response Problems	Prof. Peretz Friedmann UCLA
3/1/83	Rotor Aeromechanics	Dr. Chee Tung Aeromechanics Lab. AVRADCOM
3/28/83	Recent Developments in Rotorcraft Aerodynamic Technology	Dr. Michael Summa Sr. Research Scientist Analytical Methods, Inc.
3/30/83	The Helicopter: Radio Controlled vs Pull Scale (Jointly with RPI Chapter of the AHS)	Mr. John Burkam Engineering Specialist Boeing-Vertol Company
4/5/83	"daVinci's VTOL Comes of Age" (as part of "Rensselaer Salutes 200 Years of Manned Flight")	Mr. Robert Zincone Sr. Vice President Sikorsky Div., U.T.C.
4/19/83	"A Dynamic Inflow Model for Rotorcraft Flight Dynamics"	Dr. Gopal Gaonkar Visit'g Prof., Wash. U.
6/29/83	Consideration of Spanwise-Variable Elastic Axis Offset in Aeroelastic Modelling of Rotor Blades	Dr. Richard Bielawa Supervisor, Dynamics Group, United Technologies Research Ctr.
7/20/83	Nonlinear Effects in Rotor Blade Dynamics	Dr. Dewey H. Hodges Leader, Theoretical Group, Aeromechanics Lab., Ames Res. Ctr. (AVRADCOM)

Date	Subject	Speaker
10/6/83	Experiments in Rotorcraft Stability	Mr. William G. Bousman Research Scientist, Aeromechanics Lab, Ames Res. Ctr.
11/16/83	Use of Composites in the Helicopter Industry	Dr. Gary Cheatham Sikorsky Aircraft Div., U.T.C.
11/29/83	Perturbation Methods and a Numerical/ Perturbation Analysis of the Flap-Lead Lag Response of a Rotor Blade in Forward Flight	Dr. M. Crespo da Silva Professor of Aerospace Engineering and Applied Mechanics, University of Cincinnati
2/20/84	Overview of U.S. Rotorcraft Development (in general), at Bell Helicopter (in particular), and the Status of Tilt Rotors	Dr. Jing G. Yen Manager, Flight Tech., Bell Helicopter Textron
3/5/84	Computer Aided Engineering Applications at Hughes Helicopter	Mr. Grant Parker Chief of Dynamics Finite Element Analysis Hughes Helicopter
4/2/84	Dynamics of Rotor-Bearing Systems	Dr. K. N. Gupta Indian Inst. of Techn.
4/26/84	6th Annual Paul E. Hemke Lecture: A Glance at Soviet vs Western Schools of Helicopter Design	Dr. W. Z. Stepniewski President, International Technical Associates, Ltd.
8/8/84	Ductile Fracture	Prof. J. W. Hancock, University of Glascow
9/11/84	An Implicit Time Integration Scheme for Inelastic Constitutive Equations with Internal State Variables	Prof. F. G. Kollmann, Technische Hochschule Darmstadt
10/9/84	Rotor Testing and Unsteady Aerodynamics	Prof. F. D. Smetana, US Army Research Office
10/16/84	Developments at Hughes Helicopters	Mr. F. K. Straub, Hughes Helicopters

Date	Subject	Speaker
10/31/84	Dynamic Response of Mechanical Systems by a Weak Hamiltonian Formulation	Prof. Marco Borri, Politecnico, Di Milano, Italy
11/15/84	Reducing Helicopter Vibration through Rotor Blade Design	Mr. F. Tarzanin, Boeing Vertol
11/15/84	NASA Ames Research Center & The Army Aeromechanics Lab.	Mr. M. Lewis, Army Aeromechanics Lab, NASA Ames
2/12/85	Advanced Composite Applications at McDonnell Aircraft	Mr. H. Siegel, Director Product Engrg, McDonnell Aircraft Company
2/18/85	Design of Composite Structures	Mr. D. S. Adams Hercules Aerospace
2/22/85	Unsteady Aerodynamics and Composite Structures	Profs. U. Leiss & S. Wagner, University of the Federal Armed Forces, Munich, FRG
2/25-26/85	R & D Activities at Hughes Helicopters	Messrs R. Prouty & J. Schibler, Hughes Helicopters, Culver City, CA & Mesa, AZ
3/26/85	Interlaminar Fracture Toughness of Composite Structures	Prof. L. Rehfield, Georgia Institute of Technology
4/9/85	A Viewpoint on Aerospace Engineering (7th Annual Paul E. Hemke Lecture)	Mr. R. H. Widmer General Dynamics Corp. St. Louis, MO
4/17/85	Damage Zone Modeling of Notched Composites Under Tension	Prof. J. Bäcklund, Royal Institute of Tech. Stockholm, Sweden
10/8/85	"The Overstress Concept and Its Application to Creep-Fatigue Analysis"	Prof. Y. Asada, University of Tokyo
10/29/85	"Large Deflection Analysis of Elasto-Plastic Structures"	Dr. M. Bieniek, Columbia University

Date	Subject	Speaker
11/11/85	"Using Wind Tunnels to Help Solve Dynamic Problems of the V-22 Tilt Rotor"	Mr. R. Smith Boeing-Vertol
3/8/86	Some Size Effects in the Mechanical Behavior of Materials	Prof. I. Finnie University of Cal. Berkeley, CA
4/1/86	New Approaches to Aerodynamic Modeling of Helicopter Rotors	Mr. T. R. Quackenbush Princeton Univ.
4/8/86	Computational Fluid Dynamics in Engineering & Education	Prof. D. B. Spalding, F.R.S., Imperial College, London, U.K.
4/9/86	Optimum Twist of Tilt Rotor Aircraft Propellers	Messrs. H. Alexander & H. Bishop, Boeing-Vertol
4/15/86	Fluid Flow & Heat Transfer in Materials Processing	Prof. M. M. Chen, Univ. of Illinois, Urbana-Champaign
11/11/86	"Great Mysteries of Helicopter Aerodynamics"	Mr. R. W. Prouty McDonnell Douglas Helicopter Co.
3/25/87	"Statistical Linearization in Structural Dynamics"	Prof. Pol. Spanos, Dept. of Civil Eng. Rice University, Houston, TX
4/15/87	Advanced Programs in Rotorcraft Propulsion Developments	Messrs. J. Acurio, H. Bill and D. Brewe, U.S. Army Propulsion Lab, Lewis Res. Center, Cleveland, Ohio
4/30/87	Helicopter Weapon Gust Effects Modeling and Testing	Mr. B. Webster, Kaman AviDyne, Burlington, MA

Table 22

Rotorcraft Technology Papers Published During the Contract Period

Rensselaer RTC

"Shear Fatigue Properties of Tapered Composite Laminates under Axial Loading", S. Hakim, W. Kim and R. Loewy, RPI RTC Report No. M-84-1, February 15, 1984.

"Nonlinear Finite Element Analysis of an ITR Flexure Under Limit Loading", M. H. Ackroyd, R. G. Loewy, M. S. Shephard and M. E. Yerry, RPI RTC Report No. S-84-1, March 5, 1984.

"A Uniaxial Fatigue Study of Near-Unidirectional Composite Tubes for Negative R-Ratios", E. Krempl and D. M. Elzey, RPI RTC Report No. M-84-2, April 15, 1984.

"The Army Research Office Center of Excellence in Rotorcraft Technology at Rensselaer", R. Loewy, Proceedings of the 92nd Annual ASEE Conference, Salt Lake City, Utah, June 24-26, 1984.

"An Improved Technique for Testing Helicopter Rotor-Pylon Aeromechanical Stability Using Measured Rotor Dynamic Impedance Characteristics", R. Bielawa, Proceedings of the 10th European Rotorcraft Forum, August 28-31, 1984.

"Biaxial Fatigue Properties of Thin-Walled Composite Tubes", E. Krempl, R. Loewy and D. Elzey, Proceedings of the American Helicopter Society Midwest Region Helicopter Fatigue Specialist's Meeting, October 16-18, 1984.

"Combined Finite Element - Transfer Matrix Method Based on a Mixed Formulation", E. E. Degen, M. Shephard and R. Loewy, Symposium on Advances and Trends in Structures and Dynamics, October 23, 1984.

"Unsteady Two-Dimensional Potential Flow Interactions", R. Mayle and P. Renzoni, Workshop on Blade Vortex Interaction, NASA Ames Research Center, Octovber 29-31 1984.

"Supercritical Airfoil Drag Reduction by Passive Shock Wave/Boundary Layer Control in the Mach Number Range .75 to .90", H.T. Nagamatsu, R. Dyer & R.V. Ficarra Proceedings of the 23rd AIAA Aerospace Sciences Meeting, Reno, NV, January 1985.

"Use of Twisted Principal Coordinates in Blade Analysis", A. Rosen, R.G. Loewy and M.B. Mathew; Proceedings of the ARO-AHS International Conference on Rotorcraft Basic Research, Research Triangle Park, NC, February 1985.

"Optimal Design of Composite Power Transmission Shafting", M.S. Darlow and J.W. Lim, Proceedings of the ARO-AHS International Conference on Rotorcraft Basic Research, Research Triangle Park, NC, February 1985. (Also RPI RTC Report No. S-85-1, February 15, 1985.)

"Hygrothermally Curvature Stable Laminates with Tension-Torsion Coupling", S. Winckler, Proceedings of the ARO-AHS International Conference on Rotorcraft Basic Research, Research Triangle Park, NC, Feburary 1985.

"Toward Automated Finite Element Modeling for the Unification of Engineering Design and Analysis", M.S. Shephard, Proceedings of the 8th UFEM Symposium, U. of Conn., Storrs, CT, May 1985.

"Combined Finite Element-Transfer Matrix Method Based on a Mixed Formulation", E.E. Degen, M.S. Shephard and R.G. Loewy, Computers and Structures, Vol. 20, 1985.

"A Simplified Orthotropic Formulation of the Viscoplasticity Theory Based on Overstress", M. Sutcu; Proceedings of the Third Army Conference on Applied Mathematics and Computing, Georgia Institute of Technology, Atlanta, GA, May 1985.

"Hygrothermally Curvature Stable Laminates with Tension-Torsion Coupling", S. Winckler, Journal of the American Helicopter Society, July 1985.

"Interactive Computer Modeling of Airframe Structures", B. Johnston and M. Shephard; Journal of the American Helicopter Society, July 1985.

"Finite Element Approach to Rotor Blade Modeling", O. Bauchau and C. Hong; Journal of the American Helicopter Society, October 1985.

"Application of Mixed Finite Elements in the Formulation of Transfer Matrices", E. Degen, Y. Chang and M. Shephard; Proceedings of the ASME Winter Annual Mtg, Hybrid and Mixed Finite Element Models, Miami, FL, November 1985.

"Finite Element Modeling Within an Integrated Geometric Modeling Environment; Part 2 - Attribute Specification, Domain Differences, and Indirect Element Types", M. Shephard; ASCE Engineering with Computers, December 1985.

"Optimal Sizing of Composite Power Transmission Shafting", J.W. Lim and M.S. Darlow, Journal of the American Helicopter Society, Vol. 31, No. 1, January 1986.

"Passive Shock Wave/Boundary Layer Control for Transonic Drag Reduction for Rotor Blade", A.D. Barnard and H.T. Nagamatsu, AIAA Aerospace Science Meeting, Reno, NV, Paper No. 86-0288, January 6-9, 1986.

"The Effect of Interlaminar Normal Stresses on the Uniaxial Zero-to-Tension Fatigue Behavior of Graphite/Epoxy Tubes", E. Krempl and D. An, RPI MML 86-1, Rensselaer Polytechnic Institute, published February 1986.

"Application of the Principal Curvature Transformation to Nonlinear Rotor Blade Analysis", R.G. Loewy, A. Rosen, and M.B. Mathew, Proceedings of the 27th Structures, Structural Dynamics and Materials Conference, San Antonio, TX, May 19-21, 1986.

"Effects of Type of Boundary Layer, Cavity Depth and Surface Porosity Distribution and Supercritical Airfoil Drag Reduction by Shock Wave/Boundary Layer Control", H. Nagamatsu and R. Dyer, Proceedings of the High Speed Aerodynamics I Mtg at Aachen, Edited by A. Natase, pps 85-100, Published by Haag-Herichen, Frankfurt, Germany, May 1986.

"Relaminarization of the Boundary Layer Over a Flat Plate in Shock Tube Experiments", J.N. Hinckel and H.T. Nagamatsu, AIAA Journal, (AIAA-86-1238), June 1986.

"Large Displacement Analysis of Naturally Curved and Twisted Composite Beams", O. A. Bauchau and C. H. Hong, RPI RTC Report D-86-1, July 1986.

"An Approach to Ideal Twist Distribution in Tilt-Rotor VTOL Blade Design", O. A. Bauchau, R. G. Loewy and P. S. Bryan, RPI RTC Report D-86-2, July 1986.

"A Solution of the Eigen Problem for Undamped Gyroscopic Systems with the Lanczos Algorithm", O.A. Bauchau, Int. J. Num. Meth. Eng., Vol. 23, 1705-1713, Sept. 1986.

"Validation of a Method for Air Resonance Testing of Helicopters at Model Scale Using Active Control of Pylon Dynamic Characteristics", R.L. Bielawa, (paper No. 82) Proceedings of the Twelfth European Rotorcraft Forum, Gramisch-Partenkirchen, F.R.G., September 22-25, 1986.

"Geometrically Based Automatic Finite Element Modeling Procedures", M.S. Shephard, Reliability of Methods for Engineering Analysis, K.J. Bathe and R.J. Owen, Eds., Pineridge Press, UK, 1986, pp. 289-304.

"Preprocessor Development for the RPI Model Rotor Impedance Test Facility, Part I - Conceptual Development", K. D. Hsueh and R. L. Bielawa, RPI RTC Report D-86-3, Dec. 30, 1986.

"Passive Shock Wave/Boundary Layer Control of a Helicopter Rotor Airfoil in a Contoured Transonic Wind Tunnel", H.T. Nagamatsu, T.J. Mitty and G. A. Nyberg, AIAA Aerospace Sciences Conf., Reno, NV, Paper No. 87-0438, Jan. 1987.

"Application of the Principal Curvature Transformation to Nonlinear Rotor Blade Analysis", R.G. Loewy, A. Rosen and M.B. Mathew, VERTICA, Vol. 11, No. 1/2, 1987 (special 10th anniversary issue).

"Automated Finite Element Modeling: How Close Is It", M. Shephard, Vol. 1, Proceedings of the MSC 1987 World Users Conference, Los Angeles, CA, March 11, 1987.

"Nonlinear Analysis of Pretwisted Rods Using 'Principal Curvature Transformation', Part I: Theoretical Derivation", A. Rosen, R.G. Loewy and M.B. Mathew, AIAA Journal, Vol. 25, No. 3, March 1987.

"The Generation of Finite Element Models Using an Expert System", B.L. Gregory and M.S. Shephard, Engineering and Computers, Vol. 2, pp. 65-77, 1987.

"Nonlinear Analysis of Pretwisted Rods Using 'Princpal Curvature Transformation', Part II: Numerical Results", A. Rosen, R.G. Loewy and M.B. Mathew, AIAA Journal, Vol. 25, No. 4, April 1987.

"Nonlinear Dynamics of Slender Rods", A.Rosen, R.G. Loewy and M.B. Mathew, AIAA Journal Vol. 25, No. 4, April 1987.

"Design and Experimental Studies of Composite Power Transmission Shafts", R.G. Kraus and M.S. Darlow, Proceedings of the 43rd AHS Annual Forum, St. Louis, MO, May 18-21, 1987.

"Use of Twisted Principal Coordinates and Non-Physical Coordinates in Blade Analysis", A. Rosen, R.G. Loewy and M.B. Mathew, VERTICA, Vol. 11, No. 3, 1987.

"Passive Drag Reduction on a Complete NACA 0012 Airfoil at Transonic Mach Numbers", H.T. Nagamatsu, T.W. Trilling and J.A. Bossard, AIAA Fluid Dynamics and Plasma Conf., Honolulu, Hawaii, Paper No. 87-0140, June 1987.

"Notes Regarding Fundamental Understandings of Rotorcraft Aeroelastic Instability", R. L. Bielawa, Journal of the American Helicopter Society, Oct. 1987.

"Elastic Hingeless Scissor Design", M. Niederer and D. B. Goetschel, VERTICA, Vol. 11, No. 4, 1987.

"Preprocessor Development for the RPI Model Rotor Impedance Test Facility, Part II - Computer Programs", K. Hsueh, RPI RTC Report No. D-87-3, 1987.

"Large Displacement Analysis of Naturally Curved and Twisted Beams", O. A. Bauchau and C. H. Hong, AIAA Journal, Vol. 25, No. 11, pp 1469-1475, Nov. 1987.

Table 23

Rotorcraft Technology Papers Presented During the Contract Period

Rensselaer RTC

"Helicopter Vibrations: A Technological Perspective", R. G. Loewy, 4th Alexander Nikolsky Memorial Lecture, 40th American Helicopter Society Annual Forum, May 17, 1984.

"The Army Research Office Center of Excellence in Rotorcraft Technology at Rensselaer", R. Loewy, 92nd Annual ASEE Conference, Salt Lake City, Utah, June 24-26, 1984.

"Finite Element Approximation to Theodorsen's Solution for Non-Steady Aerodynamics of a Two-Dimensional Airfoil Section", R. E. Duffy and E. Czajkowski, 17th AIAA Fluid Dynamics, Plasma Dynamics and Lasers Conference, June 25-27, 1984.

"An Improved Technique for Testing Helicopter Rotor-Pylon Aeromechanical Stability Using Measured Rotor Dynamics Impedance Characteristics", R. Bielawa, 10th European Rotorcraft Forum, August 28-31, 1984.

"Biaxial Fatigue Properties of Thin-Walled Composite Tubes", E. Krempl, R. Loewy and D. Elzey, American Helicopter Society Midwest Region Helicopter Fatigue Specialist's Meeting, October 16-18, 1984.

"Combined Finite Element - Transfer Matrix Method Based on a Mixed Formulation", E. E. Degen, M. Shephard and R. Loewy, Symposium on Advances and Trends in Structures and Dynamics, October 23, 1984.

"Unsteady Two-Dimensional Potential Flow Interactions", R. Mayle and P. Renzoni, Workshop on Blade Vortex Interaction, NASA Ames Research Center, October 19-31, 1984.

"Supercritical Airfoil Drag Reduction by Passive Shock Wave/Boundary Layer Control in the Mach Number Range .75 to .90", H.T. Nagamatsu, R. Dyer & R.V. Ficarra; 23rd AIAA Aerospace Sciences Meeting, Reno, NV, January 1985.

"Use of Twisted Principal Coordinates in Blade Analysis", A. Rosen, R.G. Loewy and M.B. Mathew; ARO-AHS International Conference on Rotorcraft Basic Research, Research Triangle Park, NC, February 1985.

"Optimal Design of Composite Power Transmission Shafting", M.S. Darlow and J.W. Lim; ARO-AHS International Conference on Rotorcraft Basic Research, Research Triangle Park, NC, February 1985.

"Hygrothermally Curvature Stable Laminates with Tension-Torsion Coupling", S. Winckler; ARO-AHS International Conference on Rotorcraft Basic Research, Research Triangle Park, NC, Feburary 1985.

"Helicopter Vibrations: A Technological Perspective", R. Loewy, 4th A. Nikolsky Lecture, given to and at invitation of Tobacco Valley AHS Chapter, Hartford, CT, 2/14/85.

"Investigation of Composite materials Applications to Rotorcraft Shafting", M.S. Darlow; "Work-in-Progress" session of the 26th AIAA Structures, Structural Dynamics and Materials Conference, Orlando, FL, April 1985.

"Toward Automated Finite Element Modeling for the Unification of Engineering Design and Analysis", M.S. Shephard, 8th UFEM Symposium, U. of Conn., Storrs, CT, May 1985.

"A Simplified Orthotropic Formulation of the Viscoplasticity Theory Based on Overstress", M. Sutcu; Third Army Conference on Applied Mathematics and Computing, Georgia Institute of Technology, Atlanta, GA, May 1985.

"Automatic Generation and Control of Finite Element Models", M. Shephard, Worcester Polytechnic Inst., Worcester, MA., 11/7/85.

"Aeronautical Engineering Education in the PRC", R. Loewy, Meeting of the Hampton Roads Section of AHS, Ft. Eustis, VA, 11/20/85.

"Application of Mixed Finite Elements in the Formulation of Transfer Matrices", E. Degen, Y. Chang and M. Shephard; ASME Winter Annual Mtg, Hybrid and Mixed Finite Element Models, Miami, FL, November 1985.

"The Effect of Biaxial Cycling on the Residual Strength of $[+/-45]_S$ Gr/Epoxy Thin-Walled Tubes", E. Krempl, Second International Conference on Biaxial/Multiaxial Fatigue, Sheffield, United Kingdom, December 1985.

"Inclusion of a Generalized Anisotropic Beam Force - Deformation Relationship in Normal Mode Rotor Aeroelastic Analyses", R. Bielawa; ARO & Georgia Tech. Workshop on Dynamic and Aeroelastic Stability Modeling of Rotor Systems, Atlanta, GA, December 1985.

"A Comparison of Composite Rotor Blade Models", O. Bauchau; ARO & Georgia Tech. Workshop on Dynamic and Aeroelastic Stability Modeling of Rotor Systems, Atlanta, GA, December 1985.

"Finite Element Approach to Rotor Blade Modeling", O. Bauchau; ARO & Georgia Tech. Workshop on Dynamic and Aeroelastic Stability Modeling of Rotor Systems, Atlanta, GA, December 1985.

"Application of Principal Curvature Velocity Component Transformations in Blade Dynamics", R. Loewy, A. Rosen and M.B. Mathew; ARO & Georgia Tech. Workshop on Dynamic and Aeroelastic Stability Modeling of Rotor Systems, Atlanta, GA, December 1985.

"Generalized Mobility Coupling of Substructures", B. Jetmundsen; Regional AHS Lichten Award Competition, Kaman Aerospace Corp. Headquarters, Bloomfield, CT, December 1985.

"A Study of the Influence of Predeformations on the Free Vibrations of Blades", M.B. Mathew; presented at the Regional AHS Lichten Award Competition, Kaman Aerospace Corp. Headquarters, Bloomfield, CT, December 1985.

"Passive Shock Wave/Boundary Layer Control for Transonic Drag Reduction for Rotor Blade", A.D. Barnard and H.T. Nagamatsu, AIAA Aerospace Science Meeting, Reno, NV, Paper No. AIAA 86-0288, January 6-9, 1986.

"Aeronautical Research and Education in the Peoples Republic of China", R.G. Loewy, AHS Chapter, Philadelphia, PA, March 17, 1986.

"Recent Advances in the Generation and Control of the Finite Element Method", M. Shephard, Rutgers University, May 7, 1986.

"Application of the Principal Curvature Transformation to Nonlinear Rotor Blade Analysis", R.G. Loewy, A. Rosen, and M.B. Mathew, 27th Structures, Structural Dynamics and Materials Conference, San Antonio, TX, May 19-21, 1986.

"Effects of Type of Boundary Layer, Cavity Depth and Surface Porosity Distribution and Supercritical Airfoil Drag Reduction by Shock Wave/Boundary Layer Control", H. Nagamatsu and R. Dyer, High Speed Aerodynamics Mtg at Aachen, FRG, May 1986.

"Supercritical Composite Shafting", M.S. Darlow, AHS Tobacco Valley Chapter, Windsor, CT, presented June 29, 1986.

"Torsional Buckling Analysis and Damage Tolerance of Graphite/Epoxy Shafts", O.A. Bauchau, Workshop on Composite Materials and Structures for Rotorcraft, RPI, September 10-11, 1986.

"Optimal Design and Evaluation of Supercritical Composite Helicopter Power Transmission Shafts", M.S. Darlow, Workshop on Composite Materials and Structures for Rotorcraft, RPI, September 10-11, 1986.

"Designing for Thermal Twist Stability in Rotor Blades with Tension-Torsion Coupling", S. Winckler, Workshop on Composite Materials and Structures for Rotorcraft, RPI, September 10-11, 1986.

"The Filament Winding of Complex Shape Composites", R.J. Diefendorf, Materials Technology Laboratory - U.S. Army, Watertown, MA, September 12, 1986.

"Validation of a Method for Air Resonance Testing of Helicopters at Model Scale Using Active Control of Pylon Dynamic Characteristics", R.L. Bielawa, Twelfth European Rotorcraft Forum, Gramisch-Partenkirchen, F.R.G., September 22-25, 1986.

"Asymmetric Composites", R.J. Diefendorf, Sixth International Symposium on Composite Materials, Stara Lesna, Czechoslovakia, October 27-30, 1986.

"Blade Vortex Interaction Research at RPI", R.E. Mayle, Boeing Vertol Company; Essington, Pa; Oct. 30, 1986.

"Asymmetric Composites - Flat Plates", R.J. Diefendorf, ASM/SAMPE/ESD Advanced Composites Meeting, Detroit, MI, November 19-20, 1986.

"DAMVIBS Related Activities at RPI", R.L. Bielawa, DAMVIBS Workshop NASA Langley Research Center, Dec. 1-4, 1986.

"Passive Shock Wave/Boundary Layer Control of a Helicopter Rotor Airfoil in Contoured Transonic Wind Tunnel", H.T. Nagamatsu, T.J. Mitty and G.A. Nyberg, AIAA Aerospace Sciences Conf., Reno, NV, Jan. 1987.

"Composite Structures", R.J. Diefendorf, University of Delaware, Newark, DE., February 2, 1987.

"Automated Finite Element Modeling: How Close Is It", M. Shephard, MSC 1987 World Users Conference, Los Angeles, CA, March 11, 1987.

"Composite Processing", R.J. Diefendorf, Sach's Memorial Lecture at Syracuse University, Syracuse, NY, April 21, 1987.

"Adaptive Analysis for Automated Finite Element Modeling", M. Shephard, Conference on The Mathematics of Finite Elements and Applications, Brunel U., West London, UK, April 28-May 1, 1987.

"Design and Experimental Studies of Composite Power Transmission Shafts", R.G. Kraus and M.S. Darlow, 43rd AHS Annual Forum, St. Louis, MO, May 18-21, 1987.

"Comparison of High Performance Fibers", R. J. Diefendorf, General Electric C&D Whitney Lecture on Science & Technology, Rensselaerville, N.Y., June 11-13, 1987.

"Passive Drag Reduction on a Complete NACA 0012 Airfoil at Transonic Mach Numbers", H.T. Nagamatsu, T.W. Trilling and J.A. Bossard, AIAA Fluid Dynamics and Plasma Conf., Honolulu, Hawaii, June 1987.

"Nonlinear Composite Beam Theory", and "An Approach to Ideal Twist Distribution in Tilt Rotor VTOL Blade Design", O. Bauchau, Workshop on Dynamics and Aeroelasticity Stability Modeling of Rotor Systems held at Florida Atlantic University, Boca Raton, FL, Nov. 18-20, 1987.

"A Unified Perturbation Analysis of the Nonlinear Flap-Lag Response of a Rotor Blade in Forward Flight or in Hover", M.R.M. Crespo da Silva, R.P.I., Workshop on Dynamics and Aeroelasticity Stability Modeling of Rotor Systems, Florida Atlantic University, Boca Raton, FL, Nov. 18-28, 1987.

"The Chemical Nature of the Fiber/Resin Interface in Composite Materials", R. J. Diefendorf, Fall Meeting of the Materials Research Society, Boston, MA, Nov. 30-Dec. 5, 1987.

Table 24

Rotorcraft Technology Discussions or Informal Presentations

on the Site of the

Rensselaer RTC

Date	Subject	Participants	"Outside" Organization
10/29/82	Plans for the Rensselaer Rotorcraft Technology Center	Mr. K. Kelly	Sikorsky Aircraft Div., U.T.C.
11/3/82	RRTC Wind Tunnel & Composite Materials Laboratories	Messrs. J. M. DelBalzo, T. L. Hartnett, R. L. Fulton, J. Haight and N. A. Owens,	Eastern Region, FAA
10/5/82	Composites Research	Messrs. E. Hooper, P. Dixon	Boeing-Vertol
10/6/83	Experiments in Rotorcraft Stability	Mr. W. G. Bousman Res. Scientist, Aeromechanics Lab.	Ames Res. Ctr.
11/16/83	Use of Composites in the Helicopter Industry	Dr. Gary Cheatham	Sikorsky Aircraft Div., U.T.C.
1/18/84	Composite Structures Research; Analysis & Testing	Messrs. E. Hooper, L. Marchinski, P. Dixon & E. Mychalowycz	Boeing-Vertol Co.

Date	Subject	Participants	"Outside" Organization
2/6/84	Review of RPI RTC Activities	Drs. F. Oertel & R. Singleton	U.S. Army Res. Office
3/5/84	Computer Graphics, Structures & Structural Dynamics	Mr. Grant Parker Chief of Dynamics, Finite Element Analysis	Hughes Helicopter
3/6/84	Unsteady Aerodynamics and Composite Structures	Mr. R. Killough	Hughes Helicopters
4/10/84	Rotor Testing Research	Messrs. A. J. Landgrebe, R. Olsen & W. Weller	U.T.R.L. of UTC
10/16/84	Review of Engr. CAD/CAM	Mr. M. Adami	Sikorsky Aircraft
3/27/85	Structures, Dynamics & Materials Aspects of RRTC Program	Dr. G. Anderson	Army Res. Office
9/3/85	Research in the FAA	Mr. R. Adams	Systems Control Tech., Inc., West Palm Bch, FL
4/9/86	Optimum Twist of Tilt Rotor Aircraft Propellers	Messrs. H. Alexander, H. Bishop	Boeing-Vertol
8/5/86	Passive Drag Control Research	Mr. M. Jenks	Boeing-Vertol

Date	Subject	Participants	"Outside" Organization
8/15/86	Applications of Carbon Fiber Composites	Mr. M. Katz	E.I. duPont deNemours & Co.
9/10/86	Composite Shaft Test Facility	Mr. N. Krebs	Kaman Aerospace
9/26/86	Response of Helicopters to Control Input and Tip Path Tilt	Mr. K. Raisner	U.S. Army, Picatinny Arsenal
9/26/86	Reinforcements for Metal Matrix Composites	Mr. S. Harris	Imperial Chemical Inc. Wilmington, De.
10/8/86	The Mechanics of Composites and Structural Applications	Mr. D. Adams	Center for Composite Materials, Univ. of Wyoming
11/11/86	Transonic Flow Phenomena	Mr. R. Prouty	McDonnell-Douglas Helicopter Co.
11/13/86	Fracture in Structural Applications	Mr. W. Sutton	U.T.R.C. East Hartford, CT
11/17/86	Filamentary Composites	Prof. J. Saint-Romain	M.I.T.
11/17/86	Optimization of Composite Shafts	Mr. W. Taylor	USARDL Ft. Eustis, VA
12/15/86	Response of Helicopters to Control Input and Tip Path Tilt	Mr. K. Raisner	U.S. Army, Picatinny Arsenal

Date	Subject	Participants	"Outside" Organization
12/19/86	Rotor Unsteady Aerodynamics and Aeroelasticity	Dr. F. Caradonna	Aeroflight Dynamics Directorate, U.S. Army, Ames Res. Ctr.
2/3/87	Rotorcraft Center Plans & Programs	Dr. R. Singleton	Army Res. Office
3/10/87	Composite Design & Fabrication	Dr. B. Fioretto	U.S. Army TACOM
4/8/87	Composite Materials at RPI	Committee Personnel	Capital Region Technology Com.
5/26/87	RPI Programs & Plans in Rotorcraft Technology Research	Drs. H. Somerson, J. Shaw, Messrs. C. Albrecht & P. Teare	Boeing-Vertol Co.
		Prof. Wang Shi-Cun	Nanjing Aero. Inst., Nanjing, P.R.C.
11/9/87	Rotorcraft Structures and Dynamics Research at RPI	Dr. G. Anderson	U.S. Army Res. Office

TABLE 25

Special Short Courses Offered Since Establishment of the Rensselaer RTC

Course Title (Faculty)	Dates Given	Location	Attendance Statistics			
			Total	Different Companies	Different Universities	Different Government Agencies
Advanced Composite Materials and Structures (R.J. Diefendorf, O. Bauchau*, G. Dvorak**, RPI; S. Tsai, USAFML; B. Riley***, MacDAC	07/11-15/83	RPI	21	14	2	3
	07/23-27/84	RPI	27	17	2	4
	07/22 26/85	RPI	16	9	0	4
	07/21-25/86	RPI	17	13	0	3
	07/27-31/87	RPI	26	9	1	9
Composite Materials and Structures for Rotorcraft (R.J. Diefendorf and O. Bauchau)	10/08-31/85 12/05-19/85 02/07-21/86	Sikorsky Aircraft Division U.T.C.	Sikorsky Employees Only No Statistics Available			
Rotor Structural Dynamics, Aero-elasticity & Vibration (R. Loewy, R. Bielawa, O. Bauchau, RPI; F. Caradonna, USA Ames R.C.; D. Bliss, Duke University)	07/14-18/86	Naval Post-Graduate School, Monterey, CA	24	4	3	7
	06/01-05/87	RPI	9	6	0	3
	07/20 24/87	Naval Post-Graduate School, Monterey, CA	18	2	2	6

* Replaced Dr.G. Helwig, Dornier
** Replaced Drs. L. Phoenix, Cornell University or W. Rosen, Materials Sciences Corporation
*** Replace D. Wilkins who participated in the earlier of these years

Table 26

Steering Committee

Workshop on Composite Materials and Structures

September 10th and 11th, 1986

Rensselaer RTC

Dr. Gary Anderson, Chairman
U. S. Army Research Office

Carl Albrecht
Boeing-Vertol

G. Reis Alsmiller
Bell Helicopter

Frank Camaratta, Jr.
Sikorsky Aircraft

John Dugundji
M. I. T.

Dan Good
U. S.Army AATD

Len Marchinski
DuPont

Table 27

Rotorcraft Related Placement of Graduates Since ARO RTC was Established

Rensselaer RTC

Organization	Year 82/83	83/84	84/85	85/86	86/87
Aerojet General				J. Bossard*[2]	
Aerospace Corp				M. Kolotylo[2]	
Bell			D. Speaker[1]		
Boeing Vertol		M. Jenks*[2] R. Smith*[2] M. Niederer[2] A. Bertolazzi[2]	P. Welles[1] R. Tomlin*[2]	J. Doran[2] J. Hayes*[2] J. Nickerson[2]	
Corning Glass				R. Bergman*[2]	
Det Norske Veritas, Norway				B. Jetmundsen*[3]	
Garrett Turbine					T. Harris[1] M. Morris[1] R. Musiol[1]
G. E. (Turbine Lab)		D. Elzey*[2]	E. Degen*[3]		J. Carboni[1]
Grumman				J. Colasante[2]	
Helicopter Pilot Train.					M. O'Connor[2]
Kaman		P. Vrionides[2]			
LSI - Logic Corp.				B. Gregory*[2]	
Link-Singer			S. Garing*[2]		G. Feder[2] P. Lewis[2]
MDHC (formerly Hughes)			J. Schorn[1] S. Casabella[1]		
NASA LaRC		C. Rumsey*[2]			
RPI				S. Winckler*[3]	B. Mathew*[3]
Sikorsky	P. Bogucki[1] P. Novoa[1] P. Dripnak[1]	W. Kim[3] J. Rios[1] S. Baxter[1] K. Furnes[2] P. Zoons[2]	R. Martin[1] J. Philcox[1] A. Trudeau[2] T. Kron[2] W. Beck[2]	S. Morris[1] S. Poulin[1] S. Sammatro[1]	D. Belluardo[1] S. Clarkson[1] M. Consolini[1] P. Dansreau[1] R. Halvorson*[2] C. Jaran*[3]
USA St. Louis			J. Planchak[2]		
US Air Force				T. Bidlack*[3]	
UTRC		M. Malorin[1] J. Regelman[1]			
Ph.D. Programs Elsewhere		E. Czajkowski*[2] (MIT)	J. Lim*[2] (U of MD)		T. Mitty*[2] (Princeton)

* With support under ARO contract.
1. B.S., 2. M.S., 3. Ph.D., (3, Ph.D

8. References

1. "Vertical Lift Review" A Final Report of the U.S. Army's Vertical Lift Technology ad hoc Sub Group, Chairman, Norman R. Augustine, July 26, '80

2. "Program Guide Centers of Excellence: Rotary Wing Technology" U.S. Army Research Office, Durham, N.C. September '81

3. RPI, Proposal "A Center of Excellence in Rotary Wing Aircraft Technology" No. 189(22R)8259(2F), Dec. 31, 1981

4. U. S. Army Research Office Contract No. DAAG 29-82-K-0093, July 1, 1982

5. "Introduction to Composite Materials", S. W. Tsai & H. T. Hahn, Technomic. 1980.

6. "Unsymmetrically Laminated Composites", M. W. Hyer, Proceedings of ICCM IV, Vol. 1, 1982, pp. 373-380.

7. "The Effects of Fabrication and Moisture on the Curvatures of Thin Unsymmetric Graphite/Epoxy Laminates", M. Wong, MSc. Thesis, MIT, February 1982.

8. "Hygrothermally Curvature Stable Laminates with Tension-Torsion Coupling", S. Winckler, AHS Journal, July 1985.

9. Rehfield, L. W. and Atilgen, A.R. "Structural Technology for Elastic Tailoring of Composite Rotor Blades", 2nd Technical Workshop on Dynamics and Aeroelastic Stability Modeling of Rotorcraft Systems", Nov. 18-20, 1987, Boca Raton, Fla.

10. "Graphite/Epoxy $[+/-45]_8$ Tubes. Their Static Axial and Shear Properties and Their Fatigue Behavior Under Completely Reversed Load Controlled Loading", E. Krempl and Tyan-Min Niu, Journal of Composite Materials, 16, 172-187, 1982.

11. "Biaxial Fatigue of Graphite/Epoxy $[+/-45]_8$ Tubes", Tyan-Min Niu, Doctoral Dissertation, RPI, 1983.

12. "The Effect of Interlaminar Normal Stresses on the Uniaxial Zero-to-Tension Fatigue Behavior of Graphite/Epoxy Tubes", E. Krempl and D. An, RPI Report MML 86-1, February 1986.

13. "A Simplified Orthotropic Formulation of the Viscoplasticity Theory Based on Overstess", M. Sutcu and E. Krempl, Transactions of the Third Army Conference on Applied Mathematics and Computing, ARO Report 86-1, The Army Mathematics Steering Committee, Department of Defense, 307-337, 1986.

14. "Stress Fracture Criteria for Laminated Composites Containing Stress Concentrations", J. R. Whitney and R. J. Nuismer, Journal of Composite Materials, July 1974, pp 253-265.

15. "Design Manual for Impact Damage Tolerant Aircraft Structure", Avery, J. G., AGARD ograph No. 238, 1981.

16. "Comparison of the Ballistic Impact Response of Metals and Composites for Military Aircraft Applications", Avery, J. G. and Porter, T. R., ASTM STP 568, 1975, pp. 3-29.

17. "Residual Strength Characterization of Laminated Composites Subjected to Impact Loading", Husman, G. E., Whitney, J. M. and Halpin, J. C., ASTM STP 568, pp 92-113, 1975.

18. "Comparison of Residual Strength of Composite and Metal Structures After Ballistic Damage", Suarez, J. A. and Whiteside, J. B., ASTM STP 568, 1975, pp 72-91.

19. "Hard Object Impact Damage of Metal Matrix Composite", Awerbach, Jr. and Hahn, H. T., J. Composite Materials, Vol. 10, July 1976, pp 231.

20. "Impact Properties of Carbon Fibre/Kevlar 49 Fiber Hybrid Composites", Drey, G., Sidey, G. R. and Hutchings, J., Composites, Jan. 1976, pp 25-32.

21. "Delamination-Crack Propagation in Ballistically Impacted Gloss/Epoxy Composite Laminates", Takeda, N., Sierakowski, R. L., Ross, C. A. and Malvern, L. E., Experimental Mechanics, Jan. 1982, pp 19-25.

22. "Torsional Buckling Analyses and Damage Tolerance of Graphite Epoxy Shafts", Bauchau, O. A., Krafchak, T. M. and Hayes, J. F., Journal of Composite Materials to appear, Spring '88.

23. "Elastic Hingeless Scissor Design", M. Niederer and D.B. Goetschel, VERTICA, Vol. 11, No. 4, 1987.

24. "The Optimal Design of Composite Drive Shafts", Lim, J. W. and Darlow, M. S., Proc. 1st Int'l Conf. on Rotorcraft Basic Research, 1985.

25. "Optimal Sizing of Composite Power Transmission Shafting", Lim, J. W. and Darlow, M. S., JAHS, Vol. 31, No. 1, pp. 75-83, January 1986.

26. "Design and Experimental Studies of Composite Power Transmission Shafting", Kraus, R. F. and Darlow, M. S., Proc. 43rd AHS Annual Forum, pp. 733-738, 1987.

27. "Experimental Verification of Optimized Driveshaft Designs", Kraus, R. F., Darlow, M. S., Conley, W. P. and Jones, P. L., Proc. 2nd Int'l Conf. on Rotorcraft Basic Research, University of Maryland, Feb. 16-18, 1988.

28. "Finite Element Modeling Within an Integrated Geometric Modeling Environment", Engineering with Computers, Vol. 1, 1985, pp. 73-85.

29. "Interactive Computer Modeling of Airframe Structures:, B.J. Johnson and M.S. Shephard, J. of the American Helicoper Society, Vol. 30, No. 3, 1985, pp. 59-61.

30. "Design of a Knowledge-Based System to Convert Airframe Geometric Models to Finite Element Models", B. G. Gregory and M.S. Shephard, Expert Systems in Civil Engineering, C.N. Kostem and M.L. Maher, Eds. ASCE, NY, NY, 1986, pp. 133-144.

31. "The Generation of Airframe Finite Element Models Using and Expert System", B.G. Gregory and M.S. Shepahrd, Engineering with Computers, Vol. 2, 1987, p. 65-77.

32. "Combined Finite Element - Transfer Matrix Method Based on a Mixed Formulation", E.E. Degen, M.S. Shephard and R.G. Loewy, Computers and Structures, Vol. 20, 1985, pp. 173-180.

33. "Application of Mixed Finite Elements in the Formulation of Transfer Matrices", E.E. Degen, Y.H. Chang and M.S. Shephard, Hybrid and Mixed Finite Element Methods, R.L. Spilker and K.W. Reed, Eds, ASME, AMD-Col. 73, ASME, N.Y. 1985, pp. 11-18.

34. "Structural System Identification Technology Verification", N. Giasante, A. Berman, W. G. Flannelly and E. J. Nagy, USMURADCON-TR-81-D28, November 1981.

35. "Investigation of Passive Shock-Wave-Boundary Layer Control for Transonic Airfoil Drag Reduction", NASA Grant # NSG 1624.

36. "Passive Shock Wave/Boundary Layer Control for Transonic Airfoil Drag Reduction", L. Bahi, J. M. Ross and H. T. Nagamatsu, AIAA Paper No. 83-0137, January 1983.

37. "Porosity Effect on Supercritical Airfoil Drag Reduction by Shock Wave/Boundary Layer Control", H. T. Nagamatsu, R. D. Orozco and D. C. Ling, AIAA Paper No. 84-1682, June 1984.

38. "Supercritical Airfoil Drag Reduction by Passive Wave/Boundary Layer Control in the Mach Number Range .75 to .90", H. T. Nagamatsu, R. Dyer and R. V. Ficarra, AIAA Paper No. 85-0207, January 1985.

39. "Determination of Profile Drag at High Speeds by Pitot Traverse Method", C. Lock, W. Hilton and S. Goldstain, A.R.C. R&M, 1971, September 1940.

40. "Transonic Drag Reduction on a Helicopter Rotor Blade Tip (NACA 0012 Airfoil Section) by Passive Shock Wave/Boundary Layer Control", A.D. Barnard and H. T. Nagamatsu, AIAA Paper No. 86-0288, January 1986.

41. "Passive Shock Wave/Boundary Layer Control of a Helicopter Rotor Airfoil in a Contoured Transonic Wind Tunnel", H.T., T.J. Mitty and G.A. Nyberg, AIAA Paper No. 87-0438, January 1987.

42. "Passive Drag Reduction on a Complete NASA 0012 Airfoil at Transonic Mach Numbers", H.T. Nagamatsu, T.W. Trilling and J.A. Bossard, AIAA Paper No. 87-1263, June 1987.

43. "Passive Transonic Drag Reduction of Supercritical and Helicopter Rotor Airfoils", H.T. Nagamatsu and T.W. Trilling, Proceedings of 2nd International Conference on rotorcraft Basic Research, University of Maryland, College Park, Maryland, February 1988.

44. "Some Conclusions from an Investigation of Blade Vortex Interaction", N.D. Ham, J. of the American Helicopter Society, Vol. 20, No. 4, October 1975.

45. "Aerodynamics of Two-Dimensional Blade-Vortex Interaction", G.R. Srinivasan, W.J. McCroskey and J.D. Baeder, AIAA Journal, Vol. 24, No. 10, Oct. 1986.

46. "Aerodynamics, Noise and the Sonic Boom", W.R. Sears, AIAA Journal, Vol. 7, No. 4, April 1969.

47. "Airfoil Pressure Measurements During a Blade-Vortex Interaction and a Comparison with Theory", J. Straus, P. Renzoni, and R.E. Mayle, AIAA Paper No. 88-0669, 1988.

48. "Theoretical Prediction of Dynamic Inflow Derivatives", D.M. Pitt and D.A. Peters, VERTICA, Vol. 5, 1981.

49. "A Method for Computing Rotary Wing Airload Distributions in Forward Flight", R.A. Piziali and P.A. DuWalt, TCREC TR 62-44, November 1962.

50. "Finite Element Approximation to Theodorsen's Solution for Non-Steady Aerodynamics of an Airfoil Section", R. E. Duffy, E. Czajkowski and C. Jaran, AIAA 17th Fluid Dynamics, Plasma Dynamics and Lasers Conference, AIAA Paper No. 84-1640, Snowmass, CO, June 1984.

51. "Effect of Finite Span on the Airload Distribtuion for Oscillating Wings - Part I: Aerodynamic Theory of Oscillatory Wings of Finite Span", E. Reissner, NACA TN 1194, March 1947.

52. "Effect of Finite Span on the Airload Distribution for Oscillating Wings - Part II: Method of Calculation and Exmaple of Application:, E. Reissner, NACA TN 1195, October 1947.

53. "Unsteady Transonic Flow Calculations for Two-Dimensional Canard-Wing Configurations", J.T. Batina, AIAA Journal of Aircraft, Vol. 23, No. 4, April 1986.

54. "Unsteady Kutta Condition at High Values of the Reduced Frequency Parameter", F.S. Archibald, AIAA Journal of Aircraft, Vol. 12, No. 6, June 1975.

55. "A Two-Dimensional Approximation to the Unsteady Aerodynamics of Rotary Wings", R.G. Loewy JAS, Vol. 124, No. 2, February 1957.

56. "New Approach to Finite-State Modeling of Unsteady Aerodynamics", C. Venkatesan and P.P. Friedmann, J. AIAA, Vol. 24, No. 12, December 1968.

57. "Aeroelasticity", R.L. Bisplinghoff, H. Ashley and R.L. Halfman, Addison-Wesley, 1955.

58. "Foundations of Aerodynamics", A.M. Kuethe and C.Y. Chow, Fourth Edition, Wiley, New York 1986.

59. "Summary of Airfoil Data", I.H. Abbott, A.E. von Doenhoff and L.S. Stivers, NACA Technical Report No. 824, National Advisory Committee for Aeronautics, 1948.

60. "A Theoretical and Experimental Study of the Snap-Through Airfoil and its Potential as a Higher Harmonic Control Device", R.E. Duffy, J. Dubben, J. Nickerson and J. Colasante, AIAA 26th Aerospace Sciences Meeting, Reno, NV, January 1988.

61. "Finite Element Approach to Rotor Blade Modeling", O. Bauchau and C. Hong; Journal of the American Helicopter Society, Vol. 32, No. 1, pp. 60-67, Jan. 87.

62. "Nonlinear Composite Beam Theory", O. Bauchau and C. Hong, J. Applied Mechanics, Vol. 55, No. 1, pp. 156-163, March 1980.

63. "A Solution of the Eigen Problem for Undamped Gyroscopic Systems with the Lanczos Algorithm", O.A. Bauchau, Int. J. Num. Meth. Eng., Vol. 23, 1705-1713, Sept. 1986.

64. "Composite Box Beam Analysis: Theory & Experiments", O. Bauchau, B. Coffenberry and L. J. Rehfield. Reinforced Plastics & Composites, Vol. 6, No. 1, pp 45-85, January 1987.

65. "An Experimental Study of the Nonlinear Stiffness of a Rotor Blade Undergoing Flap, Lag and Twist Deformations", E.H. Dowell and J. Traybar, AMS Report No. 1194, (and its addendum, AMS Report No. 1257) Department of Aerospace and Mechanical Sciences, Princeton University, 1975.

66. "An Experimental-Theoretical Correlation Study of Nonlinear Bending and Torsion Deformations of a Cantilever Beam:, E.H. Dowell, J. J. Traybar and D. H. Hodges, J. Sound Vibration, Vol. 50, p 533-544, 1977.

67. "An Experimental Investigation of the Structural Dynamics of a Torsionally Soft Rotor in Vacuum", A.V. Srinivasan, D.G. Cutts and H.T. Shu, NASA Contractor Report 177418, July 1986.

68. " Nonlinear Vibration of a Beam Under Harmonic Excitation", W. Tseng & J. Dugundji, J. Applied Mechanics, Vol. 38, pp 467-476, June 1971.

69. "Restructuring the Rotor Analysis Program C-60", P. G. Phelan and F. J. Tarzanin, Jr., NASA Conference Publication 2400, Proceedings of the 2nd Decennial Specialists Meeting on Rotorcraft Dynamics, November 1985.

70. "Use of Twisted Principal Coordinates and Non Physical Coordinates in Blade Analysis", A. Rosen, R. G. Loewy and M. B. Mathew, Vertica, Vol. 11, No. 3, 1987.

71. "A Method of Principal Curvature Transformation for Analysing the Coupled Bending-Torsion of Pretwisted Rods - Part I Theoretical Derivation", A. Rosen, R.G. Loewy and M.B. Mathew, AIAA Journal, Vol. 25, No. 3, March 1987.

72. "Knickung Verwundener Stäbe Unter Druck" (Buckling of Twisted Bars Under Compression), E. Hui, Österr. Ing. - Arch. Vol. 9, No. 4, 1955, pp. 288-319.

73. "Theoretical and Experimental Investigation of the Nonlinear, Planar Bending of Rotating Beams", A. Rosen and E. Nevo, Israel J. Tech., Vol. 19, pp 89-97, 1981.

74. "Nonlinear Analysis of Pretwisted Rods Using Principal Curvature Transformation, Part II: Numerical Results", A. Rosen, R.G. Loewy and M.B. Mathew, AIAA Journal, Vol. 25, No. 4, April 1987.

75. "Nonlinear Dynamics of Slender Rods", A. Rosen, R.G. Loewy and M.B. Mathew, AIAA Journal, Vol. 25, No. 4, April 1987.

76. "Theory of Elastic Stability", S.P. Timoshenko and J.M. Gere, McGraw Hill Book Co., 1961, Chap. 6, pp. 251-277.

77. "Elastic Stability of Pretwisted Rods", A. Rosen, R. G. Loewy and M. B. Mathew, to appear in the Josef Singer Anniversary Volume, 1988.

78. "Application of the Principal Curvature Transformation to Nonlinear Rotor Blade Analysis", R. G. Loewy, A. Rosen and M. B. Mathew, Vertica, Vol. 11, No. 1/2, 1987.

79. "Nonlinear Effects in Helicopter Rotor Forward Flight Forced Response", R. G. Loewy and M. B. Mathew, Proceedings of the Second Technical Workshop on Dynamics and Aeroelastic Stability Modeling of Rotorcraft Systems, Boca Raton, Fla., November 18-20, 1987.

80. "The Dynamic Antiresonant Vibration Isolator", W. G. Flannelly, Proceedings of the 22nd Annual Forum of the American Helicopter Society, Washington, D. C., May 1966.

81. "Fuselage Nodalization", D. P. Shipman, J. A. White and J. D. Cronkhite, Proceedings of the 42nd Annual Forum of the American Helicopter Society, Washington, D.C., 1972.

82. "Design and Finite Element Analysis of a Model Helicopter Rotor Test Hub", J-L. Terng, Master's Thesis, Rensselaer Polytechnic Institute, December 1987.

83. "Developmental Status of the RPI Model Rotor Impedance Test Facility", R. L. Bielawa, K. D. Hsueh, R. D. Martin and J-L. Terng, Proceedings of the Second International Conference on Rotorcraft Basic Research, University of Maryland, College Park, MD, February 1988.

84. "Theory of Self-Excited Mechanical Oscillations of Hinged Rotor Blades", R. P. Coleman, NACA A.R.R. 3G29, July 1943.

85. "Airborne and Ground Resonance of Hingeless Rotors", R. T. Lytwyn, W. Miao and W. Woitsch, Journal of the American Helicopter Society, Vol. 16, No. 2, Apr. 1971.

86. "Theory of Vibration with Applications:, W. T. Thomson, Prentice Hall, pg. 388, 1981.

87. "Rotor-Fuselage Dynamic Coupling Characteristics of Helicopter Air and Ground Resonance", R. A. Ormiston, Presented at the American Helicopter Society/Nanjing Aeronautical Institute Vertical Flight Technology Seminar, Nanjing, China, November 1985.

88. "AHIP: The OH-58D From Conception to Production", F. D. Harris, presented at the 42nd Annual Forum of the American Helicopter Society, Washington,D. C. June 1986.

89. "Linear Flap-Lag Dynamics of Hingeless Helicopter Rotor Blades in Hover", R. A. Ormiston and D. H. Hodges, Journal of the American Helicopter Society, Vol. 17, No. 2, April 1972.

90. "An Experimental Investigation of the Effects of Aeroelastic Couplings on Aeromechanical Stability of a Hingeless Rotor Helicopter", W. G. Bousman, Journal of the American Helicopter Society, Vol. 26, No. 1, January 1981.

91. "Aeroelastic Stability Analysis of a Composite Blade", C. Hong and I. Chopra, Proceedings of the 40th Annual AHS National Forum, Crystal City, VA, May 1984.

92. "An Approach to the Ideal Twist Distribution in Tilt Rotor VTOL Blade Design", O. A. Bauchau, R. G. Loewy and S. J. Winckler, Proceedings of the Second Technical Workshop on Dynamics and Aeroelastic Stability Modeling of Rotor Systems, Boca Raton, FL, Nov. 18-20, 1987.

Appendix A

Final Agenda

ARO Site Visit
RPI Center of Excellence in
Rotorcraft Technology

June 28, 1983
JEC 3012

8:00 A.M.	Introduction	R. Loewy
	1. Organization	
	2. Principal Investigators	
	3. Fiscal Matters and Modus Operandi	
	4. RPI as the Center's Base	
	5. External Interactions	
8:40 A.M.	Educational Aspects	R.J. Diefendorf
	1. Distinguished Fellowship Program	
	2. Graduate Research Assistants	
	3. Courses Given	
	4. New Course Plans	
	5. Continuing Education Program	
9:00 A.M.	Research Program	
	1. Structures and Materials - Overview	R.J. Diefendorf
	a. Fatigue in Composite Materials	D. Elzey*
	b. Fatigue in Tapered Tension Members	W. Kim
	c. Mechanical Connectors in Composite Shafts	K. Furnes*
	d. Shear Lag in Airframe Structure	D. Goetschel
10:45 A.M.	BREAK	
11:00 A.M.	Research Program	
	1. Structures and Materials (Cont'd.)	
	e. Fracture Mechanisms in Composites	M. Shephard
	f. Environmental Effects & Fracture in Resin Matrices	S. Sternstein
	g. Sikorsky Composite Scissors	M. Niederer*

* Graduate Student

12:00 NOON	LUNCH	
1:00 P.M.	Research Program (Cont'd.)	
	2. Unsteady Aerodynamics - Overview	R. Loewy
	a. Passive Control of Wave Drag	H. Nagamatsu
	b. Vortex-Lifting Surface Interaction	R. Mayle
	c. 3-D, Unsteady Aero Coefficients	E. Czajkowski*
		C. Rumsey*
2:00 P.M.	3. Structural Dynamics and Aeroeleasticity - OVERVIEW	R. Loewy
	a. Passive Blade Pitch Control Through Composites	E. Brunelle
	b. Fully Coupled Rotational Dynamics	R. Smith*
	c. Indicial Admittance & Non-Integer Harmonics	R. Loewy
	d. Blade Dynamics and Mathieu's Equations	C. Shen
3:30 P.M.	BREAK	
3:45 P.M.	3. Structural Dynamics and Aeroelasticity (Cont'd.)	
	e. Fuselage Analysis through FEM	E. Degen*
	f. Fuselage Analysis and CAD/CAM	M. Shephard
4:15 P.M.	Lab Tour	
	Computer Graphics	
	Patigue Lab	
	Composites Lab	
	Transonic Tunnels	
5:15 P.M.	Plans for 83-84	R. Loewy
	1. Expenditure Forecast	
	2. Planned Equipment Purchases	
	3. Recommendations of the Budget Committee	
	4. Alternative Projects Summary	
5:30 P.M.	Executive Sessions	
	1. ARO Evaluations Group	R. Singleton
	2. Industry Advisory Committee	R. Loewy
6:30 P.M.	Debriefing	
	ARO Evaluation Group and RPI RTC Administration	R. Singleton
7:00 P.M.	ADJOURN	R. Singleton

Final Agenda

ARO Site Visit
RPI Center of Excellence in
Rotorcraft Technology

June 19, 1984
JEC 3117

8:00 A.M.	Introduction	R. Loewy
	1. Organization	
	2. Principal Investigator Changes	
	3. Fiscal Matters and Modus Operandi	
	4. Update on RPI as the Center's Base	
	5. Status of External Interactions	
8:40 A.M.	Educational Aspects	R.J. Diefendorf
	1. Distinguished Fellowship Program	
	2. Graduate Research Assistants	
	3. Status of Rotorcraft Courses	
	4. Continuing Education Program	
9:00 A.M.	Research Program	
	1. Structures and Materials - Overview	R.J. Diefendorf
	a. Asymmetric Laminates	D. Radford*
	b. Stable Laminates with Coupling	S. Winckler**
	c. Fatigue in Composite Materials	D. Elzey***
10:05 A.M.	BREAK	
10:20 A.M.	Research Program	
	1. Structures and Materials (Cont'd.)	
	d. Mechanical Connectors in Composite Shafts Torsion	D. Goetschel
	Axial Load and Bending	P. Vaney*
	e. Optimal Composite Drive Shafting	M. Darlow
	f. Composite Shafts and Ballistic Damage	O. Bauchau
	g. Shear Lag and Stringer Crippling	D. Goetschel
11:40 A.M.	LUNCH	

* Graduate Student
** ARO Distinguished Fellow
*** Recent Graduate

1:00 P.M.	Research Program (Cont'd.)	
	2. Unsteady Aerodynamics - Overview	R. Loewy
	a. Passive Control of Wave Drag	H. Nagamatsu
	b. Vortex-Lifting Surface Interaction	R. Mayle
	c. Unsteady Aero Coefficients	C. Jaran*
	d. Snap-Through Airfoil Unsteady Coefficients	M. Kolotylo*
		M. Tomlin*
2:05 P.M.	3. Structural Dynamics and Aeroeleasticity - OVERVIEW	R. Loewy
	a. Vibration of Blades with Multiply Connected Cross Sections	G. Amazigo
	b. Fully Coupled Rotational Dynamics	M. Mathew*
	c. Finite Element Approach to Blade Dynamics	O. Bauchau
3:10 P.M.	BREAK	
3:25 P.M.	3. Structural Dynamics and Aeroelasticity (Cont'd.)	
	d. Fuselage Analysis Using FE-TM Methods	E. Degen*
	e. Fuselage Design and CAD/CAM	W. Bayles*
	f. Rotor Impedance Test Rig	R. Biewlawa
4:25 P.M.	Lab Tour	
	Computer Graphics Composites Lab } or Transonic Tunnels	
5:00 P.M.	Plans for 84-85	R. Loewy
	1. Expenditure Forecast	
	2. Planned Equipment Purchases	
	3. Recommendations of the Budget Committee	
	4. Future Projects Summary	
5:20 P.M.	Executive Sessions	
	1. ARO Evaluations Group	R. Singleton
	2. Industry Advisory Committee	R. Loewy
6:30 P.M.	Debriefing	
	ARO Evaluation Group and RPI RTC Administration	R. Singleton
7:00 P.M.	ADJOURN	R. Singleton

Final Agenda

ARO Site Visit
RPI Center of Excellence in
Rotorcraft Technology

June 12, 1985
JEC 3117

8:00 A.M.	Introduction	R. Loewy
	1. Organizational Review	
	2. Principal Investigator Changes	
	3. Fiscal Matters and Modus Operandi	
	4. Update on RPI as the Center's Base	
	5. Status of External Interactions	
8:30 A.M.	Educational Aspects	R.J. Diefendorf
	1. Distinguished Fellowship Program	
	2. Graduate Research Assistants	
	3. Status of Rotorcraft Courses	
	4. Continuing Education Program	
8:45 A.M.	Research Programs	
	1. Structures and Materials - Overview	R.J. Diefendorf
	a. Asymmetric Laminates	D. Radford*
	b. Stable Laminates with Coupling	S. Winckler**
	c. Fatigue in Composite Materials	D. Elzey***
9:50 A.M.	BREAK	
10:05 A.M.	Research Program	
	1. Structures and Materials (Cont'd.)	
	d. Optimal Composite Drive Shafting	M. Darlow
	e. Ballistic Damage Tolerance in Composite Shafts	O. Bauchau
	f. Shear Lag	O. Bauchau

* Graduate Student
** ARO Distinguished Fellow
*** Recent Graduate

10:55 A.M.	Research Program (Cont'd.)	
	2. Unsteady Aerodynamics - Overview	R. Loewy
	a. Passive Control of Wave Drag	H. Nagamatsu
	b. Vortex-Lifting Surface Interaction	R. Mayle
11:40 A.M.	Tour of Wind Tunnel Area	R. Mayle
12:10 P.M.	LUNCH	
12:40 P.M.	Research Program (Cont'd.)	
	2. Unsteady Aerodynamics (Cont'd.)	R. Loewy
	c. Unsteady Aero Coefficients	C. Jaran**
	d. Snap-Through Airfoil	R. Duffy
1:20 P.M.	3. Structural Dynamics and Aeroeleasticity - OVERVIEW	R. Loewy
	a. Non-Linear Effects in Blade Structural Dynamics - Theory	A. Rosen
	b. Non-Linear Effects in Blade Structural Dynamics - Results	M. Mathew*
	c. Finite Element Approach to Blade Dynamics	O. Bauchau
2:25 P.M.	BREAK	
2:40 P.M.	3. Structural Dynamics and Aeroelasticity (Cont'd.)	
	d. Fuselage Analysis Using FE-TM Methods	E. Degen
	e. An Expert Systems Approach to the Generation of Fuselage Analysis Models	M. Shephard
	f. Rotor Impedance Test Rig	R. Bielawa
3:40 P.M.	Plans for 85-86	R. Loewy
	1. Expenditure Forecast	
	2. Planned Equipment Purchases	
	3. Recommendations of the Budget Committee	
	4. Future Projects Summary	
4:00 P.M.	Simultaneous Discussions	
	1. ARO Evaluation Group (Executive Session)	R. Singleton
	2. Industry Advisory Committee	R. Loewy
4:45 P.M.	Debriefing	
	ARO Evaluation Group and RPI RTC Administration	R. Singleton
5:15 P.M.	ADJOURN	R. Singleton

Itinerary

Visit of
Gary Anderson, Thomas Doligalski, and Robert Singleton
Army Research Office
Research Triangle Park

February 3, 1987

8:00 A.M. DR. ANDERSON (Room 3117) — Dr. Bauchau

1. Damage in Composite Shafts
2. FEM for Nonlinear Rotor Dynamics

DR. DOLIGALSKI & DR. SINGLETON (Room 4001) -- Dr. Nagamatsu

1. Passive Wave Drag Reduction

9:15 A.M. DR. ANDERSON (Room 3117) — Dr. Diefendorf & Dr. Winckler

1. Composite Applications to Helicopters

DR. DOLIGALSKI & DR. SINGLETON (Room 4001) -- Dr. Mayle

1. Blade Vortex Interaciton

10:30 A.M. DR. ANDERSON (Room 3117) — Dr. Darlow

1. Optimum Composite Shafting Design

DR. DOLIGALSKI & DR. SINGLETON (Room 4001) -- Dr. Duffy

1. Snap-Through Airfoils
2. Unsteady Aerodynamics

11:45 A.M. DR. ANDERSON, DR. DOLIGALSKI, & DR. SINGLETON -- Dr. Shephard

1. Graphics
2. Fuselage Dynamics Analysis

12:30 P.M. LUNCH

(Drs. Anderson, Doligalski, Singleton; Profs. Bielawa, Loewy, Mayle, and Crespo da Silva)

1:30 P.M. DR. ANDERSON, DR. DOLIGALSKI, & DR. SINGLETON — Dr. Bielawa

1. Fuselage Dynamics Testing
2. Rotor Impedance Rig

2:45 P.M. DR. ANDERSON, DR. DOLIGALSKI, & DR. SINGLETON — Dr. Loewy

1. Nonlinear Rotor Forced Response

Appendix B

Agenda

ARO Distinguished Fellowships: A Rotorcraft Technology Review

"Challenges in Rotorcraft Development; 1983-plus"
August 22-23, 1983
Communications Center Room 337

Rensselaer Rotorcraft Technology Center

August 22, 1983

Welcome	Professor R.G. Loewy Director Rotorcraft Technology Center	9:00 A.M.
Introductions	Professor R.J. Diefendorf Associate Director Rotorcraft Technology Center	9:05 A.M.
Helicopter Aerodynamics	Mr. Leo Dadone Engineering Specialist Boeing-Vertol	9:15 A.M.
Helicopter Stability and Control	Mr. Ray Prouty Chief, Stability and Control Analysis Hughes Helicopter	10:00 A.M.
Break		10:45 A.M.
Helicopter Structures and Structural Dynamics	Dr. Frank Camaratta Manager of Airframe Stress Sikorsky Aircraft Mr. Robert Blackwell Senior Dynamicist Sikorsky Aircraft	11:00 A.M.
Tilt Rotor Design and Development	Mr. Troy Gaffey Manager, JVX Technology Bell Helicopter Textron	11:45 A.M.
Lunch	JEC 3rd Floor Lounge	12:30 P.M.
Advanced Rotorcraft Configurations	Dr. Daniel Schrage Director of Advanced Systems AVRADCOM	1:15 P.M.
Laboratory Tours	Composites Lab Computer Graphics	2:00 P.M.

Break		3:00 P.M.
Materials Opportunities for Future Rotorcraft	Dr. G.L. Roderick Chief, Army Aeronautical Research Group Langley Research Center	3:15 P.M.
Helicopter Applied Technology	Dr. D.E. Hammond Chief, Aeromechanics Technical Area Applied Technology Labs Fort Eustis, Virginia	4:00 P.M.
Adjourn		4:45 P.M.
Dinner	Speaker: Mr. Allen Haggerty Class of '61 Senior Vice President for Operations of Hughes Helicopter	6:00 P.M.

August 23, 1983

Rotorcraft Research at NASA	Mr. Robert J. Huston Rotorcraft Manager Langley Research Center	9:00 A.M.
The Role of RPI's Rotorcraft Technology Center	Professor R.G. Loewy Director Rotorcraft Technology Center	9:45 A.M.
Break		10:30 A.M.
Lab Tours	Wind Tunnels Computer Center/Library	10:45 A.M. 11:15 A.M.
Steak Roast	JEC Courtyard	12:00 NOON
Adjourn		

Appendix C

List of Theses on Rotorcraft Technology Topics

1983

"Determination of The Position of Trailing Vortex Systems in a Closed Rectangular Wind Tunnel", M. Jenks, May '83, M.E. Aero. Eng. (Duffy)*

"Bolted Connections in Composite Shafts", K. Furnes, Aug. '83, M. Mech. (Goetschel)

"Elastic Hingeless Scissor Design for a Helicopter Upper Control System", M. M. Niederer, Aug. '83, M.S. (Goetschel)

"Determination of Non-Steady Aerodynamic Characteristics of Helicopter Rotors in Forward Flight", C. Rumsey, Aug. '83, M.E. Aero. Eng. (Duffy)

"Design Studies of a Composite Bearingless Tail Rotor for a Radio Controlled Helicopter", P. G. Vrionides, Aug. '83, M.S. (Loewy)

"Finite Element Approximation to Theodorsen's Solution for Non-Steady AeroDynamics of a Two-Dimensional Airfoil Section", E. Czajkowski, Dec. '83, M.E. Aero. Eng. (Duffy)

1984

"Analysis and Design of Bonded Composite Tubular Joints with Consideration of Thermal Effects", S. Anderson, May '84, M.S. Mech. Eng. (Goetschel)

"A Uniaxial Fatigue Study of Near-Unidirectional Composite Tubes for Negative R-Ratios", D. Elzey, May '84, M.S. Mech. (Krempl)

"Interactive Computer Modelling of Airframe Structures", B. Johnson, May '84, M.S. Civil Eng. (Shephard)

"The Optimal Design of Composite Drive Shafts", J. Lim, Aug. '84, M.S. Mech. Eng. (Darlow)

"Optimization of a Composite Scissor Assembly for a Helicopter Upper Control System", P. Vaney, Aug. '84, M.S. Mech. Eng. (Goetschel)

* The faculty member responsible as thesis advisor is shown in parenthesis, in each case.

"Transonic Drag Reduction on a Helicopter Rotor Blade Tip (NASA 0012 Airfoil Section) by Passive Shock Wave/Boundary Layer Control", D. Barnard, Dec. '84, M.S. (Nagamatsu)

"Design and Performance of a Blade-Vortex Interaction Experiment", R. Bergman, Dec. '84, M. E. Mech. Eng. (Mayle)

"Investigation of the Snap-Through Airfoil Concept for Control of Helicopter Rotors", M. Kolotylo, Dec. '84, M.E. Aero. Eng. (Duffy)

"A Method for Determining the Non-Steady Aerodynamic Loads and Moments on Helicopter Rotors in Forward Flight", J. Planchak, Dec. '84, M.S. Aero. Eng. (Duffy)

"Preliminary Design of a Snap-Through Helicopter Rotor Blade", R. M. Tomlin, Dec. '84, M.E. Aero. Eng. (Duffy)

"Turbine Aerodynamic Cascade Secondary Flow analysis", E. White, Dec. '84, M.S. Mech. Eng. (Nagamatsu)

1985

"Bolted Connections in Composite Rotor Shafts", R. Benson, May '85, M.S. Mech. Eng. (Goetschel)

"Preliminary Experimental Evaluation of a Five-Hole Probe Subjected to Varying Flow Conditions", M. Berube, May '85, M.S. Aero. Eng. (Nagamatsu)

"Post Processor Waveform Generator for the RPI Rotor Test Stand", May '85, S. Garing, M.S. Aero. Eng. (Bielawa)

"Improving the Strength Prediction for Advanced Composite Material With Stress Concentration", G. Hu, May '85, Ph.D. (Goetschel)

"Preliminary Conceptual Design of Mechanical Components of a Model Helicopter Rotor Impedance Test Rig", P. Singh, May '85, M.S. Aero. Eng. (Bielawa)

"Residual Static Torsional Strength of Composite Shafts After Simulated Impact Damage", R. Krafchak, Aug. '85, M.S. Aero. Eng. (Bauchau)

"Determination of Rotating Mode shapes and Natural Frequencies of a Helicopter Rotor Blade Using the Non-Rotating Mode Shapes as Generalized Coordinates", R. Smith, Aug. '85, M.S. Aero. Eng. (Loewy)

"Investigation of the Effects of Tunnel Size, Use of Top Wall Inserts and Trailing Edge Static Pressure on the Transonic Drag Reduction on Helicopter Rotor Blade Tips (NACA 0012 and Bell FX69-H-098 Airfoil Sections) by Passive Shock Wave/Boundary Layer Control", Dec. '85, N. Portier, M.S. Aero. Eng. (Nagamatsu)

"An Orthotropic Formulation of the Viscoplasticity Theory Based on Overstress", M. Sütcü, Dec. '85, Ph. D. Mech. Eng. (Krempl)

"Design and Performance of a Blade-Vortex Interaction Experiment", R. Bergman, Dec. '85 M.S. (Mayle)

1986

"Passive Drag Reduction on a Complete NASA 0012 Airfoil at Transonic Mach Numbers", J. Bossard, May '86, M.S. Aero. Eng. (Nagamatsu)

"Implementation of an Expert System Preprocessor", B. Gregory, M.S. Comp. Sc. May '86. (Shephard)

"The Elastic Stability of Composite Cylindrical Shells Under Combined Torsional and Axial Loading", J. Hayes, May '86, M.S. Mech. Eng. (Bauchau)

"On Frequency Domain Methodologies for Prescribed Structural Modification and Subsystem Synthesis", B. Jetmundsen, Aug. '86, Ph.D. Mech. Eng. (Bielawa)

"A Theory for Warp-Free Unsymmetric Composite Plates and Beams with Extension-Bending Couplings", S. J. Winckler, Aug. '86, Ph.D. M.E. (Diefendorf)

"Passive Shock Wave/Boundary Layer Control for the Bell FX69-H-098 Airfoil", T. J. Bidlack, Dec. '86, Ph.D. Aero. Eng. (Nagamatsu)

"Cumulative Damage Theory in Multiaxial Fatigue of Graphite/Epoxy [+45] Composites and Weight Function Theory For a Rectilinear Anisotropic Body", D. An, Dec. '86, Ph.D. Mechanics. (Krempl)

"An Evaluation of Design for Assembly Methodologies", D. Avidar, Dec. '86, M.S. Mech. Eng. (Darlow)

"The Effects of The Snap-Through Airfoil on the Elastic Twist of Rotor Blades", J. Colasante, Dec. '86, M.E. Aero. Eng. (Duffy)

"Hamiltonian Weak Principle in a Finite Element in Time Formulation as Applied to a Simple Beam Problem", R. Halvorsen, M.S. Aero. Eng., Dec. '86 (Bauchau)

"A Theoretical and Experimental Study of the Aerodynamic Characteristics of the Snap-Through Airfoil Higher Harmonic Control Device", J. Nickerson, Dec. '86, M.E. Aero. Eng. (Duffy)

"Airfoil Pressure Measurements for a Two Dimensional Blade Vortex Interaction", J. Straus, Dec. '86, M.S. Aero. Eng. (Mayle)

1987

"An Approach to Ideal Twist Distributions in Tilt Rotor VTOL Blade Designs Using Composite Materials Tailored to Produce Extension-Twisting Coupling Behavior", P. Bryan, May '87, M.S. Mech. Eng. (Bauchau)

"Shape Stability in Composites", D. Radford, May '87, Ph.D. Materials Eng. (Diefendorf)

"The Prototype Development of a Practical Design for the Precision Waveform Generator Portion of the RPI Rotor Impedance Test Facilities Postprocessor Subsystem", R. Martin, Aug. '87, M.S. Mech. Eng. (Bielawa)

"An Investigation of Unsteady Flow Over a Helicopter Rotor-Tip Airfoil with Solid and Porous Surfaces", T. Mitty, Aug. '87, M.S. Aero. (Nagamatsu)

"Passive Shock Wave/Boundary Layer Control of a Helicopter Rotor Airfoil (Bell FX69-H-098) Using a Contoured Transonic Wind Tunnel", G. Nyberg, Aug. '87, M.S. Aero. (Nagamatsu)

"A Theoretical and Experimental Study of the Aerodynamic Characteristics at the Snap-Through Airfoil", M. O'Connor, Aug. '87, M. Aero. Eng. (Duffy)

"The Scaling and Sizing of a Froude Scale Free-Flying Model Helicopter to be Used in Air Resonance Stability Testing and the Design of its Hingeless Rotor", K. Deyo, Dec. '87, M.S. Mech. Eng. (Bielawa)

"A Helicopter Airframe Structural Dynamics Test Facility: Design, Analysis, and Experimental Verification", J. Gordis, Dec. '87, M.S. Mech. Eng. (Bielawa)

"Preprocessor Development for the RPI Model Rotor Impedance Test Facility", K. Hsueh, Dec. '87, Ph.D. Mech. Eng. (Bielawa)

"Finite Element Approach to the Dynamic Analysis of Composite Helicopte Blades", C. H. Hong, Dec. '87, Ph.D. (Bauchau)

"Nonlinear Effects in Helicopter Forward Flight Forced Response", M. B. Mathew, Dec. '87, Ph.D. Mech. Eng. (Loewy)

"Discrete Vortex Modeling of a Blade-Vortex Interaction", P. Renzoni, Dec. '87, Ph.D. Aero. Eng. (Mayle)

"Design and Finite Element Analysis of a Model Helicopter Rotor Test Hub", J-L. Terng, Dec. '87, M.S. Mech. Eng. (Bielawa)

"The Effect of Incident Wake Flow on Blunt-Body Transfer Rates", N. VanDresar, Dec. '87, Ph.D. Mech. Eng. (Mayle)

Appendix D

RENSSELAER ROTORCRAFT TECHNOLOGY CENTER

Brown Bag Lunch Schedule

Spring of 1983

DATE	TOPIC	RESP. FACULTY
Feb. 21	Administrative Report Lightly Loaded Structures	J. Diefendorf D. Goetschel
Feb. 28	Vertol Composites Project Rotor Unsteady Aerodynamics	E. Krempl, W. Kim R. Duffy
Mar. 7	Transonic Airfoils Vortex Interaction Wind Tunnel	H. Nagamatsu R. Mayle
Mar. 21	Rotor Dynamics Analysis FEM Analysis for Fuselages	R. Loewy M. Shephard
Mar. 28	Administrative Report Report on AHS Specialists Mtg. Mechanical Connections in Composite Shafts	R. Loewy J. Diefendorf D. Goetschel
Apr. 4	Fundamental Fatigue Studies Blade Coupling Through Elastic Tailoring	E. Krempl E. Brunelle
Apr. 11	FEM Analysis for Fuselages Rotor Unsteady Aerodynamics	M. Shephard R. Duffy
Apr. 18	Report on AGARD Meeting Vortex Interaction Wind Tunnel	R. Loewy R. Mayle
Apr. 25	Administrative Report Lightly Loaded Structures Rotor Dynamics Analysis	J. Diefendorf D. Goetschel R. Loewy
May 2	Transonic Airfoils Mechanical Connections in Composite Shafts	H. Nagamatsu D. Goetschel

RENSSELAER ROTORCRAFT TECHNOLOGY CENTER

Brown Bag Lunch Schedule

Fall of 1983

DATE	TOPIC	RESP. FACULTY
Sep. 26	Administrative Report	J. Diefendorf
	Lightly Loaded Structures	D. Goetschel
Oct. 3	Administrative Report	R. Loewy
	Boeing-Vertol Project	E. Krempl W. Kim
Oct. 10	Rotor Unsteady Aerodynamics	R. Duffy
	Vortex Interaction Wind Tunnel	R. Mayle
Oct. 24	Composite Shaft Dynamics	M. Darlow
	FEM Analysis for Fuselages	M. Shephard
Oct. 31	Administrative Report	J. Diefendorf
	Transonic Airfoils	H. Nagamatsu
	Composite Fabrication Research	J. Diefendorf
Nov. 7	Mechanical Connections in Composite Shafts	D. Goetschel
	Fundamental Fatigue Studies	E. Krempl
Nov. 14	FEM Analysis for Fuselages	M. Shephard
Nov. 21	Administrative Report	R. Loewy
	Vortex Interaction Wind Tunnel	R. Mayle
	Research at NASA Langley	R. Loewy
Nov. 28	Rotor Unsteady Aerodynamics	R. Duffy
	Rotor Dynamic Analysis	R. Loewy
Dec. 5	Transonic Airfoils	H. Nagamatsu
	Lightly Loaded Structures	D. Goetschel
Dec. 12	Composite Shaft Dynamics	M. Darlow
	Boeing-Vertol Flex-Strap Research	V. Paedelt S. Hakim
	Nieschel Elastic Hinge	P. Vaney

RENSSELAER ROTORCRAFT TECHNOLOGY CENTER

Brown Bag Lunch Schedule

Spring of 1984

DATE	TOPIC	RESP. FACULTY
Jan. 16	Administrative Report	R. Loewy
	Boeing-Vertol Flex Strap Analysis	M. Shephard
	Lightly Loaded Structures	D. Goetschel
Jan. 23	Fundamental Fatigue Studies	E. Krempl
	Composite Shaft Dynamics	M. Darlow
Jan. 30	Fabrication Processes	J. Diefendorf
	Rotor Unsteady Aerodynamics	R. Duffy
Feb. 6	Administrative Report	Visitor: Dr. R. Singleton (ARO)
	FEM Analysis for Fuselages	M. Shephard
	Vortex Interaction Wind Tunnel	R. Mayle
		Visitor: Dr. F. Oertel (ARO)
Feb. 13	Transonic Airfoils	H. Nagamatsu
	Mechanical Connections in Composites	D. Goetschel
Feb. 20	Rotor Dynamics Analysis	R. Loewy
	Fundamental Fatigue Studies	E. Krempl
		Visitor: Dr. Jing G. Yen (Be
Feb. 27	Administrative Report	R. Loewy
	Composite Shaft Dynamics	M. Darlow
	Fabrication Processes	J. Diefendorf
Mar. 5	Rotor Unsteady Aerodynamics	R. Duffy
	FEM Analysis for Fuselages	M. Shephard

RENSSELAER ROTORCRAFT TECHNOLOGY CENTER

Brown Bag Lunch Schedule

Spring of 1984 - Cont'd.

DATE	TOPIC	RESP. FACULTY
Mar. 19	Vortex Interaction Wind Tunnel	R. Mayle
	Transonic Airfoils	H. Nagamatsu
Mar. 26	Lightly Loaded Structures	D. Goetschel
	Fundamental Fatigue Studies	E. Krempl
Apr. 2	Composite Shaft Dynamics	M. Darlow
	Fabrication Processes	J. Diefendorf
Apr. 9	Administrative Report	R. Loewy
	AGARD Report	R. Loewy
Apr. 16	FEM Analysis for Fuselages	M. Shephard
	Vortex Interaction Wind Tunnel	R. Mayle
Apr. 23	Transonic Airfoils	H. Nagamatsu
	Mechanical Connections in Composites	D. Goetschel
Apr. 30	Administrative Report	R. Loewy
	Fundamental Fatigue Studies	E. Krempl
	Composite Shaft Dynamics	M. Darlow

RENSSELAER ROTORCRAFT TECHNOLOGY CENTER

Brown Bag Lunch Schedule

Fall of 1984

DATE	TOPIC	RESP. FACULTY
Sep 10	Administrative Report	R. Loewy
	Composite Shaft Dynamics	M. Darlow
	FEM Analysis of Rotor Blade Aeroelasticity	O. Bauchau
Sep 17	Vortex-Interaction Wind Tunnel	R. Mayle
	Transonic Airfoils	H. Nagamatsu
Sep 24	Report on European Forum	R. Bielawa
	FEM Analysis for Fuselages	M. Shephard
Oct 1	Administrative Report	R. Loewy
	Rotor Dynamic Analysis	R. Loewy
	Rotorcraft Research at Technion-Israel Inst. of Tech.	A. Rosen
Oct 8	Rotor Unsteady Aerodynamics	R. Duffy
	Ballistic Damage Tolerance	O. Bauchau
Oct 15	Composites Fabrication	J. Diefendorf
	Mechanical Connections in Composites	D. Goetschel
Oct 22	Composite Shaft Dynamics	M. Darlow
	Composites Fatigue	E. Krempl
	Report on AHS Specialist's Mfg on Fatigue	E. Krempl
Oct 29	Vortex-Interaction Wind Tunnel	R. Mayle
	FEM Analysis of Rotor Blade Aeroelasticity	O. Bauchau
Nov 5	Administrative Report	R. Loewy
	Rotor Impedance Test Rig	R. Bielawa
	Transonic Airfoils	H. Nagamatsu
Nov 12	FEM Analysis for Fuselages	M. Shephard
	General Model of Blade Dynamics	A. Rosen
Nov 19	Rotor Dynamic Analysis	R. Loewy
	Rotor Unsteady Aerodynamics	R. Duffy
Nov 26	Composites Fatigue	E. Krempl
	Ballistic Damage Tolerance	O. Bauchau
Dec 3	Administrative Report	R. Loewy
	Composites Fabrication	J. Diefendorf
	Mechanical Connections in Composites	D. Goetschel
Dec 19	Composite Shaft Dynamics	M. Darlow
	FEM Analysis of Rotor Blade Aeroelasticity	O. Bauchau

RENSSELAER ROTORCRAFT TECHNOLOGY CENTER

Brown Bag Lunch Schedule

Spring of 1985

DATE	TOPIC	RESP. FACULTY
14 Jan	Administrative Report	Diefendorf
	Composite Shaft Dynamics	Darlow
	Composites Fabrication	Diefendorf
21 Jan	FEM Anal. of Rotor Blade Aeroelasticity	Bauchau
	Composite Fatigue	Krempl
28 Jan	Administrative Report	Loewy
	Vortex Interaction	Mayle
	Transonic Airfoils	Nagamatsu
04 Feb	Rotor Impedance Test Rig	Bielawa
	FEM Analysis of Fuselages	Shephard
11 Feb	Administrative Report	Loewy
	Rotor Dynamic Analysis	Loewy
	General Model of Blade Dynamics	Rosen
18 Feb	Rotor Unsteady Aerodynamics	Duffy
	Ballistic Damage Tolerance	Bauchau
	VISITOR: D. Adams, Hercules Aerospace	
25 Feb	Composite Shaft Dynamics	Darlow
	Composites Fabrication	Diefendorf
	VISITORS: R. Prouty & J. Shibler, Hughes Helicopters	
04 Mar	Analytical Testing	Bielawa
	Composite Fatigue	Krempl
11 Mar	Spring Recess	
18 Mar	Administrative Report	Loewy
	Rpt on Sikorsky Plant Visit - Composite Rotor Blades for "Black Hawk" Helicopter	Winckler
	Transonic Airfoils	Nagamatsu

RENSSELAER ROTORCRAFT TECHNOLOGY CENTER

Brown Bag Lunch Schedule

Spring of 1985 - Cont'd.

DATE	TOPIC	RESP. FACULTY
25 Mar	Rotor Impedance Test Rig	Bielawa
	FEM Analysis of Fuselages	Shephard
	VISITOR: Dr. M. Lessen, Prof. Emeritus, Univ. of Rochester	
01 Apr	Rotor Dynamic Analysis	Loewy
	General Model of Blade Dynamics	Rosen
08 Apr	Rotor Unsteady Aerodynamics	Duffy
	FEM Anal. of Rotor Blade Aeroelasticity	Bauchau
15 Apr	Administrative Report	Diefendorf
	Vortex Interaction	Mayle
	Composites Fabrication	Diefendorf
22 Apr	Composite Shaft Dynamics	Darlow
	Transonic Airfoils	Nagamatsu
29 Apr	Ballistic Damage Tolerance	Bauchau
	Composite Fatigue	Krempl
	VISITOR: P. LaMicq, SEP, France	

RENSSELAER ROTORCRAFT TECHNOLOGY CENTER

Brown Bag Lunch Schedule

Fall of 1985

DATE	TOPIC	RESP. FACULTY
09-Sep	Administrative Report	Krempl
	Rotor Unsteady Aerodynamics	Duffy
	FEM Anal. of Rotor Blade Aeroelasticity	Bauchau
16-Sep	General Discussion Topic - Technical Challenges in Human-Powered Helicopter Flight	Winckler**
23-Sep	Administrative Report	Diefendorf
	Composite Shaft Dynamics	Darlow
	European Rotorcraft Forum	Bielawa
30-Sep	General Discussion Topic - Composite Applications to Rotorcraft	Diefendorf
07-Oct	Administrative Report	Diefendorf
	Composite Fatigue	Krempl
	Vortex-Interaction	Mayle
14-Oct	General Discussion Topic - Rotor-Fuselage Coupling	Bielawa
21-Oct	Administrative Report	Diefendorf
	Transonic Airfoils	Nagamatsu
	FEM Analysis of Fuselages	Shephard
28-Oct	General Discussion Topic - Unsteady Aerodynamics of Rotors	Duffy
04-Nov	Administrative Report	Diefendorf
	Composites Fabrication	Diefendorf
	Ballistic Damage Tolerance	Bauchau

** ARO Distinguished Fellow

RENSSELAER ROTORCRAFT TECHNOLOGY CENTER

Brown Bag Lunch Schedule

Fall of 1985 - Cont'd.

DATE	TOPIC	RESP. FACULTY
11-Nov	General Discussion Topic - Rotor Blade Modeling	Bauchau
18-Nov	Administrative Report	Loewy
	Rpt on AHS Inter Mtg on the Theoreical Basis of Helicopter Technology, Nanjing, China	Loewy
	Rotor Unsteady Aerodynamics	Duffy
25-Nov	General Discussion Topic - Application of Principal Curvature Transformation & Velocity Components in Blade Dynamics	Mathew*
02-Dec	Administrative Report	Bielawa
	Ballistic Damage Tolerance	Bauchau
	Composite Shaft Dynamics	Darlow
09-Dec	General Discussion Topic - Vortex Aerodynamics	Mayle
	VISITORS: C. J. Weizenecker, Natl SAMPE President T. Quackenbush, Princeton University	

* Graduate Student

RENSSELAER ROTORCRAFT TECHNOLOGY CENTER

Brown Bag Lunch Schedule

Spring of 1986

DATE	TOPIC	RESP. FACULTY
13-Jan	Administrative Report	Loewy
	Composites Fabrication	Diefendorf
	FEM Anal. of Rotor Blade Aeroelasticity	Bauchau
20-Jan	General Discussion Topic -	
	Rotorcraft Vibrations	Loewy
27-Jan	Administrative Report	Diefendorf
	Composite Fatigue	Krempl
	Vortex-Interaction	Mayle
03-Feb	General Discussion Topic -	
	Planning for Annual Forum	Diefendorf
	Composite Applications to Rotorcraft	Diefendorf
10-Feb	Administrative Report	Diefendorf
	Transonic Airfoils	Nagamatsu
	Rotor Impedance Test Rig	Bielawa
17-Feb	Administrative Report	Loewy
	General Discussion Topic -	
	State of Rotor Aerodynamics	Duffy
24-Feb	Administrative Report	Diefendorf
	FEM Analysis of Fuselages	Shephard
	Rotor Dynamic Analysis	Loewy
03-Mar	General Discussion Topic -	
	Rotor-Fuselage Coupled Phenomena	Bielawa
10-Mar	Administrative Report	Diefendorf
	Rotor Unsteady Aerodynamics	Duffy
	Ballistic Damage Tolerance	Bauchau
17-Mar	Spring Recess (No Meeting)	

RENSSELAER ROTORCRAFT TECHNOLOGY CENTER

Brown Bag Lunch Schedule

Spring of 1986 - Cont'd.

DATE	TOPIC	RESP. FACULTY
24-Mar	General Discussion Topic - Optimization in Rotorcraft Design VISITOR: Mr. Karl Kowalski, M.I.T.	Gabriel
31-Mar	Administrative Report Composite Shaft Dynamics Composites Fabrication	Loewy Darlow Diefendorf
07-Apr	General Discussion Topic - Rotorcraft Crashworthiness (nonlinear FEM studies)	Shephard
14-Apr	Administrative Report Time Integration Formulation for FEM Anal. of Rotor Blade Aeroelasticity Composite Fatigue VISITOR: Ms. Ann Peck, Boeing Vertol	Loewy Bauchau Krempl
21-Apr	General Discussion Topic - Power Transmission in Rotorcraft	Darlow
28-Apr	Administrative Report Vortex-Interaction Transonic Airfoils	Loewy Mayle Nagamatsu

RENSSELAER ROTORCRAFT TECHNOLOGY CENTER

Brown Bag Lunch Schedule

Fall of 1986

DATE	TOPIC	RESP. FACULTY
08-Sep	Administrative Report	Diefendorf
	Some Dynamics Aspects of the Tilt-Rotor	Khader
	An Approach to Ideal Twist Distribution in Tilt-Rotor VTOL Blade Design	Bauchau
15-Sep	Rpt on Future NASA Rotorcraft Research	Bielawa/Mayle/ Nagamatsu
22-Sep	Administrative Report	Loewy
	Composite Shaft Dynamics	Darlow
	Rotor Unsteady Aerodynamics	Duffy
29-Sep	General Discussion - Composite Applications to Rotorcraft	Diefendorf
06-Oct	Administrative Report	Loewy
	Rotor Dynamic Response	Loewy
	Nonlinear Rotor Analysis	Crespo da Silva
13-Oct	General Discussion - Nonlinear Beam Kinematics	Bauchau
20-Oct	Administrative Report	Diefendorf
	Rotor Impedance Test Rig	Bielawa
	Composite Fatigue	Krempl

RENSSELAER ROTORCRAFT TECHNOLOGY CENTER

Brown Bag Lunch Schedule

Fall of 1986 - Cont'd.

DATE	TOPIC	RESP. FACULTY
27-Oct	General Discussion - Rotorcraft Crashworthiness	Shephard
03-Nov	Vortex-Interaction	Mayle
	Transonic Airfoils	Nagamatsu
10-Nov	General Discussion - Computer-Aided-Design of Rotorcraft	Gabriele/Trainer
17-Nov	Administrative Report	Diefendorf
	FEM Analysis of Fuselages	Shephard
	Ballistic Damage Tolerance	Bauchau
24-Nov	General Discussion - Rotor-Fuselage Coupling	Bielawa
01-Dec	Administrative Report	Diefendorf
	FEM Anal. of Rotor Blade Aeroelasticity	Bauchau
	Composite Fabrication	Diefendorf
08-Dec	Administrative Report	Loewy
	Ground/Air Resonance	Loewy
	Fuselage Dynamic Testing	Bielawa

RENSSELAER ROTORCRAFT TECHNOLOGY CENTER

Brown Bag Lunch Schedule

Spring of 1987

DATE	TOPIC	RESP. FACULTY
Jan 12	Administrative Report Composite Shaft Dynamics Ground/Air Resonance	Diefendorf Darlow (Zotto)
Jan 19	Administrative Report Rotor Unsteady Aerodynamics Nonlinear Strain Vibration	Loewy Duffy Crespo da Silva
Jan 26	General Discussion - Finite Element vs Modal Blade Dynamic Analysis	Bauchau/Loewy
Feb 2	Administrative Report Ballistic Damage Tolerance Report on AIAA Mtg in Reno and Recent Transonic Passive Drag Results	Bielawa Bauchau Nagamatsu (Mitty)
Feb 9	Administrative Report FEM Analysis of Fuselages Rotor Impedance Test Rig	Loewy Shephard Bielawa
Feb 16	General Discussion - Composite Applications to Rotorcraft	Diefendorf/Winckler
Feb 23	Administrative Report Vortex-Interaction Rotor Dynamic Response (Visitor: J. Oppedisano, RPI Office of Human Resources)	Loewy Mayle Loewy
Mar 2	Administrative Report Composites Fabrication Fuselage Dynamic Testing	Diefendorf Diefendorf Bielawa

RENSSELAER ROTORCRAFT TECHNOLOGY CENTER

Brown Bag Lunch Schedule

Spring of 1987 - Cont'd.

DATE	TOPIC	RESP. FACULTY
Mar 9	General Discussion - Compressible Rotor Aerodynamics	Nagamatsu/Brower/Cole
Mar 16	No Meeting (Spring Break)	
Mar 23	Administrative Report FEM Anal. of Rotor Blade Aeroelasticity Rotor Unsteady Aerodynamics	Loewy Bauchau Duffy
Mar 30	Administrative Report Composite Shaft Dynamics Rotor Impedance Test Rig	Diefendorf Darlow Bielawa
Apr 6	General Discussion - Computer-Aided-Design of Rotorcraft	Gabriele (Trainer)
Apr 13	Administrative Report Ballistic Damage Tolerance Vortex-Interaction	Loewy Bauchau Mayle
Apr 20	Administrative Report FEM Analysis of Fuselages Rotor Dynamic Response	Loewy Shephard Loewy
Apr 27	General Discussion - Rotor-Fuselage Coupling	Bielawa

RENSSELAER ROTORCRAFT TECHNOLOGY CENTER

Brown Bag Lunch Schedule

Fall of 1987

DATE	TOPIC	RESP. FACULTY
Sep 14	Welcome and Administrative Report	R.J. Diefendorf
	Finite Element in Time Solution for Rotor Dynamics	O. Bauchau
Sep 21	Administrative Report	R.J. Diefendorf
	Report on DaVinci Project	R. Bielawa
	Optimizing Composite Drive Systems	M. Darlow
Sep 28	Administrative Report	R.J. Diefendorf
	Unbalanced Laminates	R.J. Diefendorf
	Affine Transformations in Fluid Mechanics	E. Brunelle
Oct 5	Administrative Report	R.G. Loewy
	Effect of Rotor Shaft Flexibility on Ground/Air Resonance	R.G. Loewy
	Use of Generalized Coordinates in Blade Dynamics	R.G. Loewy
Oct 12	Administrative Report	R.G. Loewy
	Transonic Drag Reduction	H. Nagamatsu
	Rotor Unsteady Aerodynamics	R. Duffy
Oct 19	General Discussion: Helicopter Fuselage Shake Testing: What's Needed?	R. Bielawa R.G. Loewy H. Scarton
Oct 26	Administrative Report	R.J. Diefendorf
	Vortex Interaction Testing	J. Straus

RENSSELAER ROTORCRAFT TECHNOLOGY CENTER

Brown Bag Lunch Schedule

Fall of 1987 - Cont'd.

DATE	TOPIC	RESP. FACULTY
Nov 2	Administrative Report	R.G. Loewy
	Vertol C-60 Project	M.B. Mathew
	Use of Elastic Coupling in Blade Design	S. Winckler
Nov 9	Administrative Report	R.J. Diefendorf
	FEM in Blade Dynamics	O. Bauchau
	Optimizing Composite Drive Systems	M. Darlow
Nov 16	Administrative Report	R. Loewy
	Unbalanced Laminates	R.J. Diefendorf
	Affine Transformations in Fluid Mechanics	E. Brunelle
Nov 23	Administrative Report	R.J. Diefendorf
	Impedance Test Rig	R. Bielawa
	Transonic Drag Reduction	H. Nagamatsu
Nov 30	General Discussion: Calculating Rotor Loads in Violent Maneuvers	R.G. Loewy M. Crespo da Silva O. Bauchau
Dec 7	Adminisatrative Report	R.J. Diefendorf
	Rotor Unsteady Aerodynamics	R. Duffy
	Ballistic Damage in Composite Shafts	O. Bauchau
Dec 14	Administrative Report	R. G. Loewy
	Vortex Interaction Testing	J. Straus
	Effect of Rotor Shaft Flexibility on Ground/Air Resonance	R. G. Loewy